Quantitative and qualitative analysis of nano-sized vesicles released by dendritic cells and T cells

Towards deciphering the role of extracellular vesicles in immune cell communication

The research described in this thesis was performed at the Department of Biochemistry and Cell Biology, Faculty of Veterinary Medicine, Utrecht University.

The printing of this thesis was financially supported by the Department of Biochemistry and Cell Biology of the Faculty of Veterinary Medicine at Utrecht University, Infection and Immunity Center Utrecht, BD Biosciences, and the J.E. Jurriaanse Stichting.

ISBN: 978-90-393-5956-3

Cover photo: Dick van der Vlist
Cover design: Ilse Leen
Lay-out: Els van der Vlist and Joost van der Lit
Printed by Wöhrmann Print Service, Zutphen

Paranymphs: Marian Aalberts and Marijke Zonneveld

Quantitative and qualitative analysis of nano-sized vesicles released by dendritic cells and T cells

Towards deciphering the role of extracellular vesicles in immune cell communication

Kwantitatieve en kwalitatieve analyse van door dendritische cellen en T cellen afgegeven nano-membraanblaasjes: Richting het ophelderen van de rol van extracellulaire membraanblaasjes in de communicatie tussen immuuncellen *(met een samenvatting in het Nederlands)*

Proefschrift

ter verkrijging van de graad van doctor aan de Universiteit Utrecht op gezag van de rector magnificus, prof.dr. G.J. van der Zwaan, ingevolge het besluit van het college voor promoties in het openbaar te verdedigen op donderdag 30 mei 2013 des ochtends te 10.30 uur

door

Elizabeth Johanan van der Vlist

geboren op 30 mei 1985 te Zaltbommel

Promotoren: Prof. dr. M.H.M. Wauben
Prof. dr. W. Stoorvogel

Co-promotor: Dr. E.N.M. Nolte-’t Hoen

Table of contents

Life begins at the end of your comfort zone - Neale Donald Walsch

Chapter 1

General Introduction

Extracellular vesicles in immunology

Els J. van der Vlist, Esther N.M. Nolte-'t Hoen and Marca Wauben

In: Micro/nanovesicles and exosomes in health and disease,
Pan Stanford Publishing (in press)

Abstract

Communication between cells of the immune system was originally thought to occur either via direct cell-cell contact or via soluble factors released by cells. Over the last two decades, however, it has become clear that cell-derived vesicles also play an important role in intercellular communication (1, 2). This chapter focuses on the role of T cell-derived vesicles and dendritic cell (DC)-derived vesicles in immune regulation. Interaction and crosstalk between T cells and DC is the key-event in the initiation of adaptive immune responses. During their crosstalk, both T cells and DC increase the release of vesicles. In contrast to DC-derived vesicles, T cell-derived vesicles attracted less attention in relation to a possible role in immune regulation. We here give a comprehensive overview of the current knowledge on T cell-derived and DC-derived vesicles and their biological activities.

Introduction

Intercellular communication via vesicles has several clear advantages. First, the selective sorting of proteins, lipids and RNA into vesicles allows the transfer of unique combinations of multiple signaling molecules within one vehicle (1). Second, vesicles uniquely allow the intercellular transfer of transmembrane proteins. These proteins can be involved in adhesion, targeting and/or signaling of the vesicle to the target cell. Third, cytosolic proteins and RNA present in the lumen of the vesicle are sequestered and thereby protected against degradation and shielded for unwanted collateral effects. Fourth, after their release into the extracellular space, vesicles can bind soluble factors from their environment, which can also be transferred to target cells. Finally, cell-derived vesicles can be targeted not only to cells in their direct environment but can also reach target cells over longer distances via circulation in body fluids. Hence, the selective incorporation of different molecules into vesicles and the regulated release and targeting of vesicles ensures the timely spread of custom-made vehicles for intercellular communication.

Many, if not all, cells types can release vesicles either constitutively or upon specific triggers (1, 2). Vesicles derived from viable cells range in size between 50 – 1000 nm and can be roughly divided into two groups: vesicles that are released into their environment after shedding from the plasma membrane and vesicles derived from endosomal compartments. Multivesicular bodies (MVB) are late endosomal compartment that contain multiple intraluminal vesicles, which are formed through the inward budding of the limiting membrane of the MVB. Once proteins are incorporated into intraluminal vesicles they can either be degraded, when the MVB fuses with lysosomes, or be released into the extracellular space when the MVB fuses with the plasma membrane (3). Both MVB pathways can be simultaneously operational in one cell (4). The intraluminal vesicles released in the extracellular space are generally referred to as exosomes (3). Exosomes have been described to be 50 - 150 nm in size and have a buoyant density in sucrose ranging between 1.10 – 1.19 g/ml (1, 3). They contain endosomal proteins such as Tsg101 and Alix and tetraspanins such as CD9 and CD63 (1, 3). Depending on their parental cell, exosomes can also carry cell-type specific proteins such as MHCII for DC-derived exosomes and TCR for T cell-derived exosomes (5, 6). DC and T cell-derived exosomes also carry a selective set of small RNAs which differs from the RNA composition of their parental cells (7, 8).

Vesicles that are shed from the plasma membrane, which are often referred to as microvesicles, microparticles or ectosomes, are very heterogeneous in size (50 - 1000 nm) (2, 9). Plasma membrane-derived vesicles are formed by budding at particular regions of the plasma membrane. Specific cytosolic and plasma membrane-derived proteins can be sorted into or excluded from these buds (2). In addition to formation at MVBs, exosome biogenesis can also occur at specialized plasma membrane microdomains enriched in

endosomal proteins, as was shown for T cells (10). Although the exact mechanisms of protein sorting into different types of cell-derived vesicles have yet to be elucidated, cholesterol-rich microdomains are believed to be involved in this process (2, 11).

The currently used classification of vesicles is mainly based on the cell type of origin or the presumed subcellular origin of the vesicle. This has resulted in a rather confusing nomenclature including terms such as prostasomes, exosomes, microvesicles, microparticles, ectosomes, and shedding vesicles. Although in theory these different vesicle types can be quite well-defined based on their (sub)cellular origin, once released in extracellular space this classification is very difficult. First, endosomally-derived vesicles and plasma membrane-derived vesicles can overlap in size and in buoyant density. Second, up to now there are no markers described that are exclusively present on one vesicle type. Consequently, it is not yet possible to phenotypically classify a released vesicle based on its subcellular origin. Classification based on function is also complicated. The molecular composition of a released vesicle is dynamic and not only depends on the subcellular origin of the vesicle but also on the producing cell type and the activation status of these cells. Hence, the total population of released vesicles is heterogeneous and probably consists of a mixture of different vesicles types (12, 13).

Extracellular vesicles can affect their target cells by signaling via receptor-ligand interactions (14), via modulatory lipids (15) or through transfer of regulatory (small) RNAs (16). Besides the molecular composition of the vesicles, the status of the target cell determines the functional outcome of the crosstalk between vesicles and target cells. Altogether, these different factors might explain the pleiotropic biological functions that have been described for extracellular vesicles.

Methods to characterize individual vesicles and vesicle populations

The majority of the vesicles released by cells is smaller than 300 nm (17, 18). As a result, high-resolution imaging techniques, such as electron microscopy (EM) or atomic force microscopy (AFM), are required to visualize individual nano-sized vesicles. These high-resolution imaging techniques, however, are not suitable to study large numbers of vesicles, needed to reliably characterize vesicle populations that are largely heterogeneous.

Techniques such as western blotting, proteomics, lipidomics and transcriptomics, have been used to characterize bulk-isolates of entire vesicle populations. These techniques yield valuable information on the molecular composition at the level of the total vesicle population, but are less suited to study the heterogeneity of vesicle populations. Detection of a certain molecule, for instance, will not reveal whether this molecule is present in all vesicles or uniquely expressed in a certain vesicle subset. More importantly, molecules characteristic for a small vesicle subset may be missed in such bulk-based approaches. Furthermore, the lack of 'household' markers, which are constitutively

sorted into vesicles, precludes reliable quantitative analysis of vesicles using bulk-based analysis techniques.

To analyze different vesicle types or subpopulations within a heterogeneous vesicle population, multi-parameter high-throughput analysis of individual vesicles is required. Nano-particle Tracking Analysis (NTA) allows accurate size determination of individual vesicles based on their Brownian motion (19). However, our recent data indicate that heterogeneously sized vesicle populations are difficult to quantify and characterize using NTA.

Flow cytometry is a powerful technique that can be used to combine high-throughput and multi-parameter analysis on cells. However, since most conventional flow cytometers have a lower limit for light scatter detection of 300 – 500 nm, they are unable to detect nano-sized vesicles (20). We have therefore developed a fluorescence-based high-resolution flow cytometric method which can be used for quantitative and qualitative analysis of individual nano-sized vesicles smaller than 300 nm (21, 22). By using bright fluorescent labeling of vesicles combined with reduced wide-angle light scattering on a high-end flow cytometer, this method is suitable for the analysis of vesicles down to ~70 nm in size. This high-resolution flow cytometric method allows multi-parameter analysis on individual vesicles and can thus be used for the analysis of vesicle subsets within heterogeneous vesicle populations. NTA can complement the flow cytometry-based analysis of nano-sized vesicles since with the latter method only relative and approximate size information can be obtained, whereas NTA measurements provide more accurate information on the absolute size of vesicles. The recent and future development of methods to analyze large numbers of individual vesicles will allow more insight in the physiological role of changes in the composition of both individual vesicles and vesicle subsets.

T cell-derived vesicles

T cells are key effector cells of the adaptive immune response and are also important in the regulation of B cell and T cell responses. $CD4^+$ T cells recognize their cognate peptide presented in the context of MHCII and provide help to enhance both humoral responses and cellular immunity mediated by $CD8^+$ cytotoxic T cells (CTL). Depending on numerous polarizing signals $CD4^+$ T cells can be skewed to many different functional subsets, such as Th1, Th2, Th17 cells or regulatory T cells (23). Each subset secretes different effector molecules and can actively regulate other T cell subsets. Vesicles derived from T cells might therefore differ in their molecular composition depending on the T cell subset they originate from. Remarkably, only a limited number of studies have focused on T cell-derived vesicles. Due to large variations in the source of T cells and exogenously applied stimuli in these studies, the molecular composition of the released vesicles is likely to vary substantially. Additionally, the use of different vesicle isolation procedures further

complicates inter-study comparisons. Nevertheless, these studies show that vesicles derived from T cells can be targeted to many different cell types and may induce a large range of immune modulatory effects (**Fig. 1**).

Table I gives an overview of the variation in parental T cell sources, type and duration of activation stimuli, vesicle isolation protocols, target cells and functional assays that were used to study the role of T cell-derived vesicles. In addition, the morphological and molecular characteristics of the different vesicle populations, as well as the methods used to characterize these vesicles are listed in this table. As cellular sources of vesicles, primary T cells, different T cell clones and cell lines, such as Jurkat cells, were used. These cells were triggered to release vesicles by mitogens, such as PMA or PHA (24-30), or (antibody-mimicked) cognate interactions with antigen presenting cells (6, 12, 26, 29, 31-35). T cells were allowed to release vesicles for different time periods ranging from 1 hour up to 4 days (6, 24, 25, 30, 36). However, the release of T cell-derived vesicles was mostly limited to 10 – 24 hours of culture (6, 12, 26, 29, 31, 33-35, 37, 38). In most studies, vesicles were isolated from cell culture supernatants by differential steps of centrifugation. Vesicle sedimentation was most often performed at 100,000g, but in some studies lower g-forces, such as 15,000g or 20,000g, were used (27-29, 32). Sedimentation at lower g-forces yields a vesicle population of larger or aggregated vesicles. Only three studies used density gradient floatation to further characterize the T cell-derived vesicles (10, 12, 32). The size and composition of the isolated vesicles were determined by electron microscopy, western blotting or flow cytometric analysis (of bead-associated vesicles). TCR/CD3 complexes, MHCI, CD2, and LFA-1 were frequently detected on the surface of T cell-derived vesicles. The pro-apoptotic protein FasL was also detected in multiple studies. For *in vitro* functional studies, isolated vesicles were incubated with different target cells, after which proliferation, cytokine production and/or apoptosis induction were measured. For *in vivo* functional studies, mice were injected i.v. with isolated T-cell derived vesicles, after which tumor growth, killing of injected target cells, or the onset of diabetes were assessed (**Table I**).

$CD8^+$ T cell-derived vesicles

Activated $CD8^+$ T cells kill infected cells or tumor cells by releasing the content of their secretory lysosomes in the synaptic cleft formed between the $CD8^+$ T cell and target cell. Secretory lysosomes are late endosomal compartments that contain lethal components, such as perforin and granzymes. Interestingly, these secretory lysosomes also contain multiple nano-sized intraluminal vesicles that carry the T cell receptor (TCR), CD3, CD8 and MHCI (36). Peters *et al*. were the first to describe the intracellular presence and release of $CD8^+$ T cell-derived vesicles based on elaborate EM studies (36). At that time,

it was hypothesized that perforin and granzymes were released in a vesicle-mediated or -associated manner (39). The presence of CD3/TCR, CD8, and possibly other proteins on these nano-sized vesicles were proposed to ensure unidirectional delivery of the lethal compounds to the target cell to avoid bystander damage (40). Later, the pro-apoptotic transmembrane protein Fas ligand (FasL) was identified on both the limiting membrane and on nano-sized intraluminal vesicles (41). Based on this subcellular origin FasL-bearing vesicles are often referred to as exosomes. The receptor of FasL, named Fas (or Fas receptor), is expressed on various immune and non-immune cells. Binding of FasL to Fas triggers apoptosis of Fas-bearing cells (42). In this perspective, it is likely that FasL, present on $CD8^+$ T cell-derived vesicles, is also involved in the vesicle-mediated killing in the lytic synapse. It is unclear whether membrane-bound FasL can also be released via plasma membrane-derived vesicles. However, the sorting of FasL to late endosomal compartments avoids inactivation of FasL, which normally occurs at the cell surface through cleavage of FasL by metalloproteases (43). Hence, the sorting to the endosomal compartment and the subsequent release of exosomes ensures the delivery of active membrane-bound FasL to target cells.

After the initial description of $CD8^+$ T cell-derived exosomes, the function of $CD8^+$ T cell-derived vesicles has been addressed by a few other groups. These studies focused on the total pool of vesicles released by $CD8^+$ T cells, which may be a mixture of plasma membrane-derived vesicles and exosomes (6, 32, 38). More importantly, the vesicles studied were isolated from cell culture supernatant and might therefore be different from the population of $CD8^+$ effector vesicles released in the lytic synapse between $CD8^+$ T cell and target cell. Indeed, these studies demonstrated that $CD8^+$ T cell-derived vesicles released in culture supernatant have immune regulatory properties.

Immune suppressive effects of $CD8^+$ T cell-derived vesicles

The immune-suppressive effect of $CD8^+$ T cell-derived vesicles became clear from a study that described that vesicles derived from OTI $CD8^+$ T cells could inhibit $CD8^+$ cytotoxic responses both *in vitro* and *in vivo* (38) (**Fig. 1**). These vesicles blocked MHCI-OVA-peptide complexes on DC, thereby reducing in vitro $CD8^+$ proliferation without affecting $CD4^+$ proliferation. Besides shielding of MHCI, these $CD8^+$ T cell derived vesicles induced apoptosis of OVA-pulsed DC, which could be prevented by incubating the vesicles with FasL blocking antibodies before incubation with the DC. Remarkably, despite the fact that the $CD8^+$ T cell-derived vesicles induced apoptosis of OVA-pulsed DC, *in vitro* $CD4^+$ T cell proliferation remained unaffected in this study (38). *In vivo* administration of vesicles from OTI $CD8^+$ T cells were shown to be beneficial in an autoimmune DC_{OVA}-induced diabetes model, since they inhibited the $CD8^+$ T cell-mediated killing of pancreatic beta cells (38). Blocking of MHCI-peptides complexes and apoptosis induction via the Fas/FasL-pathway have both

been suggested to be involved in this process. It is however unclear whether one vesicle population released by activated OVA-specific $CD8^+$ T cells can perform either functions or that different subpopulations of vesicles are responsible for these effects. Besides the beneficial immune suppressive role of $CD8^+$ T cell vesicles on autoimmune diseases, these vesicles can also be exploited to promote tumor development. In the latter study, *in vivo* administration of the $CD8^+$ T cell-derived vesicles resulted in an inhibition of cytotoxic T cell responses against OVA-expressing tumor cells (38). In a more recent study, another mechanism via which $CD8^+$ T cell-derived vesicles might promote tumor development was described. Incubation of Fas-resistant tumor cells with vesicles from activated $CD8^+$ T cells promoted their invasion both *in vitro* and *in vivo* (34). This effect was dependent on FasL, and may involve vesicle-induced upregulation of matrix metalloproteinase 9 (MMP9) in tumor cells, which plays an important role in the breakdown of extracellular matrix (34).

Immune activating effects of $CD8^+$ T cell-derived vesicles

The immune-activating potential of $CD8^+$ T cell-derived vesicles became clear from a study describing increased antiviral properties of $CD4^+$ T cells after binding of $CD8^+$ T cell-derived vesicles (32) (**Fig. 1**). Both acute and chronically infected $CD4^+$ T cells showed increased suppression of HIV-1 replication *in vitro* upon binding of the $CD8^+$ T cell-derived vesicles. The poorly understood antiviral mechanism displayed by $CD8^+$ T cells remained unsolved for a long time, since it was attributed to a soluble protein (e.g. cytokine or chemokine). However, recently Tumne *et al*. proved that 15,000g sedimented vesicles, but also isolated homogenized $CD8^+$ T cell membranes, were able to suppress HIV-1 replication (32). $CD3^+$ $MHCII^+$ vesicles enriched in tetraspanins were shown to be responsible for this effect. Although cell culture supernatant from $CD8^+$ T cells was able to suppress HIV-replication, cell-to-cell contact between $CD8^+$ T cells and HIV-1-infected $CD4^+$ T cells was necessary for maximal inhibition of virus replication. This direct cell-cell contact may be a trigger for the $CD8^+$ T cell to release vesicles or allow more efficient targeting of vesicles to the $CD4^+$ T cell.

A recent study suggested that vesicles released by activated human $CD3^+$ T cells carry RANTES (CCL5), which may be involved in the observed vesicle-induced proliferation of $CD8^+$ T cells population and release of MIP1β (35). Since this $CD3^+$ T cell population was not further sorted, it is unclear if these vesicles are released by $CD4^+$ or $CD8^+$ T cells. Furthermore, future research should resolve whether T cell vesicle-associated RANTES is also involved in the earlier described antiviral effects of these vesicles.

CD4$^+$ T cell-derived vesicles

Similar to CD8$^+$ T cell-derived vesicles released in the lytic synapse between a CD8$^+$ T cell and target cell (36), CD4$^+$ T cell-derived vesicles can be released in the immune synapse formed between a CD4$^+$ T cell and antigen presenting cell (APC) (7). It has been demonstrated that cognate interaction between T cells and APC induces the directional release of microRNA-containing vesicles from the T cell toward the interacting APC (7). These T cell-derived vesicle-associated microRNAs were functionally transferred to the interacting APC (7). Besides the direct targeting of T cell-derived vesicles to the interacting APC, CD4$^+$ T cell-derived vesicles can also be isolated from cell culture supernatant. In analogy with CD8$^+$ T cell-derived vesicles, these non-directionally released vesicles can play a role in immune regulation via the targeting of bystander cells.

Immune suppressive effects of CD4$^+$ T cell-derived vesicles

Vesicles released by either suppressive CD4$^+$ T cells or effector CD4$^+$ T cells can be involved in the down regulation of immune responses, via interaction with other T cells or DC (**Fig. 1**). Similar to CD8$^+$ T cells, FasL and another apoptosis-inducing ligand, APO2L, are sorted to the MVBs of CD4$^+$ T cells (41). Upon activation, CD4$^+$ T cells can release APO2L/FasL-bearing vesicles through fusion of MVBs with the plasma membrane (24, 25). These FasL-bearing vesicles can be targeted to non-activated CD4$^+$ T cells and induce apoptosis in these cells (24), which may be a mechanism for dampening of immune responses. The fact that these vesicles were released within 1 hour, well before their parental cells showed signs of activation-induced cell death, clearly distinguishes them from apoptotic blebs.

Another type of immune cell that is targeted by CD4$^+$ T cell-derived vesicles is the antigen presenting cell (APC). Our group was the first to show that proteins derived from rat T cells, such as TCR and MHCII (present on activated human and rat T cells), were transferred to APC in a vesicle-mediated manner (37). We showed that vesicles derived from anergic CD4$^+$ T cells, which can suppress T cell responses similar to regulatory T cells, could endow APC with immune-suppressive properties. APC incubated with these anergic T cell-derived vesicles down-modulated CD4$^+$ T cell responses during subsequent antigen exposure (37). In contrast, vesicles from non-anergic T cells did not change the T cell stimulatory capacity of these APC. The vesicles derived from anergic T cells exhibited higher levels of MHCII, IL2-Rα and ICAM-1. It is however unclear whether these molecules are responsible for the immune suppressive effect or for improved targeting of other immune suppressive entities e.g. microRNAs.

More recently, it was shown that OVA-specific (OTII) CD4$^+$ T cells release FasL-positive vesicles that can bind to OVA-pulsed DC (DC_{OVA}) in a MHCIIp/TCR and ICAM-1/LFA-1 dependent manner (33). DC_{OVA} incubated with vesicles derived from OTII CD4$^+$ T

cells that had been activated via cognate interactions showed decreased capacity to induce proliferation of naïve OTII $CD4^+$ T cells *in vitro*. Immunization of mice with DC_{OVA} in combination with OTII $CD4^+$ T cell vesicles resulted in severely reduced numbers of OVA-specific $CD8^+$ T cells as compared to immunization with DC_{OVA} alone or DC_{OVA} together with vesicles from control ConA-stimulated polyclonal $CD4^+$ T cells. Subsequent cytotoxicity assays demonstrated that *in vivo* administration of vesicles derived from OTII $CD4^+$ T cells inhibit DC_{OVA}-stimulated effector $CD8^+$ cytotoxic responses (33). This effect could be either due to masking of MHCII-peptide complexes on the DC_{OVA} by vesicle-associated OVA-specific TCR, resulting in less efficient $CD4^+$ T cell mediated help for $CD8^+$ T cells. Alternatively, vesicle-associated FasL could have led to apoptosis induction of Fas-expressing DC_{OVA}. Although *in vitro* binding of the T cell-derived vesicles to DC_{OVA} could be blocked by anti-MHCII antibodies, it was not investigated whether either anti-MHCII or anti-FasL blocking could inhibit the described *in vivo* effects. Yet another study indicates that $CD4^+$ T cell-derived vesicles could be involved in suppression of immune responses via blocking of MHC-peptide complexes on DC (31). DC that acquired TCR molecules from OVA-specific $CD4^+$ T cells were shown to be less efficient in activating naïve OVA-specific $CD4^+$ T cells, whereas their ability to prime OVA-specific $CD8^+$ T cells was unaffected. Addition of an excess of OVA-peptide restored the capacity of TCR-bearing DC to activate OVA-specific $CD4^+$ T cells. This suggests that transferred TCR complexes had masked the OVA-peptide bearing MHCII molecules, thereby reducing their accessibility for $CD4^+$ T cells (31). Hence, these findings indicate that $CD4^+$ T cell derived vesicles could play a role in the antigen-specific dampening of immune responses.

Immune activating effects of $CD4^+$ T cell-derived vesicles

Vesicles released by $CD4^+$ T cells have also been described to be involved in enhancement of immune responses, e.g. via activation of innate monocytes and mast cells (27-30) (**Fig. 1**). Incubation of human monocytes with vesicles derived from mitogen-activated $CD4^+$ T cells induced the production of pro-inflammatory cytokines such as TNFα and IL-1β (27, 28, 30). The vesicle-induced production of these cytokines could be inhibited by high-density lipoprotein (HDL) from human serum, whereas the release of other factors such as sIL-1Ra and CCL2 remained unaffected (27, 28). Incubation of monocytes with 100 – 800 nm sized T cell-derived vesicles was also shown to lead to the accumulation of cholesterol in the cytosol of these cells. This accumulation was thought to occur through the uptake of the cholesterol-rich vesicles by the monocyte and could be inhibited by blocking the phosphatidylserine (PS) receptor (30). Since both activated T cells and monocytes are present in atherosclerotic plaques, it has been suggested that activated T cell-derived vesicles may promote atherogenesis by inducing intracellular cholesterol accumulation in monocytes and creating a pro-inflammatory cytokine-rich environment (30). Whether

HDL could plays a role in inhibiting this vesicle-mediated process remains to be elucidated.

When targeted to mast cells, vesicles derived from anti-CD3/anti-CD28 activated T cells caused degranulation and release of IL-8 and oncostatin M. These effects were also observed after incubation of mast cells with crude membrane fragments derived from these T cells (29). Degranulation induced by activated T cell-derived vesicles was dose-dependent and increased over time to almost 20% degranulation after 20 hours, whereas incubation with vesicles from non-activated T cells led to less than 5% degranulation. This effect may be ERK-dependent, since vesicles from activated T cells were shown to induce phosphorylation of ERK in mast cells and pretreatment of mast cells with an ERK-inhibitor significantly reduced the ability of activated T cell vesicles to induce mast cell degranulation (29). Since in these studies the T cell-derived vesicles displayed similar activity as solubilized membranes and membrane fragments (27-30), it is not clear whether the described effects were mediated by a specifically released population of vesicles or by non-specifically shed plasma membrane fragments.

Assessing the quality and quantity of T cell-derived vesicles

The studies described above show that T cell-derived vesicles are targeted to various types of immune cells and can regulate immune responses at distinct levels (**Fig. 1**). The broad spectrum of target cells and functions of these vesicles may be caused by differences in the molecular composition of vesicles released by functionally distinct T cell subsets. Few studies have addressed the changes in the population of vesicles released by T cells upon activation. Based on analyses of bulk isolates of T cell-derived vesicles, it was suggested that TCR engagement is an important trigger for $CD4^+$, and possibly also $CD8^+$, T cells to increase vesicle release (6, 26). Using our flow cytometric method for detection and characterization of individual vesicles, we showed that $CD4^+$ T cells indeed released higher numbers of vesicles upon TCR-triggering. Moreover, additional co-stimulatory signals via CD28 further increased the number of released vesicles (12). Using this technique, we also showed that the population of vesicles released by T cells is heterogeneous and that T cells differentially regulate the release of distinct vesicle subpopulations depending on their activation status (12). Hence, different vesicle populations within the total pool of vesicles might be targeted to distinct cell types and exert different functions. In order to understand the pleiotropic effects of T cell derived vesicles it is therefore important to further unravel the triggers for the release of different vesicle subsets and to study their molecular composition and target cells.

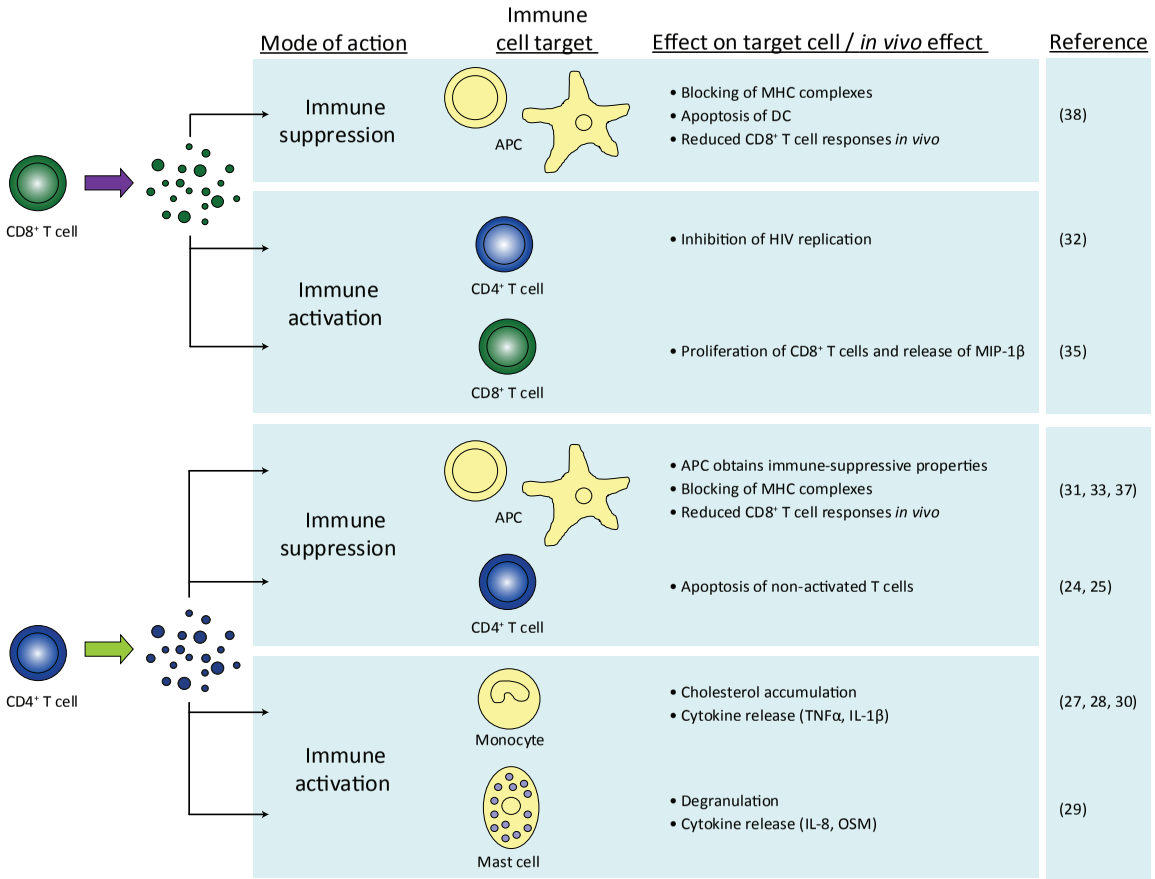

Figure 1 –Targets and pleiotropic effects of T cell-derived vesicles This figure summarizes the immune cell targets and the effects that have been described for vesicles derived from $CD4^+$ and $CD8^+$ T cells. The effects summarized in this figure are observed *in vitro* unless indicated otherwise.

Dendritic cell-derived vesicles

A key-player in immune regulation is the dendritic cell (DC). In all tissues DC constantly sample their environment and present peptides on MHC molecules which can be recognized by T cells bearing a T cell receptor (TCR) specific for this complex (cognate DC-T cell interaction). DC that are not activated by danger signals, e.g. pathogens or tissue damage, are called immature DC. Immature DC do not induce effector T cell responses and can play an important role in the maintenance of tolerance by inhibition of effector T cells and/or expansion of regulatory T cells (44). Danger signals, such as the presence of bacterial derived lipopolysaccharide (LPS), can induce DC to mature and become efficient inducers of effector T and B cells (44, 45). The interaction between mature DC and $CD4^+$ T cells lies at the heart of the adaptive immune response and is crucial for efficient eradication of invading pathogens and maintenance of homeostasis (45). Consequently, the functional outcome of cognate DC-T cell interactions is tightly regulated and depends on the subtype and activation status of the cells engaged in this interaction. The balance between activation and tolerance is regulated via direct cell-cell interactions, secreted soluble factors and released vesicles.

The first report on vesicle release by antigen presenting cells (APC) came from Raposo and coworkers (14) who described that B cells could secrete vesicles containing MHCII. These vesicles were thought to amplify the antigen-presenting capacity of APC and were quickly recognized as potential therapeutic agents. As a consequence, both the triggers for release and the molecular composition of vesicles released by APC have been studied far more extensively than T cell-derived vesicles and many excellent reviews have been written (see (1, 46) for examples). In this section we focus on vesicles derived from DC, since these professional antigen presenting cells are key to initiation of immune responses. The proposed functions and immune target cells of DC-derived vesicles are summarized in **Fig. 2.** Various studies indicate that vesicles derived from DC can be targeted to $CD4^+$ and $CD8^+$ T cells, DC, and natural killer (NK) cells. The effects of DC-derived vesicles have been studied both *in vitro* and *in vivo*. Importantly, the composition and number of vesicles released by DC depend on the activation (maturation) status of the parental cell and in turn determine how these vesicles modify the function of target cells.

Both immature DC and mature DC release vesicles. It was originally postulated that lipopolysaccharide (LPS)-matured DC release 2-3 fold less vesicles than immature DC (5, 47). This suggestion was based on western blot detection of specific proteins and analysis of total protein content of vesicle populations. However, a recent study and our own unpublished data, in which high-resolution flow cytometry and NTA were used for quantification of vesicles, indicate that LPS-matured DC release approximate 2-fold more vesicles than non-activated DC (48). Importantly, we found that also during cognate DC - $CD4^+$ T cell interactions the release of DC-derived vesicles strongly increased,

demonstrating a link between vesicle production and productive T cell-DC interactions (4, 21).

Besides the number of released vesicles, also the molecular composition of the DC-derived vesicles differs depending on the activation status of the parental cell. Vesicles derived from mature DC were shown to contain higher levels of MHC class II, CD86, and ICAM-1, but lower levels of MFG-E8 compared to vesicles from immature DC (21, 47 and our own unpublished data). Vesicles derived from immature and mature DC also differ in their miRNA content (8). These data indicate that the release and cargo-composition of DC-derived vesicles are regulated, which allows a timely spread of tailor-made messengers for intercellular communication.

Vesicles derived from either immature or mature DC were shown to be efficiently targeted to other DC (49, 50) and to $CD4^+$ T cells (50, 51). However, the fate of the bound vesicles differs between these target cells. $CD4^+$ T cells capture DC-vesicles via high-affinity LFA-1 and retain the recruited DC-derived vesicles at their cell-surface for at least 24 hours (4, 50). This suggests that stable receptor-ligand interactions are formed between vesicle-associated membrane proteins and T cell plasma membrane proteins. In addition to vesicle binding, these receptor-ligand interactions may be involved in signaling towards T cells and modulation of their function. In contrast, DC-derived vesicles captured by DC rapidly fuse with the plasma membrane or are endocytosed by these cells (8). Upon fusion with either the plasma membrane or the endosomal membrane, luminal contents of the vesicles, e.g. miRNAs, can be released in the cytosol of DC and can modulate DC functions (8). Consequently, the functional outcome of cross-talk between DC-derived vesicles and their target cells not only depends on the molecular composition of the vesicles but also on the target cell type.

Immune-activating effects of DC-derived vesicles

Stimulation of $CD4^+$ T cells by DC-derived vesicles

The presence of MHC molecules and co-stimulatory molecules on DC-derived vesicles sparked the idea that these vesicles could have a function in T cell activation. Indeed, several *in vitro* and *in vivo* studies demonstrated the T cell activating potential of these vesicles. In general mature DC-derived vesicles are more potent *in vitro* in inducing T cell responses than vesicles derived from immature DC (52). Immature DC-derived vesicles could only activate $CD4^+$ T cell clones weakly (14, 53) and were not able to stimulate naive $CD4^+$ T cells *in vitro* (49). However, activation of naive $CD4^+$ T cells could be induced when immature DC-derived vesicles were recruited by bystander DC (49, 54). The presence of ICAM-1 on DC-vesicles was critical for the ability of these vesicles to induce $CD4^+$ T cell proliferation and might be required for the efficient recruitment of these vesicles to bystander DC (47). Activation of naive T cells was stronger when immature DC-derived vesicles were recruited on mature bystander DC versus immature bystander

DC (49, 54). DC-vesicles captured by MHCII-negative DC could also induce naive $CD4^+$ T cell proliferation, indicating the functional transfer of MHCII-peptide complexes to the surface of bystander DC (49) (**Fig. 2**). On the other hand, immature DC-vesicles captured by costimulation-deficient (CD80/CD86-deficient) bystander DC were unable to induce proliferation of naive $CD4^+$ T cells (49). This indicates that, besides MHCII complexes on the DC-vesicles, additional co-stimulatory molecules on the bystander DC were required to activate naive $CD4^+$ T cells (47, 49).

In vivo, mature DC-derived vesicles injected, into the footpath of mice, were shown to bind to $CD8\alpha^+$ DC present in the draining lymph node through LFA-1/ICAM-1 interactions. This allowed these $CD8\alpha^+$ DC to prime naive $CD4^+$ T cells *in vivo* (47, 55), leading to rapid rejection of male skin grafts in female mice in an antigen-specific fashion (47) (**Fig. 2**).

Vesicles released by DC can also induce humoral responses *in vivo*. Immunization of mice with vesicles from Diphtheria Toxoid (DT)-pulsed DC induced primary IgM and IgG anti-DT responses in naive mice (56). Vesicles derived from mature DT-pulsed DC showed an enhanced ability to induce primary IgG responses as compared to vesicles from immature DC (56). Likewise, immunization with vesicles derived from whole protein (ovalbumine)-pulsed mature DC were shown to elicit potent Th1 and B cell responses *in vivo* (53). Whether the DC-derived vesicles eliciting strong humoral responses *in vivo* via DC targeting and/or B cell targeting remains to be elucidated.

In conclusion, these findings demonstrate that both immature and mature DC-derived vesicles can activate $CD4^+$ T cells, but that the requirements with respect to the need for accessory DC differ. Furthermore, DC-derived vesicle-induced activation of antigen-experienced $CD4^+$ T cells is more easily achieved than priming of naive $CD4^+$ T cells.

Stimulation of $CD8^+$ T cells by DC-derived vesicles

Similar to $CD4^+$ T cell activation, vesicles derived from mature antigen-pulsed DC are more potent inducers of $CD8^+$ T cell activation than immature DC-derived vesicles. Indeed, vesicles from both immature and mature antigen-pulsed DC were able induce proliferation of antigen-experienced $CD8^+$ T cell clones *in vitro* (57). However, mature DC-derived vesicles induced a 2-fold higher proliferation of these $CD8^+$ T cell clones (57). Mature DC-derived vesicles loaded with viral peptides were also shown to induce IFN-γ production during recall responses of freshly isolated human $CD8^+$ T cells, whereas immature DC-derived vesicles were poor inducers of IFN-γ production (58). These studies indicate that antigen-experienced $CD8^+$ T cells can be directly activated by vesicles derived from antigen-pulsed DC without the requirement of bystander DC (**Fig. 2**). In contrast, priming of naive $CD8^+$ T cells by DC-derived vesicles requires recruitment of these vesicles onto bystander DCs (54). Both peptide-loaded immature and mature DC-derived vesicles could activate naive $CD8^+$ T cells upon transfer to bystander DC *in vitro*. *In vivo*, however,

only mature DC-derived vesicles were able to promote the differentiation of naive $CD8^+$ T cells into $CD8^+$ effector cells (54).

In early studies, Zitvogel *et al*. showed that tumor-antigen loaded DC-derived vesicles could promote anti-tumor $CD8^+$ T cell responses, which led to the rejection of established tumors in mice (59). Based on these results, clinical trials were initiated using vesicles derived from immature DC pulsed with tumor antigen (60). However, anti-tumor T cell responses were not efficiently induced with these immature DC-derived vesicle-based vaccines. With the novel insights regarding the potency of activated DC-derived vesicles, a phase II clinical trial is currently ongoing based on vesicles derived from IFN-γ activated DC, which have enhanced immuno-stimulatory properties (61).

Since DC-derived vesicles recruited by $CD4^+$ T cells remain at the cell surface for at least 24 hours (4, 50), the acquired MHC-peptide loaded complexes could be involved in antigen presentation to other T cells (4, 50). Indeed, it has been demonstrated that MHC-peptide complexes derived from vesicles released by OVA-protein pulsed DC can be presented *in vitro* by ConA-stimulated splenic $CD4^+$ T cells, thereby inducing OVA-specific $CD8^+$ T cell proliferation as potently as the peptide-pulsed DC themselves (51). Vaccination of these DC vesicle-decorated $CD4^+$ T cells led to an increase in the number of OVA-specific $CD8^+$ T cells in the spleen of mice. The magnitude of this response was again comparable to vaccination with OVA peptide-pulsed DC, while injection of the OVA-pulsed DC-derived vesicles alone induced only a slight increase in the number of OVA-specific $CD8^+$ T cells (51). It is however not clear whether the injected DC-derived vesicles were recruited to activated $CD4^+$ T cells *in vivo* and whether the decoration of $CD4^+$ T cells by DC-derived vesicles plays a physiological role in the stimulation of effector $CD8^+$ T cell responses *in vivo*.

Activation of NK cells through immature DC-derived vesicles

Natural killer (NK) cells have also been identified as targets for DC-derived vesicles (**Fig. 2**). Vesicles from immature DC can carry ligands for NKp30 and NKG2D, two activating receptors of the NK cell (62, 63). Upon incubation with immature DC-derived vesicles, NK cells were activated as was shown by the release of TNF-α and IFN-γ (62). This release was further increased in response to vesicles derived from heat shock-treated immature DC (62). *In vivo* administration of immature DC-derived vesicles induced proliferation of NK cells in mice, which was dependent on vesicle-associated IL-15Rα, and triggered NK cell-mediated cytotoxicity against tumor metastases in the lungs of mice (63). It has been postulated that the presence of IL-15Rα on the surface of human immature DC-derived vesicles can synergize the effect of soluble IL-15 on NK cell activation, possibly via 'trans-presentation' of IL-15 to NK cells.

Immune-suppressive effects of DC-derived vesicles

DC-derived vesicles, especially those released by immature DC, can also mediate immune-suppressive and/or tolerizing effects (**Fig. 2**). Although immature DC-derived vesicles can activate NK cells and induce minor levels of $CD4^+$ T cell proliferation, they are mainly thought to play a role in tolerance induction. The immune suppressive properties of immature DC-derived vesicles have primarily been investigated *in vivo*. It has been demonstrated that the administration of vesicles derived from immature DC either before or after allograft transplantation can induce tolerance and thereby prolong allograft survival (64, 65). The combined administration of an immune-suppressive drug (LF 15-0195) and donor DC-derived vesicles after transplantation significantly improved survival of cardiac allografts (64). Since LF can inhibit DC maturation *in vivo*, it has been proposed that donor vesicle-derived MHC complexes are presented by immature host DC, thereby inducing donor-specific tolerance (64). In another study, pre-treatment of rats with vesicles derived from immature donor DC prolonged survival of intestinal grafts (65). *Ex vivo* analysis of splenic T cells, derived from pre-treated allograft recipients, showed higher levels of IL-10, lower levels of IFN-γ and less proliferation in response to donor splenocytes as compared to allograft recipients that did not receive pre-treatment. Additionally, total Foxp3 levels were higher in spleen homogenates from allograft recipients pre-treated with donor DC-derived vesicles (65). Altogether these findings indicate that immature donor DC-derived vesicles could be exploited to induce donor-specific tolerance in allograft transplantation.

In an experimental sepsis model, administration of immature DC-derived vesicles improved the clearance of apoptotic cells and reduced the release of sepsis-related cytokines, thereby significantly reducing mortality (66). The enhanced phagocytosis was abrogated by the inhibition of MFG-E8 before vesicle administration (67). In this model, immature DC-derived vesicles might provide a source of MFG-E8, which is a crucial component for the uptake of apoptotic cells. This could also explain why mature DC-derived vesicles, which contain lower levels of MFG-E8 (21, 52, 66) did not show these beneficial effects (66).

In contrast to the strong immune suppressive potential of immature DC-derived vesicles in the allograft transplantation and sepsis models, these vesicles could poorly interfere in already established immune responses e.g. collagen-induced arthritis (68). This suggests that immature DC-derived vesicles contain tolerogenic properties, but that these can be overruled during strong immune activation. Thus, although immature DC-derived vesicles are interesting candidates to be used as therapeutic agents for the treatment of diseases that require dampening of immune responses, the molecular composition of these vesicles should be optimized in order to retain the suppressive capacity in a primed environment. Several investigators tried to modify the molecular composition of these vesicles in order to increase their immune suppressive properties. Robbins and coworkers

generated tolerizing DC by culturing them in the presence of recombinant IL-10 or by transducing them with vectors encoding IL-10, IL-4 or FasL (69, 70). Vesicles derived from these DC could reduce *in vitro* proliferation in Mixed Lymphocyte Reactions (69), as well as delayed-type hypersensitivity responses and collagen-induced arthritis *in vivo* (69). The potential of DC-derived vesicles to exert immune suppressive functions, like their parental cell, and the fact that they are much more stable in circulation, make them interesting therapeutic agents for the treatment of e.g. auto-immune diseases.

DC-derived vesicles as antigen-source

DC-derived vesicles can function as vehicles for the spreading of antigen. In many studies it is, however, unclear how antigen is transferred to target cells via these vesicles and whether the antigen is further processed by the target cell. A first possibility is the functional transfer of MHC-peptide complexes or intact antigen to the surface of the target cell. This mechanism was illustrated by the ability of MHCII-negative DC to stimulate $CD4^+$ T cell responses after recruitment of MHCII-bearing vesicles, so-called 'cross-dressing' (49). These vesicle-derived MHCII-peptide complexes can be presented at the target cell surface directly after vesicle binding, or after fusion of the vesicle with the plasma membrane. Vesicle-associated intact antigens exposed at the plasma membrane of the target cell can play a role in antigen presentation to B cells (53, 56). Indeed, intact OVA-protein on the surface of vesicles derived from mature DC pulsed with OVA-protein elicited production of OVA-specific IgG upon injection in mice, whereas vesicles directly loaded with OVA-peptides did not (53). However, vesicles derived from DC pulsed with complete diphtheria toxoid (DT) were also able to induce IgG responses, while no intact DT could be found in or on these vesicles (56). Hence the exact mechanism via which DC-derived vesicles transfer intact antigens and induce humoral responses remains to be elucidated. Alternatively, the transferred antigens can be processed by the target cell for antigen (cross-)presentation (71). It was, for example, shown that DC can process allogenic MHC-derived peptides transferred via vesicles, and present these allo-peptides via self-MHC (71). Altogether, these findings demonstrate that DC-derived vesicles have a physiological role in antigen spreading.

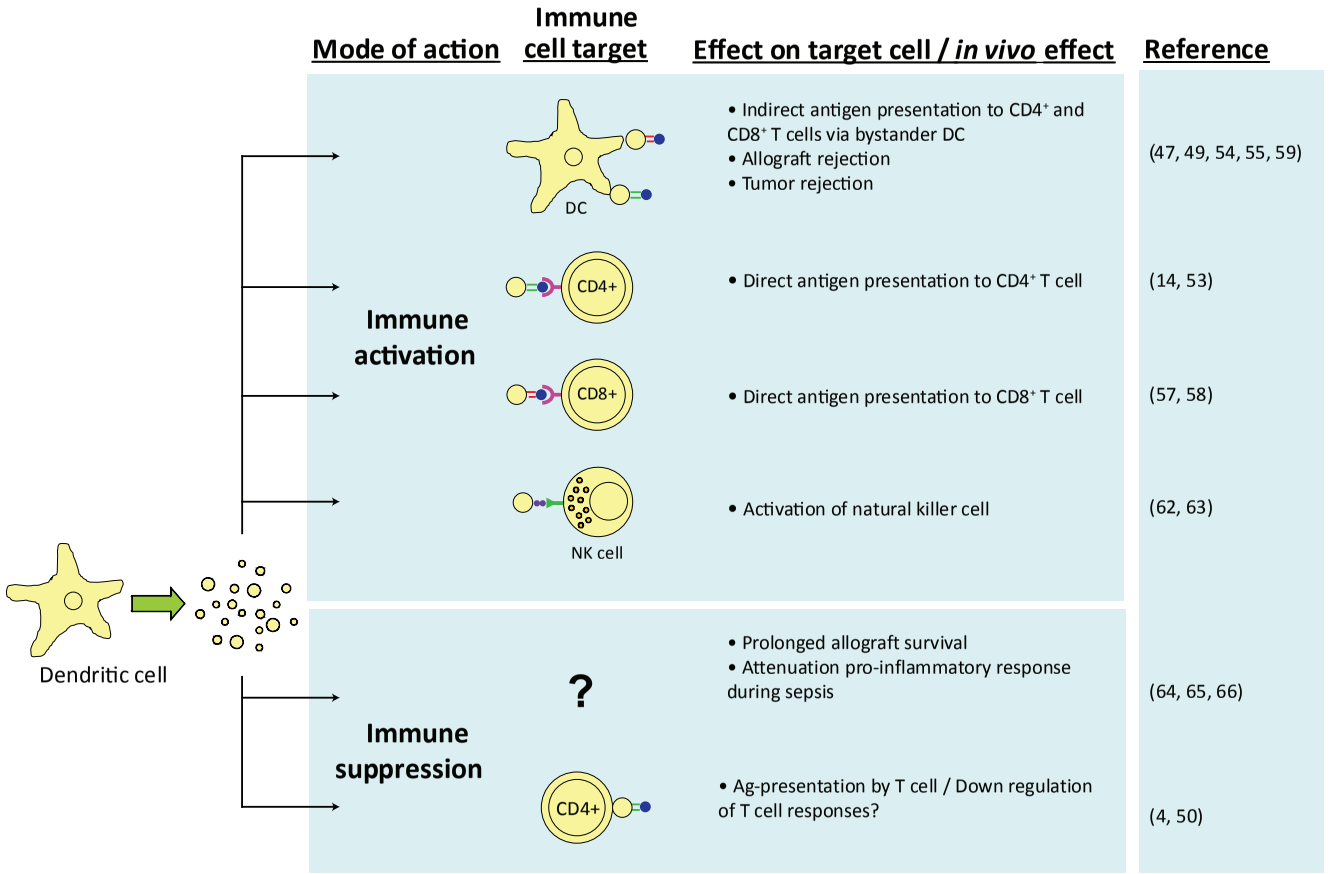

Figure 2 – Targets and pleiotropic effects of dendritic cell-derived vesicles This figure summarizes the main targets and effects of vesicles released by dendritic cells (DC) on immune cells both *in vitro* and *in vivo*.

DC- and CD4$^+$ T cell-derived vesicles for the balancing of immune responses

Intense crosstalk between DC and CD4$^+$ T cells takes place during cognate interaction. This ensures proper immune response to tackle infections and to prevent senescence and tumor-development. These responses have to be strictly regulated in order to prevent immunopathology, autoimmune diseases, and chronic inflammation. Immune stimulatory and immune suppressive events therefore need to be carefully balanced in ongoing immune responses. We propose that vesicles released by DC and T cells during cognate interaction participate in the balancing of immune responses (**Fig. 3**). During cognate interactions, DC release higher numbers of MHCII-containing vesicles (4, 21). These vesicles could amplify the antigen presenting capacity of the DC both by direct antigen presentation to T cells and indirect antigen presentation after recruitment on bystander DC (49, 53, 54, 57). Furthermore, the antigen presenting capacity could be prolonged, since DC-derived vesicles can remain at the surface of CD4$^+$ T cells after T cells and DC have dissociated. However, whether or not this antigen spreading will have an immune activating effect depends on both the maturation status of the parental DC and on the cell type and the activation or maturation status of the target cell. Besides the targeting to bystander DC, activated T cells can also efficiently bind DC-derived vesicles, thereby recruiting MHCII onto their surface (4, 50). This may allow for T cell-to-T cell antigen presentation, which might lead to down-regulation of immune responses (72, 73). However, the recruitment of DC-vesicles might also enable CD4$^+$ T cells to activate CD8$^+$ T cells responses (51). In addition to these active immune modulatory properties, the respective blocking of TCR and MHCII complexes by DC and T cell-derived vesicles could lead to suppression of immune responses (31, 33, 38). The passive blocking limits the number of available specific TCR and/or MHC peptide complexes on the surface of the CD4$^+$ T cell and DC, respectively. Finally, T cells can release vesicles carrying FasL, which can induce apoptosis of both DC and bystander T cells and possibly also of other immune cells (24, 25).

The studies discussed here clearly indicate that DC- and T cell-derived vesicles can play a major role in regulation of immune responses. The rapid expansion of this research field and the increasing interest in vesicle-mediated intercellular communication will catalyze progress in determining the physiological role and potential therapeutic applications of DC and T cell-derived vesicles,

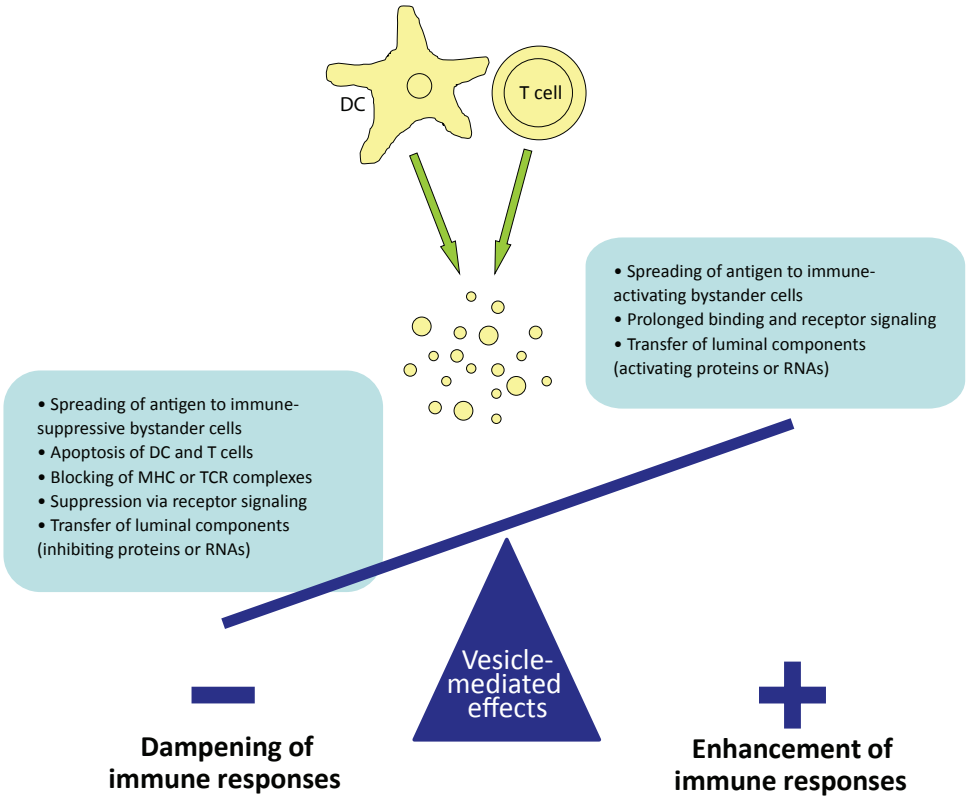

Figure 3 – DC- and CD4⁺ T cell-derived vesicles for balancing of immune responses Dendritic cells and CD4⁺ T cells release vesicles that can have both immune activating and/or immune suppressive effects. These vesicles contribute to the spreading of both activating and suppressive signals that are involved in the regulation of immune responses.

Table I – Characteristics of T cell-derived vesicles as described by different studies

Vesicle-producing T cell		T cell activation protocol	Vesicle isolation protocol	Vesicle size	Vesicle composition	Target cell	Effect on target cell	Reference
$CD4^+$	OVA-specific T cells generated by co-culture of naïve $CD4^+$ T cells from OTII mice with OVA-pulsed BMDC	Cognate interaction with OVA-pulsed DC 24 hours	300g (5 min) 1,200g (20 min) 10,000g (30 min) 100,000g (1h)	50-100 nm (based on EM)	CD4, TCR, LFA-1, CD25 and FasL (analyzed by conventional FC) Lamp-1, TCR and LFA-1, no calnexin (analyzed by WB)	OVA-pulsed BMDC	Inhibition of $CD4^+$ T cell proliferation *in vitro* Inhibition of CD4+ dependent CD8+ CTL responses (tumor killing and cytotoxicity assay *in vivo*)	33
	OTII, DO11.10 $CD4^+$ T cells and human peripheral $CD4^+$ T lymphocytes	Cognate interaction with OVA-peptide / SEB-pulsed DC 24 hours	1,500g (10 min) 4,000g (20 min) 100,000g (2.5h)	< 0.4 µm for $CD3^+$ vesicles (based on pore-size Transwell system)	CD2, CD3, CD27, OX40 (based on transfer to DC, analyzed by FC) CD28 was not transferred	Spleen- (for mouse) or monocyte- (for human) derived DC	Masking of MHCII complexes (by CD3-positive vesicles)	31
	Murine $CD4^+$ T cell clone KO4C1	Different levels of plate-bound anti-CD3 and anti-CD28 20 hours	200g (2x 10 min) 500g (2x 10 min) 10,000g (30 min) 100,000g (65 min) Sucrose density gradient (192,000g for < 15h)	50 -250 nm	3 distinct subpopulations could be identified based on light scattering and fluorescence of a general membrane dye (analyzed by high-resolution FC)	Not tested	Not tested	12
	Rat $CD4^+$ T cell clones A2b and Z1a	T cell-T cell Ag presentation 24 hours	300g (10 min) 1,200g (20 min) 0.22 µm filter 100,000g (1h)	50-200 nm (based on EM)	MHCII (analyzed by EM) TCR, IL-2Rα, MHCII, ICAM-1, CD80, CD86 (analyzed by conventional FC) Higher levels of IL-2Rα, MHCII and ICAM-1 on vesicles from anergic T cells	Spleen-derived B cells and DC	Responder T cells stimulated by APC exposed to vesicles derived from anergic T cells showed a diminished response to subsequent presentation of their specific antigen	37
	Jurkat T cells Human T cell blasts	anti-CD3 30 min – 24 hours	300g (6 min) 0.22 µm filter 100,000g (1h)	50-100 nm (based on EM)	CD3ε, CD2, MHCI. Upon activation (higher) levels of TCR, CD3ε, CXCR4, CD2, CD18, MHCI, MHCII and CD63. No FasL, CD28 or CD45 (analyzed by WB, bead-based FC)	Not tested	Not tested	6

$CD4^+$ *(continued)*	Jurkat T cells Human T cell blasts	PHA pulse (50 µg/ml) anti-CD59	800g (10 min) 10,000g (20 min) 100,000g (18h) or 100,000g (8h) alone	100-200 nm (based on EM)	FasL and APO2L (analyzed by WB, conventional FC and EM)	Non-activated Jurkat T cells	Apoptosis of non-activated Jurkat T cells	24, 25
	Jurkat E6.1 J-HM1-2.2 (Jurkat T cells expressing HM1R) Human T cell blasts	CCh (trigger HM1R) anti-CD3 PHA pulse (50 µg/ml) 10 hours	800g (10 min) 10,000g (20 min) 100,000g (12h)	Not tested	CD63, FasL, no CD45 or CD28 (analyzed by WB)	Other Jurkat T cells	Apoptosis of Jurkat T cells	26
	Jurkat T cells Human peripheral blood T lymphocytes	PMA (5 ng/ml) anti-CD3 / anti-CD28 coated Dynal beads 20 hours	800g (5 min) 4500g (5 min) 100kDa Centricon cut-off (4,000g, 10 min) or 20,000g or 100,000g (1h)	100-800 nm (based on EM)	Positive for annexinV-staining (analyzed by conventional FC) , LFA-1 (analyzed by WB)	Mast cells (LAD2 or human cord blood mast cells)	B-hexosaminidase release (degranulation). Release of IL-8 and OSM, ERK phosphorylation	29
	Jurkat E6-1 T cell Resting $CD4^+$ T lymphocytes from peripheral blood	PHA (20 µg/ml) 3 – 4 days	200g (10min) 0.22 µm filter 100,000g (1.5h)	50 nm (based on EM)	Positive for annexinV -staining (analyzed by IF) CD81, no CD45 (analyzed by WB)	Monocytes isolated from peripheral blood	Accumulation of cholesterol Release of TNFα	30
	T cell line HUT-78 Human peripheral blood T lymphocytes	PHA (1 µg/nl) PMA (5 ng/ml) 6 hours	800g (5 min) 7,000g (5 min) 20,000g (45 min)	100-800 nm (based on EM)	Positive for annexinV -staining (analyzed by conventional FC)	Monocytes isolated from peripheral blood	Release of pro-inflammatory cytokines TNFα, IL-1β and sIL1-Ra (also IL-6, IL-8, CCL3, CCL4 and CCL2)	27, 28
	Jurkat T cells	No activation	2,000g (5 min) 0.22 µm filter 10,000g (30 min) 70,000g (1h) Sucrose density gradient (270,000g for 16h)	100-300 nm (based on EM)	CD81, CD63, no CD45 (in sucrose gradient, analyzed by WB)	Not tested	Not tested	10

Table I (continued)

Vesicle-producing T cell		T cell activation protocol	Vesicle isolation protocol	Vesicle size	Vesicle composition	Target cell	Effect on target cell	Reference
$CD8^+$	CTL clone JS-132	Triggering vesicle release by interaction with target cell (within 10 minutes)	n.a.	40-70 nm (based on EM)	TCR, CD3, CD8 and MHCI (analyzed by EM)	Target cell of CTL	Not tested	36, 39
	OVA-specific T cells generated by co-culture of naïve $CD8^+$ T cells from OTI or OTI/Fas-ko mice	Cognate interaction with OVA-pulsed DC 24 hours	300g (5 min) 1,200g (20 min) 10,000g (30 min) 100,000g (1h)	50-90 nm (based on EM)	CD8, CD28, ICAM-1, TCR, LFA-1, FasL (analyzed by FC) TCR, LFA-1, ICAM-1, no calnexin (analyzed by WB)	OVA-pulsed BMDC	Blocking of MHCIp and induction of apoptosis by DC. Inhibition of both anti-tumor responses and autoimmunity *in vivo*.	38
	OVA-specific $CD8^+$ T cells	Addition of cognate peptide to naïve lymphocytes from OTI mouse 24 hours	300g (5 min) 1,200g (20 min) 10,000g (30 min) 100,000g (1h)	50-100 nm (based on EM)	FasL, CD8, TCR, CD9 (analyzed by FC) Hsp70, Tsg101 and FasL, no GRP94 (analyzed by WB)	Thymocytes, B16 and 3LL tumor cell lines	Upregulation of MMP9 and increase invasiveness of tumor cells *in vitro* and *in vivo*	34
	$CD8^+$ T cell line TG and primary $CD8^+$ T cells from HIV infected patients	anti-CD3	300g (10 min) 800g (30 min) 6,000g (30 min) 15,000g (30 min) or 60,000g (1h) 15,000g pellet used for sucrose gradient at 90,000g	30-100 nm (based on EM)	MHCII, CD9, CD63, CD81, CD3, no CD8 (captured on anti-MHCII beads, analyzed by FC)	TZM-bl cells (HeLa cells expressing CD4, CXCR4 and CCR5 and an additional reporter system) Expanded primary $CD4^+$ T cells	Inhibition of HIV replication in both acute and chronically infected $CD4^+$ T cells	32
$CD3^+$ ($CD4^+$ and $CD8^+$)	Human peripheral $CD3^+$ T lymphocytes	anti-CD28 and plate-bound anti-CD3 4 days	400g (10 min) 16,500g (30 min) 0.22 µm filter 120,000g (70 min)	54nm (based on Zetasizer Nano ZS and DLS)	Not tested	Non-stimulated human peripheral CD3+ T lymphocytes	Induction of $CD8^+$ T cell proliferation and release of MIP1β (CCL5)	35

APC, antigen presenting cell; BMDC, bone marrow-derived DC; CTL, cytotoxic T lymphocyte; DC, dendritic cells; DLS, dynamic light scattering; EM, electron microscopy; FC, flow cytometry; HIV, human immunodeficiency virus; HM1R, human muscarinic type 1 receptor; IF, immune fluorescence microscopy; OVA, ovalbumin; PHA, phyto-hemagglutinin; PMA, phorbol myristate acetate; SEB, staphylococcal enterotoxin B; WB, western blotting

References

1. Thery C, Ostrowski M, Segura E. Membrane vesicles as conveyors of immune responses. Nature reviews. 2009 Aug;9(8):581-93.
2. Cocucci E, Racchetti G, Meldolesi J. Shedding microvesicles: Artefacts no more. Trends in cell biology. 2009 Feb;19(2):43-51.
3. Simons M, Raposo G. Exosomes--vesicular carriers for intercellular communication. Curr Opin Cell Biol. 2009 Aug;21(4):575-81.
4. Buschow SI, Nolte-'t Hoen EN, van Niel G, Pols MS, ten Broeke T, Lauwen M, et al. MHC II in dendritic cells is targeted to lysosomes or T cell-induced exosomes via distinct multivesicular body pathways. Traffic. 2009 Oct;10(10):1528-42.
5. Thery C, Regnault A, Garin J, Wolfers J, Zitvogel L, Ricciardi-Castagnoli P, et al. Molecular characterization of dendritic cell-derived exosomes. selective accumulation of the heat shock protein hsc73. J Cell Biol. 1999 Nov 1;147(3):599-610.
6. Blanchard N, Lankar D, Faure F, Regnault A, Dumont C, Raposo G, et al. TCR activation of human T cells induces the production of exosomes bearing the TCR/CD3/zeta complex. J Immunol. 2002 Apr 1;168(7):3235-41.
7. Mittelbrunn M, Gutierrez-Vazquez C, Villarroya-Beltri C, Gonzalez S, Sanchez-Cabo F, Gonzalez MA, et al. Unidirectional transfer of microRNA-loaded exosomes from T cells to antigen-presenting cells. Nat Commun. 2011;2:282.
8. Montecalvo A, Larregina AT, Shufesky WJ, Stolz DB, Sullivan ML, Karlsson JM, et al. Mechanism of transfer of functional microRNAs between mouse dendritic cells via exosomes. Blood. 2012 Jan 19;119(3):756-66.
9. Sadallah S, Eken C, Schifferli JA. Ectosomes as immunomodulators. Semin Immunopathol. 2011 Sep;33(5):487-95.
10. Booth AM, Fang Y, Fallon JK, Yang JM, Hildreth JE, Gould SJ. Exosomes and HIV gag bud from endosome-like domains of the T cell plasma membrane. J Cell Biol. 2006 Mar 13;172(6):923-35.
11. de Gassart A, Geminard C, Fevrier B, Raposo G, Vidal M. Lipid raft-associated protein sorting in exosomes. Blood. 2003 Dec 15;102(13):4336-44.
12. van der Vlist EJ, Arkesteijn GJA, van de Lest CHA, Stoorvogel W, Nolte - 't Hoen,Esther N.M., Wauben MHM. $CD4^+$ T cell activation promotes the differential release of distinct populations of nanosized vesicles. Journal of Extracellular Vesicles. 2012;1(1):18364.
13. Bobrie A, Colombo M, Krumeich S, Raposo G, Théry C. Diverse subpopulations of vesicles secreted by different intracellular mechanisms are present in exosome preparations obtained by differential ultracentrifugation. Journal of Extracellular Vesicles. 2012;1(1):18397.
14. Raposo G, Nijman HW, Stoorvogel W, Liejendekker R, Harding CV, Melief CJ, et al. B lymphocytes secrete antigen-presenting vesicles. J Exp Med. 1996 Mar 1;183(3):1161-72.
15. Subra C, Grand D, Laulagnier K, Stella A, Lambeau G, Paillasse M, et al. Exosomes account for vesicle-mediated transcellular transport of activatable phospholipases and prostaglandins. J Lipid Res. 2010 Aug;51(8):2105-20.
16. Valadi H, Ekstrom K, Bossios A, Sjostrand M, Lee JJ, Lotvall JO. Exosome-mediated transfer of mRNAs and microRNAs is a novel mechanism of genetic exchange between cells. Nat Cell Biol. 2007 Jun;9(6):654-9.
17. Gyorgy B, Modos K, Pallinger E, Paloczi K, Pasztoi M, Misjak P, et al. Detection and isolation of cell-derived microparticles are compromised by protein complexes resulting from shared biophysical parameters. Blood. 2011 Jan 27;117(4):e39-48.
18. Yuana Y, Oosterkamp TH, Bahatyrova S, Ashcroft B, Garcia Rodriguez P, Bertina RM, et al. Atomic force microscopy: A novel approach to the detection of nanosized blood microparticles. J Thromb Haemost. 2010 Feb;8(2):315-23.

19. Dragovic RA, Gardiner C, Brooks AS, Tannetta DS, Ferguson DJ, Hole P, et al. Sizing and phenotyping of cellular vesicles using nanoparticle tracking analysis. Nanomedicine. 2011 May 4;7(6):780-8.
20. Lacroix R, Robert S, Poncelet P, Dignat-George F. Overcoming limitations of microparticle measurement by flow cytometry. Semin Thromb Hemost. 2010 Nov;36(8):807-18.
21. Nolte-'t Hoen EN, van der Vlist EJ, Aalberts M, Mertens HC, Jan Bosch B, Bartelink W, et al. Quantitative and qualitative flow cytometric analysis of nano-sized cell-derived membrane vesicles. Nanomedicine. 2011 Jul Oct 21;8(5):712-20.
22. van der Vlist EJ, Nolte - 't Hoen,Esther N.M., Stoorvogel W, Arkesteijn GJA, Wauben MHM. Fluorescent labeling of nano-sized vesicles released by cells and subsequent quantitative and qualitative analysis by high resolution flow cytometry. Nature Protocols. 2012 Jun;7(7):1311-26.
23. Sallusto F, Lanzavecchia A. Heterogeneity of CD4+ memory T cells: Functional modules for tailored immunity. Eur J Immunol. 2009 Aug;39(8):2076-82.
24. Martinez-Lorenzo MJ, Anel A, Gamen S, Monle nI, Lasierra P, Larrad L, et al. Activated human T cells release bioactive fas ligand and APO2 ligand in microvesicles. J Immunol. 1999 Aug 1;163(3):1274-81.
25. Monleon I, Martinez-Lorenzo MJ, Monteagudo L, Lasierra P, Taules M, Iturralde M, et al. Differential secretion of fas ligand- or APO2 ligand/TNF-related apoptosis-inducing ligand-carrying microvesicles during activation-induced death of human T cells. J Immunol. 2001 Dec 15;167(12):6736-44.
26. Alonso R, Rodriguez MC, Pindado J, Merino E, Merida I, Izquierdo M. Diacylglycerol kinase alpha regulates the secretion of lethal exosomes bearing fas ligand during activation-induced cell death of T lymphocytes. J Biol Chem. 2005 Aug 5;280(31):28439-50.
27. Carpintero R, Gruaz L, Brandt KJ, Scanu A, Faille D, Combes V, et al. HDL interfere with the binding of T cell microparticles to human monocytes to inhibit pro-inflammatory cytokine production. PLoS One. 2010 Jul 29;5(7):e11869.
28. Scanu A, Molnarfi N, Brandt KJ, Gruaz L, Dayer JM, Burger D. Stimulated T cells generate microparticles, which mimic cellular contact activation of human monocytes: Differential regulation of pro- and anti-inflammatory cytokine production by high-density lipoproteins. J Leukoc Biol. 2008 Apr;83(4):921-7.
29. Shefler I, Salamon P, Reshef T, Mor A, Mekori YA. T cell-induced mast cell activation: A role for microparticles released from activated T cells. J Immunol. 2010 Oct 1;185(7):4206-12.
30. Zakharova L, Svetlova M, Fomina AF. T cell exosomes induce cholesterol accumulation in human monocytes via phosphatidylserine receptor. J Cell Physiol. 2007 Jul;212(1):174-81.
31. Busch A, Quast T, Keller S, Kolanus W, Knolle P, Altevogt P, et al. Transfer of T cell surface molecules to dendritic cells upon CD4+ T cell priming involves two distinct mechanisms. J Immunol. 2008 Sep 15;181(6):3965-73.
32. Tumne A, Prasad VS, Chen Y, Stolz DB, Saha K, Ratner DM, et al. Noncytotoxic suppression of human immunodeficiency virus type 1 transcription by exosomes secreted from CD8+ T cells. Journal of virology. 2009 May;83(9):4354-64.
33. Zhang H, Xie Y, Li W, Chibbar R, Xiong S, Xiang J. CD4(+) T cell-released exosomes inhibit CD8(+) cytotoxic T-lymphocyte responses and antitumor immunity. Cell Mol Immunol. 2011 Jan;8(1):23-30.
34. Cai Z, Yang F, Yu L, Yu Z, Jiang L, Wang Q, et al. Activated T cell exosomes promote tumor invasion via fas signaling pathway. J Immunol. 2012 Jun 15;188(12):5954-61.
35. Wahlgren J, Karlson Tde L, Glader P, Telemo E, Valadi H. Activated human T cells secrete exosomes that participate in IL-2 mediated immune response signaling. PLoS One. 2012;7(11):e49723.
36. Peters PJ, Geuze HJ, Van der Donk HA, Slot JW, Griffith JM, Stam NJ, et al. Molecules relevant for T cell-target cell interaction are present in cytolytic granules of human T lymphocytes. Eur J Immunol. 1989 Aug;19(8):1469-75.
37. Nolte-'t Hoen EN, Wagenaar-Hilbers JP, Peters PJ, Gadella BM, van Eden W, Wauben MH. Uptake of membrane molecules from T cells endows antigen-presenting cells with novel functional properties. European journal of immunology. 2004 Nov;34(11):3115-25.

38. Xie Y, Zhang H, Li W, Deng Y, Munegowda MA, Chibbar R, et al. Dendritic cells recruit T cell exosomes via exosomal LFA-1 leading to inhibition of CD8+ CTL responses through downregulation of peptide/MHC class I and fas ligand-mediated cytotoxicity. J Immunol. 2010 Nov 1;185(9):5268-78.
39. Peters PJ, Borst J, Oorschot V, Fukuda M, Krahenbuhl O, Tschopp J, et al. Cytotoxic T lymphocyte granules are secretory lysosomes, containing both perforin and granzymes. J Exp Med. 1991 May 1;173(5):1099-109.
40. Peters PJ, Geuze HJ, van der Donk HA, Borst J. A new model for lethal hit delivery by cytotoxic T lymphocytes. Immunol Today. 1990 Jan;11(1):28-32.
41. Zuccato E, Blott EJ, Holt O, Sigismund S, Shaw M, Bossi G, et al. Sorting of fas ligand to secretory lysosomes is regulated by mono-ubiquitylation and phosphorylation. J Cell Sci. 2007 Jan 1;120(Pt 1):191-9.
42. Suda T, Okazaki T, Naito Y, Yokota T, Arai N, Ozaki S, et al. Expression of the fas ligand in cells of T cell lineage. J Immunol. 1995 Apr 15;154(8):3806-13.
43. Mariani SM, Matiba B, Baumler C, Krammer PH. Regulation of cell surface APO-1/fas (CD95) ligand expression by metalloproteases. Eur J Immunol. 1995 Aug;25(8):2303-7.
44. Reis e Sousa C. Dendritic cells in a mature age. Nat Rev Immunol. 2006 Jun;6(6):476-83.
45. Guermonprez P, Valladeau J, Zitvogel L, Thery C, Amigorena S. Antigen presentation and T cell stimulation by dendritic cells. Annu Rev Immunol. 2002;20:621-67.
46. Viaud S, Thery C, Ploix S, Tursz T, Lapierre V, Lantz O, et al. Dendritic cell-derived exosomes for cancer immunotherapy: What's next? Cancer Res. 2010 Feb 15;70(4):1281-5.
47. Segura E, Nicco C, Lombard B, Veron P, Raposo G, Batteux F, et al. ICAM-1 on exosomes from mature dendritic cells is critical for efficient naive T-cell priming. Blood. 2005 Jul 1;106(1):216-23.
48. Soo CY, Song Y, Zheng Y, Campbell EC, Riches AC, Gunn-Moore F, et al. Nanoparticle tracking analysis monitors microvesicle and exosome secretion from immune cells. Immunology. 2012 Jun Feb 20;136(2):192-7.
49. Thery C, Duban L, Segura E, Veron P, Lantz O, Amigorena S. Indirect activation of naive CD4+ T cells by dendritic cell-derived exosomes. Nat Immunol. 2002 Dec;3(12):1156-62.
50. Nolte-'t Hoen EN, Buschow SI, Anderton SM, Stoorvogel W, Wauben MH. Activated T cells recruit exosomes secreted by dendritic cells via LFA-1. Blood. 2009 Feb 26;113(9):1977-81.
51. Hao S, Yuan J, Xiang J. Nonspecific CD4(+) T cells with uptake of antigen-specific dendritic cell-released exosomes stimulate antigen-specific CD8(+) CTL responses and long-term T cell memory. J Leukoc Biol. 2007 Oct;82(4):829-38.
52. Segura E, Amigorena S, Thery C. Mature dendritic cells secrete exosomes with strong ability to induce antigen-specific effector immune responses. Blood Cells Mol Dis. 2005 Sep-Oct;35(2):89-93.
53. Qazi KR, Gehrmann U, Domange Jordo E, Karlsson MC, Gabrielsson S. Antigen-loaded exosomes alone induce Th1-type memory through a B-cell-dependent mechanism. Blood. 2009 Mar 19;113(12):2673-83.
54. Andre F, Chaput N, Schartz NE, Flament C, Aubert N, Bernard J, et al. Exosomes as potent cell-free peptide-based vaccine. I. dendritic cell-derived exosomes transfer functional MHC class I/peptide complexes to dendritic cells. J Immunol. 2004 Feb 15;172(4):2126-36.
55. Segura E, Guerin C, Hogg N, Amigorena S, Thery C. CD8+ dendritic cells use LFA-1 to capture MHC-peptide complexes from exosomes in vivo. J Immunol. 2007 Aug 1;179(3):1489-96.
56. Colino J, Snapper CM. Exosomes from bone marrow dendritic cells pulsed with diphtheria toxoid preferentially induce type 1 antigen-specific IgG responses in naive recipients in the absence of free antigen. J Immunol. 2006 Sep 15;177(6):3757-62.
57. Utsugi-Kobukai S, Fujimaki H, Hotta C, Nakazawa M, Minami M. MHC class I-mediated exogenous antigen presentation by exosomes secreted from immature and mature bone marrow derived dendritic cells. Immunol Lett. 2003 Oct 31;89(2-3):125-31.
58. Admyre C, Johansson SM, Paulie S, Gabrielsson S. Direct exosome stimulation of peripheral human T cells detected by ELISPOT. Eur J Immunol. 2006 Jul;36(7):1772-81.

59. Zitvogel L, Regnault A, Lozier A, Wolfers J, Flament C, Tenza D, et al. Eradication of established murine tumors using a novel cell-free vaccine: Dendritic cell-derived exosomes. Nat Med. 1998 May;4(5):594-600.
60. Escudier B, Dorval T, Chaput N, Andre F, Caby MP, Novault S, et al. Vaccination of metastatic melanoma patients with autologous dendritic cell (DC) derived-exosomes: Results of thefirst phase I clinical trial. J Transl Med. 2005 Mar 2;3(1):10.
61. Chaput N, Thery C. Exosomes: Immune properties and potential clinical implementations. Semin Immunopathol. 2011 Sep;33(5):419-40.
62. Simhadri VR, Reiners KS, Hansen HP, Topolar D, Simhadri VL, Nohroudi K, et al. Dendritic cells release HLA-B-associated transcript-3 positive exosomes to regulate natural killer function. PLoS One. 2008;3(10):e3377.
63. Viaud S, Terme M, Flament C, Taieb J, Andre F, Novault S, et al. Dendritic cell-derived exosomes promote natural killer cell activation and proliferation: A role for NKG2D ligands and IL-15Ralpha. PLoS One. 2009;4(3):e4942.
64. Peche H, Renaudin K, Beriou G, Merieau E, Amigorena S, Cuturi MC. Induction of tolerance by exosomes and short-term immunosuppression in a fully MHC-mismatched rat cardiac allograft model. Am J Transplant. 2006 Jul;6(7):1541-50.
65. Yang X, Meng S, Jiang H, Zhu C, Wu W. Exosomes derived from immature bone marrow dendritic cells induce tolerogenicity of intestinal transplantation in rats. J Surg Res. 2011 Dec;171(2):826-32.
66. Miksa M, Wu R, Dong W, Komura H, Amin D, Ji Y, et al. Immature dendritic cell-derived exosomes rescue septic animals via milk fat globule epidermal growth factor-factor VIII [corrected. J Immunol. 2009 Nov 1;183(9):5983-90.
67. Miksa M, Wu R, Dong W, Das P, Yang D, Wang P. Dendritic cell-derived exosomes containing milk fat globule epidermal growth factor-factor VIII attenuate proinflammatory responses in sepsis. Shock. 2006 Jun;25(6):586-93.
68. Kim SH, Bianco N, Menon R, Lechman ER, Shufesky WJ, Morelli AE, et al. Exosomes derived from genetically modified DC expressing FasL are anti-inflammatory and immunosuppressive. Mol Ther. 2006 Feb;13(2):289-300.
69. Kim SH, Lechman ER, Bianco N, Menon R, Keravala A, Nash J, et al. Exosomes derived from IL-10-treated dendritic cells can suppress inflammation and collagen-induced arthritis. J Immunol. 2005 May 15;174(10):6440-8.
70. Ruffner MA, Kim SH, Bianco NR, Francisco LM, Sharpe AH, Robbins PD. B7-1/2, but not PD-L1/2 molecules, are required on IL-10-treated tolerogenic DC and DC-derived exosomes for in vivo function. Eur J Immunol. 2009 Nov;39(11):3084-90.
71. Morelli AE, Larregina AT, Shufesky WJ, Sullivan ML, Stolz DB, Papworth GD, et al. Endocytosis, intracellular sorting, and processing of exosomes by dendritic cells. Blood. 2004 Nov 15;104(10):3257-66.
72. Helft J, Jacquet A, Joncker NT, Grandjean I, Dorothee G, Kissenpfennig A, et al. Antigen-specific T-T interactions regulate CD4 T-cell expansion. Blood. 2008 Aug 15;112(4):1249-58.
73. Taams LS, van Rensen AJ, Poelen MC, van Els CA, Besseling AC, Wagenaar JP, et al. Anergic T cells actively suppress T cell responses via the antigen-presenting cell. Eur J Immunol. 1998 Sep;28(9):2902-12.

Effective inquiry often proceeds by a series of increasingly intelligent mistakes
– R.E. Young, A.L. Becker and K.L. Pike

Chapter 2

Quantitative and qualitative flow cytometric analysis of nanosized cell-derived membrane vesicles

Esther N.M. Nolte-'t Hoen, Els J. van der Vlist, Marian Aalberts, Hendrik C.H. Mertens, Berend Jan Bosch, Willem Bartelink, Enrico Mastrobattista, Ethlinn V.B. van Gaal, Willem Stoorvogel, Ger J.A. Arkesteijn and Marca M.H. Wauben

Nanomedicine. 2012 Jul;8(5):712-20

Abstract

Nanosized cell-derived membrane vesicles are increasingly recognized as therapeutic vehicles and high-potential biomarkers for several diseases. Currently available methods allow bulk analysis of vesicles but are not suited for accurate quantification and fail to reveal phenotypic heterogeneity in membrane vesicle populations. For such analyses, single vesicle-based, multiparameter, high-throughput methods are needed. We developed a fluorescence-based, high-resolution flow cytometric method for quantitative and qualitative analysis of nanosized membrane vesicles. Proof of principle was obtained by single-particle analysis of virions and liposomes. Further validation was obtained by quantification of cell-derived nanosized membrane vesicles from cell cultures and body fluids. An important aspect was that the technology was extended to detect specific proteins on individual vesicles. This allowed identification of exosome subsets and phenotyping of individual exosomes produced by dendritic cells (DCs) undergoing different modes of activation. The described technology allows quantitative, multiparameter, and high-throughput analysis of a wide variety of nanosized particles and has broad applications

Introduction

Cells release membrane vesicles with specific lipid, protein, and RNA contents (1, 2). Regulated secretion of membrane vesicles and recruitment by target cells have been hypothesized to play a role in many pathophysiological processes (2-14). Cell-derived membrane vesicles are either shed from the plasma membrane (microparticles/ microvesicles, 50–1000 nm) or exocytosed by fusion of multivesicular endosomes with the plasma membrane (exosomes, 50–100 nm) (1, 2). The heterogeneity of cell-derived membrane vesicles in body fluids reflects the plethora of cellular origins. The abundance of a specific vesicle type may reflect the health or disease status of the tissue of origin, making these vesicles good candidates for biomarkers for noninvasive detection and monitoring of several diseases (7, 11, 15, 16). Furthermore, exosomes derived from dendritic cells (DCs) or tumor cells have been applied as "cell-free vaccines" in experimental tumor models and clinical trials in cancer patients (8, 17). Conversely, application of tumor exosomes can also result in accelerated tumor growth (18). Both for the development of the biomarker field and for the safe clinical application of membrane vesicles, high-resolution analysis methods are needed for vesicle characterization and/or quality control. Proteomics, western-blotting, and lipidomics have been applied to characterize bulk isolates of membrane vesicles. However, a standardized, multiparameter, high-throughput method is required to analyze individual membrane vesicles and heterogeneity in membrane-vesicle populations. Microscopic analysis revealed that the vast majority of membrane vesicles present in cell culture supernatants or body fluids are significantly smaller than 300 nm (3, 19, 20). Although vesicles as small as 50–100 nm can be accurately visualized and characterized using specific imaging techniques (19-22), these techniques preclude analysis of the large numbers of vesicles needed to study their quantity and heterogeneity (3, 19). Flow cytometry on the other hand is an ideal technique to simultaneously quantify and qualify high numbers of cells and vesicles with a diameter > 300 nm (23-25). However, this method falls short for the analysis of smaller membrane vesicles (< 300 nm) (26, 27). We here describe a novel high-resolution flow cytometry-based method for fluorescence-based detection of single nanosized particles that can be used for both standardized quantification and multiparameter characterization.

Materials and Methods

Cell culture

Bone-marrow-derived DCs were generated from C57BL/6 mice as described (28) with minor modifications. Bone marrow cells were maintained in Iscove's Modified Dulbecco's medium lacking L-glutamine (BioWhittaker, Frederick, Maryland) supplemented with 2 mM Ultraglutamine (BioWhittaker), 10% heat inactivated fetal calf serum (FCS, Sigma-Aldrich, St. Louis, Missouri), 100 IU/mL penicillin and 100 mg/mL streptomycin (Life Technologies, Bleiswijk, The Netherlands), 50 µM β-mercaptoethanol and 30% conditioned medium from GM-CSF producing NIH 3T3 cells (R1). At days 3, 6, and 8, medium was added or replaced. On day 9, nonadherent cells were collected and plated in new dishes with fresh medium. Cells were activated with 10 µg/mL LPS on day 13. Semi-adherent and nonadherent cells were harvested on day 14 and replated for exosome production in medium containing overnight ultracentrifuged (100,000g) FCS and conditioned R1 medium to deplete bovine and R1 cell exosomes. The p53-specific $CD4^+$ T-cell clone, generated in a C57BL/6 $p53^{-/-}$ mouse (29) and provided by Prof. C. Melief (Leiden University Medical Center, Leiden, The Netherlands), was cultured as described previously (30). When indicated, DCs were preloaded with 2.5 µM p53 peptide (amino acid 77–96) simultaneous with LPS activation, mixed in a 1:1 ratio with T cells on day 14, and co-cultured for 20 hours. All cultures were maintained at 37°C, 5% CO2. Experiments were approved by the Institutional Ethical Animal Committee at Utrecht University (Utrecht, The Netherlands).

Exosome isolation and labeling

Exosomes were collected from culture supernatants of 3×10^6 DC, 3×10^6 T cells or 3×10^6 DCs co-cultured with 3×10^6 T cells by differential centrifugation as described (3). As a negative control, culture medium that had not been in contact with cells was used. Exosomes were pelleted by ultracentrifugation at 100,000g for 65 minutes in a SW40 rotor (Beckman Coulter Inc., Fullerton, California). Freshly isolated exosomes were resuspended in 20 µl PBS containing 0.2% BSA from a stock solution cleared from aggregates by ultracentrifugation and fluorescently labeled with 7.5 µM PKH67 (Sigma-Aldrich) in an end volume of 200 µl, following the manufacturer's recommendations. For antibody staining, exosomes resuspended in 20 µl PBS/0.2% BSA were incubated with 0.5 µg R-PE-labeled or APC-labeled anti-mouse MHC class II antibody (clone M5/114, eBioscience, San Diego, California), 0.5 µg B-PE-labeled anti-mouse MFG-E8 antibody (clone 2422, MBL, labeled according protocol with B-Phycoerythrin [B-PE] conjugation kit [Innova Biosciences, Cambridge, United Kingdom]) or with similarly labeled isotype controls for 45 minutes at room temperature (18–24°C), after which PKH67 labeling was performed. Exosomes were mixed with 2.5 M sucrose, overlaid with a linear sucrose gradient (2.0–0.4 M sucrose in PBS) and floated into the gradient by centrifugation in a

SW40 tube (Beckman) for 16 hours at 192,000g. Gradient fractions were collected from the bottom of the tube, diluted 20-fold with PBS and measured on the flow cytometer. Fraction densities were determined by refractometry.

Flow cytometric analysis of nanosized particles

The BD Influx flow cytometer (Becton Dickinson, Brussels, Belgium) was triggered on the fluorescence signal derived from the fluorescently labeled particles and thresholding was applied on this fluorescence channel. Fluorescence thresholding was based on measuring 0.22 μm filtered PBS, allowing an event rate of ≤ 6 events per second. Light scattering detection was performed in log mode. All relevant BD Influx features and settings are listed in **Supplementary Table S1** and full details of experimental procedures are described in Supplementary Methods.

When indicated for quantification, serial twofold dilutions of 100-nm fluorescent beads in an input concentration range of 1.64×10^6 to 3.2×10^3 beads per mL (stock solutions specified by the manufacturer) were mixed with a fixed number (3.8×10^5) of 200-nm fluorescent beads. After measurement (30 seconds), the ratio of 100- and 200-nm beads was calculated. Alternatively, the quantity of particles detected in a fixed timeframe of 30 seconds was determined. The numbers of detected particles in this timeframe were plotted against the dilution factor. Linear regression analysis was performed using Prism (version 3.0, GraphPad Software). The intersample variation was determined by preparing seven individual tubes with identical bead dilutions, after which the mean ± standard deviation (SD) of the number of beads detected in 30 seconds was calculated. The intrasample variation was determined by repeated measurements of the same bead dilution with 30-second time intervals. Between measurements the sample was not removed from the cytometer to prevent volume changes due to fluid back-flush. PE-labeled antibodies were measured by excitation with the 561-nm laser and using a 585/42 band pass filter.

Virus labeling and purification

LR7 cells were maintained as monolayer cultures in Dulbecco modified Eagle medium (DMEM) (BioWhittaker) supplemented with 10% FCS (Bodinco, Alkmaar, The Netherlands), 100 IU of penicillin/mL, and 100 μg of streptomycin/mL (Life Technologies). LR7 cells were inoculated with MHV (strain A59) in Opti-MEM (Invitrogen, Carlsbad, California). At t = 2 hours, 5 μM HR2 peptide was added to prevent syncytia formation.31 At t = 7 hours, cells were fluorescently labeled with 5 μM carboxy-fluorescein succinimidyl ester (CFSE, Invitrogen), according to the manufacturer's recommendations, and incubated for another 2 hours in Opti-MEM containing 10% FCS and 5 μM HR2 peptide. At t = 9 hours, culture medium was harvested and centrifuged for 10 minutes at 1200 rpm and for 15 minutes at 10,000g at 4°C to remove cellular debris. Virions were sedimented through a 20% sucrose

cushion (wt/wt) in TN buffer [10 mM Tris pH 7.4, 100 mM NaCl] by ultra-centrifugation at 100,000g for 1.5 hours at 4°C in a Beckman SW40 rotor. Pelleted MHV virions were resuspended in TN buffer and floated by centrifugation to equilibrium density into a 2.0- to 0.4-M sucrose gradient by ultracentrifugation at 100,000g. Different sucrose fractions were collected, diluted 1/10 and analyzed by flow cytometry-based measurements. The infectivity was checked by using the median tissue culture infective dose ($TCID_{50}$) end-point dilution assay. This assay confirmed that the majority of virus, as detected by flow cytometry-based analysis, was present in the 1.14 g/mL gradient fraction. Virion size was 100 ± 30 nm, as measured by NTA, which is in accordance with previous measurements (32).

Liposome preparation

Liposomes were prepared using the lipid film hydration method. Briefly, EPC-35, EPG and cholesterol (molar ratio 2:0.06:1) were dissolved in chloroform:methanol (1:1, v/v) in a round-bottom flask. After evaporation of the solvent under reduced pressure using a rotary evaporator, the lipid film was hydrated with HEPES buffered saline (HBS; 10 mM HEPES, 137 mM NaCl, 1mM EDTA, pH 7.4). For calcein-labeled liposomes, lipid films were hydrated with 0.25 mM calceine in HBS. Differently sized liposomes were prepared by 10 extrusions through 100- or 400-nm polycarbonate membranes (Nuclepore, Whatman, Clifton, New Jersey) using a Lipex high-pressure extruder (Northern Lipids, Vancouver, Canada). Sized liposomes were dialyzed in 10,000 MWCO Slide-A-Lyzer Dialysis Cassettes (Thermo Scientific, Bremen, Germany) against HBS for at least 3 days with regular exchange of HBS. Liposome sizes were 95 ± 26 nm or 123 ± 45 nm, as measured by Nanoparticle Tracking Analysis (NTA).

NTA

For nanoparticle (NP) size determination, the Brownian motion of the particles was followed using the NanoSight LM10SH (NanoSight, Amesbury, United Kingdom), equipped with a 532-nm laser. Samples were introduced into the sample chamber and measured for 120 or 150 seconds at 20°C with manual shutter and gain adjustments. The data were captured and analyzed using NTA 2.0 Build 0252 software (NanoSight). Indicated sizes and SDs are averages of at least three individual measurements. At least 2000 tracks of individually traced particles were detected in total.

Isolation and labeling of vesicles from seminal fluid

Human semen was obtained after informed consent from vasectomized men following a postoperative period of > 3 months. Residual cells were removed by centrifugation at 3,000g for 10 minutes. Supernatants were pooled from 5–7 donors per batch, diluted 1:1 in PBS and cleared of large particles by centrifuging twice at 10,000g for 20 minutes.

Remaining small membrane vesicles were pelleted at 100,000g for 1 hour in an SW28 rotor (Beckman). The pellet was resuspended in PBS and 3% samples were stained with PKH67 as described above. Vesicles were loaded on top of a linear sucrose gradient (2.0–0.4 M sucrose in PBS) in a SW40 tube (Beckman) and centrifuged for 16 hours at 192,000g. Sucrose gradient fractions were diluted 1:1000 in PBS before flow cytometry-based analysis.

SDS-PAGE and immunoblotting

Sucrose gradient fractions were diluted with PBS and centrifuged for 60 minutes at 100,000g using a SW60 rotor (Beckman). The pellets were solubilized in nonreducing SDS-PAGE sample buffer and separated by 12.5% SDS-PAGE. For western blotting, proteins were transferred to PVDF membranes (Millipore, Bedford, Massachusetts), which were blocked in PBS containing 5% (w/v) nonfat dry milk (Protifar plus; Nutricia, Zoetermeer, The Netherlands) and 0.1% (v/v) Tween-20, and immunolabeled with mouse anti-human CD9 (clone HI9a; Santa Cruz Biotechnology, Santa Cruz, California). Horseradish peroxidase-conjugated rabbit anti-mouse (Pierce, Rockford, Illinois) was used as secondary antibody and detected using Supersignal west pico chemiluminescent substrate (Pierce).

Results

Flow cytometry-based detection of nanosized particles

We optimized the configuration of a high-end, but commercially available, flow cytometry system for optical detection of light scatter and fluorescence signals generated by nanosized particles (**Supplementary Table S1**). For cells and particles larger than 500 nm the amount of light scattered at small angles (0.5–15 degrees), i.e., forward scatter (FSC), is commonly used as a rough indication of their size (26). However, particles with sizes near and below the wavelength of light (NPs) scatter proportionally more light at larger angles (15–150 degrees) (26, 27, 33). We have used a flow cytometer equipped with a photomultiplier tube detecting forward scattered light at 2–25 degrees (wide-angle forward scatter detection). We further increased the sensitivity for small particle detection by increasing the minimum detection angle to 14 degrees, resulting in an increased signal-to-noise ratio (27). In addition, we used fluorescence threshold triggering to discriminate fluorescently labeled particles of interest from noise signals (**Supplementary Figure S1 A–D**). With this set-up, 100- and 200-nm fluorescent beads could be selectively detected above the fluorescence threshold, and we achieved an unprecedented clear wide-angle FSC-based separation of these bead populations (**Supplementary Figure S1 C–D**). Light scattered at 90 degrees (side scatter, SSC) has also been used for analysis of small particles (34). However, SSC and backward scatter are more sensitive to changes in the geometry and internal structures of small particles (33). More important, we observed that the resolving power (change in light scatter with particle size) of the wide-angle FSC was greater than that of the SSC (**Supplementary Figure S1 E**). Based on these findings, we selected wide-angle FSC for relative sizing of nanosized particles.

Until now, high-throughput methods for absolute quantification of nanosized cellular membrane vesicles were lacking. To determine whether our flow cytometry-based method can be used to quantify nanosized particles, dilutions of 100-nm beads were mixed with a fixed number of 200-nm beads as a reference and measured. The ratio of detected 100- versus 200-nm beads correlated linearly with the dilution factor ($R^2 = 0.999$) with the predicted slope (**Figure 1A**), demonstrating that nanosized particles could be accurately quantified at a large range of concentrations. A disadvantage of using reference beads is that they can stick to the biological NPs of interest. Therefore, as an alternative we used a fixed timeframe for quantification (**Figure 1B**). An important finding was that the absolute number of measured 100-nm beads deviated < 10% from the specified number of input beads over a large range of concentrations (**Figure 1B**), confirming that the complete population of beads was detected above the fluorescence threshold and that noise signals were eliminated. Using this time-based quantification method, the inter- and intrasample variations were 5.3% and 0.6%, respectively.

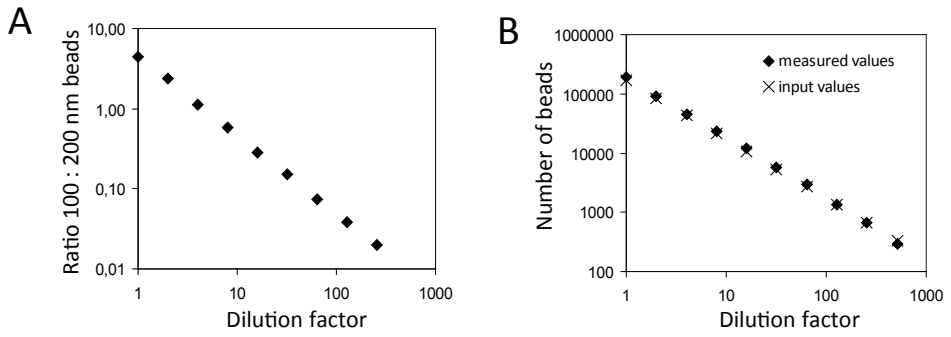

Figure 1 - Quantification of nanosized particles by flow cytometric analysis (**A**) Serial twofold dilutions of fluorescent 100-nm beads were mixed with a fixed number of fluorescent 200-nm beads. Samples were measured using fluorescence threshold triggering and the absolute numbers of 100-nm and 200-nm beads were analyzed. Expressed is the ratio of 100-nm beads versus 200-nm bead at each dilution (slope -0.9637 ± 0.064, R^2 = 0.999, as determined by linear regression). One representative experiment out of three is shown. (**B**) Serial twofold dilutions of fluorescent 100-nm beads were prepared and measured using fluorescence threshold triggering. The absolute number of beads measured in a fixed time window (30 sec) was plotted against the dilution factor (slope -1.012 ± 0.012, R^2 = 1.00, as determined by linear regression). The measured values (black diamonds) are plotted together with the calculated amount of input beads ('x' symbol) based on the specified concentration of beads in the stock solution. One representative experiment out of three is shown.

Analysis of nanosized virions and liposomes

Next, we analyzed CFSE-labeled mouse hepatitis coronavirus, representing a homogeneous population of membrane-enveloped NPs, and differently sized calcein-labeled liposome preparations. To determine their size with an independent method, we used NTA. Virions were 100 ± 30 nm (corroborating previous data, (32)), and liposome preparations I and II were 95 ± 26 nm and 123 ± 45 nm, respectively (**Figure 2C, G**). Using our flow cytometry approach, CFSE-labeled mouse hepatitis coronavirus could be clearly discerned based on fluorescence, and the wide-angle FSC level was in the range of the 100-nm fluorescent beads (**Figure 2A, B**). In addition, the calcein-labeled liposomes were clearly detected above the fluorescence threshold (**Figure 2D, E**), and the largest liposome preparation showed a slightly increased wide-angle FSC level. In comparison with 100-nm beads and the virions, the liposomes displayed a relatively low wide-angle FSC value (**Figure 2F**). This finding is most likely due to the low refractive index of these liposome preparations, indicating that particle composition also influences wide-angle FSC levels. Although the light scattering values cannot be used for absolute sizing, we conclude that wide-angle FSC can be used for approximate sizing, as well as for relative sizing of nanosized membrane particles and vesicles with a comparable composition.

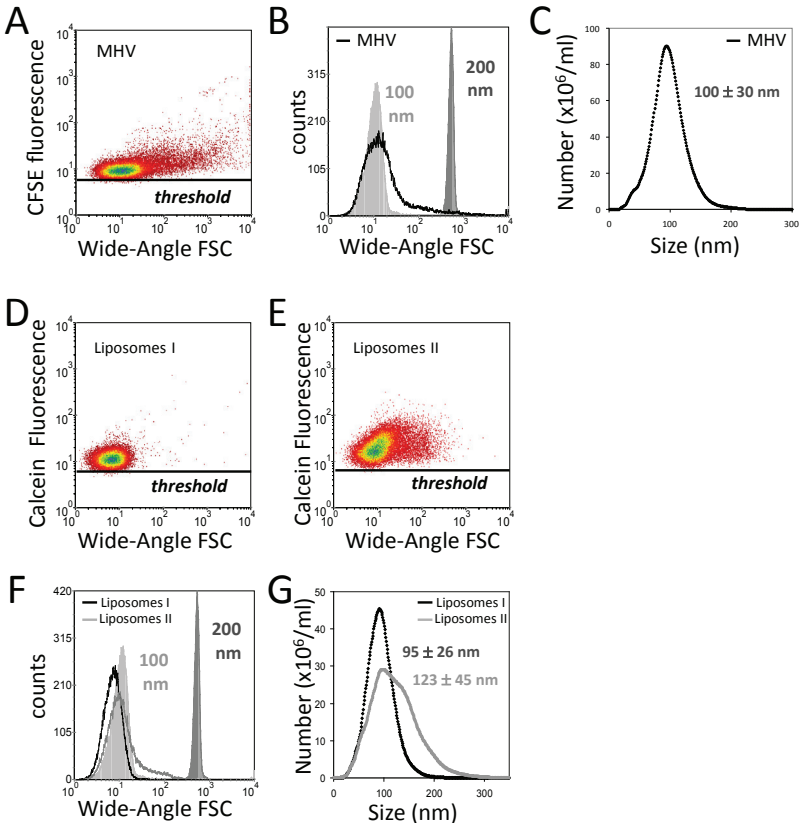

Figure 2 - Analysis of nanosized virions and liposomes (**A-B, D-F**) Flow cytometric analysis of CFSE-labeled mouse hepatitis virions (MHV) and calcein-labeled liposome preparations I and II using fluorescence threshold triggering. Wide-angle FSC levels were compared with those of 100- and 200-nm fluorescent beads as indicated. (**C, G**) Virions and liposomes were sized by NTA.

Flow cytometric analysis of nanosized membrane vesicles from cell culture supernatant and body fluid

To analyze nanosized membrane vesicles (exosomes) secreted by *in vitro* cultured cells, we developed a labeling method to obtain brightly fluorescent exosomes free of unbound dye. Exosomes secreted by murine DCs were isolated from cell culture supernatant by differential centrifugation, fluorescently labeled with PKH67 and floated by centrifugation to equilibrium density into a sucrose gradient (30). This experimental set-up (**Figure 3A**) ensured separation of labeled exosomes from unbound dye or aggregates thereof that severely hamper exosome measurements. We found that the vast majority (84 ± 4%; mean ± SD of four individual experiments) of DC vesicles equilibrated at sucrose densities of 1.11–1.18 g/mL (**Figure 3B**), corresponding to the representative density range of

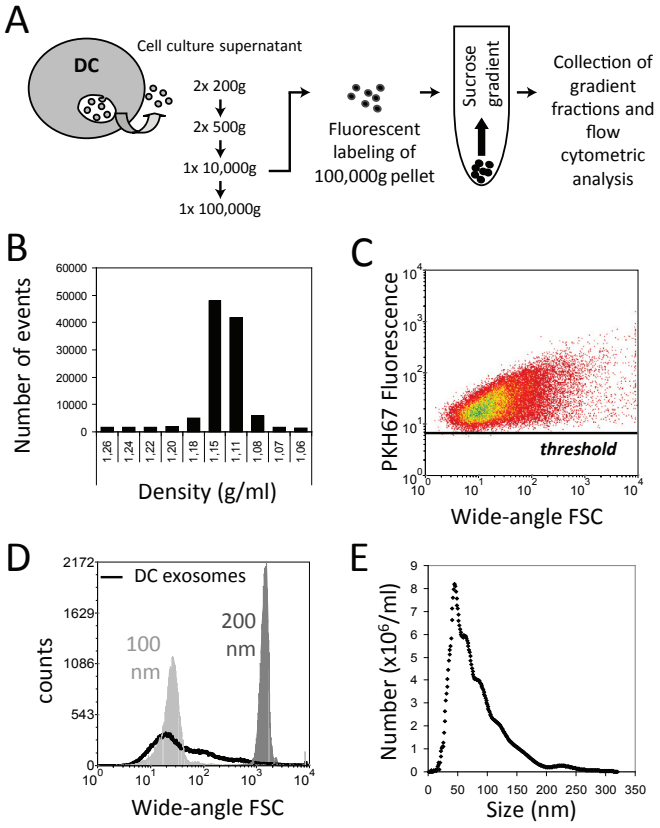

Figure 3 - Flow cytometric analysis of exosomes from cell culture supernatant (**A**) Schematic diagram of the method developed to quantify and characterize cellular membrane vesicles by flow cytometric analysis. Exosomes were isolated from culture supernatants of LPS-activated DC cultures by differential centrifugation. Pelleted (100,000g) exosomes were fluorescently labeled with PKH67 and loaded at the bottom of a sucrose gradient, after which the vesicles were floated to equilibrium by ultracentrifugation. Sucrose gradient fractions were analyzed using a threshold on PKH67 fluorescence. (**B**) Time-based quantification of fluorescent membrane vesicles detected in collected gradient fractions. Indicated are the numbers of events measured in 30 sec. One representative experiment out of five is shown. (**C**) Dot plot of wide-angle FSC versus PKH67 fluorescence of DC exosomes pooled from 1.11–1.18 g/mL fractions. (**D**) Histogram indicating the wide-angle FSC of DC exosomes relative to the scatter levels of 100- and 200-nm beads. (**E**) Exosome size was determined by NTA. The mean size of these DC exosomes was estimated to be 83 ± 47 nm.

exosomes (1). An important finding was that the entire population of fluorescently labeled DC-exosomes (pool of densities 1.11–1.18 g/mL) was detected above the fluorescence threshold, indicating that the labeling approach was sufficient to visualize the vast majority of exosomes (**Figure 3C**). The size distributions of these DC exosomes as determined by wide-angle FSC level (**Figure 3D**) and NTA (**Figure 3E**) were comparable.

We next applied our method to the detection and quantification of nanosized membrane vesicles in a body fluid. We selected human seminal fluid that contains vesicles derived from various cell types, e.g., from prostate epithelial cells (prostasomes, (35)). Using western blotting, we found that in sucrose gradients the exosomal marker CD9 migrated to densities of 1.09–1.17 g/mL (**Figure 4A**). Quantification by time-based flow cytometric analysis demonstrated that the vesicles distributed in a manner similar to that of CD9 (**Figure 4B**), indicating the suitability of this method to detect nanosized membrane vesicles in body fluids.

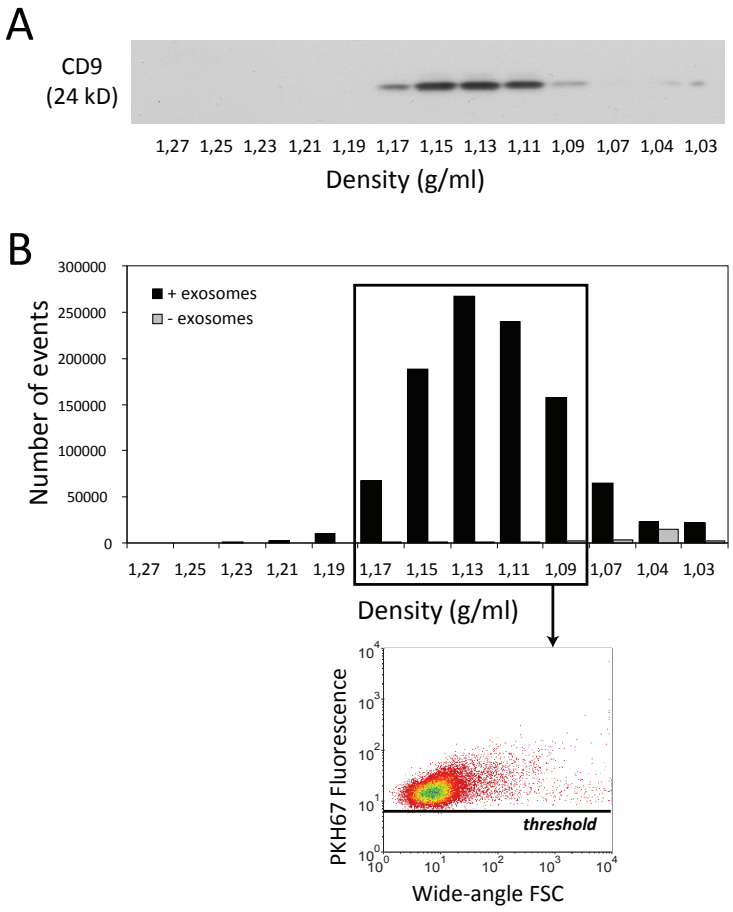

Figure 4 - Detection and quantification of human seminal fluid nanosized membrane vesicles by flow cytometric analysis Membrane vesicles were isolated from seminal fluid, fluorescently labeled with PKH67, loaded onto a sucrose gradient and centrifuged to equilibrium density. One representative experiment out of two independent experiments is shown. (**A**) Gradient fractions were analyzed for the presence of CD9 by western blotting. (**B**) Sucrose gradient fractions were analyzed using a threshold on PKH67 fluorescence. Time-based (30 sec) quantification of fluorescent

Flow cytometric characterization of exosome subsets

Next, we applied fluorescent antibody staining for phenotypic characterization of individual exosomes in heterogeneous populations using our murine DC-T cell co-culture system (30). Quantitative analysis of exosomes derived from DC-T cell co-culture revealed that the number of exosomes increased 2.1 ± 0.5-fold (mean ± SD of four individual experiments) during cognate DC-T cell interaction (**Figure 5A**). This finding can be explained either by T cell-induced secretion of DC exosomes (30) and/or the additional presence of T cell exosomes (36). To discriminate between T cell- and DC-derived exosomes, DC exosomes were in addition to PKH67 also selectively labeled with fluorescently labeled antibodies against MHC class II (MHCII). MHCII is incorporated into DC exosomes (30, 37) but is absent on mouse T cells and T cell-derived exosomes. MHCII stained vesicles were detected in those sucrose fractions containing DC exosomes (**Figure 5B**), with signals well above isotype control antibody staining (**Figure 5B, C**). The MHCII staining levels of DC exosomes were variable. Vesicles floating at a relative high density (1.18 g/mL) contained the highest amount of MHCII (**Figure 5B**). Besides MHCII-positive exosomes, MHCII-negative vesicles also were observed (**Figure 5C**). This suggests that DC can also secrete vesicles that contain little or no MHCII. Exosomes derived from murine T cells were all negative for MHCII (**Figure 5C**). In DC-T cell co-culture supernatants, both MHCII-positive and MHCII-negative populations of exosomes were found (**Figure 5C**). In comparison with DC cultures, the relative amount of MHCII-negative exosomes was increased in DC-T cell co-cultures, indicating a contribution of T cell exosomes.

To further test the sensitivity of our method to reveal conditional phenotypic changes of exosomes, we performed a double labeling for MHCII and milk-fat globule-EGF factor 8 (MFG-E8; a protein described to be present on DC exosomes, (1)) and compared exosomes produced by LPS-activated with nonactivated murine DCs. Based on the combined analysis of MFG-E8 and MHCII, different exosome subsets could be distinguished in both populations of DC exosomes (**Figure 5D**). MHCII staining was higher on LPS-activated DC exosomes in comparison with nonactivated DC exosomes. In contrast, exosomes derived from nonactivated DC contained higher levels of MFG-E8 in comparison with LPS-activated DC exosomes, as had previously been suggested based on western blot analysis (38). These data demonstrate that subtle changes in the molecular make-up of a subset of nanosized membrane vesicles can be analyzed with our method.

Figure 4 (*continued*) membrane vesicles (black bars) detected in different gradient fractions and dot plot of wide-angle FSC versus PKH67 fluorescence representing fluorescent vesicles pooled from fractions with densities of 1.09–1.17 g/mL. As a control for unbound dye aggregates, PKH67 dye-only without membrane vesicles was loaded onto a sucrose gradient (gray bars).

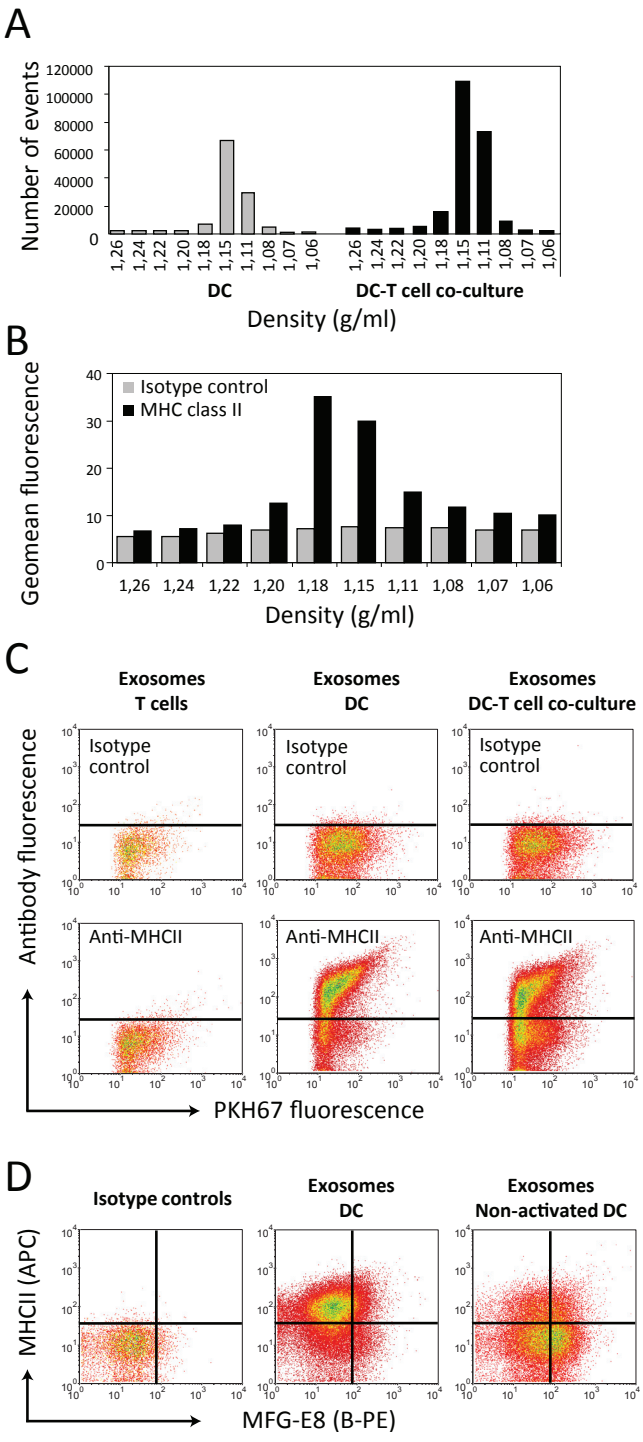
A
Number of events
120000
100000
80000
60000
40000
20000
0
1,26 1,24 1,22 1,20 1,18 1,15 1,11 1,08 1,07 1,06
1,26 1,24 1,22 1,20 1,18 1,15 1,11 1,08 1,07 1,06
DC
DC-T cell co-culture
Density (g/ml)
B
Geomean fluorescence
Isotype control
MHC class II
40
30
20
10
0
1,26 1,24 1,22 1,20 1,18 1,15 1,11 1,08 1,07 1,06
Density (g/ml)
C
Exosomes T cells
Exosomes DC
Exosomes DC-T cell co-culture
Antibody fluorescence
Isotype control
Anti-MHCII
PKH67 fluorescence
D
Isotype controls
Exosomes DC
Exosomes Non-activated DC
MHCII (APC)
MFG-E8 (B-PE)

Figure 5 - Flow cytometric characterization of exosome subsets Exosomes were isolated from culture supernatants of murine DC, T cell or DC-T cell co-cultures. (**A**) Time-based quantification of fluorescent exosomes detected in different gradient fractions. Indicated are the numbers of events measured in 30 sec. One representative experiment out of four is shown. (**B**) Exosomes from LPS-activated DC cultures were additionally stained with R-PE-labeled anti-MHCII (black bars) or isotype control (gray bars) antibodies. Indicated are the geometric mean fluorescence intensities of events measured in each of the gradient fractions. One representative experiment out of three is shown. (**C**) Dot plots representing PKH67 and anti-MHCII-R-PE or isotype control antibody-labeled exosomes (pools of 1.11–1.18 g/ml sucrose fractions) derived from T cell cultures (left), LPS-activated DC cultures (middle) or DC/LPS-T cell co-cultures (right). One representative experiment out of three is shown. (**D**) Dot plots representing PKH67 and anti-MHCII (APC-labeled) / anti-MFG-E8 (B-PE-labeled) double-labeled exosomes or corresponding isotype control labeled exosomes derived from nonactivated or LPS-activated DC cultures.

Discussion

Biomarker profiling of cellular membrane vesicles and quality control of exosome-based vaccines depend heavily on accurate methods to analyze the quantity and phenotype of these vesicles. However, current methods fall short in the identification and characterization of individual membrane vesicles and vesicle subsets in heterogeneous populations. For the larger membrane vesicles in human blood (> 300 nm), FSC-based flow cytometric analysis appeared to be a reproducible method for high-throughput, multiparameter analysis at the particle level (23-25, 39). However, the majority of secreted membrane vesicles in body fluids are in the nanoscale size range (50–100 nm) (19) which cannot be visualized by conventional FSC-based analysis (23-25). Techniques that allow phenotypic analysis of individual nanosized membrane vesicles, including immunoelectron microscopy and atomic force microscopy, preclude analysis of large numbers of vesicles needed to study their quantity and heterogeneity (3, 19). Recently, NTA has been described as a method to analyze cell-derived membrane vesicles (21). Although NTA is a powerful method for size analysis, quantitative measurements are less precise in samples containing differently sized vesicles (21) and the number of parameters that can be analyzed simultaneously is limited. These limitations pose a disadvantage for the analysis of biological fluids containing many different types of cellular membrane vesicles. We here described a novel flow cytometry-based method allowing simultaneous high-throughput quantitative analysis and multiple-parameter phenotyping of individual nanosized membrane vesicles. This methodology proved suitable for the accurate and absolute quantification of nanosized particles over a wide range of concentrations, setting the stage for its applicability in biomarker analysis. Importantly, we demonstrated that antibody-mediated detection of multiple specific proteins on individual membrane vesicles allowed discrimination of phenotypically different vesicle subsets.

Several features of the selected high-end flow cytometer contributed to the high sensitivity of fluorescence and light scatter detection. First, the selected BD Influx flow cytometer, like some other new generation flow cytometers (23), uses wide-angle FSC instead of the conventional FSC (< 15 degrees) to improve small-particle detection. Second, the BD Influx is fitted with a high-performance photomultiplier tube instead of a photodiode (used in other flow cytometers) for detection of FSC signals. Third, we used fluorescence threshold triggering, which was crucial to distinguish nanosized fluorescently labeled particles of interest from noise signals with overlapping light scattering properties. Importantly, the sensitivity by which the BD Influx detected fluorescently labeled membrane vesicles above the threshold was higher in comparison with other flow cytometers, such as the BD FACS Canto II and the Beckman Coulter Gallios, making it better suited for accurate quantification and characterization of complete vesicle populations. Because our method is based on both optimized wide-angle FSC detection and fluorescence thresholding, the exact lower detection limit for the described technology not only depends on the size of the particles but also on the brightness of labeling, allowing the detection of the entire population above the fluorescence threshold. There are two important advantages of using a labeling method for indiscriminative detection of the entire membrane vesicle population above the fluorescence threshold. First, particles of interest can be accurately quantified because all noise signals are eliminated. Second, by combining the general fluorescent labeling with labeling for a specific marker, vesicle subsets can be identified and related to the entire membrane vesicle population. To analyze fluorescently labeled membrane vesicles, removal of unbound soluble and aggregated dye is very important. Simple washing by sedimentation through ultracentrifugation was not efficient to remove dye aggregates, which appeared above the fluorescence threshold with scatter levels just below those of 100-nm beads. Density gradient ultracentrifugation was therefore crucial to separate the vesicles from unbound dye and simultaneously allowed the identification of membrane vesicles subsets with distinct buoyant densities.

Accurate and standardized quantification and detailed phenotypic analysis of (subsets of) membrane vesicles is important for biomarker profiling and therapeutic applications. We here demonstrated that our method allows accurate and absolute quantification of nanosized particles over a wide range of concentrations. Furthermore, we showed proof of principle that specific proteins can be detected on individual exosomes using fluorescent antibodies. In addition, we showed the suitability of this method for liposome and virion analyses. Therefore, this method opens new avenues for NP analysis in the fields of medicine, virology, and nano-drug development.

Acknowledgments

We thank M. de Boer-Brouwer and M. van Steenbergen for excellent technical assistance and N.P.H. van Adrichem and M. van Wijnen (Meander Medical Center, Amersfoort, The Netherlands) for providing seminal fluid samples. We thank Drs R. Wubbolts and M. Nolte for critical reading of the manuscript.

References

1. Thery C, Ostrowski M, Segura E. Membrane vesicles as conveyors of immune responses. Nat Rev Immunol 2009; 9: 581-93.
2. Cocucci E, Racchetti G, Meldolesi J. Shedding microvesicles: artefacts no more. Trends Cell Biol 2009; 19: 43-51.
3. Raposo G, Nijman HW, Stoorvogel W, Liejendekker R, Harding CV, Melief CJ, et al. B lymphocytes secrete antigen-presenting vesicles. J Exp Med 1996; 183: 1161-72.
4. Puddu P, Puddu GM, Cravero E, Muscari S, Muscari A. The involvement of circulating microparticles in inflammation, coagulation and cardiovascular diseases. Can J Cardiol 2010; 26: 140-5.
5. Chironi GN, Boulanger CM, Simon A, Dignat-George F, Freyssinet JM, Tedgui A. Endothelial microparticles in diseases. Cell Tissue Res 2009; 335: 143-51.
6. Nomura S. Dynamic role of microparticles in type 2 diabetes mellitus. Curr Diabetes Rev 2009; 5: 245-51.
7. Clayton A, Mason MD. Exosomes in tumour immunity. Curr Oncol 2009; 16: 46-9.
8. Escudier B, Dorval T, Chaput N, Andre F, Caby MP, Novault S, et al. Vaccination of metastatic melanoma patients with autologous dendritic cell (DC) derived-exosomes: results of thefirst phase I clinical trial. J Transl Med 2005; 3: 10.
9. Nolte-'t Hoen EN, Buschow SI, Anderton SM, Stoorvogel W, Wauben MH. Activated T cells recruit exosomes secreted by dendritic cells via LFA-1. Blood 2009; 113: 1977-81.
10. Morelli AE, Larregina AT, Shufesky WJ, Sullivan ML, Stolz DB, Papworth GD, et al. Endocytosis, intracellular sorting, and processing of exosomes by dendritic cells. Blood 2004; 104: 3257-66.
11. Beyer C, Pisetsky DS. The role of microparticles in the pathogenesis of rheumatic diseases. Nat Rev Rheumatol 2009; 6: 21-9.
12. Sullivan R, Saez F, Girouard J, Frenette G. Role of exosomes in sperm maturation during the transit along the male reproductive tract. Blood Cells Mol Dis 2005; 35: 1-10.
13. Kim SH, Lechman ER, Bianco N, Menon R, Keravala A, Nash J, et al. Exosomes derived from IL-10-treated dendritic cells can suppress inflammation and collagen-induced arthritis. J Immunol 2005; 174: 6440-8.
14. Zhang HG, Grizzle WE. Exosomes and cancer: A newly described pathway of immune suppression. Clin Cancer Res 2011.
15. Mathivanan S, Simpson RJ. ExoCarta: A compendium of exosomal proteins and RNA. Proteomics 2009; 9: 4997-5000.
16. Keller S, Ridinger J, Rupp AK, Janssen JW, Altevogt P. Body fluid derived exosomes as a novel template for clinical diagnostics. J Transl Med 2011; 9: 86.
17. Chaput N, Taieb J, Schartz N, Flament C, Novault S, Andre F, et al. The potential of exosomes in immunotherapy of cancer. Blood Cells Mol Dis 2005; 35: 111-5.
18. Iero M, Valenti R, Huber V, Filipazzi P, Parmiani G, Fais S, et al. Tumour-released exosomes and their implications in cancer immunity. Cell Death Differ 2008; 15: 80-8.

19. Yuana Y, Oosterkamp TH, Bahatyrova S, Ashcroft B, Garcia Rodriguez P, Bertina RM, et al. Atomic force microscopy: a novel approach to the detection of nanosized blood microparticles. J Thromb Haemost 2010; 8: 315-23.
20. Gyorgy B, Modos K, Pallinger E, Paloczi K, Pasztoi M, Misjak P, et al. Detection and isolation of cell-derived microparticles are compromised by protein complexes resulting from shared biophysical parameters. Blood 2011; 117: e39-48.
21. Dragovic RA, Gardiner C, Brooks AS, Tannetta DS, Ferguson DJ, Hole P, et al. Sizing and phenotyping of cellulars vesicles using Nanoparticle Tracking Analysis. Nanomedicine 2011.
22. Filipe V, Hawe A, Jiskoot W. Critical evaluation of Nanoparticle Tracking Analysis (NTA) by NanoSight for the measurement of nanoparticles and protein aggregates. Pharm Res 2010; 27: 796-810.
23. Lacroix R, Robert S, Poncelet P, Kasthuri RS, Key NS, Dignat-George F. Standardization of platelet-derived microparticle enumeration by flow cytometry with calibrated beads: results of the International Society on Thrombosis and Haemostasis SSC Collaborative workshop. J Thromb Haemost 2010; 8: 2571-2574.
24. Orozco AF, Lewis DE. Flow cytometric analysis of circulating microparticles in plasma. Cytometry A 2010; 77: 502-14.
25. Freyssinet JM, Toti F. Membrane microparticle determination: at least seeing what's being sized! J Thromb Haemost 2010; 8: 311-4.
26. Shapiro HM. Practical Flow Cytometry, Fourth Edition, Wiley Liss, New York. 2003.
27. Steen HB. Flow cytometer for measurement of the light scattering of viral and other submicroscopic particles. Cytometry A 2004; 57: 94-9.
28. Lutz MB, Kukutsch N, Ogilvie AL, Rossner S, Koch F, Romani N, et al. An advanced culture method for generating large quantities of highly pure dendritic cells from mouse bone marrow. J Immunol Methods 1999; 223: 77-92.
29. Lauwen MM, Zwaveling S, de Quartel L, Ferreira Mota SC, Grashorn JA, Melief CJ, et al. Self-tolerance does not restrict the CD4+ T-helper response against the p53 tumor antigen. Cancer Res 2008; 68: 893-900.
30. Buschow SI, Nolte-'t Hoen EN, van Niel G, Pols MS, ten Broeke T, Lauwen M, et al. MHC II in dendritic cells is targeted to lysosomes or T cell-induced exosomes via distinct multivesicular body pathways. Traffic 2009; 10: 1528-42.
31. Bosch BJ, van der Zee R, de Haan CA, Rottier PJ. The coronavirus spike protein is a class I virus fusion protein: structural and functional characterization of the fusion core complex. J Virol 2003; 77: 8801-11.
32. Barcena M, Oostergetel GT, Bartelink W, Faas FG, Verkleij A, Rottier PJ, et al. Cryo-electron tomography of mouse hepatitis virus: Insights into the structure of the coronavirion. Proc Natl Acad Sci U S A 2009; 106: 582-7.
33. Kerker M, Chew H, McNulty PJ, Kratohvil JP, Cooke DD, Sculley M, et al. Light scattering and fluorescence by small particles having internal structure. J Histochem Cytochem 1979; 27: 250-63.
34. van Gaal EV, Spierenburg G, Hennink WE, Crommelin DJ, Mastrobattista E. Flow cytometry for rapid size determination and sorting of nucleic acid containing nanoparticles in biological fluids. J Control Release 2010; 141: 328-38.
35. Sahlen GE, Egevad L, Ahlander A, Norlen BJ, Ronquist G, Nilsson BO. Ultrastructure of the secretion of prostasomes from benign and malignant epithelial cells in the prostate. Prostate 2002; 53: 192-9.
36. Blanchard N, Lankar D, Faure F, Regnault A, Dumont C, Raposo G, et al. TCR activation of human T cells induces the production of exosomes bearing the TCR/CD3/zeta complex. J Immunol 2002; 168: 3235-41.
37. Stoorvogel W, Kleijmeer MJ, Geuze HJ, Raposo G. The biogenesis and functions of exosomes. Traffic 2002; 3: 321-30.

38. Segura E, Amigorena S, Thery C. Mature dendritic cells secrete exosomes with strong ability to induce antigen-specific effector immune responses. Blood Cells Mol Dis 2005; 35: 89-93.
39. Zwicker JI. Tissue factor-bearing microparticles and cancer. Semin Thromb Hemost 2008; 34: 195-8.

Supplementary information

The following is supplemenatry information to this chapter.

Supplementary Methods

Flow cytometric analysis of nano-sized particles (full details)

The BD Influx™ flow cytometer (Becton Dickinson) was originally equipped with a small particle detector consisting of a high NA long working distance 20x objective, a 0.7 mm diameter pinhole and two PMTs collecting light of different polarization directions. Since we and others were unable to demonstrate a correlation between particle size and direction of polarization for particles <200 nm, we removed the option of polarization measurement in the small particle detector. Instead, we measured light scattering only, in straight line with the laser excitation beam (collection angle is 14-25°). Sheath tanks were filled with PBS and connected to the machine via a sheath in-line 0.22 µm filter. A nozzle size of 140 µm was found to yield optimal signal-to-noise ratios. Samples were run at low pressure (5 PSI on the sheath fluid and 4.2 PSI on the sample) in order to maximize the particle dwell time in the laser beam and thereby the sensitivity of fluorescent light collection.

Lasers were aligned at the start of each experiment. For calibration, we established fixed positions for fluorescent 100 and 200 nm polystyrene beads (yellow-green–fluorescent FluoSpheres, Invitrogen) in wide-angle FSC (14-25°)/SSC and wide-angle FSC (14-25°)/FL1 plots as a reference. Samples were measured at event rates lower than 10,000 events per second. The two bottom fractions of the sucrose gradients were left out since unbound staining reagents in these fractions severely hampered the analysis. Sample measurements were performed as follows: 1) Install sample tube, 2) Boost the system for 5 sec, 3) Wait 30 sec till fluidics have equilibrated and event rate has stabilized, 4) Acquire data for 30 sec, 5) Remove sample tube, 6) Flush by running soap solution in boost-mode (10 PSI) for 5 sec 7) Flush by running PBS in boost-mode for 5 sec.

Supplementary Table S1 - Configuration of BD Influx™ and settings relevant to nano-particle analysis

Feature	**Technical details**
488 nm laser	Sapphire (Coherent, USA), 190 mW (95% of its maximum)
561 nm laser	Jive (Cobolt, Sweden), 100 mW
Scatter optics for small particles	
20x microscope objective	Mitutoyo (Japan), Long distance N.A. 0.42
Blocker bar in front of the FSC lens	5 mm width, allowing to collect scatter at an angle between 14-25 degrees
Pinhole behind FSC lens	0.7 mm
PMT on each scatter position	Type R3896, Hamamatsu (Japan)
Parameter	**Value**
Nozzle size	140 micrometer
Sheath pressure	5 PSI
Sample pressure	4.2 PSI
Flow rate	20.8 micro liter per minute
Trigger signal	On fluorescence (528/38)
Threshold FL1	Threshold level was set such that 6 events per second were observed in filtered PBS
PMT filter sets and positions	488/10 FSC detector 488/10 SSC detector 528/38 pinhole 1 585/42 pinhole 3
Other	- Measure with closed blinds - Standard 0.2 micron filter for sheath fluid

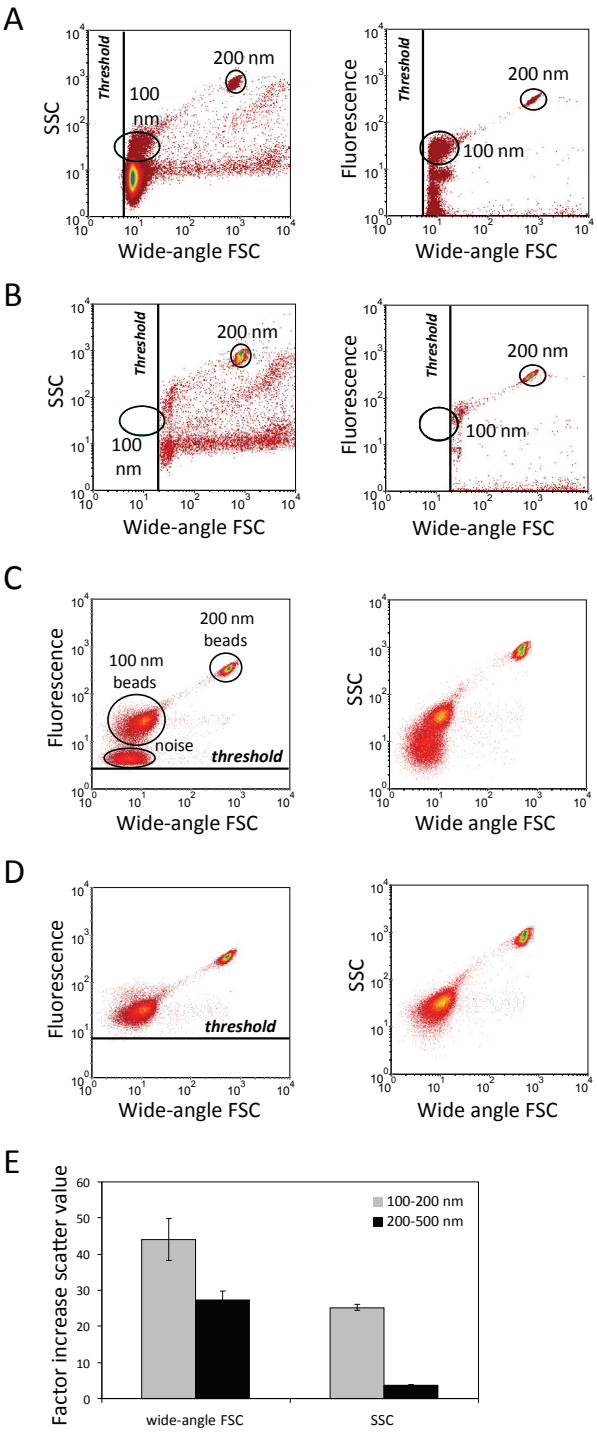

Supplementary Figure 1 - Flow cytometric detection of nano-sized particles by FSC-based or fluorescence-based thresholding

(**A, B**) Conventional FSC-based thresholding was used to analyze a mixture of fluorescent 100 nm and 200 nm beads on the BD Influx™ flow cytometer. Measurements were performed using a low FSC threshold (**A**) or a high FSC threshold (**B**). For each threshold, wide-angle FSC/SSC and wide-angle FSC/Fluorescence dotplots are shown. In these plots, gates indicate the positions of the 100 and 200 nm beads. In contrast to measurements with fluorescence-based thresholds (**C, D**), measurements with the depicted FSC-based thresholding do not allow discrimination of the 100 nm particles from noise signals. (**C, D**) Fluorescence-based measurements of mixed 100 and 200 nm beads. Dot plots represent fluorescence and wide-angle FSC levels or wide-angle FSC and SSC levels of the two different beads. Thresholding on the fluorescence channel was applied to eliminate noise events. With a low fluorescence threshold, noise events are visible (**C**). By raising the fluorescence threshold, noise events could be eliminated (**D**). (**E**) Wide-angle FSC and SSC values of 100, 200, and 500 nm fluorescent beads were analyzed. Bars depict the ratio of the scatter values (mean ± s.d. of three independent experiments) for 200 nm beads versus 100 nm beads (grey bars) or for 500 nm beads versus 200 nm beads (black bars).

It always seems impossible until it's done – Nelson Mandela

Chapter 3

Fluorescent labeling of nano-sized vesicles released by cells and subsequent quantitative and qualitative analysis by high-resolution flow cytometry

Els J. van der Vlist, Esther N.M. Nolte-'t Hoen, Willem Stoorvogel, Ger J.A. Arkesteijn and Marca H.M. Wauben

Nature Protocols. 2012 Jun 14;7(7):1311-26

Abstract

We provide a protocol for a high-resolution flow cytometry–based method for quantitative and qualitative analysis of individual nano-sized vesicles released by cells, as developed and previously described by our group. The method involves (i) bright fluorescent labeling of cell-derived vesicles and (ii) flow cytometric analysis of these vesicles using an optimized configuration of the commercially available BD Influx flow cytometer. The method allows the detection and analysis of fluorescent cell-derived vesicles of ~100 nm. Integrated information can be obtained regarding the light scattering, quantity, buoyant density and surface proteins of these nano-sized vesicles. This method can be applied in nanobiology to study basic aspects of cell-derived vesicles. Potential clinical applications include the detailed analysis of vesicle-based biomarkers in body fluids and quality control analysis of (biological) vesicles used as therapeutic agents. Isolation, fluorescent labeling and purification of vesicles can be done within 24 h. Flow cytometer setup, calibration and subsequent data acquisition can be done within 2–4 h by an experienced flow cytometer operator.

Introduction

Cells release 50–1,000-nm vesicles into their environment either by direct shedding from the plasma membrane or as exosomes through the fusion of late endosomal compartments (multivesicular bodies) with the plasma membrane (1, 2). Such cell-derived vesicles can be detected both in cell culture–conditioned medium and in various body fluids, where they may function as vehicles for intercellular communication (1, 2). Different characteristics of cell-derived vesicles have been described by various research groups, depending on the source of the vesicles and isolation procedure used (2, 3). This has largely complicated the nomenclature and definition of these vesicles (**Box 1**).

Specific sets of proteins, lipids and RNA are selectively incorporated during the formation of vesicles that will be released into the extracellular space. Both the molecular composition of vesicles and the dynamics of their release are dependent on the subcellular origin of the vesicles, the donor cell type and the activation status of the donor cell (2). This leads to large heterogeneity in the quantity and quality of vesicles released by cells. Cell-derived vesicles can be targeted to other cells and impose signaling via protein-mediated receptor-ligand interactions (4), the action of modulatory lipids (5) or transfer of regulatory (small) RNAs (6). Hence, the composition and the number of transferred vesicles determine how the function of target cells is modified.

From a clinical perspective, cell-derived vesicles are interesting as they are present in many body fluids, such as blood (7, 8), semen (9, 10), urine (11, 12) , saliva (13, 14) and milk (15, 16). Several studies have indicated the biomarker potential of these vesicles, allowing the development of novel, noninvasive disease screening procedures (8, 12, 17-20). Furthermore, extracellular vesicles may be used as therapeutic agents (21, 22). For example, a clinical phase 2 trial using autologous dendritic cell (DC)–derived exosomes for the treatment of lung cancer patients is ongoing (23, 24). Basic research, biomarker profiling and clinical application of cell-derived vesicles requires high-resolution methods for accurate quantitative and qualitative vesicle analysis.

Although the size of cell-derived vesicles ranges from 50 to 1,000 nm, the vast majority of vesicles are smaller than 300 nm (25-27). This severely complicates the analysis of individual vesicles. The currently available techniques that allow the visualization of nano-sized vesicles (electron microscopy, atomic force microscopy) preclude analysis of large numbers of vesicles, which is needed to analyze quantity and heterogeneity (25, 26, 28). Proteomics, lipidomics, flow cytometry of bead-captured vesicles, and western blotting are powerful methods for analyzing the molecular composition of bulk isolates of cell-derived vesicles (29-32). However, these methods are not suited for studying the heterogeneity of vesicle populations, as changes in the number of vesicles cannot be discriminated from changes in the molecular composition of vesicles. Currently, no proteins are known that are constitutively sorted into vesicles independently of the

subcellular origin of the vesicle and the activation status of the producing cell. This lack of invariant 'household' markers hampers the quantitative analysis of vesicles using bulk-based analysis techniques. Notably, small changes in specific vesicle subsets may be leveled out by bulk-based analysis and will therefore be easily overlooked.

Nanoparticle tracking analysis (NTA) is a relatively new technique for analyzing individual vesicles (28, 33, 34). NTA allows the accurate determination of vesicle size on the basis of Brownian motion. However, quantification of a pool of heterogeneously sized vesicles is less precise. In addition, the total number of vesicles that can be tracked and the number of parameters that can be analyzed simultaneously are limited (33).

Flow cytometry is an ideal technique for high-throughput quantification and multiparameter characterization of individual cells and particles. However, many flow cytometers fall short in the analysis of nano-sized vesicles. For most conventional flow cytometers, the lower detection limit for light scattering is 300–500 nm (35-37). In addition, these cytometers cannot distinguish between particles that differ by <200 nm in size. A few studies describe the use of custom-constructed flow cytometers for detection of nano-sized particles based on scattering (38-40). By collecting scattered light over an angle of 16°–70°, polymer beads of > 74 nm and virus particles could be detected with a very high resolution (38). However, such hand-built machines are not available for use by most researchers. In a comparative study of commercially available high-end flow cytometers, the Apogee A40 was recently shown to have the highest sensitivity for nano-sized particle detection (41). Although the BD Influx performed less well in that study, the described BD Influx machine had not been optimized for many parameters that are crucial for the analysis of nano-sized particles.

We recently developed a high-resolution flow cytometry–based method, which uniquely allows quantitative and multiparameter qualitative analysis of nano-sized cell-derived vesicles (42). For this method, we selected the BD Influx flow cytometer and optimized this system to detect particles with sizes as small as 100 nm and with sufficient resolution to easily distinguish between 100- and 200-nm particles on the basis of light scatter. With the defined adaptations of the BD Influx and an optimized protocol for fluorescent vesicle labeling and measurement, this method is superior in the detection and characterization of nano-sized cell-derived vesicles.

Applications of the method

The method described here allows for the analysis of individual cell-derived nano-sized vesicles. This method yields integrated information on their buoyant density, light scattering (for approximate and relative sizing), quantity and protein content. By combining these parameters, different vesicle subsets can be identified within heterogeneous populations. In addition, dynamic changes in nano-sized vesicle populations (e.g., in response to

cellular activation) can be analyzed. We anticipate that the application of this method will result in a better understanding of basic aspects of vesicle-mediated communication between cells. Another key area for the application of this method is the characterization of nano-sized cell-derived vesicle subsets present in body fluids as biomarkers for disease. Nano-sized vesicles in body fluids can derive from a large range of different cell types and tissues (2). High-resolution techniques, such as our novel flow cytometry–based method, are therefore essential to detect (pathology-associated) changes in small vesicle subsets within the total vesicle population. In addition, our method can be applied to more accurate quality control analysis of vesicles used as therapeutic agents. Besides the analysis of nano-sized cell-derived vesicles, this method also allows analysis of ~100-nm-sized liposomes and virions (42). We therefore envision that the described method may also find novel applications in the fields of virology and nano-drug development.

Box 1 | The realm of cell-derived vesicles

The diversity in cell systems, body fluids and isolation procedures used by different research groups to study cell-derived vesicles has led to the identification of many different vesicle types. This has driven individual research groups to create their own nomenclature for their vesicles of interest. Terminologies were based on cell type of origin, presumed subcellular origin, or vesicle morphology, and include terms like exosomes, microvesicles, membrane particles, ectosomes, shedding vesicles, and exosome-like vesicles. This heterogeneity in nomenclature, combined with the large variation in protocols to purify and characterize vesicles has obscured the field and it is currently unknown how many fundamentally distinct types of extracellular vesicles actually exist. This is largely due to the lack of specific markers, e.g. to distinguish vesicles derived from late endosomal compartments from plasma membrane-derived vesicles. Consequently, once vesicles are released into the extracellular space it is impossible to trace their subcellular origin. Most likely, the total vesicle pool released by cells consists of a mixture of different vesicles types. Since the population of vesicles described in this protocol, which were collectively termed 'exosomes' in our original research article (42), may also contain plasma membrane-derived vesicles, we here decided to use the more general term 'cell-derived vesicles'.

Recently, the International Society of Extracellular Vesicles (ISEV) has been established (www.isevmeeting.org). One of the aims of this society is to define a proper nomenclature for extracellular vesicles and establish minimum requirements for their purification and characterization.

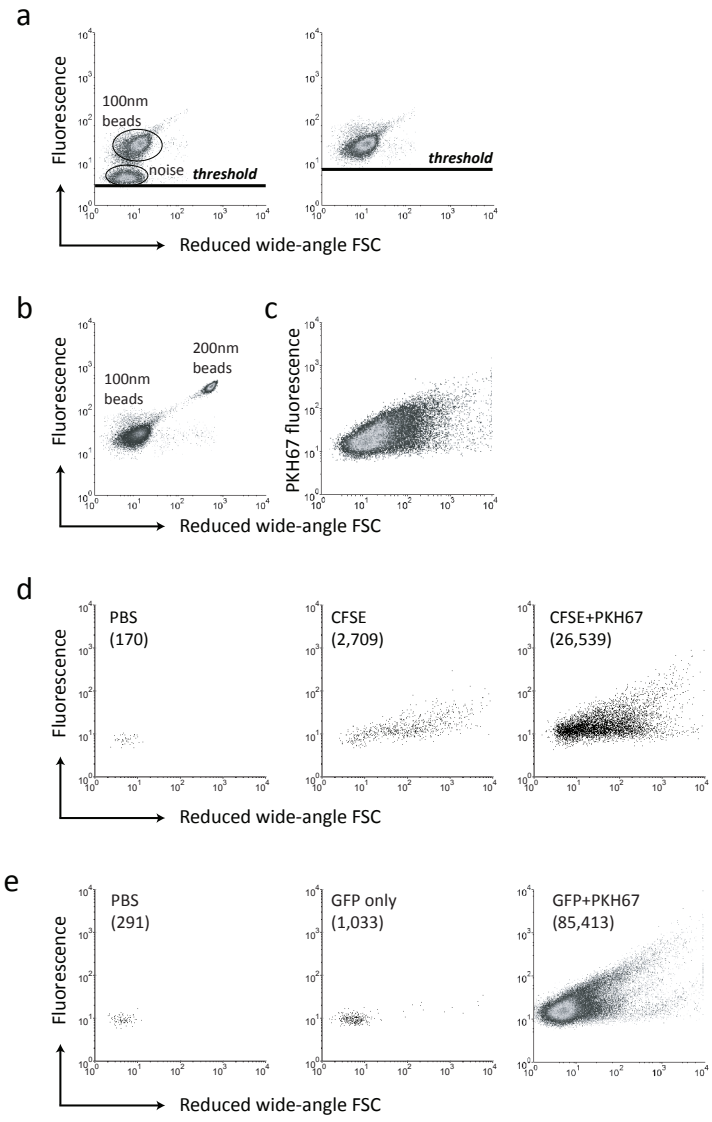

Figure 1 - Flow cytometric detection of nano-sized beads and cell-derived vesicles by fluorescence-based thresholding (**a**) Fluorescence-based thresholding was used to analyze fluorescent 100-nm beads on the BD Influx flow cytometer. Dot plots represent levels of fluorescence versus reduced wide-angle FSC. With a low fluorescence threshold, noise events are visible (left). By raising the fluorescence threshold, noise events could be eliminated (right). (**b**) A mixture of 100- and 200-nm-sized fluorescent beads was subjected to flow cytometric analysis as described in a. (**c**) Nano-sized vesicles released by lipopolysaccharide-stimulated mouse DCs were fluorescently labeled with PKH67 and floated to equilibrium density into a sucrose gradient. Vesicles derived from pooled 1.12–1.17 g ml^{-1} density fractions were subjected to flow cytometric analysis using fluorescence-based thresholding. Indicated is a dot plot of reduced wide-angle FSC levels versus PKH67 fluorescence.

Experimental design

Flow cytometry–based detection of individual nano-sized particles

We selected the jet-in-air–based BD Influx flow cytometer (originally purchased as Cytopeia Influx) for analysis of individual cell-derived vesicles. Jet-in-air systems allow for relatively easy manual adjustments before each experiment, which is an absolute requirement for measurements that reach the limits of detection. With the adapted settings of the BD Influx, we developed a method with exceptionally high sensitivity for fluorescence and light scatter detection (42). The flow cytometer used is equipped with a high-power 488-nm laser (200 mW, compared with 25 mW for most conventional benchtop flow cytometers), leading to increased intensity of the scattered light and optimal excitation of fluorochromes to gain the highest possible fluorescence signal per vesicle. Although the resolution of jet-in-air–based flow cytometers is generally less than that of the cuvette-based systems, measurements on jet-in-air–based cytometers are not hampered by dust or dirt build-up on cuvette surfaces and in the immersion gels. The use of lasers with higher output power compensates in part for the loss in resolution.

Flow cytometry–based detection of vesicles and particles smaller than 300 nm is severely hampered by noise derived from buffers, optics and electronics. The overlap in light scattering between noise and nano-sized vesicles precludes the discrimination of vesicles based on light scattering. As an alternative, we developed a method in which fluorescence threshold triggering was applied to discriminate fluorescently labeled vesicles from nonfluorescent noise (42). In addition, measurements were performed at low sheath pressure to increase the dwell time of the vesicles in the laser beam, thereby maximizing the amount of fluorescence and scattered light induced by these vesicles (42). With this setup, 100-nm fluorescent beads could be distinguished from noise events on the basis of fluorescence (42) (**Fig. 1a**).

Figure 1 (*continued*) (**d**) Mouse $CD4^+$ T cells were fluorescently labeled with the cytoplasmic dye CFSE (2 μM). Released vesicles with (right) or without (middle) additional PKH67 labeling were floated to equilibrium density into a sucrose gradient. Indicated is the analysis and time-based quantification (numbers of events in dot plots) of fluorescent vesicles detected in pools of fractions with densities of 1.11–1.16 g ml^{-1}. Dot plots represent reduced wide-angle FSC versus fluorescence levels of fluorescently labeled vesicles (middle and right) or the PBS control sample (left). (**e**) Vesicles were isolated from blood plasma of mice in which EGFP was expressed as soluble fluorescent protein under the control of the actin promoter (48). Citrated plasma was centrifuged for 30 min at 2,000g and 30 min at 10,000g, and vesicles were pelleted during 60 min of centrifugation at 100,000g. Vesicles with (right) or without (middle) additional PKH67 labeling were floated to equilibrium density into a sucrose gradient. Indicated is the analysis and time-based quantification (numbers of events in dot plots) of fluorescent vesicles detected in the 1.15 g ml^{-1} fraction. Dot plots represent reduced wide-angle FSC versus fluorescence levels of fluorescently labeled vesicles (middle and right) or the PBS control sample (left). Panels **a–c** are reprinted from ref. 42 with permission from Elsevier.

Box 2 | FSC-based sizing of nano-sized vesicles

Flow cytometric forward scatter (FSC) detection is widely used for the estimation of cell size. FSC-based sizing of small (< 1 µm) biological particles, such as cell-derived vesicles and virions, has been performed by comparison with different nano-sized latex or polystyrene calibration beads (50-53). However, FSC signals of small particles are not only influenced by particle size but also by their refractive index, surface roughness, shape and possibly light absorption (41, 43) Hence, the overall characteristics of cell-derived vesicles will determine whether their FSC signals can be compared to the FSC of calibration beads for size determination. Comparison of beads and cell-derived vesicles has led to conflicting results and it is debated how the FSC signals of different biological vesicles and similarly sized calibration beads compare (54-56).

We and others observed that biological vesicles, such as exosomes, 100 nm virions (42) or 400 nm virions (56) induce FSC signals largely comparable to FSC signals of polystyrene beads with the same size. However, we also found that the FSC levels of artificial membrane vesicles with a low relative refractive index, such as empty liposomes, were much less in comparison to those of calibration beads (42). Thus, care should be taken when comparing nano-sized particles and vesicles with different molecular compositions.

Part of the discrepancies in the field might be explained by differences in the angles at which FSC signals are collected in different types of flow cytometers (54). Collection of scattered light at highly enlarged angles is believed to correspond more to SSC detection than conventional FSC detection. A detailed description of the optical design of flow cytometers including light collection angles used for FSC-based sizing of nano-sized particles should therefore be included in scientific publications.

Conclusively, calibration beads can be useful tools for FSC-based sizing of nano-sized vesicles by flow cytometry. However, the predictive value of these beads for sizing will depend both on the composition of the studied vesicles and on the FSC collection angles of the flow cytometer. The inclusion of various biological standards, e.g. virions, will increase the reliability of FSC-based size measurements.

In addition to the high-power 488-nm laser, the small-particle detector (SPD) equipped on the BD Influx contributes to the high sensitivity for forward scatter (FSC) detection. The SPD includes high-performance photo multiplier tubes (PMTs), which are more sensitive than the photodiodes used in many conventional flow cytometers. The lens of the SPD has a high numeric aperture and magnification factor, allowing forward scattered light to

be detected over a wider maximal angle than most conventional flow cytometers (wide-angle FSC). This improves the detection of nano-sized particles, which scatter light to larger angles (38, 43, 44). By increasing the minimal FSC detection angle (reduced wide-angle FSC), the signal-to-noise ratio could be further improved (38). By using these features, the reduced wide-angle FSC signal of 100-nm fluorescent polystyrene beads could be clearly detected above background levels, and 100- and 200-nm beads could be clearly detected as separate populations, further illustrating the high resolution for such small particles (42) (**Fig. 1b**). The reduced wide-angle FSC resolution was most optimal when using a large nozzle size (140 µm).

Side scatter (SSC, light scattered at 90°) has also been used for the analysis of small particles (45, 46). However, SSC is influenced to a higher degree than FSC by changes in the geometry and internal structures of small particles (44). Notably, in our hands, the resolving power (change in light scatter with particle size) was higher for the reduced wide-angle FSC compared with SSC (42). It should be noted, however, that FSC signals from nano-sized particles are not only determined by their size but also by other factors such as the refractive index and the shape of the particle (41, 43). Therefore, FSC signals can only be used for approximate and relative sizing of nano-sized particles (42) (**Box 2**).

To allow for interexperimental comparison of data, we implemented a strategy for calibration of the reduced wide-angle FSC, SSC and fluorescence signals. Fixed regions for 100-, 200- and 500-nm calibration beads in FSC/FL1 and FSC/SSC plots were defined and used to optimize the laser alignment at the start of each measurement (42) (see EQUIPMENT SETUP).

To summarize, flow cytometric detection of nano-sized particles requires high-power lasers, reduced wide-angle FSC measurements, a sensitive FSC detector (PMT) and fluorescence threshold triggering (42). In theory, these features can be installed on any high-end flow cytometer. The BD Influx has an open architecture and can therefore easily be modified for small-particle detection. The flow cytometer brand and type will determine whether these adaptations can be easily implemented.

General vesicle-labeling strategy

Uniform and bright fluorescent labeling is a prerequisite for fluorescence threshold-based analysis of individual nano-sized vesicles. We experimentally determined that the brightest labeling of vesicles was achieved using the fluorescent membrane intercalating dye PKH67 (42). By using this dye, the vast majority of vesicles produced in an *in vitro* DC culture could be detected, as evidenced by the fact that the density core of the vesicle population appeared well above the fluorescence threshold (42) (**Fig. 1c**). Indeed, slight lowering of the fluorescence threshold did not substantially increase the number of detected events. Although the current methodology heavily relies on efficient and homogeneous labeling

of vesicles, we cannot formally exclude the possibility that vesicles harboring much less PKH67 are missed using this method.

We noticed that removal of unbound dye from the labeled vesicle fractions was very important. Simple washing by pelleting the vesicles by ultracentrifugation was not sufficient to remove dye aggregates. Floatation of vesicles up into density gradients or sedimentation through block gradients using ultracentrifugation has previously been used to separate vesicles from protein aggregates (4, 47). We observed that floatation up into sucrose gradients was crucial for separating the vesicles from unbound dye and did not induce substantial aggregation of vesicles. Floatation of vesicles into a sucrose gradient also allowed the separation of vesicle subsets on the basis of their differential buoyant densities and their subsequent characterization by flow cytometry. To control for the presence of unbound dye aggregates and nano-sized membrane particles in fresh culture medium, control experiments should be performed. These should include the comparison of material sedimenting at 100,000g from equal volumes of cell culture supernatant and fresh culture medium. Notably, culture medium should always be prepared with fetal calf serum (FCS) depleted from cell-derived vesicles and large protein aggregates (see REAGENT SETUP). We have applied the current protocol to analyze vesicles derived from *in vitro* cultured DCs and T cells and different body fluids (see (42) and the current protocol). On the basis of these results, we expect that the protocol is suitable for the analysis of vesicles from a wide range of cellular sources, as long as they are uniformly stained for fluorescence threshold triggering. As an alternative approach, we tested various strategies for labeling parental cells, resulting in the release of fluorescently labeled vesicles. This circumvents the vesicle-labeling step and allows for the direct analysis of vesicles from the cell culture supernatant after removal of cells and cellular debris. However, we identified several shortcomings of this approach. In the case of labeling cells with cytoplasmic dyes, such as calcein and 5,6-carboxy-succinimidyl-fluoresceine ester (CFSE), we experienced that high cell labeling concentrations of the dye were required to obtain vesicles containing sufficient fluorescence to be detected above the fluorescence threshold. However, such high dye concentrations (e.g., 5 μM for CFSE) were detrimental to the function of immune cells. Moreover, the level of fluorescence of CFSE-labeled vesicles was much lower in comparison with PKH67-labeled vesicles and only vesicles high in FSC, which may represent larger vesicles, could be detected above the threshold (**Fig. 1d**). In addition, the fluorescence level of vesicles released from cells in which EGFP was expressed as soluble fluorescent protein under the control of the actin promoter (48) (a kind gift from R.E. Mebius, Vrije Universiteit Medisch Centrum, Amsterdam) was lower compared with PKH67-labeled vesicles. As a result, the majority of these GFP-labeled vesicles could not be detected above the threshold (**Fig. 1e**). Improved fluorescent labeling may in the future be achieved by GFP tagging of those proteins that

are specifically and constitutively sorted into vesicles.

In conclusion, we found that the PKH67 dye was optimal for obtaining brightly labeled vesicles, which were well detected above a fluorescence threshold that eliminated nonfluorescent noise. Purification of labeled vesicles by ultracentrifugation between sucrose layers or into sucrose gradients was crucial for separating vesicles from unbound dye.

Characterization by antibody labeling

In addition to the characterization of vesicles on the basis of light scatter and PKH67 fluorescence, vesicles can be further characterized by staining with fluorochrome-conjugated antibodies. This allows further identification of different vesicle subsets within heterogeneous pools of vesicles. The surface area of a vesicle is multiple orders of magnitude smaller than cells, which limits the overall labeling intensities. The ability to detect certain proteins is therefore largely dependent on the abundance of this

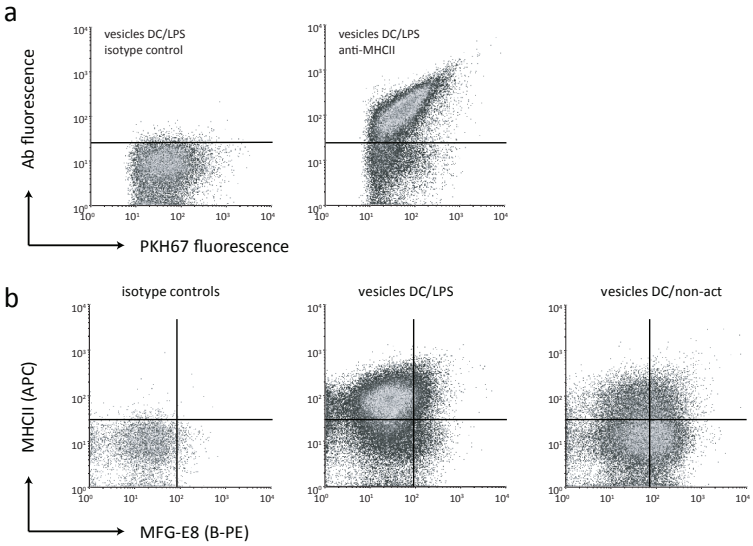

Figure 2 - Antibody-mediated detection of specific proteins on cell-derived vesicles Nano-sized vesicles released by nonactivated or LPS-activated mouse DCs and labeled with PKH67 were additionally stained with fluorochrome-labeled specific antibodies or isotype control antibodies and floated to equilibrium density into a sucrose gradient. The vesicles in the collected sucrose gradient fractions were measured using fluorescence threshold triggering. (**a**) Dot plots represent PKH67 labeling and isotype control (left) or anti-MHCII-R-PE (right) antibody (Ab) staining of vesicles derived from LPS-activated DCs (pools of 1.11–1.18 g ml^{-1} sucrose fractions). (**b**) Dot plots represent anti-MFG-E8 (B-PE-labeled)/anti-MHCII (APC-labeled) double-labeled vesicles derived from LPS-activated (middle plot) or nonactivated (right plot) DCs. As a negative control, vesicles were stained with rat APC-conjugated isotype control and B-PE–labeled rat anti-CD4. This figure is reprinted from ref. 42 with permission from Elsevier.

protein on the vesicle surface, the affinity of the antibody for this protein, the number of fluorochromes conjugated to the antibody and the brightness of fluorochromes. As a consequence, the presence of low-abundance proteins might be overlooked using the current methodology. We therefore aimed to use antibodies conjugated to the brightest available fluorochromes, such as B-phycoerythrin (B-PE) and R-PE, which have high extinction coefficients and quantum yields. By using an R-PE-conjugated antibody, we could detect MHCII on the surface of nano-sized vesicles from mouse DCs (**Fig. 2a**) (42). We experienced that antibodies conjugated to less-bright fluorochromes, such as allophycocyanin (APC) or Alexa Fluor 647, could be used only in case of sufficient abundance of proteins and high-affinity antibodies. To analyze heterogeneities in vesicle subsets, we combined an APC-labeled antibody against the highly abundant MHCII with a B-PE–labeled antibody specific to milk-fat globule-epidermal growth factor 8 (MFG-E8). This multicolor labeling strategy allowed us to demonstrate large differences in the protein composition of vesicle populations derived from lipopolysaccharide (LPS)-activated and nonactivated DCs (**Fig. 2b**) (42). Ongoing improvement of dyes and detectors over a broader range of the light spectrum will allow the detection of lower-abundance proteins and the use of lower-affinity antibodies.

Quantification of nano-sized vesicles and particles

The flow of particles is hydrodynamically focused in the center of the sheath fluid. This forces larger particles (e.g., cells) to pass the lasers one by one, which is needed for accurate quantification. Smaller particles such as nano-sized vesicles have a greater freedom of space in a core stream of the same diameter. This could allow the simultaneous passage of two or more particles through the laser beam. Furthermore, it enables the particles to pass at different interrogation positions of the laser. It was therefore crucial to analyze vesicle samples at low sample pressure. This reduced the core stream diameter and forced the nano-sized particles to pass the laser at a more-defined position. At rates below 10,000 events per second, relevant numbers of stored events could be combined with a relative low coincidence of particles. Furthermore, the electronics did not show relevant aborts at this rate.

By using these settings, we showed that nano-sized particles could be accurately quantified within a large range of concentrations (42). We tested this by measuring serial dilutions of 100-nm beads mixed with a fixed number of 200-nm reference beads (**Fig. 3a**). Care should be taken when using reference beads to spike biological samples. We found that some of the biological nanoparticles stuck to the reference beads, thereby hampering quantification. We therefore developed an alternative protocol for quantification that uses a fixed time frame (42) (see PROCEDURE). This allowed us to quantify absolute numbers of 100-nm beads over a broad range of concentrations (**Fig. 3b**). In addition, cell-derived

vesicles present in sucrose gradient fractions could be quantified using this time-based quantification protocol (**Fig. 3c**). For quantitative comparison of different samples, sheath and sample pressure must be optimized and kept constant, allowing the measurement of all samples within the constraints of the core diameter and the maximal accepted event rate.

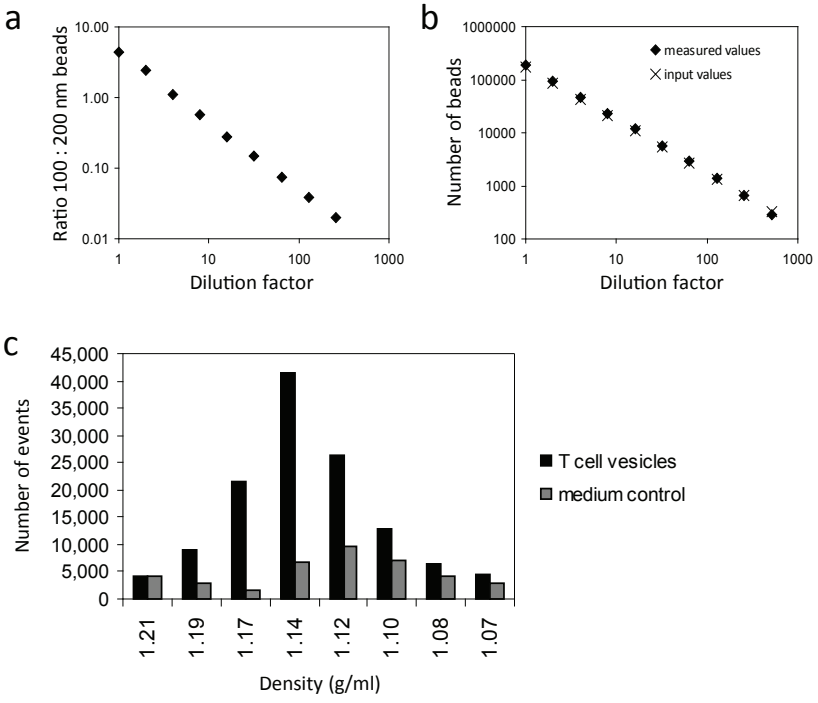

Figure 3 - Quantification of nano-sized beads and cell-derived vesicles by flow cytometric analysis (**a**) Serial twofold dilutions of fluorescent 100-nm beads were mixed with a fixed number of fluorescent 200-nm beads. Samples were measured using fluorescence threshold triggering, and the absolute numbers of 100- and 200-nm beads were analyzed. Expressed is the ratio of 100-nm beads versus 200-nm beads at each dilution (slope –0.9637 ± 0.064, R^2 = 0.999, as determined by linear regression). One representative experiment out of three is shown. (**b**) Serial twofold dilutions of fluorescent 100-nm beads were prepared and measured using fluorescence threshold triggering. The absolute number of beads measured in a fixed time window (30 s) was plotted against the dilution factor (slope −1.012 ± 0.012, R^2 = 1.00, as determined by linear regression). The measured values (black diamonds) are plotted together with the calculated amount of input beads ('×' symbol) on the basis of the specified concentration of beads in the stock solution. One representative experiment out of three is shown. (**c**) Time-based quantification of PKH67-labeled vesicles derived from $CD4^+$ T cells (black bars) detected in different sucrose gradient fractions. Indicated are the numbers of events measured in 30 s. Gray bars represent the number of events detected in control gradients containing 100,000g-sedimented material from fresh culture medium and unbound PKH67 aggregates. Panels **a** and **b** are reprinted from ref. 42 with permission from Elsevier.

Limited potential for sorting nano-sized vesicles

Although the use of a jet-in-air–based system opens up the possibility of sorting, the currently described adaptations of the flow cytometer for the analysis of nano-sized vesicles do not allow efficient sorting of these vesicles. The use of a large nozzle diameter and low pressure, necessary for improved detection of individual nano-sized particles, determines a large sort envelope compared with the size of the vesicle, while the drop frequency is low. This implies that sorts can only be performed at low event rates. Consequently, long sorting times will be required to obtain sufficient numbers of vesicles for further analysis. Furthermore, the sorted fraction will have an unfavorable low concentration of particles owing to the high volume of the sorted drop in relation to the size of the vesicle. To optimize the sorting of nano-sized vesicles, fine-tuning with smaller nozzle sizes and higher pressure will be necessary.

Materials

REAGENTS

- Cultured cells (e.g., mouse bone marrow–derived DCs and KO4C1 T cells (42)) or tissue or fluid sample (e.g., blood plasma from transgenic mice with EGFP under the chicken actin promoter (48))
- LPS from Escherichia coli (Sigma-Aldrich, http://www.sigmaaldrich.com/, cat. no. 62325)
- Deionized sterile water (purified with Millipore, http://www.millipore.com/, cat. no. Q-GARD2)
- PBS (without calcium or magnesium pH 7.2; Gibco, http://www.invitrogen.com/, cat. no. 20012-019)
- Albumin from bovine serum (Sigma-Aldrich, http://www.sigmaaldrich.com/, cat. no. A4503)
- PKH67 Green Fluorescent Cell Linker Midi Kit (including PKH67 and diluent C, Sigma www.sigmaaldrich.com cat.no. MIDI67-1KT) **CAUTION** PKH67 is highly flammable and evaporates quickly. Keep away from flame and seal tube containing dye with parafilm after use. Also protect PKH67 from bright direct light.
- Fetal calf serum (FCS) (Sigma, www.sigmaaldrich.com cat.no. F9665) **CRITICAL** Prepare 30% vesicle-free FSC in IMDM in advance (see REAGENT SETUP)
- Iscove's Modified Dulbecco's Media (IMDM) (Lonza, www.lonza.com, cat.no. BE12-726F)
- Sucrose (Mallinckrodt Baker, http://www.avantormaterials.com cat.no. 0334)
- Sodium azide (Merck, www.merck.com cat.no. 106688) **CAUTION** Sodium azide is toxic. Avoid skin contact and inhalation
- Anti-mouse MHCII (R-)PE-conjugated (eBioscience, www.ebiosience.com cat.no. 12-5321-83)
- Anti-mouse MHCII APC-conjugated (eBioscience, www.ebiosience.com cat.no. 17-5321-82)
- Rat IgG2b K Isotype Control (R-)PE-conjugated (eBioscience, www.ebioscience.com cat.no 12-4031-83)
- Rat IgG2b K Isotype Control APC-conjugated (eBioscience, www.ebioscience.com cat.no 17-4031-82)
- Anti-mouse MFG-E8 (MBL, www.mblintl.com cat.no. D161-3)
- Anti-mouse CD4 (eBioscience, www.ebioscience.com cat.no. 14-0041-81)
- Lightning-Link B-Phycoerythrin (B-PE) conjugation kit (Innova Bioscience, www.innova biosciences.com cat.no. 716-0010)

- Calibration beads: Yellow-Green Fluorescent FluoSpheres (Invitrogen, www.invitrogen.com cat. no. F8888)
- Fluoresbrite YG Carboxylate Microspheres 2.00 µm (Polysciences, http://www.polysciences.com cat. no. 09847)
- Cyto-Cal Multifluor plus Violet beads (Duke Scientific www.thermo.com cat.no. FC3MV)
- BD FACSRinse Solution (BD, www.bd.com cat.no. 340346)
- 10x DPBS without calcium or magnesium (Lonza, www.lonza.com cat.no. 17-515F)

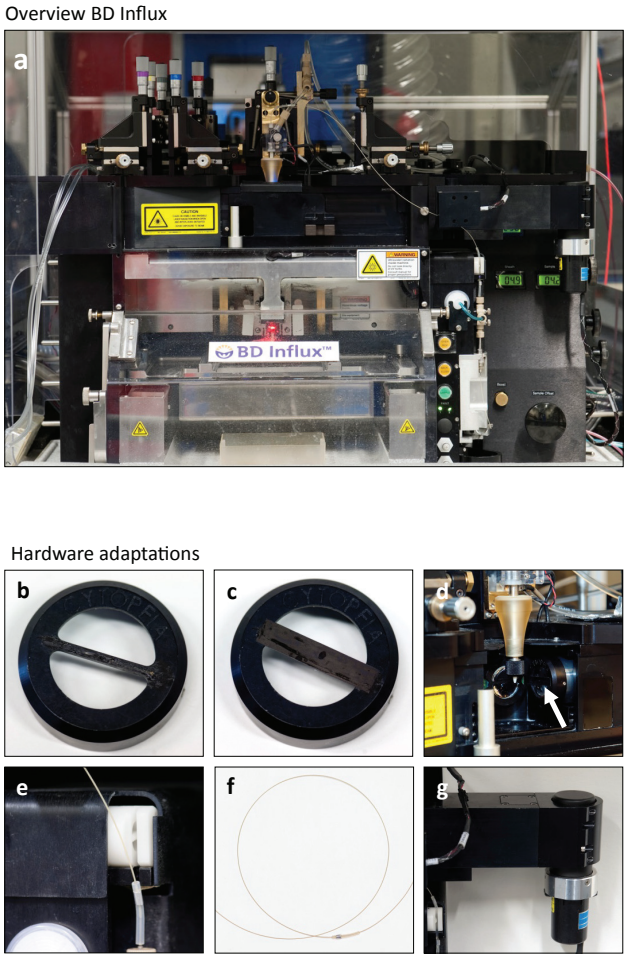

Figure 4 - Hardware adaptations of the BD Influx flow cytometer for analysis of individual nano-sized vesicles. (**a**) Overview of the BD Influx cell sorter. (**b**) Original FSC obscuration bar (2 mm in width). (**c**) Adapted obscuration bar (5 mm in width) placed over the original obscuration bar. (**d**) Adapted obscuration bar (indicated with white arrow) installed in front of the FSC lens. (**e**) Installed PEEK tubing without silicone tubing in front of the pinch valve. (**f**) PEEK tubing without silicone tubing. (**g**) FSC PMT after removal of the polarization unit.

EQUIPMENT

- 50 ml centrifuge tubes (Corning, www.corning.com cat.no. 430829)
- Polyallomer SW40 centrifuge tubes (14x95 mm, Beckman, www.beckmancoulter.com cat.no. 331374) **CRITICAL** The use of polyallomer instead of Ultra-clear centrifugation tubes is essential to prevent loss of vesicles due to sticking to the wall of the tube.
- Polyallomer SW28 centrifuge tubes (25x89 mm, Beckman, www.beckmancoulter.com cat.no. 326823)
- Polypropylene 5 ml tubes (BD Falcon, www.bdbiosciences.com cat.no. 352063)
- 1.5 ml safe-lock Eppendorf tubes (Eppendorf, www.Eppendorf.com cat.no. 0030120086)
- 3 ml plastic Pasteur pipette (Copan, www.copanswabs.com cat.no. 200C)
- 0.22 µm Millipore stericup filter (Sigma, www.sigmaaldrich.com cat.no. SCGPT05RE)
- Disposable capillary pipette 25 µl (Capilette Boehringer Mannheim, www.roche.com)
- Parafilm (Pechiney Plastic Packaging, www.parafilm.com cat.no. PM-996)
- Tissues (Satino, www.daxtrio.nl cat.no 170547)
- Balance with d = 0.001 g (Radwag www.radwag.pl cat.no. PS 510/C/1)
- Vacuum pump (using a vacuum line and a Sep-T-Vac container from Sherwood, Davis & Geck, www.covidien.com cat.no 8888-310052)
- Timer (Huger laboratory timer, cat.no. N388)
- Eppendorf centrifuge (Eppendorf, www.eppendorf.com cat.no. 5415R)
- Vortex (Scientific Industries, www.scientificindustries.com cat.no G-560E)
- Cell Culture Centrifuge (Beckman Coulter www.beckmancoulter.com Allegra X-12R)
- Centrifuge (Sorvall www.sorvallcentrifuge.co.uk, RC5B)
- SLA-600TC rotor for Sorvall (Thermo Fisher Scientific, www.thermofisher.com cat.no. 096-145001)
- Ultra centrifuge (Beckman Coulter www.beckmancoulter.com Optima LE-80K or L-90K)
- Ultra centrifuge rotors (Beckman Coulter www.beckmancoulter.com SW40 and SW28)
- Peristaltic pump (Medorex, www.medorex.com cat.no. TI/20 with 3 rollers and 1.6 x 1.6 tubing)
- Refractometer (Atago, www.atago.net)
- Beckton Dickinson (www.bd.com) Influx™ cell sorter (**Fig. 4**, purchased as Cytopeia Influx cell sorter), which was equipped by Cytopeia and BD with:
  - 488 nm (200 mW) laser (Coherent Sapphire, www.coherent.com cat.no. 488-200 CDRH)
  - 561 nm (100mW) laser (Cobolt Jive, www.cobolt.se cat.no. 561-04-01-100-300)
  - 635 nm (30 mW) Cube laser (Coherent, www.coherent.com cat.no. 1069410)
  - Small particle detector, containing a Mitutoyo Plan Apo 20x (NA 0.42) lens, a 0.7 mm pinhole and a polarization unit with two FSC PMTs
  - Optical filters (all from Semrock, Rochester, New York)
  - Amplifier board with 2 'fast' pre-amplifiers (0.12 µs) and 6 'slow' pre-amplifiers (1.2 µs)
  - Spigot software, version 6.1 (Beckton Dickinson www.bd.com)
- Modifications to the Influx™ cell sorter with (see EQUIPMENT SETUP):
  - Alternative tubing (IDEX Health & Science, www.idex-hs.com cat.no. 1542)
  - Sheath fluid nylon capsule filters 0.2 µm (Sterlitech, www.sterlitech.com cat.no. CNY0208RR)
  - Obscuration bar made out of paper tape and black marker
  - Pressure meter (Comark, http://www.comarkltd.com cat.no. C9557)

REAGENT SETUP

Preparation of 5% BSA stock solution and 0.2% BSA solution

Prepare a solution of 5% BSA (wt/vol) in sterile deionized water. Divide the solution over SW28 ultracentrifugation tubes (37 ml per tube). Spin solution in SW28 rotor at

100,000g at 4°C for 14-20 hrs to remove aggregates. After centrifugation carefully collect 30 ml solution from top, without disturbing the solution close to the pellet. Filter-sterilize through 0.22-µm Millipore filter. The 5% BSA stock solution can be stored at -20°C up to one year. Before each experiment dilute the 5% BSA stock solution in PBS to prepare a fresh 0.2% BSA solution.

Preparation of vesicle-free 30% fetal calf serum in IMDM

Prepare a solution of 30% fetal calf serum (FCS) (vol/vol) in Iscove's Modified Dulbecco's Media (IMDM). Divide the solution over SW28 ultracentrifugation tubes (37 ml per tube). Spin solution in SW28 rotor at 100,000g at 4°C for 14-20 hrs to remove serum-derived vesicles and large protein aggregates. After centrifugation carefully collect 30 ml solution from top, without disturbing the solution close to the pellet. Filter-sterilize through 0.22 µm Millipore filter. The 30% FCS stock solution can be stored at -20°C up to one year.

Conjugation of antibody with B-PE fluorochrome

Use the Innova Bioscience Lightning-Link B-PE conjugation kit (see manufacturer's instructions for details) to conjugate purified anti-MFG-E8 monoclonal antibody (MBL) and isotype control antibody (eBioscience) with B-Phycoerythrin (B-PE) at room temperature (21°C). In short, use 50 µg (= 50 µl of purified anti-MFG-E8) add 1 µl of LL-modifier reagent per 10 µl antibody and mix gently. Add antibody mixture to lyophilized Lightning-LinkTM mix and resuspend gently. Allow conjugation overnight at room temperature in the dark. Add 1 µl of LL-quencher reagent for every 10 µl of antibody used. The conjugated antibody can be used after 30 minutes.

Pre-spinning and dilution of antibodies

Spin antibodies prior to use for 5 min at 16,000g to pellet large aggregates. Use 0.5 µg antibody (cleared from aggregates) diluted in 20 µl 0.2% BSA solution per vesicle pellet, derived from 10 ml cell culture supernatant. **CRITICAL** Large antibody aggregates could cause aggregation of vesicles (49).

Preparation of PKH67 solution in diluent C

Use 1.5 µl PKH67 diluted in 100 µl diluent C for 100,000g sedimented material derived from 10 ml cell culture supernatant. When staining more than one sample, make a stock solution of PKH67 in diluent C in an Eppendorf tube. Vortex solution gently and pipette 100 µl per sample in separate SW40 ultra centrifuge tubes. **CRITICAL** Make the solution just before staining.

Preparation of 2.5M sucrose stock solution

Use 427.9 g of sucrose to make a stock solution of 500 ml 2.5 M sucrose. Dissolve sucrose

in 200 ml sterile deionized water in a beaker while stirring. Seal with parafilm and heat the sucrose solution (max. 60°C) to speed up the process. This results in a saturated solution in which the sucrose crystals will no longer dissolve. Transfer the solution to a graduated cylinder, to determine the remaining volume of sterile deionized water that should be added. Use this volume to flush remaining sucrose from the beaker and add to the sucrose solution. Allow the sucrose to dissolve completely. Filter the solution through a 0.22 µm Millipore stericup filter and store at 4°C up to half a year. **CRITICAL** It takes up to 24 hrs to prepare this solution.

Preparation of sucrose gradient fractions

Make 25 ml of a 2.0 M sucrose stock solution by mixing 20 ml of 2.5 M sucrose solution with 2.5 ml 10x PBS and 2.5 ml sterile deionized water. Make 25 ml of a 0.4 M sucrose stock solution by mixing 4 ml of 2.5 M sucrose with 2.5 ml 10x PBS and 18.5 ml sterile deionized water. When sucrose samples need to be stored longer than 2 days, add 0.02% (wt/vol) sodium azide to 2.0 M and 0.4 M stock solutions and store up to 3 months at 4°C. Make sucrose gradient fractions by mixing the 2.0 M and 0.4 M sucrose stock solutions according to **Table 1**. The volumes in **Table 1** are sufficient for 2 sucrose gradients.

Table 1 - Sucrose gradient fraction preparations

fraction	Sucrose (M)	2.0 M sucrose volume (ml)	0.4 M sucrose volume (ml)
1	1.886	1.857	0.143
2	1.771	1.714	0.286
3	1.657	1.571	0.429
4	1.543	1.429	0.571
5	1.429	1.286	0.714
6	1.314	1.143	0.857
7	1.200	1.000	1.000
8	1.086	0.857	1.143
9	0.971	0.714	1.286
10	0.857	0.571	1.429
11	0.743	0.429	1.571
12	0.629	0.286	1.714
13	0.514	0.143	1.857
14	0.400	0.000	2.000

The molarities of the different fractions are calculated based on the volumes of 0.4 and 2.0 M sucrose solutions that are mixed.

EQUIPMENT SETUP

Configuration of pulse processing channels

The PMTs that provide the signals for fluorescence threshold triggering and FSC are connected to the first two channels on the amplifier board (using a short time constant of 0.12 µs). All the other fluorescence and side scatter PMT signals are connected to channels with a time constant of 1.2 µs. For the first fluorescence (triggering) signal it is necessary to use a fast pulse processing channel, whereas reduced wide-angle FSC can also be measured in slow pulse processing channels.

Making an obscuration bar

The original obscuration bar of the BD Influx is 2 mm in width. To be able to reduce the forward scatter detection at lower angles, we created an obscuration bar of 5 mm using paper tape stained black with a permanent marker pen and placed it over the original obscuration bar (**Fig. 4b-d**). We thereby raised the minimal detection angle for FSC from 2° to 15°, allowing 15°-25° reduced wide-angle FSC detection. **CAUTION** This extra obscuration bar is not compatible with high energy wavelength (355 nm) laser light, which can burn holes in the paper tape.

Tubing

The standard configuration of the Influx has a sample line that consists of PEEK tubing interrupted by a small part of silicon tubing, where a pinch valve can block back flush during sample change. We found that small particles were trapped in this small silicon tube and released at later stages, leading to cross-contamination of samples. We solved this by replacing the sample line with a line that consisted of PEEK tubing only (**Fig. 4e-f**). A consequence of this tubing is that there will be a back flush once there is no sample tube mounted. Cross-contamination between measurements was prevented by extensive washing procedures as described in PROCEDURE Steps 67 - 72.

Other hardware adaptations

The small particle detector consists of a FSC lens with a high numeric aperture and magnification factor and a unit to measure polarization differences on two high performance PMTs (**Fig. 5a**). We improved the sensitivity of the SPD by removing the polarization unit and allowing all the FSC light to reach one PMT in the same optical axis as the direction of the laser, thus rendering a modified SPD with a high numerical aperture microscope lens, a pinhole, and only one PMT (**Fig. 4g and 5b**). Additionally, neutral density filters in front of the FSC PMT were removed to increase the amount of scattered light along the light path and a 488/10 bandpass filter was mounted in front of the FSC PMT.

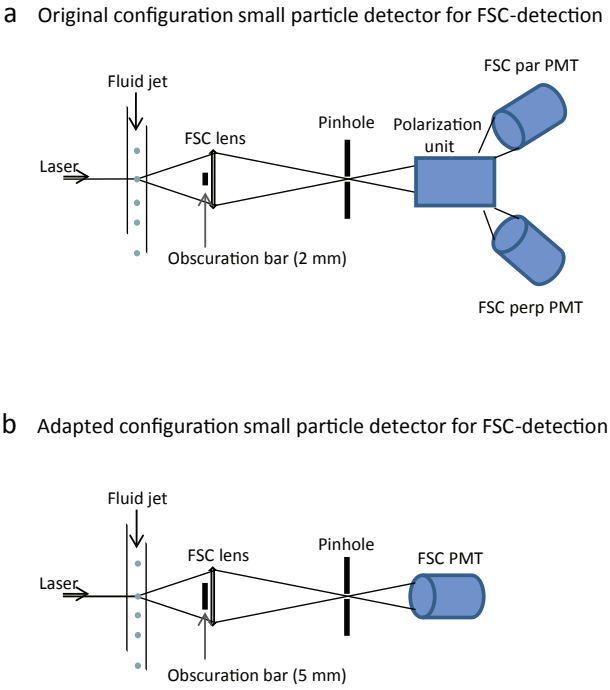

Figure 5 - Modified BD Influx configuration for reduced wide-angle FSC detection (**a**) Schematic representation of FSC detection using the small-particle detector (SPD) equipped on the BD Influx. This SPD consists of a FSC lens with a high numeric aperture and magnification factor and a unit for measuring polarization differences on two high-performance PMTs. Light is focused on a pinhole placed in front of the polarization unit to reduce the amount of unwanted light collected. (**b**) Adapted configuration for FSC detection as it is used in this protocol. The polarization block was removed, allowing all the FSC light to reach one PMT in the same optical axis as the direction of the laser. In addition, the width of the obscuration bar is increased for reduced wide-angle FSC detection. Par, parallel; perp, perpendicular.

Laser configuration

The BD Influx has flexible modular illumination and detection systems and uses an analogue triggering system. Therefore, the laser used for fluorescence threshold triggering needs to be the first laser to excite the particle of interest. For multi laser setup, we chose the largest possible distance between pinholes in order to prevent cross contamination of laser and fluorescence light. We chose pinhole 1 for the first (488 nm), pinhole 3 for the second (561 nm) and pinhole 5 for the third laser (635 nm) (**Fig. 6a**). The 561 nm laser was focused on the 3rd pinhole and all reflective mirrors in the light path behind this pinhole were shifted aside, thereby allowing the fluorescence light to reach the PMT in a straight line. The laser configuration as described in **Table 2** was used and the lasers were aligned at the start of each measurement as described in PROCEDURE Steps 41 - 50.

Calibration gates for laser alignment

Gates were created for the positioning of calibration beads (yellow-green fluorescent FluoSpheres) in FSC/FL1 and FSC/SSC dot plots (all parameters were displayed in logarithmic scale), and used for the alignment of the 488 nm laser at the start of each measurement. Calibration gates were set such that 100 nm beads appeared well above the fluorescent threshold level. The gates for 200 nm and 500 nm beads were positioned relative to the 100 nm gate as described in **Table 3** by using the procedure described in **Box 3**. **Fig. 6b** shows an example of the calibration gates in FSC/FL1 and FSC/SSC dot plots. This strategy ensured comparable FL1 fluorescence and light scatter measurements between experiments.

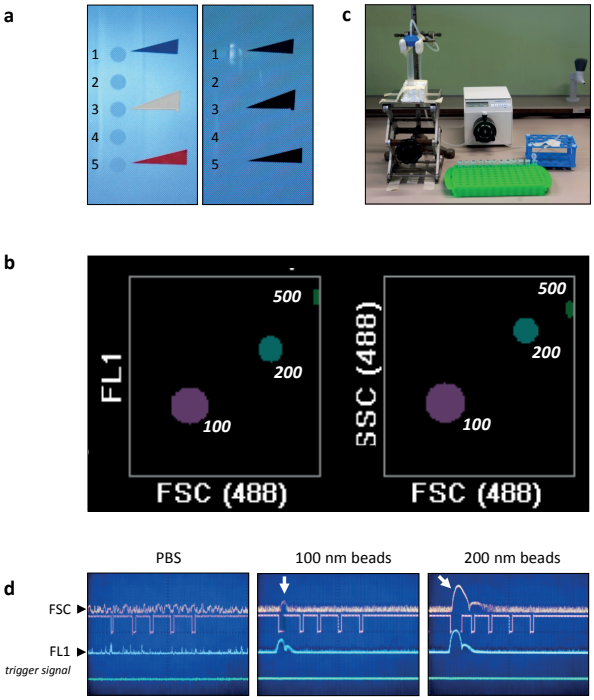

Figure 6 - Influx settings and sucrose gradient fraction collection setup (**a**) Camera view of five pinholes in front of the SSC and fluorescence PMTs (left) and of the fluorescent flash derived from yellow-green fluorescent beads in front of the first pinhole (right). (**b**) Screen print of the Spigot 6.1 software showing 100-, 200- and 500-nm calibration gates in FSC/FL1 (left) and FSC/SSC (right) dot plots. All axes are in four-decade logarithmic scale. (**c**) Overview of the sucrose gradient fraction collection setup. A disposable capillary pipette is connected to the tubing of a peristaltic pump. Fractions are collected in microcentrifuge tubes. (**d**) Electronic pulses derived from FSC and FL1 PMTs are displayed on a digital storage oscilloscope produced by PBS (background; left), fluorescent 100-nm beads (middle) or 200-nm beads (right). A clear FSC pulse could be detected above background signals for 100- and 200-nm beads (white arrows).

Box 3 | Creating calibration gates for laser alignment

The directions below should be followed to define fixed regions for 100, 200, and 500 nm calibration beads in FSC/FL1 and FSC/SSC plots, which can be used to optimize the laser alignment at the start of each measurement.

1. *Run fluorescent 100 nm Fluosphere beads.*
2. *Fine-tune 488 nm laser alignment once more to obtain the highest FL1 and scatter signals with the lowest coefficient of variation (CV).*
3. *Make sure that for each parameter a pulse can be seen above background signals on the oscilloscope (**Fig. 6d**).*
4. *To anticipate on the size distribution of the extracellular vesicles, position the 100nm beads in the lower left quadrant of the FSC/FL1 and FSC/SSC dot plot, well above the threshold level. Set a gate around the 100 nm bead position in both dot plots.*
5. *Relate the 200 nm and 500 nm bead gates to this 100 nm gate as described in **Table 3** of Equipment set-up. Note that for FSC the 500 nm beads wi- ,0ll fall off the scale. An example of our gate positions can be found (**Fig. 6b**).*
6. *Once gates have been created, continue with step 55 of the main PROCEDURE.*

Table 2 - Lasers and PMT configuration

Laser	PMT	Pinhole	Filters	Time constant amplifier	Power (Volt)
488nm	FL1 detector	1	528/38	0.12 µs	613
	SSC detector	1	488/10	1.2 µs	688
	FSC detector	FSC	488/10	0.12 µs / 1.2 µs	484 / 473
561nm	FL7 detector	3	585/42	1.2 µs	1004
635nm	FL6 detector	5	670/30	1.2 µs	888

Table 3 - Relative FL1, FSC and SSC signals of calibration beads

	100 nm → 200 nm	200 nm → 500 nm
FL1	15x	17x
FSC	67x	16x *500 nm beads fall of scale*
SSC	51x	4x

Sample and sheath pressure

Sheath pressure was set at 5.0 psi and sample pressure at 4.2 psi, allowing a flow rate of 20 µl per minute. For absolute quantification of particles the flow rate should be accurately determined on each individual machine. Sheath and sample pressures were regularly checked with an external pressure meter.

Delay time for Ab detection on vesicles

Within the sample stream of a flow cytometer, particles pass different laser beams after which scattered light and fluorescence signals will be captured by PMTs. In order to relate fluorescence and scattering signals of individual particles, the different signals generated upon passage of the same particle along the different laser beams should be interrelated. Hereto, the time delay between a vesicle passing the first and the second and possible third laser beam has to be defined. This delay time is dependent on the velocity of the particle within the sample stream, the sheath and sample pressure, and the particle type. We experienced that the time delay for particles passing the first laser (used for fluorescence threshold triggering) and subsequent laser beams was different for beads and cell-derived vesicles. For optimal detection of the fluorescently labeled antibodies bound to vesicles, this time delay should be fine tuned using PKH67 and antibody-labeled vesicles instead of beads (see PROCEDURE Steps 56 - 61).

We sometimes observed that part of the vesicle population negative for antibody labeling located on the base line instead of in the first decade of fluorescence. The relatively low auto-fluorescence levels of nano-sized vesicles may explain the complete lack of signal for some antibody-negative vesicles on subsequent PMTs.

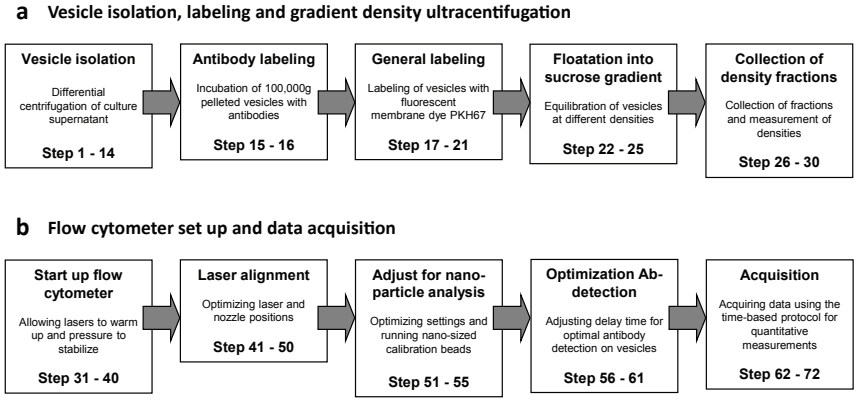

Figure 7 - Flow diagram of procedure steps (**a**,**b**) Flow diagram outlining the vesicle isolation, labeling and gradient density ultracentrifugation (**a**), and the flow cytometer setup and data acquisition (**b**). Corresponding PROCEDURE step numbers are included.

Procedure

Isolation of nano-sized extracellular vesicles • TIMING 3 hrs

1. Culture cells in culture medium with vesicle-free serum for a relevant amount of time. For DC-derived nano-sized vesicles we typically culture 3 x 10^6 DC in 12.5 ml vesicle-free culture medium for 20 hrs. A start volume of 12.5 ml cell culture supernatant is needed to obtain 10 ml 10,000g supernatant in step 12. A flow diagram summarizing the PROCEDURE steps is depicted in **Fig. 7**. **CRITICAL STEP** For vesicles in body fluids, different isolation procedures might be required. Isolate the vesicles using the preferred method and then proceed with step 17 to label the 100,000g vesicle pellet.
2. Harvest cell culture supernatant in a 50 ml tube.
3. Spin supernatant at 200g for 10 min at 4°C.
4. Retain and pour the supernatant into a new 50 ml tube and discard the pellet.
5. Repeat steps 3 and 4 once more.
6. Spin supernatant at 500g for 10 min at 4°C.
7. Retain and pour the supernatant into a new 50 ml tube and discard the pellet.
8. Repeat steps 6 and 7 once more. **CRITICAL STEP** The four low speed centrifugation steps (steps 3-8) are required to prevent the release of small vesicles as a consequence of cell damage that could occur at higher g-forces and to ensure complete removal of cells from the supernatant.
9. Spin supernatant at 10,000g for 30 min at 4°C using a SLA-600TC rotor in the Sorvall RC5Bplus centrifuge. Alternatively, the supernatant can be spun at 10,000g in SW40 buckets in an ultracentrifuge.
10. Retain and transfer 10 ml supernatant to polyallomer SW40 centrifuge tube. **CRITICAL STEP** Do not disturb the 10,000g pellet to prevent contamination of the supernatant with the pelleted material.
11. Fill up the tubes with IMDM and tare tubes in opposing rotor-buckets.
12. Pellet the vesicles by ultracentrifugation in a SW40 rotor at 100,000g for 65 min at 4°C. Use maximal acceleration and deceleration.
13. Aspirate off and discard all supernatant while decanting the ultra centrifuge tube. **CRITICAL STEP** Keep the tube upside down after aspiration to prevent back flush of residual fluid onto the pellet and continue immediately with steps 14 and 15.
14. Dry the walls of the tube using a Kleenex tissue. **CRITICAL STEP** For quantitative recovery of the pelleted material, make sure not to touch the vesicle pellet.

Labeling and floatation of vesicles up into a sucrose density gradient • TIMING 16 – 22 hrs

15. Resuspend the 100,000g pellet (from step 14) in 20 µl PBS with 0.2% BSA containing

the preferred antibody (0.5 µg) by pipetting the fluid up and down at least 10 times. When labeling with antibodies is not required, resuspend in 20 µl PBS with 0.2% BSA only and proceed directly to step 17.

16. Seal the ultra centrifuge tube with parafilm. Incubate the vesicles with the antibody suspension for 1 hour in the dark at room temperature. Flick the tubes to mix every 10 min. **CRITICAL STEP** Apply a 1 hour antibody incubation step to achieve maximal epitope binding. Control for nonspecific binding by incubating parallel samples with isotype control antibodies under similar conditions. **CRITICAL STEP** Bright fluorochrome-coupled antibodies are required for efficient staining. The use of quantum dot-coupled antibodies is not recommended since binding of such antibodies to vesicles dramatically changes their buoyant density. In addition, the multivalency of quantum dots causes the vesicles to aggregate.
17. Dilute PKH67 in diluent C as described in REAGENT SETUP. Dilute 1.5 µl PKH67 in 100 µl diluent C for every sample. Put 100 µl of the diluted PKH67 in a new SW40 ultracentrifuge tube.
18. Add 80 µl diluent C (without PKH67) to the vesicles resuspended in PBS with 0.2% BSA (from either Step 15 or Step 16). Mix by pipetting up and down 3 times.
19. Transfer the vesicles mixed with diluent C (from step 18) to the new SW40 tube containing PKH67 in diluent C (from step 17). Mix by pipetting up and down 5 times. **CRITICAL STEP** Make sure to add the vesicles to the dye (and not the other way around) to obtain homogeneous labeling.
20. Allow the PKH67 to incorporate into the lipid bilayers of the vesicles by incubating for 3 min at room temperature.
21. Stop the labeling reaction by adding 100 µl IMDM containing 10% vesicle-free FCS.
22. Add 1.5 ml 2.5 M sucrose to the stained vesicles and mix by vortexing gently for 5 sec to homogenize the solution.
23. Build a linear sucrose gradient by carefully adding 700 µl of fractions 1-14 (see **Table 1**) on top of the vesicle sucrose mixture. Layering is most convenient using a plastic Pasteur pipette.
24. Place a second sucrose gradient in the opposing bucket. Tare sucrose gradients in opposing rotor-buckets by adding extra volume of sucrose gradient fraction 14.
25. Allow the vesicles to reach their equilibrium density by spinning the sucrose gradients in an SW40 rotor at 192,000g at 4°C for 14-20 hrs. Start and stop centrifuge with slow acceleration and deceleration to prevent disturbance of the gradient. **CRITICAL STEP** Vesicles released by different cell types are heterogeneous and the centrifugation time needed to reach equilibrium density should be determined for each vesicle population of interest.
26. Carefully lower a disposable capillary pipette connected to the tubing of a peristaltic

pump (**Fig. 6c**) into the sucrose gradient to 1 mm above the bottom of the tube.

27. Start the pump and collect 1 ml gradient fractions in Eppendorf tubes.
28. Vortex each collected fraction for 5 sec. **PAUSE POINT** In our experience, samples can be stored for up to 4 days in the refrigerator without loss of quality.
29. Measure densities of the collected sucrose fractions using a refractometer.
30. For measurement on the flow cytometer, dilute sucrose gradient fractions at least 20x in PBS. Use ≥ 20 µl of the gradient fractions for accurate pipetting of high density sucrose solutions.

Start up flow cytometer • TIMING 1-3 hrs

31. Fill sheath tank with 1x PBS (dilute 10x PBS with sterile deionized water). **CRITICAL STEP** Replace entire volume of sheath fluid when measurements are performed directly after high pressure sorting.
32. Close sheath tank and apply pressure up to 5 PSI.
33. Allow pressure to equilibrate 30 min.
34. Switch on the 561 nm laser. Allow the laser to stabilize for 3 hrs.
35. Switch on the 488 nm laser. Allow the laser to stabilize for 1 hour. After one hour, adjust power to allow 95% of maximum output.
36. Place 140 µm nozzle on nozzle head.
37. Flush nozzle head and 140 µm nozzle with 70% ethanol to remove air bubbles.
38. Run cytometer with PBS to wash out ethanol.
39. Adjust the height of the nozzle. Move the nozzle up until it is just out of view of the camera showing the image of the 5 fluorescence-pinholes (**Fig. 6a**, left panel).
40. By guidance of the camera image, move fluid stream into the correct position in front of the pinholes.

Laser alignment • TIMING 15 min

41. Start Spigot software.
42. Select FL1 fluorescence on the first pinhole (488 nm excitation; 528/38 nm emission) as trigger channel.
43. Run yellow-green fluorescent beads (2 µm). Check the presence of a fluorescent flash in front of the first pinhole and adjust FL1 PMT voltage to observe dots in the middle of a FSC/FL1 dot plot.
44. Carefully move 488 nm laser position forward and backward and observe the position of the beads in the dot plot. By moving the laser position, try to maximize the signal. After that, move the forward/backward position of the nozzle assembly to maximize signal. Repeat this iterative process until no further improvement is obtained. **CRITICAL STEP** visually check if there is a well-focused sharp flash in the camera view of the fluorescence pinholes (**Fig. 6a**, right panel). In case of a blurry flash, the fluorescence

emission is not focused optimally on the pinhole.

45. Maximize the signal further by carefully moving the laser position up and down. **CRITICAL STEP** Once the fluorescence signal for the first laser is optimal, do not move the nozzle position anymore. All other lasers should be optimized relative to the position of the 488 nm laser and fluid jet.
46. Move the position of the forward scatter lens to optimize FSC signal. Focus the fluorescent flash on the FSC pinhole by guidance of the camera that shows the image of the FSC pinhole.
47. Run Cyto-Cal Multifluor plus Violet beads. Check the flash in front of the 3rd pinhole.
48. Observe the delay time on the oscilloscope and adjust if necessary. The 561 nm is in front of the 3rd pinhole and the signal should fall in the third delay bucket on the scope. Adjust the delay time if necessary. **CRITICAL STEP** The delay time needs to be fine tuned later using antibody-labeled vesicles (see steps 56 - 61).
49. Position the 561 nm laser in such a way that a maximum signal is obtained for the fluorescent beads while inspecting a corresponding dot plot.
50. Repeat steps 48 - 49 for the 635 nm laser in front of the 5th pinhole.

Flow cytometer settings and calibration for nano-particle analysis • TIMING 15 min - 2 hrs

51. Close blinds to reduce noise signals from incident light.
52. Set sheath pressure at 5 psi and sample pressure at 4.2 psi.
53. Run a sample of filtered PBS. Set threshold on FL1 fluorescence channel such that a maximum of 10 events per second is observed. **?TROUBLESHOOTING?**
54. If calibration gates for laser alignment have not already been created, carry out instructions in **Box 3** before proceeding with step 55. Otherwise, continue directly to step 55.
55. Run 200 nm Fluosphere calibration beads. Fine-tune the alignment of the 488 nm laser to optimize FSC, SSC and FL1 signals based on the Calibration gates (as described in Equipment setup). Check if 100 nm and 500 nm beads also fall within the calibration gates. **?TROUBLESHOOTING?**

Optimization of fluorochrome-conjugated Ab-detection on nano-sized vesicles • TIMING 10 min

56. Use the 561 nm laser for the detection of R-PE- or B-PE-conjugated antibodies and the 635 nm laser for detection of APC- or alexa647-conjugated antibodies.
57. Run a sample with vesicles stained with PKH67 and labeled with an isotype control-antibody.
58. Set the corresponding PMT to place the vesicles in the first decade of fluorescence.
59. Set a cross hair in the PKH67 versus antibody fluorescence dot plot, which allows

separation of vesicles positive and negative for antibody labeling.

60. Run a positive control sample containing vesicles displaying high levels of antibody staining.
61. Optimize delay time for the PMT detecting PE-fluorescence to reach the highest percentage of positive events.

Acquisition • TIMING 1.5 min per sample

CRITICAL: To ensure quantitative measurements, perform sample measurements exactly as follows:

62. Install sample tube
63. Boost system (10 psi) for 5 sec
64. Allow the pressure to stabilize for 30 sec
65. Acquire sample data for 30 sec. Do not measure more than 10,000 events per second. **?TROUBLESHOOTING?**
66. Remove sample tube
67. Back flush 2 or 3 drops of fluid
68. Install tube with FACS rinse solution
69. Flush by running FACS rinse solution for 5 sec in boost mode. Running 5 sec in boost mode is sufficient to replace all the fluid in the sample line.
70. Install tube with PBS
71. Flush by running PBS for 5 sec in boost mode
72. Back flush 2 or 3 drops

Timing

step 1 – step 14, vesicles isolation: 3 hrs
step 15 – step 16, antibody labeling: 1 hr
step 17 – step 21, general labeling of vesicles: 15 min
step 22 – step 24, building 2 sucrose gradients: 30 min
step 25, floating vesicles to equilibrium density: 14-20 hrs
step 26 – step 30, collecting and diluting sucrose density fractions: 30 min
step 31 – step 40, warm up lasers and start up flow cytometer: 1-3 hrs
step 41 – step 50, flow cytometer configuration and laser alignment: 15 min
step 51 – step 55, optimizing settings and running nano-sized calibration beads (after calibration gates have been created): 15-30 min
step 56 – step 61, optimization antibody detection on vesicles: 10 min
step 62 – step 72, sample acquisition including washing steps: 1.5 minute per sample

Troubleshooting

Table 4 - Troubleshooting table

Step	Problem	Possible reason	Solution
53	Too many events while running PBS with normal threshold settings	Contaminating light	Close blinds
		Air bubbles in nozzle assembly	Flush the whole system with ethanol and then with PBS
		Air bubbles in sheath fluid	Replace sheath fluid
		Contaminated PBS	Use a fresh bottle of PBS
55	Low FSC / fluorescence signals obtained from calibration beads	Suboptimal laser alignment	Align lasers again
65	Event rate of >10,000 per second while running sample and number of events keeps increasing	Unbound dye	Spin stained vesicles into a sucrose gradient or between 2 sucrose layers to get rid of unbound dye. The three bottom fractions of the sucrose gradient may contain unbound dye. It is best to exclude these fractions from the analysis
	Event rate of >10,000 per second while running sample	Particle concentration too high	Make several dilutions of the sample and check if number of events per second decrease concordantly. If not, the sample is most likely contaminated with unbound dye
	Too many events in control gradient with fresh culture medium and PKH67	Contamination of serum-derived vesicles	Ultracentrifuge 30% serum solution used for preparation of culture medium overnight at 100,000g
		Large aggregates of PKH67	Buy new stock of PKH67

Anticipated results

This protocol enables the quantitative and qualitative analysis of individual nano-sized cell-derived vesicles. By using an optimized fluorescent vesicle-labeling strategy, a few straightforward modifications to the commercially available BD Influx flow cytometer and fine-tuning of the flow cytometer settings, this method will allow the discrimination of ~100-nm-sized vesicles from noise (**Fig. 1a**). In addition, 100- and 200-nm-sized particles can be visualized as separate populations (**Fig. 1b**). Bright labeling of vesicles with the PKH67 membrane dye is essential for the discrimination of vesicles from nonfluorescent noise. In our hands, vesicles released by fluorescently labeled parental cells did not harbor enough fluorescence for flow cytometric detection (**Fig. 1d,e**). With the described method, integrated information can be obtained for individual fluorescently labeled nano-sized vesicles regarding their buoyant density (**Fig. 3c**), light scattering (**Fig. 1c**) and binding of different fluorochrome-conjugated antibodies (**Fig. 2**). In addition, this method allows the accurate and reproducible quantification of particles as small as 100 nm in size (**Fig. 3**). In the current protocol, the effectiveness of fluorescent antibody–mediated detection of proteins on individual vesicles is dependent on the abundance of the protein, the affinity of the antibody and the brightness of the fluorochrome coupled to the antibody (**Fig. 2**). Multicolor antibody labeling of abundant proteins present on vesicles is possible and allows for more detailed characterization of heterogeneous vesicle populations (**Fig. 2b**). As no optimized procedures for sorting vesicle populations are available yet, the current method can be combined with other techniques in order to obtain further information on vesicle subpopulations (e.g., on their morphology or RNA contents). Flow cytometric data on the presence of specific proteins on vesicle subpopulations could, for example, be used to design immunoaffinity beads on which specific vesicle populations can be absorbed. Positively or negatively selected vesicle subpopulations can thereafter be analyzed by electron microscopy or atomic force microscopy, or they can be further processed for proteomics, lipidomics or RNA analysis.

Acknowledgements

We thank H.C.H. Mertens, B.J. Bosch, W. Bartelink, E. Mastrobattista, E.V.B. van Gaal, M. Aalberts, and R.E. Mebius for providing reagents, experimental support and/or valuable discussion for validation of the method, and H. de Boer-Brouwer for technical assistance. We thank T. van Haeften, R.W. Wubbolts, and J. van der Lit for critical reading of the manuscript.

References

1. Cocucci, E., Racchetti, G. & Meldolesi, J. Shedding microvesicles: artefacts no more. Trends in cell biology 19, 43-51 (2009).
2. Thery, C., Ostrowski, M. & Segura, E. Membrane vesicles as conveyors of immune responses. Nature reviews 9, 581-93 (2009).
3. Bobrie, A., Colombo, M., Raposo, G. & Thery, C. Exosome secretion: molecular mechanisms and roles in immune responses. Traffic 12, 1659-1668 (2011).
4. Raposo, G. et al. B lymphocytes secrete antigen-presenting vesicles. J. Exp. Med. 183, 1161-1172 (1996).
5. Subra, C. et al. Exosomes account for vesicle-mediated transcellular transport of activatable phospholipases and prostaglandins. J. Lipid Res. 51, 2105-2120 (2010).
6. Valadi, H. et al. Exosome-mediated transfer of mRNAs and microRNAs is a novel mechanism of genetic exchange between cells. Nat. Cell Biol. 9, 654-659 (2007).
7. Caby, M. P., Lankar, D., Vincendeau-Scherrer, C., Raposo, G. & Bonnerot, C. Exosomal-like vesicles are present in human blood plasma. Int. Immunol. 17, 879-887 (2005).
8. Taylor, D. D. & Gercel-Taylor, C. MicroRNA signatures of tumor-derived exosomes as diagnostic biomarkers of ovarian cancer. Gynecol. Oncol. 110, 13-21 (2008).
9. Sahlen, G. E. et al. Ultrastructure of the secretion of prostasomes from benign and malignant epithelial cells in the prostate. Prostate 53, 192-199 (2002).
10. Aalberts, M. et al. Identification of Distinct Populations of Prostasomes That Differentially Express Prostate Stem Cell Antigen, Annexin A1, and GLIPR2 in Humans. Biol. Reprod. 86, 82, 1-8 (2012).
11. Pisitkun, T., Shen, R. F. & Knepper, M. A. Identification and proteomic profiling of exosomes in human urine. Proc. Natl. Acad. Sci. U. S. A. 101, 13368-13373 (2004).
12. Hoorn, E. J. et al. Prospects for urinary proteomics: exosomes as a source of urinary biomarkers. Nephrology (Carlton) 10, 283-290 (2005).
13. Palanisamy, V. et al. Nanostructural and transcriptomic analyses of human saliva derived exosomes. PLoS One 5, e8577 (2010).
14. Gonzalez-Begne, M. et al. Proteomic analysis of human parotid gland exosomes by multidimensional protein identification technology (MudPIT). J. Proteome Res. 8, 1304-1314 (2009).
15. Admyre, C. et al. Exosomes with immune modulatory features are present in human breast milk. J. Immunol. 179, 1969-1978 (2007).
16. Lasser, C. et al. Human saliva, plasma and breast milk exosomes contain RNA: uptake by macrophages. J. Transl. Med. 9, 9 (2011).
17. Clayton, A. & Mason, M. D. Exosomes in tumour immunity. Curr. Oncol. 16, 46-49 (2009).
18. Beyer, C. & Pisetsky, D. S. The role of microparticles in the pathogenesis of rheumatic diseases. Nat. Rev. Rheumatol. 6, 21-29 (2010).
19. Mathivanan, S. & Simpson, R. J. ExoCarta: A compendium of exosomal proteins and RNA. Proteomics 9, 4997-5000 (2009).
20. Keller, S., Ridinger, J., Rupp, A. K., Janssen, J. W. & Altevogt, P. Body fluid derived exosomes as a novel template for clinical diagnostics. J. Transl. Med. 9, 86 (2011).
21. Escudier, B. et al. Vaccination of metastatic melanoma patients with autologous dendritic cell (DC) derived-exosomes: results of thefirst phase I clinical trial. J. Transl. Med. 3, 10 (2005).
22. Chaput, N. et al. The potential of exosomes in immunotherapy of cancer. Blood Cells Mol. Dis. 35, 111-115 (2005).
23. Viaud, S. et al. Dendritic cell-derived exosomes for cancer immunotherapy: what's next? Cancer Res. 70, 1281-1285 (2010).
24. Chaput, N. & Thery, C. Exosomes: immune properties and potential clinical implementations. Semin. Immunopathol. 33, 419-440 (2011).

25. Gyorgy, B. et al. Detection and isolation of cell-derived microparticles are compromised by protein complexes resulting from shared biophysical parameters. Blood 117, e39-48 (2011).
26. Yuana, Y. et al. Atomic force microscopy: a novel approach to the detection of nanosized blood microparticles. J. Thromb. Haemost. 8, 315-323 (2010).
27. van der Pol, E. et al. Optical and non-optical methods for detection and characterization of microparticles and exosomes. J. Thromb. Haemost. 8, 2596-2607 (2010).
28. Sokolova, V. et al. Characterisation of exosomes derived from human cells by nanoparticle tracking analysis and scanning electron microscopy. Colloids Surf. B Biointerfaces 87, 146-150 (2011).
29. Simpson, R. J., Jensen, S. S. & Lim, J. W. Proteomic profiling of exosomes: current perspectives. Proteomics 8, 4083-4099 (2008).
30. Wubbolts, R. et al. Proteomic and biochemical analyses of human B cell-derived exosomes. Potential implications for their function and multivesicular body formation. J Biol Chem 278, 10963-72 (2003).
31. Subra, C., Laulagnier, K., Perret, B. & Record, M. Exosome lipidomics unravels lipid sorting at the level of multivesicular bodies. Biochimie 89, 205-212 (2007).
32. Clayton, A. et al. Analysis of antigen presenting cell derived exosomes, based on immuno-magnetic isolation and flow cytometry. J. Immunol. Methods 247, 163-174 (2001).
33. Dragovic, R. A. et al. Sizing and phenotyping of cellular vesicles using Nanoparticle Tracking Analysis. Nanomedicine 7, 780-8 (2011).
34. Filipe, V., Hawe, A. & Jiskoot, W. Critical evaluation of Nanoparticle Tracking Analysis (NTA) by NanoSight for the measurement of nanoparticles and protein aggregates. Pharm. Res. 27, 796-810 (2010).
35. Freyssinet, J. M. & Toti, F. Membrane microparticle determination: at least seeing what's being sized! J. Thromb. Haemost. 8, 311-314 (2010).
36. Orozco, A. F. & Lewis, D. E. Flow cytometric analysis of circulating microparticles in plasma. Cytometry A. 77, 502-514 (2010).
37. Lacroix, R. et al. Standardization of platelet-derived microparticle enumeration by flow cytometry with calibrated beads: results of the International Society on Thrombosis and Haemostasis SSC Collaborative workshop. J. Thromb. Haemost. 8, 2571-2574 (2010).
38. Steen, H. B. Flow cytometer for measurement of the light scattering of viral and other submicroscopic particles. Cytometry A. 57, 94-99 (2004).
39. Hercher, M., Mueller, W. & Shapiro, H. M. Detection and discrimination of individual viruses by flow cytometry. J. Histochem. Cytochem. 27, 350-352 (1979).
40. Yang, L., Zhu, S., Hang, W., Wu, L. & Yan, X. Development of an ultrasensitive dual-channel flow cytometer for the individual analysis of nanosized particles and biomolecules. Anal. Chem. 81, 2555-2563 (2009).
41. Lacroix, R., Robert, S., Poncelet, P. & Dignat-George, F. Overcoming limitations of microparticle measurement by flow cytometry. Semin. Thromb. Hemost. 36, 807-818 (2010).
42. Nolte-'t Hoen, E. N. et al. Quantitative and qualitative flow cytometric analysis of nano-sized cell-derived membrane vesicles. Nanomedicine (2011) In press.
43. Shapiro HM. in Practical Flow Cytometry 4th ed. Chapter 7, p273-280 (Wiley-Liss, New York, 2003).
44. Kerker, M. et al. Light scattering and fluorescence by small particles having internal structure. J. Histochem. Cytochem. 27, 250-263 (1979).
45. van Gaal, E. V., Spierenburg, G., Hennink, W. E., Crommelin, D. J. & Mastrobattista, E. Flow cytometry for rapid size determination and sorting of nucleic acid containing nanoparticles in biological fluids. J. Control. Release 141, 328-338 (2010).
46. Brussaard, C. P., Marie, D. & Bratbak, G. Flow cytometric detection of viruses. J. Virol. Methods 85, 175-182 (2000).

47. Tauro, B.J. et al. Comparison of ultracentrifugation, density gradient separation, and immunoaffinity capture methods for isolating human colon cancer cell line LIM1863-derived exosomes. Methods 56, 293–304 (2012).
48. Okabe, M., Ikawa, M., Kominami, K., Nakanishi, T. & Nishimune, Y. 'Green mice' as a source of ubiquitous green cells. FEBS Lett. 407, 313-319 (1997).
49. Aass, H. C. et al. Fluorescent particles in the antibody solution result in false TF- and CD14-positive microparticles in flow cytometric analysis. Cytometry A. 79, 990-999 (2011).
50. Dale, G. L., Remenyi, G. & Friese, P. Quantitation of microparticles released from coated-platelets. J. Thromb. Haemost. 3, 2081-2088 (2005).
51. Hunter, M. P. et al. Detection of microRNA expression in human peripheral blood microvesicles. PLoS One 3, e3694 (2008).
52. Perez-Pujol, S., Marker, P. H. & Key, N. S. Platelet microparticles are heterogeneous and highly dependent on the activation mechanism: studies using a new digital flow cytometer. Cytometry A. 71, 38-45 (2007).
53. Simak, J., Gelderman, M. P., Yu, H., Wright, V. & Baird, A. E. Circulating endothelial microparticles in acute ischemic stroke: a link to severity, lesion volume and outcome. J. Thromb. Haemost. 4, 1296-1302 (2006).
54. Mullier, F., Bailly, N., Chatelain, C., Dogne, J. M. & Chatelain, B. More on: calibration for the measurement of microparticles: needs, interests, and limitations of calibrated polystyrene beads for flow cytometry-based quantification of biological microparticles. J. Thromb. Haemost. 9, 1679-81; author reply 1681-2 (2011).
55. Chandler, W. L., Yeung, W. & Tait, J. F. A new microparticle size calibration standard for use in measuring smaller microparticles using a new flow cytometer. J. Thromb. Haemost. 9, 1216-1224 (2011).
56. Robert, S., Poncelet, P., Lacroix, R., Raoult, D. & Dignat-George, F. More on: calibration for the measurement of microparticles: value of calibrated polystyrene beads for flow cytometry-based sizing of biological microparticles. J. Thromb. Haemost. 9, 1676-8; author reply 1681-2 (2011).

Science never solves a problem without creating ten more
- George Bernard Shaw

Chapter 4

Dynamics of dendritic cell-derived vesicles: High-resolution flow cytometric analysis of extracellular vesicle quantity and quality

Esther N.M. Nolte-'t Hoen, Els J. van der Vlist, Mieke de Boer-Brouwer,
Ger J.A. Arkesteijn, Willem Stoorvogel and Marca M.H. Wauben

Journal of Leukocyte Biology. 2013 Mar;93(3):395-402

Abstract

Nano-sized membrane vesicles are secreted by many cell types. These vesicles can serve as carriers of cellular information. Dendritic cell (DC)-derived vesicles can be targeted to other immune cells and modify their function. Accurate analysis of quantitative and qualitative changes in extracellular vesicle (EV) production by DC upon different activation stimuli is needed to further reveal the immune regulatory properties of DC-derived EV. However, methods for reliable quantification of individual EV and for analysis of the heterogeneity of EV populations are limited. With our recently developed high-resolution flow cytometry-based method we can perform high-throughput, multi-parameter, and quantitative analysis of individual EV. Using this novel technique we show that, despite previous assumptions, stimulation with bacterial lipopolysaccharide (LPS) increases EV release by DC. Furthermore, we demonstrate heterogeneity in DC-derived EV regarding their buoyant density and MHC class II content. Finally, we show that cognate interaction between LPS-stimulated DC and $CD4^+$ T cells affects both the quantity and quality of LPS DC-derived EV present in the culture supernatant. These data indicate that flow cytometry-based analysis of individual EV is a valuable novel tool to study the dynamics of EV secretion and composition, offering great opportunities to unveil the function of immune cell-derived EV.

Introduction

Eukaryotic cells can release different vesicle subsets (50-1000 nm), which are either shed from the plasma membrane or exocytosed by fusion of late endosomal compartments (multivesicular bodies) with the plasma membrane (exosomes) (1). These extracellular vesicles (EV) can be detected both in cell culture conditioned medium and in a large range of body fluids (1). EV are secreted by a wide variety of cells including antigen presenting cells (APC), such as B cells and dendritic cells (DC) (reviewed in (1, 2)). Evidence is accumulating that the pool of vesicles released by cells into the extracellular milieu is heterogeneous. Cells may regulate the composition of this vesicle pool by releasing vesicles from either the endosomal compartment or the plasma membrane. Alternatively, cells may produce phenotypically different EV subpopulations within one subcellular compartment. The resulting heterogeneity in EV populations may explain why different vesicle-associated proteins distribute unequally within the classical range of densities described for exosomes (3, 4).

The function of EV mainly depends on the EV cargo (proteins, lipids, and RNA), which is determined by the nature and activation status of the producing cell (reviewed in (1, 2)). Various studies describe differences in the molecular make-up and function of EV secreted by differentially activated DC. EV derived from immature DC have been used as cell-free vaccines that can elicit T cell responses and inhibit tumor growth in mice (5, 6). However, such immature DC-derived EV cannot directly stimulate T cell responses but need to be transferred to DC (7, 8). Upon stimulation with bacterial lipopolysaccharide (LPS), DC secrete EV that are more potent inducers of T cell responses than immature DC EV (9, 10). Based on these findings a second generation of activated DC-derived EV with enhanced immune stimulatory properties is now being developed for clinical application (11).

Besides functional analysis of APC-derived EV, the identification of triggers for EV secretion is crucial to understand the physiological role of these EV in immune regulation. Based on total protein content analysis, western-blotting, ELISA or bead-capture flow cytometric analysis for quantification of EV, it has been postulated that microbial stimulation of DC decreases EV secretion. This is different from B cells, which increase EV secretion upon microbial stimulation (10, 12-15). In contrast to the reported differences in EV secretion between B cells and DC after microbial stimulation, it has been proposed that both antigen presenting cell types increase EV secretion upon cognate interaction with $CD4^+$ T cells (13, 16). However, a major obstacle in studying the dynamics of EV release and their molecular contents is the lack of reliable methods to quantify the number of secreted EV and the number of molecules per vesicle.

The currently used quantification methods are based on bulk analysis of EV rather than on quantification of individual EV. Bulk analysis of EV is however hampered by the

lack of invariable vesicle-associated 'household' markers. Consequently, bulk analysis based quantification strategies cannot discriminate between changes in EV numbers and changes in the number of molecules per EV.

We recently developed a flow cytometry-based method for multiparameter analysis of individual EV. With this method, quantification of vesicles independently of their protein content can be combined with the detection of specific proteins on individual vesicles subpopulations (17, 18). This technique therefore offers unique opportunities for the identification of different EV subpopulations.

In the present study we used this novel method to analyze the dynamics of secretion and composition of DC-derived EV upon stimulation of DC with LPS and during interaction with cognate $CD4^+$ T cells.

Materials and Methods

Cell culture

Bone marrow derived DC were generated from C57BL/6 mice as described (19), with minor modifications. In short, bone marrow cells were maintained in Iscove's Modified Dulbecco's medium supplemented with 2 mM Ultraglutamine (Biowhittaker), 10% heat inactivated fetal calf serum (FCS, Sigma-Aldrich), 100 IU/ml penicillin and 100 mg/ml streptomycin (GIBCO), 50 µM β-mercaptoethanol and 30% conditioned medium from GM-CSF producing NIH 3T3 cells (R1). At days 2, 6 and 8, medium was added or replaced. On day 9, non-adherent cells were collected by gentle pipetting and plated in new dishes with fresh medium. When indicated, cells were activated with 10 µg/ml LPS on day 13. Semi-adherent and non-adherent cells were harvested on day 14 and replated for EV production in EV-depleted medium containing overnight ultracentrifuged (100,000 x g) FCS and GM-CSF containing conditioned R1 medium (to deplete bovine and R1 cell EV). The p53-specific $CD4^+$ T-cell clone, generated in a C57BL/6 $p53^{-/-}$ mouse (20) and provided by Prof C. Melief (Leiden University Medical Center, Leiden, The Netherlands), was cultured as described previously (16). For (non-)cognate LPS DC/T cell co-culture conditions, DC were incubated with (cognate) or without (non-cognate) 2.5 µM p53 peptide (amino acid 77-96) in the presence of 10 µg/ml LPS on day 13, harvested and mixed in a 1:1 ratio with T cells on day 14, and co-cultured for 20 h. Where indicated, T cells were labeled with 0.5 µM CFSE (Invitrogen) for 15 minutes at 37°C. All cultures were maintained at 37°C, 5% CO_2. Experiments were approved by the institutional ethical animal committee at Utrecht University (Utrecht, The Netherlands).

EV isolation and labeling

EV were collected from the culture supernatants of $3x10^6$ DC or $3x10^6$ DC co-cultured with $3x10^6$ T cells by differential centrifugation (21). In short, cells were removed by two sequential centrifugations at 200 x g for 10 min. Collected supernatant was subsequently centrifuged two times at 500 x g for 10 min, followed by 10,000 x g for 30 min. EV were finally pelleted by ultracentrifugation at 100,000 x g for 65 min in a SW40 rotor (Beckman) and resuspended in 20 µl PBS containing 0.2% BSA from a stock solution that had been cleared from aggregates by ultracentrifugation. EV were fluorescently labeled with 7.5 µM PKH67 (Sigma-Aldrich) in an end volume of 200 µl, following the manufacturer's recommendations. In case of antibody staining, EV resuspended in 20 µl PBS/0.2% BSA were incubated with 0.5 µg PE-labeled anti-mouse MHC class II antibody (clone M5/114, eBioscience) for 45 min at RT, after which PKH67 labeling was performed as described above. EV were then mixed with 2.5 M sucrose, overlaid with a linear sucrose gradient (2.0-0.4 M sucrose in PBS) and floated into the gradient by centrifugation in a SW40 tube (Beckman) for 16 hours at 192,000 x g. Gradient fractions of 1 ml were collected from the bottom of the tube, diluted 20-fold with PBS and analyzed by flow cytometric analysis. Fraction densities were determined by refractometry.

Flow cytometric analysis of EV

The BD Influx™ flow cytometer (Becton Dickinson) was used for flow cytometric analysis of individual EV (17). Light scattering was measured in straight line with the laser excitation beam with a collection angle of 15-25° (wide-angle FSC). Samples were run at low pressure (5 PSI on the sheath fluid and 4.2 PSI on the sample) using a 140 µm nozzle. For all measurements, the system was triggered on the fluorescence signal derived from the fluorescently labelled EV and thresholding was applied on this fluorescence channel. Fluorescence thresholding was based on measuring 0.22 µm filtered PBS, allowing an event rate of not more than 6 events per second. For calibration of the machine, we established fixed positions for fluorescent 100 and 200 nm polystyrene beads (yellow-green-fluorescent FluoSpheres, Invitrogen) in wide-angle FSC/SSC and wide-angle FSC/FL1 plots as a reference. For all analyses, light scattering detection was performed in log mode. Samples were measured at event rates lower than 10,000 events per second. Sucrose gradient fractions were diluted in PBS and vortexed before measurement. The two bottom fractions of the gradient were left out since unbound staining reagents in these fractions severely hampered detection of labeled membrane vesicles. Sample measurements were performed as described before (18). PE-labeled antibodies were measured by excitation with the 561 nm laser and using a 585/42 band pass filter.

Western blot analysis

Sucrose gradient fractions were diluted with PBS and centrifuged for 60 min at 100,000 x g using a SW60 rotor (Beckman). The pellets were solubilized in non-reducing SDS-PAGE sample buffer and separated by 12.5% SDS-PAGE. Proteins were transferred to PVDF membranes (Millipore), which were blocked in PBS containing 5% (w/v) non-fat dry milk (Protifar plus; Nutricia) and 0.1% (v/v) Tween-20, and MHCII was detected by immunoblotting. Rabbit polyclonal antibody directed against the cytoplasmic domain of mouse MHCII-β was kindly provided by Dr N. Barois (22) and detected using horseradish peroxidase (HRP) conjugated secondary antibody (Pierce Biotechnology Inc.). CD86 was detected by immunoblotting with biotinylated anti-CD86 (GL1; eBiosciences) and HRP-conjugated Streptavidin. Proteins were detected using Supersignal west pico chemiluminescent substrate (Pierce). Protein levels were quantified by densitometry using Quantity One Basic software (Bio-Rad).

Flow cytometric analysis of cells

Cells were harvested and incubated with antibodies as indicated for 30 minutes on ice in PBS containing 1% BSA (PBS-BSA). PE-conjugated anti-I-Ab (clone M5/114), anti-TCR (CTVB11) or anti-CD69 (H1.2F3) and the corresponding isotype control antibodies were from eBiosciences. Cells were analyzed using a FACS Calibur and CellQuest (Becton Dickinson, Brussels, Belgium), and FCS Express software (De Novo software).

Statistics

The numbers of extracellular vesicles (pooled fractions 1.11-1.18 g/ml, n= 6 independent experiments) as well as differences in MHCII geomean intensity (per fraction, n=6) and percentage of MHCII-positive vesicles (per fraction, n=6) produced by DC upon different activation stimuli were compared statistically using a two-tailed, paired Student's t-test. Differences in MHCII geomean intensity between fractions within one activation condition (n=6) were compared using a one-way analysis of variance (ANOVA) with Tukey's post hoc tests. Differences in the number of MHCII-positive vesicles secreted by LPS-activated DC cultured alone or in the presence of $CD4^+$ T cells (total numbers or numbers in arbitrary gates) were tested with a one-sample T-test. All tests were two-tailed and p-values < 0.05 were considered statistically significant. Asterisks indicate p-values: $p < 0.05$ (*), $p < 0.01$ (**) or $p < 0.001$ (***).

Results and Discussion

We first determined how LPS stimulation of DC affected the number of secreted EV. EV secreted by murine bone marrow derived DC were isolated from cell culture supernatant by differential centrifugation and subsequently labeled for high-resolution flow cytometric analysis of individual EV (17). Since the light scattering of nano-sized membrane vesicles overlaps with noise signals, EV were labeled with the general lipid dye PKH67 and floated by centrifugation into an overlaid sucrose gradient (16, 17). Based on PKH67 fluorescence, labeled DC EV could be detected above the fluorescence threshold (**Figure 1A**). Quantification by time-based flow cytometric analysis demonstrated that the vast majority of vesicles produced by non-stimulated and LPS-stimulated DC equilibrated at densities of 1.11-1.18 g/ml (**Figure 1B**), corresponding to the representative density range of EV (1). Importantly, we found that LPS stimulation of DC led to a 1.9 fold increase in the number of EV in the culture supernatant as compared to EV secreted by non-stimulated DC (**Figure 1B, C**). From a physiological point of view our finding that LPS stimulation of DC increases EV production is important, since such activated DC-derived EV with strong T cell stimulatory capacity could actively contribute to amplification of immune responses. Our results seem to contradict previous reports suggesting a reduction in DC EV secretion upon LPS stimulation (10, 12, 14). Differences in EV isolation procedures, such as the addition of filtration steps or low temperature storage of cell culture supernatant (10, 14), could explain the disparity in results. More importantly, previous studies used total protein assays and western blotting to assess the amount of EV. Such assays are however far from ideal for quantification of EV. First, phospholipids present in EV and detergents commonly used to disrupt vesicle membranes can cause considerable errors in the measured protein values (23). Second, specific protein-based quantification of EV by western-blotting is difficult since the amount of a specific protein may vary between different EV subsets. Importantly, our flow cytometry-based data were recently corroborated by Soo *et al*., who demonstrated with a different EV quantification technique (Nanoparticle Tracking Analysis) and using DC from a different source (human monocyte-derived DC) that the number of released vesicles increased upon DC stimulation with LPS (24).

Next, we investigated whether LPS-stimulated and non-stimulated DC release vesicles that differ in their MHCII content by combining flow cytometric analysis of EV numbers and MHCII protein detection by western blotting (**Figures 2A-B**). The observed increase in number of EV released by LPS-stimulated DC was accompanied by an overall increase in MHCII signal obtained by western blotting. However, within the population of EV released by non-stimulated DC, we noticed that density fractions containing similar numbers of EV (densities 1.13 and 1.17 g/ml) displayed substantial differences in MHCII protein levels (**Figure 2A**). This could be due to differences in the MHCII content of EV residing in these different density fractions. Therefore, the MHCII content of antibody-stained individual

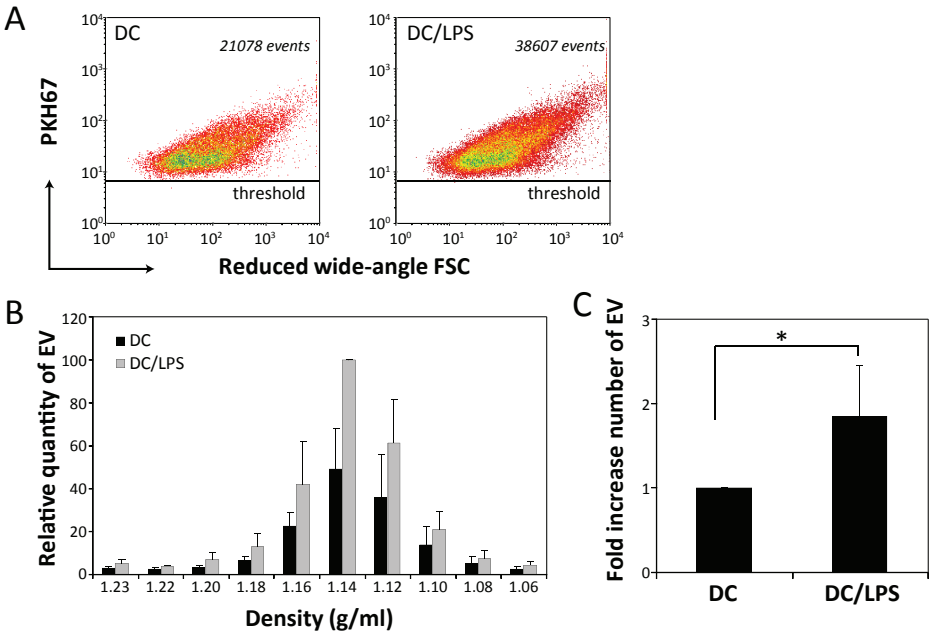

Figure 1 - DC increase EV secretion in response to LPS stimulation EV were isolated from culture supernatants of non-stimulated DC or LPS-stimulated DC (DC/LPS), fluorescently labeled with PKH67, and floated into a sucrose gradient. Sucrose gradient fractions were analyzed by high-resolution flow cytometric analysis using a threshold on PKH67 fluorescence. (**A**) Dot plots of wide-angle FSC versus PKH67 fluorescence representing fluorescent EV released by non-activated DC (left) or LPS-activated DC (right) from pooled fractions with densities of 1.11-1.18 g/ml. Indicated are the number of events measured in 30 sec. (**B**) Time-based quantification of fluorescent EV detected in different gradient fractions. Numbers of detected events were normalized to the number of EV released by LPS-activated DC with a buoyant density of 1.14 g/ml (set to 100%). Indicated are the relative quantities of EV (average ± s.d.) measured in 30 sec. Data are from four independent experiments. (**C**) Average and standard deviation of the number of EV detected in supernatants of non-stimulated versus LPS-stimulated DC of n=6 independent experiments. Indicated is the factor increase in number of EV (pools of 1.11-1.18 g/ml sucrose fractions) secreted by LPS-stimulated DC relative to non-stimulated DC (non-stimulated DC EV were set to 1). *$p < 0.05$.

EV was determined using flow cytometry-based analysis (**Figure 2C**). The geometric mean MHCII intensity of MHCII-positive EV varied between the different fractions, with EV floating at the highest density (1.18 g/ml) containing the highest amount of MHCII (**Figure 2D**). Furthermore, the MHCII content of the lower density EV from LPS-activated DC was higher compared to those EV derived from non-stimulated DC (**Figure 2D**). In addition, the percentage of MHCII-positive EV released by LPS-activated DC was substantially higher compared to non-activated DC (**Figure 2E**).

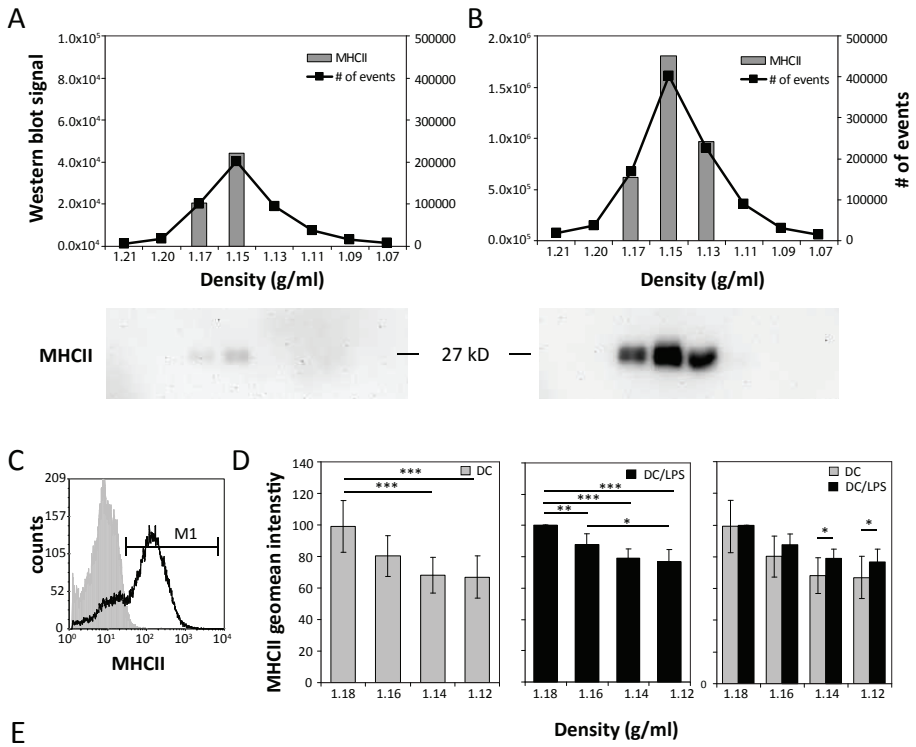

Figure 2 - Heterogeneity within DC EV populations and between EV populations secreted by differently activated DC EV were isolated from culture supernatants of non-stimulated DC or LPS- stimulated DC (DC/LPS), fluorescently labeled with PKH67 (**A-B**) or PKH67 and PE-conjugated anti-MHCII (**C-E**), and floated into a sucrose gradient. Sucrose gradient fractions were analyzed on a high-resolution flow cytometer using a threshold on PKH67 fluorescence. (**A-B**) Flow cytometric and western blot analysis of sucrose gradient fractions containing EV derived from non-stimulated DC (**A**) or LPS-stimulated DC (**B**). The left y-axis indicates the MHCII protein levels as quantified by western blotting (bars and pictures below the graphs). The right y-axis indicates the number of events detected in 30 sec by the flow cytometric approach (line). (**C**) Histogram representing anti-MHCII (black line) or isotype control antibody (grey solid) labeled EV derived from LPS-activated DC pooled from 1.11-1.18 g/ml density fractions. MHCII-positive EV were gated (M1) based on the isotype control staining. (**D**) EV derived from non-stimulated and LPS-stimulated DC were compared for MHCII labeling intensity. Indicated are the geometric mean fluorescence intensities (average ± s.d.) of MHCII staining in each of the indicated gradient fractions. Data were normalized to the intensity of the EV with buoyant density 1.18 g/ml (n=6 independent experiments). MHCII-positive events were gated as in (**C**). (**E**) The percentage of MHCII-positive EV was determined as shown in (**C**). Indicated is the comparison of the percentages of MHCII-positive EV (average ± s.d. of 6 independent experiments) released by non-stimulated and LPS-stimulated DC. *p<0.05, **p<0.01, ***p<0.001

Like MHCII, also the amount of CD86 released in the culture supernatant increased upon DC activation, as measured by western blotting (**Supplemental figure 1**). However, both the absence of high-affinity flow cytometry antibodies for co-stimulatory molecules and perhaps the lower abundance of these molecules on the vesicles currently prohibits their detection on individual EV using our flow cytometry-based assay. The present data indicate that heterogeneity exists not only between EV produced by DC undergoing different modes of stimulation, but also between EV produced during one culture condition. Collectively, our data indicate that different EV subsets produced by one cell type can be identified based on buoyant density combined with high-resolution flow cytometric analysis of the specific protein content of individual EV.

We previously showed that during cognate interactions of DC with $CD4^+$ T cells, EV-associated MHCII is released into the culture supernatant (16, 25). Besides this, part of the released MHCII is recruited to other DC (7, 9, 16, 25, 26) and part to interacting T cells in an LFA-1-dependent fashion (25). By using flow cytometry-based analysis of individual EV, we here investigated whether cognate interactions between LPS-activated, antigen-loaded DC and antigen-experienced $CD4^+$ T cells resulted in selective recruitment of specific subsets of DC EV to these T cells. First, we compared the quantity and quality of MHCII-carrying EV recovered from the DC culture supernatant in the absence or presence of cognately interacting T cells. By antibody-staining for MHCII, MHCII-positive DC-derived EV could be distinguished from MHCII-negative T cell-derived EV (17). Using this method, we found a strong decrease in the number of MHCII-positive EV in the extracellular milieu when LPS-activated DC were cultured in the presence of cognately interacting T cells (**Figure 3A-B**). Importantly, this effect was strictly dependent on cognate antigen recognition (**Figure 3B**). Flow cytometric analysis of CFSE-labeled $CD4^+$ T cells co-cultured with non-labeled, antigen pulsed, LPS-stimulated DC revealed that the T cells were activated (indicated by reduced TCR expression and increased CD69 expression) and that substantial amounts of DC-derived MHCII were recruited to the T cell surface (**Figure 4A**). We next investigated whether the cognate T cells selectively recruited specific EV subpopulations released by the interacting DC. Hence, we investigated the phenotype of DC EV present in the supernatant of DC or DC-T cell cultures. To quantify EV carrying different levels of MHCII, arbitrary gates were set for EV containing low, intermediate, or high levels of MHCII in the different density fractions (**Figure 4B**). In co-cultures of LPS-activated DC with cognate T cells, EV with buoyant densities of 1.12-1.18 g/ml that contained the highest amount of MHCII (MHCII-hi) were most efficiently eliminated from the culture supernatant (**Figure 4C-D**). A smaller decrease was observed for the number of 1.14-1.16 g/ml EV with intermediate MHCII levels, whereas the numbers of MHCII-low EV in the co-culture supernatant remained unchanged. These data suggest that EV with high MHCII contents had been preferentially recruited onto the T cells. Alternatively, interactions with T cells could have induced the DC to produce relatively more EV with lower MHCII contents.

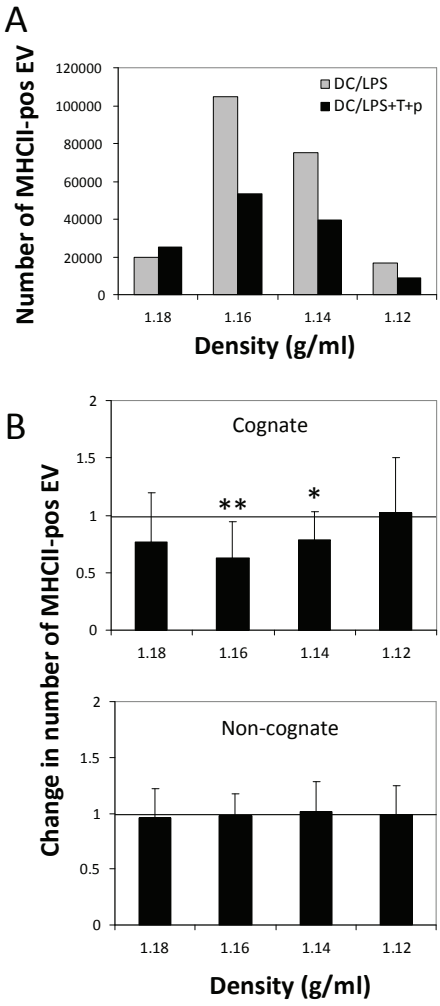

Figure 3 - Quantitative and qualitative analysis of DC EV secreted during cognate interactions with T cells EV were isolated from culture supernatants of LPS-stimulated DC (DC/LPS) cultured alone or pulsed with specific peptide and co-cultured with cognate antigen experienced $CD4^+$ T cells. EV were fluorescently labeled with PKH67 and PE-labeled anti-MHCII, and floated to equilibrium into a sucrose gradient. Sucrose gradient fractions were analyzed by high-resolution flow cytometric analysis using a threshold on PKH67 fluorescence. (**A**) Time-based quantification of MHCII positive events detected in different gradient fractions of (co-cultured) LPS-stimulated DC. Indicated are the numbers of events measured in 30 sec. One representative experiment out of three is shown. (**B**) Ratios of the number of MHCII-positive EV in culture supernatants of cognate DC-T cell cultures (upper panel) or non-cognate cultures (lower panels) over the number of MHCII-positive EV in supernatants of cultures of LPS-stimulated DC alone. Indicated are average values ± s.d. of 9 (cognate interactions) or 4 (non-cognate interactions) independent experiments. *p<0.05; **p<0.01.

This seems less likely, since the numbers of MHCII-low EV recovered from supernatants of LPS-activated DC in the presence or absence of T cells was not significantly affected. Based on these data we conclude that $CD4^+$ T cells selectively capture DC-derived EV containing the higher amounts of MHCII during cognate interactions with LPS-DC. It is currently not known whether T cells received triggers from the LPS-DC to increase the expression of receptors involved in EV binding, e.g. LFA-1 (25), or whether MHCII-high EV contain higher levels of cognate MHCII-peptide complexes or other proteins involved in T cell binding. Generally, DC EV that are not directly recruited to neighboring or interacting DC and T cells are available for targeting to other cells. We are currently investigating whether DC EV secreted in the extracellular environment during cognate interactions between LPS-stimulated DC and $CD4^+$ T cells have different immune regulatory properties.

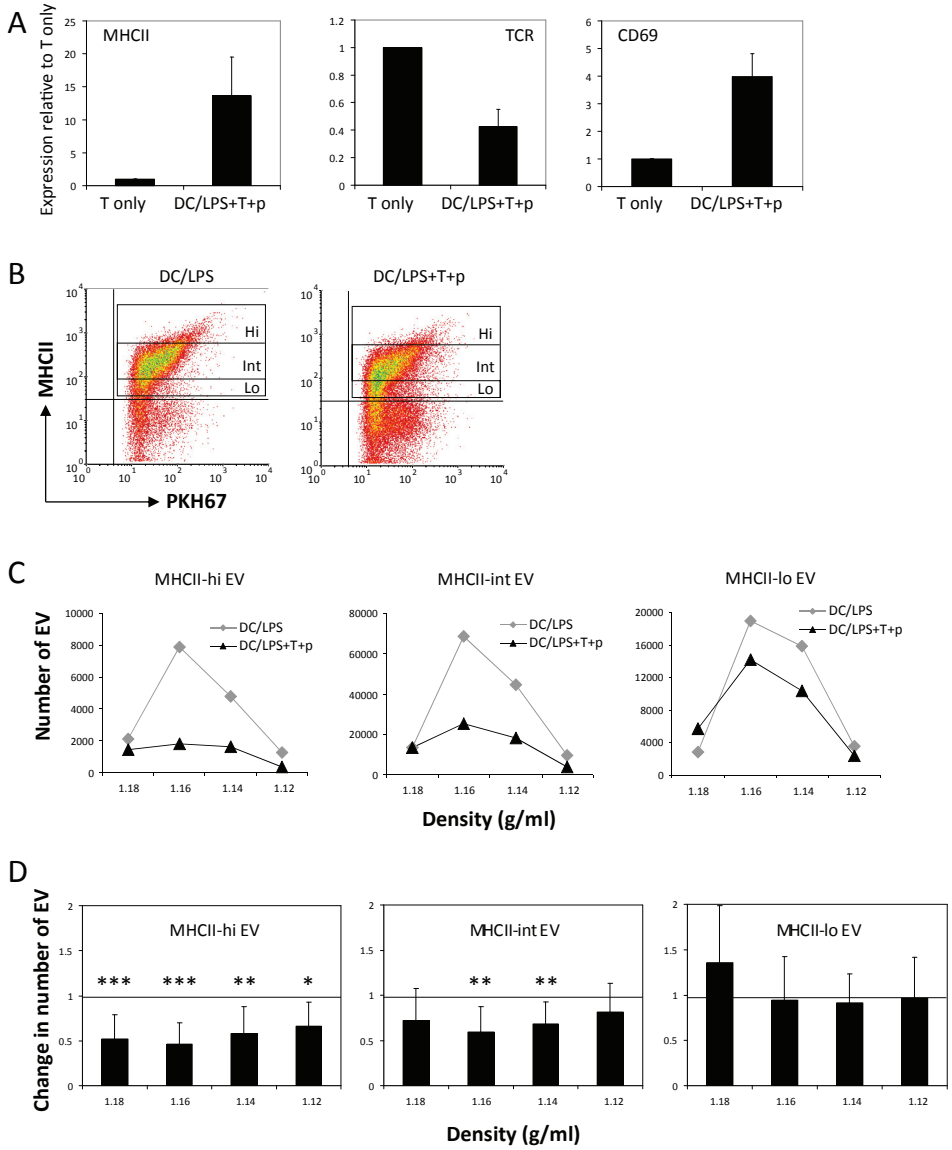

Figure 4 - Heterogeneity in MHCII contents of EV secreted in cultures of DC only and cognate DC-T cell co-cultures CFSE labeled T cells were cultured alone or in co-culture with non-labeled LPS-stimulated peptide-pulsed DC for 24 hours. (**A**) T cells were gated based on CFSE staining and analyzed for MHCII, TCR, or CD69 by flow cytometry. The levels of the indicated proteins detected on T cells in cognate co-cultures were calculated relative to those found on T cells cultured alone (set to 1). Indicated are the average values ± s.d. of 3 individual experiments. (**B-D**) DC-derived EV were labeled and analyzed as described in Figure 3. (**B**) Dot plots representing PKH67 and anti-MHCII antibody labeled EV derived from cultures of LPS-stimulated DC (left) or cognate DC/LPS-T

Conclusively, we here show that with a high-resolution, multiparameter flow cytometry-based method to analyze individual EV, detailed information can be obtained regarding the number and heterogeneity of EV secreted by DC undergoing different modes of activation. In contrast to previously used techniques, this method allows the uncoupling of quantitative and qualitative measurements in studying secreted EV. This is particularly important when the protein composition of EV changes due to environmental triggers, such as during DC activation. Using this flow cytometric approach, we showed that DC increase EV secretion upon LPS stimulation. In addition, we obtained evidence that the EV population derived from cells in one culture condition contains subsets that differ in buoyant density and protein content. The discriminative ability of our technique further allowed us to demonstrate that during cognate DC-T cell interactions, T cells preferentially capture subpopulations of DC-derived EV with higher levels of MHCII. Based on these findings we are confident that high-resolution flow cytometry-based analysis of individual EV will open up new avenues to further unravel the role of EV in immune regulation.

Figure 4 (*continued*) cell co-cultures (right). Based on isotype control stainings, quadrants were set in such a way that upper right quadrants contained only MHCII-positive DC EV. Arbitrary gates indicate low (lower 20% of positive population), intermediate and high (upper 10% of positive population) MHCII levels on DC/LPS-derived EV. The increase in MHCII negative events in the right plot represents T cell-derived EV. (**C-D**) Time-based quantification of MHCII-high (MHCII-hi), -intermediate (MHCII-int), or -low (MHCII-lo) events detected in different gradient fractions of LPS-stimulated DC cultured alone (grey diamonds) or in the presence of cognate T cells (black triangles). Indicated are the numbers of events in different gradient fractions measured in 30 sec. The data shown in (***C***) are from one representative experiment. The data shown in (**D**) represent ratios of the number of EV with different levels of MHCII in culture supernatants of cognate DC/LPS-T cell cultures over those in cultures of LPS-stimulated DC alone. Indicated are average values ± s.d. of 7 independent experiments. *p<0.05, **p<0.01, ***p<0.001

References

1. Thery, C., Ostrowski, M., Segura, E. (2009) Membrane vesicles as conveyors of immune responses. Nat Rev Immunol 9, 581-93.
2. Nolte-'t Hoen, E.N., Wauben, M.H. (2012) Immune cell-derived vesicles: modulators and mediators of inflammation. Curr Pharm Des 18, 2357-68.
3. Escola, J.M., Kleijmeer, M.J., Stoorvogel, W., Griffith, J.M., Yoshie, O., Geuze, H.J. (1998) Selective enrichment of tetraspan proteins on the internal vesicles of multivesicular endosomes and on exosomes secreted by human B-lymphocytes. J Biol Chem 273, 20121-7.
4. Bobrie, A., Colombo, M., Krumeich, S., Raposo, G., Théry, C. (2012) Diverse subpopulations of vesicles secreted by different intracellular mechanisms are present in exosome preparations obtained by differential ultracentrifugation. Journal of Extracellular Vesicles 1.
5. Zitvogel, L., Regnault, A., Lozier, A., Wolfers, J., Flament, C., Tenza, D., Ricciardi-Castagnoli, P., Raposo, G., Amigorena, S. (1998) Eradication of established murine tumors using a novel cell-free vaccine: dendritic cell-derived exosomes. Nat Med 4, 594-600.
6. Chaput, N., Schartz, N.E., Andre, F., Taieb, J., Novault, S., Bonnaventure, P., Aubert, N., Bernard, J., Lemonnier, F., Merad, M., Adema, G., Adams, M., Ferrantini, M., Carpentier, A.F., Escudier, B., Tursz, T., Angevin, E., Zitvogel, L. (2004) Exosomes as potent cell-free peptide-based vaccine. II. Exosomes in CpG adjuvants efficiently prime naive Tc1 lymphocytes leading to tumor rejection. J Immunol 172, 2137-46.
7. Thery, C., Duban, L., Segura, E., Veron, P., Lantz, O., Amigorena, S. (2002) Indirect activation of naive CD4+ T cells by dendritic cell-derived exosomes. Nat Immunol 3, 1156-62.
8. Andre, F., Chaput, N., Schartz, N.E., Flament, C., Aubert, N., Bernard, J., Lemonnier, F., Raposo, G., Escudier, B., Hsu, D.H., Tursz, T., Amigorena, S., Angevin, E., Zitvogel, L. (2004) Exosomes as potent cell-free peptide-based vaccine. I. Dendritic cell-derived exosomes transfer functional MHC class I/peptide complexes to dendritic cells. J Immunol 172, 2126-36.
9. Segura, E., Amigorena, S., Thery, C. (2005) Mature dendritic cells secrete exosomes with strong ability to induce antigen-specific effector immune responses. Blood Cells Mol Dis 35, 89-93.
10. Segura, E., Nicco, C., Lombard, B., Veron, P., Raposo, G., Batteux, F., Amigorena, S., Thery, C. (2005) ICAM-1 on exosomes from mature dendritic cells is critical for efficient naive T-cell priming. Blood 106, 216-23.
11. Viaud, S., Ploix, S., Lapierre, V., Thery, C., Commere, P.H., Tramalloni, D., Gorrichon, K., Virault-Rocroy, P., Tursz, T., Lantz, O., Zitvogel, L., Chaput, N. (2011) Updated technology to produce highly immunogenic dendritic cell-derived exosomes of clinical grade: a critical role of interferon-gamma. J Immunother 34, 65-75.
12. Thery, C., Regnault, A., Garin, J., Wolfers, J., Zitvogel, L., Ricciardi-Castagnoli, P., Raposo, G., Amigorena, S. (1999) Molecular characterization of dendritic cell-derived exosomes. Selective accumulation of the heat shock protein hsc73. J Cell Biol 147, 599-610.
13. Muntasell, A., Berger, A.C., Roche, P.A. (2007) T cell-induced secretion of MHC class II-peptide complexes on B cell exosomes. Embo J 26, 4263-72.
14. Qazi, K.R., Gehrmann, U., Domange Jordo, E., Karlsson, M.C., Gabrielsson, S. (2009) Antigen-loaded exosomes alone induce Th1-type memory through a B-cell-dependent mechanism. Blood 113, 2673-83.
15. Arita, S., Baba, E., Shibata, Y., Niiro, H., Shimoda, S., Isobe, T., Kusaba, H., Nakano, S., Harada, M. (2008) B cell activation regulates exosomal HLA production. Eur J Immunol 38, 1423-34.
16. Buschow, S.I., Nolte-'t Hoen, E.N., van Niel, G., Pols, M.S., ten Broeke, T., Lauwen, M., Ossendorp, F., Melief, C.J., Raposo, G., Wubbolts, R., Wauben, M.H., Stoorvogel, W. (2009) MHC II in dendritic cells is targeted to lysosomes or T cell-induced exosomes via distinct multivesicular body pathways. Traffic 10, 1528-42.

17. Nolte-'t Hoen, E.N., van der Vlist, E.J., Aalberts, M., Mertens, H.C., Bosch, B.J., Bartelink, W., Mastrobattista, E., van Gaal, E.V., Stoorvogel, W., Arkesteijn, G.J., Wauben, M.H. (2012) Quantitative and qualitative flow cytometric analysis of nanosized cell-derived membrane vesicles. Nanomedicine 8, 712-20.
18. van der Vlist, E.J., Nolte-'t Hoen, E.N., Stoorvogel, W., Arkesteijn, G.J., Wauben, M.H. (2012) Fluorescent labeling of nano-sized vesicles released by cells and subsequent quantitative and qualitative analysis by high-resolution flow cytometry. Nat Protoc 7, 1311-26.
19. Lutz, M.B., Kukutsch, N., Ogilvie, A.L., Rossner, S., Koch, F., Romani, N., Schuler, G. (1999) An advanced culture method for generating large quantities of highly pure dendritic cells from mouse bone marrow. J Immunol Methods 223, 77-92.
20. Lauwen, M.M., Zwaveling, S., de Quartel, L., Ferreira Mota, S.C., Grashorn, J.A., Melief, C.J., van der Burg, S.H., Offringa, R. (2008) Self-tolerance does not restrict the CD4+ T-helper response against the p53 tumor antigen. Cancer Res 68, 893-900.
21. Raposo, G., Nijman, H.W., Stoorvogel, W., Liejendekker, R., Harding, C.V., Melief, C.J., Geuze, H.J. (1996) B lymphocytes secrete antigen-presenting vesicles. J Exp Med 183, 1161-72.
22. Barois, N., Forquet, F., Davoust, J. (1997) Selective modulation of the major histocompatibility complex class II antigen presentation pathway following B cell receptor ligation and protein kinase C activation. J Biol Chem 272, 3641-7.
23. Kessler, R.J., Fanestil, D.D. (1986) Interference by lipids in the determination of protein using bicinchoninic acid. Anal Biochem 159, 138-42.
24. Soo, C.Y., Song, Y., Zheng, Y., Campbell, E.C., Riches, A.C., Gunn-Moore, F., Powis, S.J. (2012) Nanoparticle tracking analysis monitors microvesicle and exosome secretion from immune cells. Immunology 136, 192-7.
25. Nolte-'t Hoen, E.N., Buschow, S.I., Anderton, S.M., Stoorvogel, W., Wauben, M.H. (2009) Activated T cells recruit exosomes secreted by dendritic cells via LFA-1. Blood 113, 1977-81.
26. Segura, E., Guerin, C., Hogg, N., Amigorena, S., Thery, C. (2007) CD8+ dendritic cells use LFA-1 to capture MHC-peptide complexes from exosomes in vivo. J Immunol 179, 1489-96.

Supplementary information

The following is supplemenatry information to this chapter.

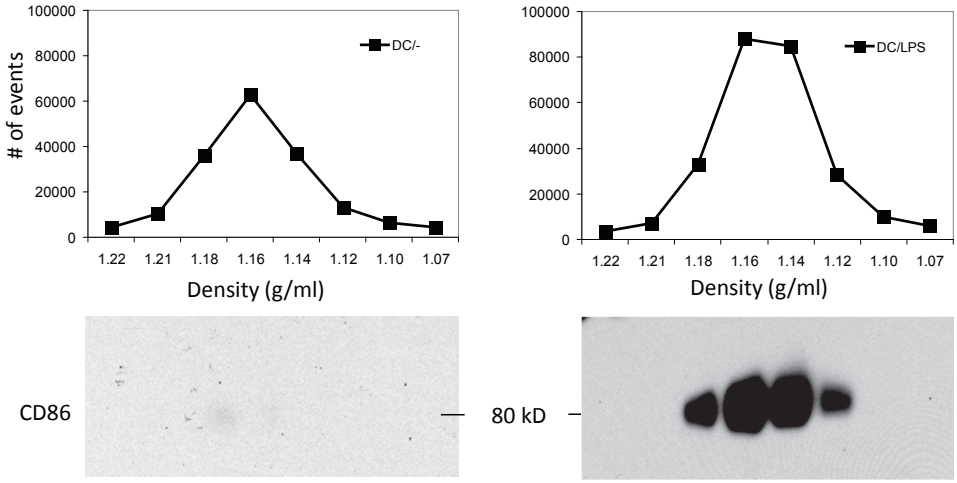

Supplementary Figure 1 - CD86 on EV released by differently activated DC EV were isolated from culture supernatants of non-stimulated DC or LPS-stimulated DC (DC/LPS), fluorescently labeled with PKH67 and floated into a sucrose gradient. Sucrose gradient fractions containing EV derived from non-stimulated DC (left) or LPS-stimulated DC (right) were analyzed on a high-resolution flow cytometer using a threshold on PKH67 fluorescence (top panels) and by western blotting (bottom panels). Top panels display the number of events detected in 30 seconds by the flow cytometric approach. Bottom panels show the CD86 protein levels as detected by western blotting.

4

Writing is easy. All you do is stare at a blank sheet of paper until drops of blood form on your forehead - Gene Fowler

Chapter 5

CD4$^+$ T cell activation promotes the differential release of distinct populations of nano-sized vesicles

Els J. van der Vlist, Ger J.A. Arkesteijn, Chris H.A. van de Lest,
Willem Stoorvogel, Esther N.M. Nolte - 't Hoen and Marca H.M. Wauben

Journal of Extracellular Vesicles 2012, 1: 18364

Abstract

Many cell types release nano-sized vesicles derived from endosomal compartments (exosomes) or the plasma membrane. Vesicles actively released by $CD4^+$ T cells have immune-modulatory characteristics. Using our recently developed high-resolution flow cytometry-based method for the analysis of individual nano-sized vesicles, we here investigated how T cell receptor (TCR)-triggering and co-stimulatory signals influence the quantity and characteristics of nano-sized vesicles released by $CD4^+$ T cells. We found that the number of released nano-sized vesicles within the buoyant density range characteristic for exosomes (1.10-1.19 g/ml) was increased by TCR-triggering and that additional co-stimulatory signals had a potentiating effect on vesicle release. However, the increase in the number of released vesicles varied substantially between density fractions within the 1.10-1.19 g/ml range and was highest for the vesicle populations in 1.14 and 1.17 g/ml fractions. Heterogeneity was also observed within the individual density fractions. Based on lipid bilayer fluorescent labeling intensity and light scattering, three distinct vesicle subpopulations were identified. One vesicle subpopulation increased significantly more upon T cell activation than the other subpopulations, and this was dependent on high levels of co-stimulation. These data show that T cells release a heterogeneous population of nano-sized vesicles and indicate that T cells differentially regulate the release of distinct vesicle subpopulations depending on their activation status.

Introduction

Cells can release different types of vesicles that are either derived from multivesicular bodies (referred to as exosomes) or shed directly from their plasma membrane (1, 2). The timely release of tailor-made vesicles by cells and their specific recruitment by target cells has led to the emerging concept that cell-derived vesicles may be important vehicles for intercellular communication (2). $CD4^+$ T cells are key-players in the initiation and regulation of adaptive immune responses. Similar to antigen presenting cells (APC), $CD4^+$ T cells can release vesicles (3, 4). After release, T cell-derived vesicles can be targeted to different types of immune cells and modify their function. For example, APO2L and FasL-containing T cell vesicles can induce apoptosis of targeted T cells (5-7). T cell-derived vesicles may also block MHC molecules on dendritic cells (DC) or induce apoptosis of DC (8, 9). Furthermore, we have shown that anergic $CD4^+$ T cells, in contrast to their non-anergic counterparts, release vesicles that can endow antigen presenting cells with immune-suppressive properties (10). Besides down-regulation of immune responses, T cell-derived vesicles can also induce immune activation. For example, vesicles secreted by activated T cells can bind to monocytes and induce the production of pro-inflammatory cytokines such as TNFα and IL-1β (11-13). Furthermore, mast cells can be triggered to degranulate and release IL-8 and oncostatin M upon binding of T cell-derived vesicles (14). Altogether these findings indicate that T cell-derived vesicles are targeted to various types of immune cells and are involved in immune regulation at distinct levels.

The number of released vesicles and their molecular composition (proteins, lipids and RNA) is dynamic and dependent on their subcellular origin and the activation status of the producing cell (2). Hence, the total pool of released vesicles can be heterogeneous (15, 16). Vesicles can be characterized based on size, using differential centrifugation and/or filtration, or on buoyant density, using density gradient ultracentrifugation (17). The nano-sized exosome population is assumed to be rather homogeneous and has a reported equilibrium buoyant density in sucrose gradients of 1.10 - 1.19 g/ml (2, 17). Exclusive molecular markers for exosomes or other types of extracellular vesicles have not yet been defined, which complicates the identification of genuine distinct vesicle populations (18). To analyze different vesicle types or subpopulations within heterogeneous vesicle populations, multi-parameter high-throughput analysis of individual vesicles is required. Given that the vast majority of cell-derived vesicles is smaller than 300 nm, high-resolution techniques are needed for their visualization and characterization (19-22). Recently, we developed a high-resolution flow cytometric method to detect, quantify and characterize individual nano-sized vesicles based on fluorescence (16). Using this novel method we were able to identify and analyze the dynamics of different nano-sized dendritic cell (DC)-derived vesicle subpopulations (16).

To understand the pleiotropic roles of $CD4^+$ T cell derived vesicles it is of utmost importance to identify the triggers for vesicle release by these T cells and to characterize the released vesicle population(s). Previously, it has been postulated that the number of released $CD4^+$ T cell-derived vesicles increases upon T cell receptor (TCR)-triggering (3, 7). This was based on an increase of total protein and increased detection of CD63 in pelleted vesicles using Western blotting (3, 7). However, since the molecular composition of the released vesicle population is dynamic (16), protein assays or Western blot analysis of bulk isolates of vesicles are not reliable for quantitative analysis. We here used our high-resolution flow cytometric method to quantify and characterize the population of nano-sized vesicles that is released by $CD4^+$ T cells in response to different activation stimuli. The individual vesicle-based analysis will be helpful to unravel the physiological role of these vesicles in communication between T cells and other immune cells.

Materials and Methods

T cell clones & cell culture

The p53-specific $CD4^+$ T cell clone (KO4C1) is generated in a C57BL/6 p53 knockout mouse and recognizes the peptide corresponding to amino acids 77-96 of murine p53 (23). As previously described (24), T cells were restimulated with peptide-pulsed irradiated splenocytes for 2-3 days and isolated through centrifugation onto Ficoll-Hypaque after which they were expanded with recombinant human IL-2 (Roche, Almere, the Netherlands). T cells were cultured in IMDM (Gibco, Invitrogen, Bleiswijk, The Netherlands) with 10% exosome-free fetal calf serum (Sigma-Aldrich, Zwijndrecht, The Netherlands), 100 UI/ml penicillin, 100 µM streptomycin, 2 mM Ultraglutamine and 30 µM βmercapto-ethanol (T cell medium) and maintained at 37°C, 5% CO2. To deplete fetal calf serum from exosomes and other vesicles, 30% FCS in IMDM was ultracentrifuged for at least 15 hrs at 100,000g (SW28 rotor). For experiments $10x10^6$ T cells were cultured in 12.5 ml T cell medium supplemented with IL-2 (5 U/ml) in 10 cm dishes for 20 hrs. To activate T cells, dishes were coated overnight with 0.1 or 10 µg/ml anti-CD3 (clone 145.2C11) alone or combined with 0.5 or 5 µg/ml anti-CD28 (clone PV-1) in PBS at 4°C. Antibody-coated dishes were washed three times with IMDM, and once with exosome-free T cell medium, before T cells were added to the coated plates. For flow cytometric analysis of cells, $4x10^6$ T cells were cultured in a separate 6 cm dishes (coated with the same antibody concentrations) parallel to the cultures in 10 cm dishes for vesicle isolation. T cells in 6 cm dishes were treated with brefeldin A (10 µg/ml) 2 hrs prior to antibody labeling to induce intracellular accumulation of IFN-γ (25). Experiments were approved by the institutional ethical animal committees at Utrecht University (Utrecht, The Netherlands).

Flow cytometric analysis of cells

After 20 hrs of culture, including 2 hrs of incubation with brefeldin A, cells were harvested and labeled for CD69 and TCR (Vβ11) for 30 min on ice in phosphate-buffered saline/1% bovine serum albumin (BSA). Interferon-gamma (IFN-γ) labeling was performed for 30 min on ice, after fixation and permeabilization. Anti–CD69-PE (H1.2F3), anti-TCR-Vβ11-PE (CTVB11), anti-IFN-γ-APC (XMG1.2), and isotype control antibodies were from eBiosciences (Vienna, Austria). Cells were analyzed by flow cytometry using a FACSCalibur and CellQuest (BD Biosciences, San Jose, USA) or FCS Express software (De Novo Software, Los Angeles, USA).

Vesicle isolation and labeling

Vesicles released by $10x10^6$ T cells during 20 hrs of culture were used for high-resolution flow cytometric analysis and nano-particle tracking analysis (NTA). Released vesicles were isolated from culture supernatants by differential steps of (ultra)centrifugation as

described previously (22, 26). In short, culture supernatants were cleared from cells by centrifugation at 200g and 500g. Both steps were performed twice for 10 min. Larger debris was removed from supernatant by centrifugation at 10,000g for 30 min using a SLA-600TC rotor in a Sorvall RC5Bplus centrifuge. Subsequently, vesicles were pelleted for 65 min at 100,000g using a SW40 rotor in a Beckman Coulter Optima L-90K ultracentrifuge. All centrifugation steps were performed at 4°C. Vesicle pellets derived from 10 ml culture supernatant were resuspended in 20 µl PBS with 0.2% BSA. For all experiments, a stock solution of 5% BSA was used that had been cleared of aggregates by ultracentrifugation at 100,000g for at least 15 hrs. Resuspended vesicle pellets were labeled with the fluorescent membrane dye PKH67 (7.5 µM, Sigma Aldrich) according to manufacturer's protocol in a total volume of 200 µl. The staining procedure was stopped after 3 min by adding 50 µl fetal calf serum that was ultracentrifuged for at least 15 hrs at 100,000g. Vesicles were then mixed with 1.5 ml 2.5 M sucrose, overlaid with a linear sucrose gradient (1.9 M - 0.4 M sucrose in PBS) and floated into the gradient by centrifugation using a SW40 rotor in a Beckman Coulter Optima L-90K ultracentrifuge for 16 hrs at 192,000g. After ultracentrifugation, fractions of 1 ml were collected from the bottom via a capillary pipette connected to the tubing of a peristaltic pump. The densities of the different fractions were determined by refractometry.

Flow cytometric analysis of nano-sized vesicles

The BD Influx™ flow cytometer optimized for high-resolution flow cytometric analysis of individual nano-sized vesicles (Becton Dickinson, San Jose, USA) was used for the analysis of vesicles in different sucrose density fractions as described previously (16). In short, the system was triggered on fluorescence signals derived from the PKH67-labeled vesicles. PKH67 was excited with a 488 nm laser and the emitted light was captured by a PMT with a 528/38 filter. Thresholding on this fluorescence channel allowed discrimination between noise events and the particles of interest. A fluorescence threshold was set based on 0.22 µm filtered PBS, allowing an event rate of not more than 6 events per second. Light scattering was measured in straight line with the laser excitation beam with a collection angle of 15-25° (reduced wide-angle FSC). Light scattering detection was performed in log mode. Samples were run at low pressure (5 PSI on the sheath fluid and 4.2 PSI on the sample) using a 140 µm nozzle. Fluorescent 100 nm and 200 nm polystyrene beads (yellow-green-fluorescent FluoSpheres, Invitrogen) were used to calibrate the fluorescence, reduced wide-angle FSC and SSC settings on the flow cytometer. Sucrose gradient fractions were diluted 20 times in PBS and vortexed before measurement. Samples were measured at event rates lower than 10,000 events per second. The three bottom fractions of the gradient were left out to avoid possible interference by unbound staining reagent in these fractions with the detection of labeled vesicles. Time-based quantitative measurements were performed as described before (16). In short, After 30 sec of equilibration time, data

were acquired for 30 sec. The sample line was extensively washed in between different samples. Data was acquired using Spigot software version 6.1 (Becton Dickinson, San Jose, USA). Acquired data was analyzed using FCS Express software (De Novo Software, Los Angeles, USA).

Nano-particle Tracking Analysis (NTA)

For size determination of the vesicles based on Brownian motion, the NanoSight LM10SH (NanoSight, Amesbury, United Kingdom), equipped with a 532 nm laser was used. The sucrose density fractions were diluted at least 100 times in PBS and vortexed before application into the sample chamber. Samples were applied with sterile syringes until the solution reached the tip of the nozzle. Samples were measured for 90 sec at 20°C with manual shutter and gain adjustments, which were kept constant for all measurements. The vesicle movement was captured and analyzed using the NTA software version 2.2 (NanoSight). Each particle was identified and its Brownian movement tracked and measured frame-to-frame. Based on the particle movement velocity, the particle size was calculated using the Stokes-Einstein equation. Post-acquisition settings were optimized and kept constant between all measurements. For each sample a batch of at least 5 individual movies was captured. For analysis the tracks (individually traced vesicles) of all movies within one batch were used. The number of tracks in each batch analysis was at least 497.

Statistics

Results are expressed as mean ± standard deviation. Significance of the fold increase in number of vesicles in pooled density fractions or per density fraction (as compared to the number of vesicles in the non-activated condition, which was set to 1) was tested with a one-sample T-test with Bonferonni correction. Differences between multiple groups were compared using the ANOVA, in which the experimental batch was introduced as a random factor, post-hoc comparisons were performed using Tukey's post-hoc test. When a significant interaction was observed between two factors (as was the case when the two density fractions with respect to the distribution of the three subpopulations were compared), both factors were analyzed separately. For comparison of the reduced wide angle FSC geometric means the paired student's T-test was applied. In all cases a two-sided p-value < 0.05 was considered statistically significant. Asterisks indicate p-values: $p < 0.05$ (*), $p \leq 0.01$ (**) or $p \leq 0.001$ (***).

Results and Discussion

In order to quantify and characterize the population of nano-sized vesicles released by $CD4^+$ T cells after different activation stimuli, T cells were activated by TCR-triggering via plate-bound anti-CD3 in the absence or presence of co-stimulation via plate-bound anti-CD28. With this approach interactions between T cells and APC were mimicked and T cell-derived vesicles could be analyzed in the absence of APC-derived vesicles.

Activation of KO4C1 T cells was confirmed by the expression of the early activation marker CD69 which was highest on T cells activated by high concentrations of both anti-CD3 and anti-CD28 (**Fig. 1A**). T cells fully down-regulated TCR and produced interferon-gamma (IFN-γ) in response to strong TCR-triggering independently of additional co-stimulation (**Fig. 1B and C**). Weaker TCR-triggering in the presence of strong co-stimulation, however, resulted in partial TCR down-regulation and lower IFN-γ production (**Fig. 1B and C**).

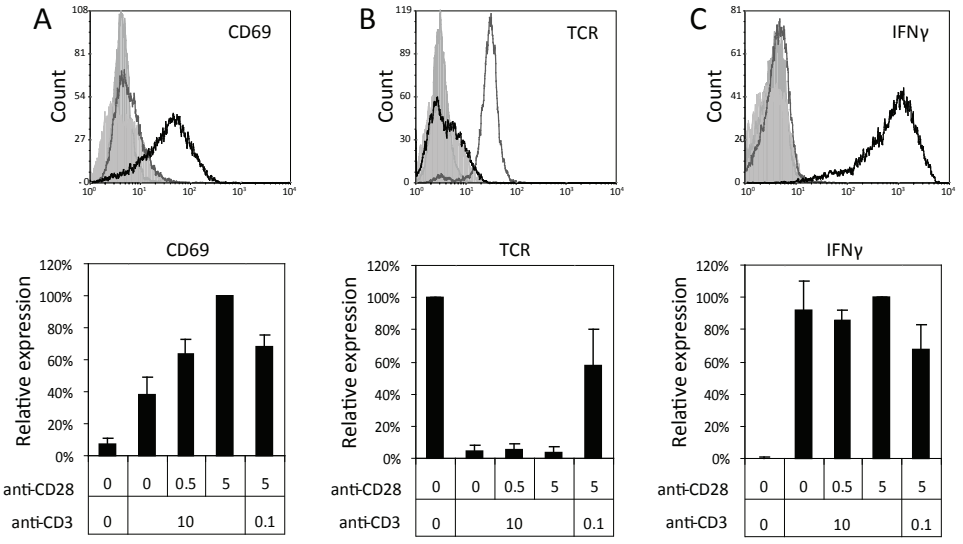

Figure 1 – Analysis of T cell activation after different levels of TCR- and co-stimulation triggering
$CD4^+$ T cells (KO4C1) were activated by TCR-triggering (0.1 or 10 µg/ml plate-bound anti-CD3), with or without additional co-stimulation (0.5 or 5 µg/ml plate-bound anti-CD28) for 20 hrs and compared to non-activated T cells. Cells were analyzed for CD69 up-regulation (**A**), TCR down-regulation (**B**), and IFN-gamma production (**C**) by flow cytometry. Histograms (top panels) show the expression of indicated markers on non-activated T cells (grey line) or on T cells activated with anti-CD3 (10 µg/ml) and anti-CD28 (5 µg/ml) (black line) or isotype control stainings (filled histograms). The bar graphs (bottom panels) show the geometric means expressed as percentages of maximal expression of the indicated markers (set to 100%) of at least three independent experiments.

To accurately assess the number of nano-sized vesicles released by these differentially activated T cells, we used our recently developed fluorescence-based high-resolution flow cytometric method (16). T cell-derived vesicles were collected from cell culture supernatants by differential (ultra)centrifugation, labeled with the fluorescent membrane dye PKH67 and then floated into a sucrose gradient. Nano-sized vesicles within the buoyant density range characteristic for exosomes (1.10-1.19 g/ml) were collected and analyzed. A threshold was set on fluorescence to distinguish vesicles from noise signals (16). T cell-derived vesicles could be detected well above this threshold (**Fig. 2A**). As shown in **Figure 2B**, KO4C1 T cells that were activated through TCR-triggering released 1.6-fold (± 0.3, p = 0.04) more vesicles in comparison to non-activated T cells. These data confirm previous indications based on bulk analyses that the number of nano-sized vesicles released by $CD4^+$ T cells increases upon TCR-triggering (3, 7). Importantly, we observed that co-stimulation had a potentiating effect on the release of T cell-derived vesicles. Simultaneous strong triggering of TCR and CD28 resulted in a 2.3-fold (± 0.6, p = 0.01) increase, as compared to non-activated T cells, whereas strong co-stimulation in the presence of weak TCR-triggering only slightly increased vesicle release (**Fig. 2B**). Although TCR down-regulation and IFN-γ production were not increased by additional co-stimulation in the KO4C1 T cell clone, the potentiating effect on CD69 up-regulation indicated that co-stimulation affected the activation status of the T cells. Concomitantly, we observed that the release of vesicles was further increased by co-stimulation.

Previously, we observed that the total pool of nano-sized vesicles released by cells can be heterogeneous (16). We therefore performed a more detailed quantitative analysis of vesicles that equilibrated at different densities in a sucrose gradient. We found that the vast majority of nano-sized vesicles derived from non-activated T cells and T cells activated with high levels of TCR-triggering and co-stimulation equilibrated at densities of 1.12-1.17 g/ml (**Fig. 2C**). The highest increase in number of released vesicles observed after T cell activation could be attributed to vesicles with a buoyant density of 1.14-1.17 g/ml (**Fig. 2D**). Moreover, the 2.7-fold increase of vesicles with a buoyant density of 1.17 g/ml was significantly higher compared to the 1.9-fold increase in vesicles equilibrating at 1.14 g/ml (**Fig. 2D**). These data indicate that heterogeneity exists within the pool of released T cell vesicles and that the release of different vesicle populations is differentially regulated upon T cell activation.

To investigate the vesicles equilibrating at 1.14 or 1.17 g/ml in more detail, we first analyzed their size by Nano-particle Tracking Analysis (NTA). NTA is a relatively new technique used to determine the size of individually tracked vesicles based on their Brownian motion (27). When compared to other techniques, such as electron microscopy or atomic force microscopy, NTA is currently the most suitable method for absolute sizing of considerable numbers of individual vesicles (20, 28). Based on NTA we found that the

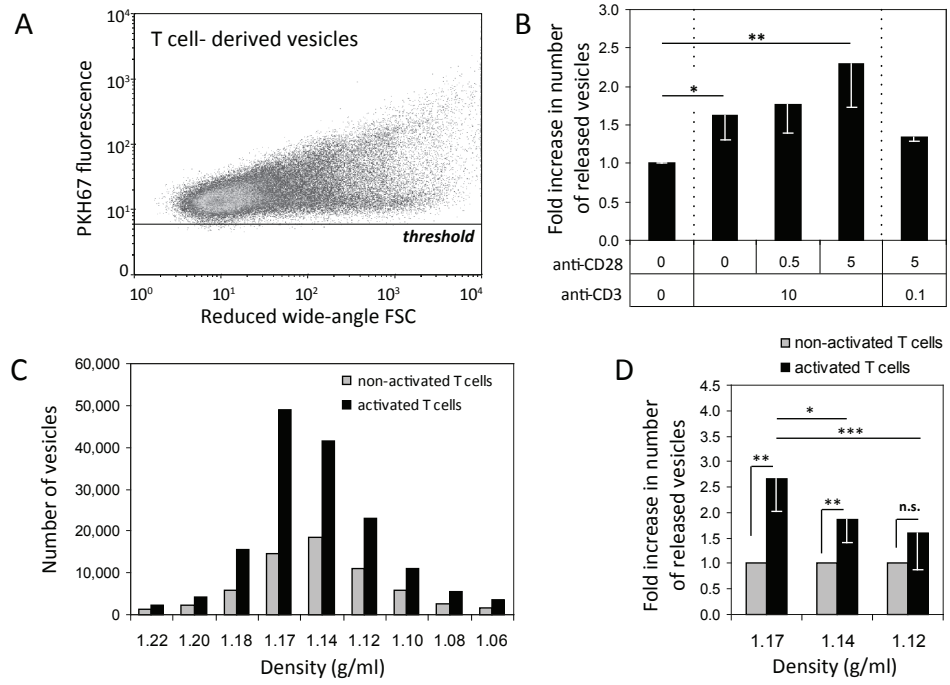

Figure 2 – Quantitative analysis of nano-sized vesicles released by T cells KO4C1 T cells were activated as described in Figure 1. Vesicles released by T cells were isolated from culture supernatants, labeled with the fluorescent membrane dye PKH67 and floated to equilibrium density into a sucrose gradient. The vesicles in the collected sucrose gradient fractions were analyzed by fluorescence-based high-resolution flow cytometry. (**A**) Dot plot of reduced wide-angle FSC versus PKH67 fluorescence representing fluorescent vesicles derived from non-activated T cells (from pooled fractions with densities of 1.12 – 1.17 g/ml). (**B**) Fluorescently labeled vesicles from differently activated T cells were quantified using our time-based quantification method. Indicated are the average and standard deviation of the number of vesicles released of 3 - 6 independent experiments (from fractions with densities of 1.10-1.19 g/ml). The number of vesicles derived from non-activated T cells was set to 1. (**C**) Fluorescently labeled vesicles from non-activated or activated (10 µg/ml anti-CD3 + 5 µg/ml anti-CD28) T cells were quantified using our time-based quantification method. Indicated is the number of events measured in 30 seconds in the indicated sucrose gradient density fractions. One representative out of six experiments is shown (**D**) Fold increase in the number of released vesicles upon activation (10 µg/ml anti-CD3 + 5 µg/ml anti-CD28) of T cells per density fraction. Indicated are the averages and standard deviations of nine independent experiments. The number of vesicles released by non-activated T cells was set to 1 for each density fraction. Asterisks denote significant differences (* = $p < 0.05$, ** = $p \leq 0.01$, *** = $p \leq 0.001$)

population of vesicles that equilibrated at 1.14 g/ml had an average size of 103 ± 50 nm (**Fig 3A**). Compared to a mono-disperse 100 nm bead population, these vesicles showed a more heterogeneous size distribution (**Fig. 3A**). Vesicles present in the higher density fraction (1.17 g/ml) were larger (166 ± 78 nm) and also displayed a broad size distribution (**Fig. 3A**).

In flow cytometry, forward scattered light (FSC) is often used as a measure for size. However, conventional flow cytometers do not allow detection of particles smaller than 300 nm based on FSC. We recently developed a flow cytometry-based method for analysis of ~100 nm fluorescent particles by optimizing the FSC detection angle and signal-to-noise ratio (16). Although forward scattering of nano-sized particles is not only influenced by their size but also by their refractive index, surface roughness, shape and possibly light absorption (29, 30), we previously demonstrated that our reduced wide-angle FSC based analysis allows for approximate and relative sizing of cell-derived nano-sized vesicles with comparable composition (16). In contrast to NTA, flow cytometry-based FSC measurements are not hampered by the size heterogeneity of vesicle populations. Moreover, high-resolution flow cytometric analysis allows the simultaneous analysis of multiple parameters on single vesicles, which is needed for the characterization of subpopulations within the total pool of vesicles. By flow cytometric analysis, we found that vesicles equilibrating at 1.17 g/ml displayed higher FSC levels than vesicles equilibrating at 1.14 g/ml (**Fig. 3C**). The FSC level distributions displayed by the two vesicles populations (**Fig. 3B**) were largely comparable to their size distribution as determined by NTA (**Fig. 3A**).

The broad size and FSC distribution of vesicles within the 1.14 and 1.17 g/ml density fractions indicated heterogeneity within these vesicle populations. To study this heterogeneity, we analyzed fluorescence and reduced wide-angle FSC levels of these vesicles in more detail. Based on their reduced wide-angle FSC (indicated as rw-FSC) and fluorescence signals (FL), we could observe three vesicle subpopulations (**Fig. 3D**). The vesicle subpopulation exhibiting low rw-FSC and low fluorescence (rw-FSC^{low}FL^{low}) may consist of relatively small vesicles. The population exhibiting higher rw-FSC and fluorescence (rw-FSC^{high}FL^{high}) may represent vesicles larger in size or aggregates of smaller vesicles. The rw-FSC^{high}FL^{low} population may consist of small vesicles (based on the low fluorescence) containing more or other cargo which induces higher levels of rw-FSC as compared to the rw-FSC^{low}FL^{low} vesicle subpopulation. Alternatively, the rw-FSC^{high}FL^{low} population may consist of larger vesicles or aggregates that have a distinct lipid bilayer compared to the rw-FSC^{high}FL^{high} vesicles and have therefore incorporated less fluorescent membrane dye. These data demonstrate that CD4^{+} T cell-derived nano-sized vesicle populations with similar buoyant densities are heterogeneous.

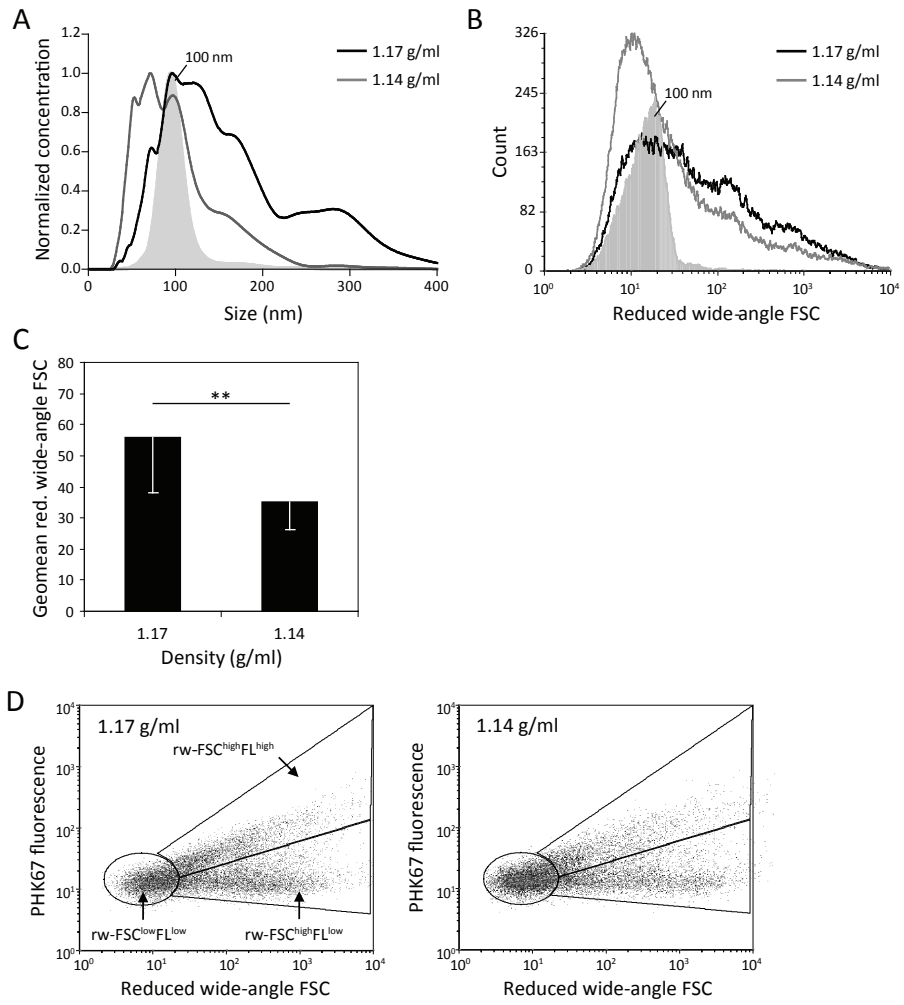

Figure 3 – Heterogeneity in T cell-derived vesicle populations with different buoyant densities
Vesicles released by non-activated T cells were isolated and analyzed as described in Figure 2. (**A, B**) Histograms indicating size as determined by NTA (**A**) or reduced wide-angle FSC as determined by high-resolution flow cytometry (**B**) of 100 nm beads (filled histograms, light grey) and T cell-derived vesicles in fractions with densities of 1.17 g/ml (black line) or 1.14 g/ml (dark grey line). (**C**) Reduced wide-angle FSC geometric means of vesicles from non-activated T cells with densities of 1.17 or 1.14 g/ml. Indicated are the averages and standard deviation of geometric mean values of six independent experiments. Asterisks denote significant differences (** = $p \leq 0.01$). Histograms in (**A**) and (**B**) are from the same experiment, representative of six (**A**) or five (**B**) experiments. (**D**) Dot plots representing wide-angle FSC and PKH67 fluorescence of vesicles from non-activated T cells floating at 1.17 (left) and 1.14 g/ml (right). Gates were set around vesicles subpopulations with low reduced wide-angle FSC levels and low fluorescence ($FSC^{low}FL^{low}$), high(er) reduced wide-angle FSC levels and high(er) fluorescence ($FSC^{high}FL^{high}$) or high(er) reduced wide-angle FSC levels and low fluorescence ($FSC^{high}FL^{low}$).

Next, we investigated whether the three subpopulations present within the 1.14 and 1.17 g/ml density fractions (**Fig. 3D**) similarly changed upon T cell activation. In both density fractions, the number of vesicles in all three subpopulations increased upon T cell activation (**Fig. 4A**). Interestingly, we found a significant difference between the two density fractions with respect to the distribution of the three subpopulations ($p < 0.01$). Indeed, the rw-FSC^{high}FL^{high} subpopulation present in the 1.17 g/ml fraction consistently increased more upon T cell activation compared to the other subpopulations within this fraction and compared to the subpopulations within the 1.14 g/ml fraction (**Fig. 4B**). This increase in number of rw-FSC^{high}FL^{high} vesicles was dependent on the presence of strong co-stimulatory signals. These data indicate that T cell activation signals can significantly alter the composition of the total pool of released vesicles.

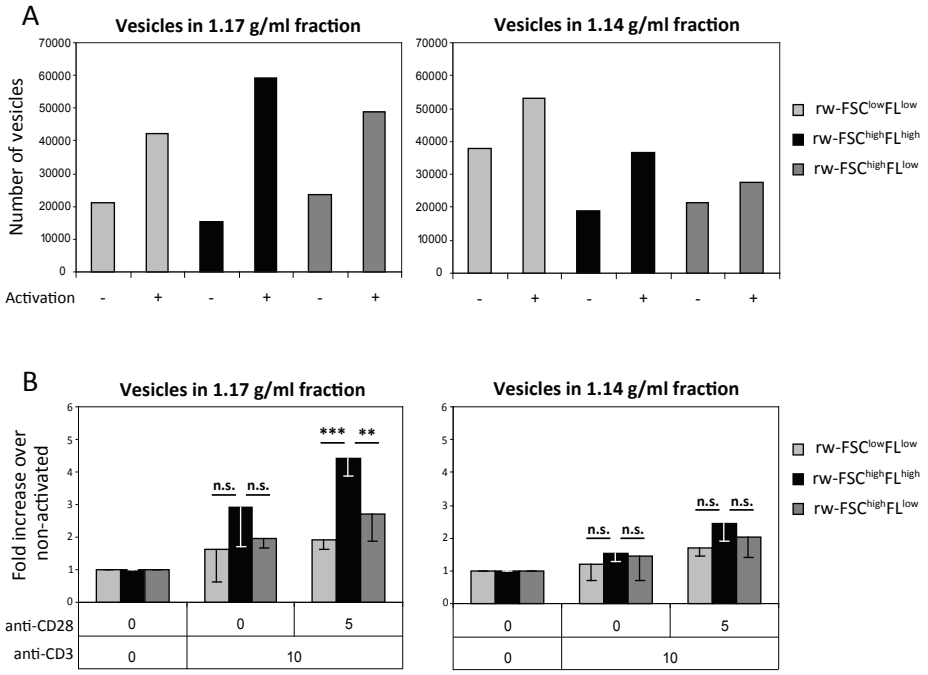

Figure 4 – T cells differentially regulate the release of distinct vesicle subpopulations upon different activation signals Vesicles from activated (10 µg/ml anti-CD3 + 5 µg/ml anti-CD28) and non-activated T cells were isolated and analyzed as described in Figure 2. (**A**) Time-based quantification of T cell-derived vesicles in different density fractions in the three different vesicle subpopulation gates, as described in Figure 3D. Indicated are the numbers of vesicles per gate measured in 30 sec. One representative experiment out of four is shown. (**B**) Indicated is the average fold increase +/- s.d. in number of vesicles released by T cells per FSC-FL gate, activated by TCR-triggering alone or with additional co-stimulation, relative to the number of vesicles from non-activated T cells (set to 1). Averages and standard deviations are displayed for vesicles with a density of 1.17 (left graph) or 1.14 g/ml (right graph) of four independent experiments. Asterisks denote significant differences (** = $p \leq 0.01$, *** = $p \leq 0.001$).

Conclusively, we here show that $CD4^+$ T cells release more vesicles upon T cell activation. This increase in vesicle release was most prominent in the vesicle population equilibrating at 1.17 g/ml and was significantly higher compared to other density fractions. Within this density fraction one vesicle subpopulation ($FSC^{high}FL^{high}$) increased significantly more as compared to the other subpopulations. This higher increase was significant upon T cell activation with TCR-triggering and additional co-stimulation, indicating that activation signals contribute to the regulated release of distinct vesicle subpopulations. Based on our findings, we hypothesize that APC displaying specific MHC-peptide complexes to T cells may be involved in the fine-tuning of T cell vesicle-mediated intercellular communication by regulating the release of vesicles via co-stimulatory signals. Furthermore, the molecular composition of T cell-derived vesicles might vary depending on the type and level of co-stimulation. It is therefore important to study the protein, lipid and RNA content of T cell-derived vesicle populations released after different co-stimulatory triggers. Currently it is not feasible to isolate vesicle subpopulations by flow cytometric sorting. Alternatively immuno-affinity bead capture of vesicles can be used for selective enrichment or depletion of vesicle subpopulations based on specific protein markers. Furthermore, we recently demonstrated that different vesicle subpopulations with the same buoyant density can be separated by limiting the floatation time into a sucrose gradient (15). The further analysis of the molecular composition of vesicle subpopulations released after different immunological cues will be helpful to determine the physiological role of $CD4^+$ T cell-derived vesicles in immune regulation.

Acknowledgements

We thank M. de Boer-Brouwer and M. van Steenbergen for excellent technical assistance. We thank prof. dr. C. Melief (Leiden University Medical Center, The Netherlands) for providing the KO4C1 T cell clone and dr. L. Boon (Bioceros, Utrecht) for providing monoclonal antibodies. We thank dr. A. Sijts for critical reading of the manuscript.

References

1. Cocucci E, Racchetti G, Meldolesi J. Shedding microvesicles: Artefacts no more. Trends in cell biology. 2009 Feb;19(2):43-51.
2. Thery C, Ostrowski M, Segura E. Membrane vesicles as conveyors of immune responses. Nature reviews. 2009 Aug;9(8):581-93.
3. Blanchard N, Lankar D, Faure F, Regnault A, Dumont C, Raposo G, et al. TCR activation of human T cells induces the production of exosomes bearing the TCR/CD3/zeta complex. J Immunol. 2002 Apr 1;168(7):3235-41.
4. Booth AM, Fang Y, Fallon JK, Yang JM, Hildreth JE, Gould SJ. Exosomes and HIV gag bud from endosome-like domains of the T cell plasma membrane. J Cell Biol. 2006 Mar 13;172(6):923-35.
5. Martinez-Lorenzo MJ, Anel A, Gamen S, Monle nI, Lasierra P, Larrad L, et al. Activated human T cells release bioactive fas ligand and APO2 ligand in microvesicles. J Immunol. 1999 Aug 1;163(3):1274-81.
6. Monleon I, Martinez-Lorenzo MJ, Monteagudo L, Lasierra P, Taules M, Iturralde M, et al. Differential secretion of fas ligand- or APO2 ligand/TNF-related apoptosis-inducing ligand-carrying microvesicles during activation-induced death of human T cells. J Immunol. 2001 Dec 15;167(12):6736-44.
7. Alonso R, Rodriguez MC, Pindado J, Merino E, Merida I, Izquierdo M. Diacylglycerol kinase alpha regulates the secretion of lethal exosomes bearing fas ligand during activation-induced cell death of T lymphocytes. J Biol Chem. 2005 Aug 5;280(31):28439-50.
8. Busch A, Quast T, Keller S, Kolanus W, Knolle P, Altevogt P, et al. Transfer of T cell surface molecules to dendritic cells upon CD4+ T cell priming involves two distinct mechanisms. J Immunol. 2008 Sep 15;181(6):3965-73.
9. Zhang H, Xie Y, Li W, Chibbar R, Xiong S, Xiang J. CD4(+) T cell-released exosomes inhibit CD8(+) cytotoxic T-lymphocyte responses and antitumor immunity. Cell Mol Immunol. 2011 Jan;8(1):23-30.
10. Nolte-'t Hoen EN, Wagenaar-Hilbers JP, Peters PJ, Gadella BM, van Eden W, Wauben MH. Uptake of membrane molecules from T cells endows antigen-presenting cells with novel functional properties. European journal of immunology. 2004 Nov;34(11):3115-25.
11. Scanu A, Molnarfi N, Brandt KJ, Gruaz L, Dayer JM, Burger D. Stimulated T cells generate microparticles, which mimic cellular contact activation of human monocytes: Differential regulation of pro- and anti-inflammatory cytokine production by high-density lipoproteins. J Leukoc Biol. 2008 Apr;83(4):921-7.
12. Carpintero R, Gruaz L, Brandt KJ, Scanu A, Faille D, Combes V, et al. HDL interfere with the binding of T cell microparticles to human monocytes to inhibit pro-inflammatory cytokine production. PLoS One. 2010 Jul 29;5(7):e11869.
13. Zakharova L, Svetlova M, Fomina AF. T cell exosomes induce cholesterol accumulation in human monocytes via phosphatidylserine receptor. J Cell Physiol. 2007 Jul;212(1):174-81.
14. Shefler I, Salamon P, Reshef T, Mor A, Mekori YA. T cell-induced mast cell activation: A role for microparticles released from activated T cells. J Immunol. 2010 Oct 1;185(7):4206-12.
15. Aalberts M, van Dissel-Emiliani FM, van Adrichem NP, van Wijnen M, Wauben MH, Stout TA, et al. Identification of distinct populations of prostasomes that differentially express prostate stem cell antigen, annexin A1 and GLIPR2 in humans. Biol Reprod. 2011 Nov 30.
16. Nolte-'t Hoen EN, van der Vlist EJ, Aalberts M, Mertens HC, Jan Bosch B, Bartelink W, et al. Quantitative and qualitative flow cytometric analysis of nano-sized cell-derived membrane vesicles. Nanomedicine. 2011 Oct 21.
17. Théry C, Amigorena S, Raposo G, Clayton A. Isolation and characterization of exosomes from cell culture supernatants and biological fluids. In: Current Protocols in Cell Biology. John Wiley & Sons, Inc.; 2001.
18. Bobrie A, Colombo M, Raposo G, Thery C. Exosome secretion: Molecular mechanisms and roles in immune responses. Traffic. 2011 Dec;12(12):1659-68.

19. Gyorgy B, Modos K, Pallinger E, Paloczi K, Pasztoi M, Misjak P, et al. Detection and isolation of cell-derived microparticles are compromised by protein complexes resulting from shared biophysical parameters. Blood. 2011 Jan 27;117(4):e39-48.
20. Sokolova V, Ludwig AK, Hornung S, Rotan O, Horn PA, Epple M, et al. Characterisation of exosomes derived from human cells by nanoparticle tracking analysis and scanning electron microscopy. Colloids Surf B Biointerfaces. 2011 Oct 1;87(1):146-50.
21. Yuana Y, Oosterkamp TH, Bahatyrova S, Ashcroft B, Garcia Rodriguez P, Bertina RM, et al. Atomic force microscopy: A novel approach to the detection of nanosized blood microparticles. J Thromb Haemost. 2010 Feb;8(2):315-23.
22. Raposo G, Nijman HW, Stoorvogel W, Liejendekker R, Harding CV, Melief CJ, et al. B lymphocytes secrete antigen-presenting vesicles. J Exp Med. 1996 Mar 1;183(3):1161-72.
23. Lauwen MM, Zwaveling S, de Quartel L, Ferreira Mota SC, Grashorn JA, Melief CJ, et al. Self-tolerance does not restrict the CD4+ T-helper response against the p53 tumor antigen. Cancer Res. 2008 Feb 1;68(3):893-900.
24. Buschow SI, Nolte-'t Hoen EN, van Niel G, Pols MS, ten Broeke T, Lauwen M, et al. MHC II in dendritic cells is targeted to lysosomes or T cell-induced exosomes via distinct multivesicular body pathways. Traffic. 2009 Oct;10(10):1528-42.
25. Assenmacher M, Schmitz J, Radbruch A. Flow cytometric determination of cytokines in activated murine T helper lymphocytes: Expression of interleukin-10 in interferon-gamma and in interleukin-4-expressing cells. Eur J Immunol. 1994 May;24(5):1097-101.
26. Nolte-'t Hoen EN, Buschow SI, Anderton SM, Stoorvogel W, Wauben MH. Activated T cells recruit exosomes secreted by dendritic cells via LFA-1. Blood. 2009 Feb 26;113(9):1977-81.
27. Filipe V, Hawe A, Jiskoot W. Critical evaluation of nanoparticle tracking analysis (NTA) by NanoSight for the measurement of nanoparticles and protein aggregates. Pharm Res. 2010 May;27(5):796-810.
28. van der Pol E, Hoekstra AG, Sturk A, Otto C, van Leeuwen TG, Nieuwland R. Optical and non-optical methods for detection and characterization of microparticles and exosomes. J Thromb Haemost. 2010 Dec;8(12):2596-607.
29. Shapiro HM. Practical flow cytometry. 4th edition ed. New York: Wiley-Liss; 2003.
30. Lacroix R, Robert S, Poncelet P, Dignat-George F. Overcoming limitations of microparticle measurement by flow cytometry. Semin Thromb Hemost. 2010 Nov;36(8):807-18.

Everything you imagine is real – Pablo Picasso

Chapter 6

Functional effects of extracellular vesicles released during cognate DC-T cell interaction

Els J. van der Vlist, Marca H.M. Wauben and Esther N.M. Nolte - 't Hoen

Abstract

Extracellular vesicles (EV) are released by many cell types and play a role in intercellular communication. Both dendritic cells (DC) and T cells increase their EV release upon activation during cognate interactions. EV that are released into the extracellular milieu during cognate DC-T cell interaction are heterogeneous and hence are likely to be targeted to different cell types and to elicit different effects. Whether these EV are involved in the amplification, dampening or skewing of immune responses is not known. We here designed an *in vitro* model system to study the functional effects of EV released during strong stimulatory cognate DC-T cell interactions on neighboring DC and T cells engaged in suboptimal cognate interactions. We found that both DC and T cells recruited these EV, and that EV recruitment during suboptimal DC-T cell interactions resulted in increased CD69 levels on DC and sustained TCR levels on T cells. No clear effects were observed on cytokine levels and expression levels of several other activation markers. Our data show that EV released during strong stimulatory cognate DC-T cell interactions are targeted to neighboring DC and T cells and might be involved in the modulation of suboptimal cognate DC-T cell interactions.

Introduction

Crosstalk between dendritic cells (DC) and $CD4^+$ T cells is crucial for the initiation and regulation of adaptive immune responses. Communication between DC and T cells can take place via direct cell-cell interactions, secretion of soluble factors or the release of extracellular vesicles. Extracellular vesicles (EV) uniquely allow transfer of transmembrane proteins, selected lipids and cytosolic components between cells. Both the molecular composition of EV and the number of released EV are dynamic and depend on the activation status of the producing cell (reviewed in (1, 2)). Hence, communication via EV represents a clever mechanism of information transfer between cells, since multiple signals can be integrated in one tailor-made vehicle.

Both DC and $CD4^+$ T cells increase their release of EV in response to activation signals. For DC, danger signals such as bacterial lipopolysaccharide (LPS) (3, 4), but also cognate interaction with $CD4^+$ T cells (5) provide activation signals that trigger EV release. DC-derived EV have been described to enhance immune responses by spreading of MHC-peptide complexes (MHCp), which can be directly or indirectly presented to $CD4^+$ T cells (6-8) and $CD8^+$ T cells (9, 10). EV from LPS- or IFN-γ-activated DC (mature DC) are often more potent in eliciting a functional T cell response than EV from immature DC (8, 11). Besides amplification of immune responses, DC-derived EV can also have tolerogenic properties. Administration of immature DC-derived EV prior to allograft transplantation, for instance, can delay acute rejection and prolong survival of the transplant (12, 13). T cells release more EV after T cell receptor (TCR) triggering and further increase their EV release in response to additional co-stimulation signals (14, 15). Up to now, EV from activated $CD4^+$ T cells have been described to have immune suppressive effects on DC and T cells, either by blocking of MHCII on DC (16, 17) or by inducing apoptosis of both DC and bystander T cells via Fas-ligand (16, 18, 19).

In most functional studies described above, EV were derived from *in vitro* single cell type cultures of DC or T cells. Activation of T cells in these cultures was often established by mimicking the antigen-specific interaction with antigen presenting cells using anti-CD3 (and anti-CD28) antibodies. Such single cell type cultures are useful to study functional effects of DC- or T cell-derived EV. However, a major disadvantage of these studies is the lack of additional DC-T cell interaction signals that might influence EV composition or release. Moreover, part of the EV released during cognate DC-T cell interaction is directly targeted to the interacting cells, for instance via the immune synapse (20). Consequently, only part of the produced EV is released in the extracellular milieu and available for targeting to neighboring cells. Finally, it is possible that EV derived from DC and T cells have additive effects on the function of target cells. Functional analysis of EV released during DC-T cell co-cultures, instead of single cell type cultures, is therefore relevant to investigate the physiological role of DC- and T cell-derived EV.

DC actively transport antigens derived from peripheral tissues to secondary lymphoid organs. Within these lymphoid organs DC interact with T cells and, upon antigen recognition and appropriate co-stimulation signals, T cell priming can take place. EV released during DC-T cell interactions may be recruited by neighboring DC and T cells present in the same lymphoid organ, and may modify the function of these recruiting cells. In this way, EV produced during cognate DC-T cell interactions may contribute to regulation of immune responses. We have previously shown that MHCII-carrying EV isolated from *in vitro* cognate DC-T cell co-cultures can be recruited by neighboring DC and activated T cells (21). Binding and surface presentation of MHCII-carrying EV by activated T cells has been proposed to be involved in dampening of immune responses (22). However, functional effects of EV produced during cognate interaction on neighboring DC or T cells were not studied.

We therefore designed an *in vitro* model system to investigate the immune modulatory potential of EV released during strong stimulatory DC-T cell interactions on neighboring DC-T cell interactions (Figure 1). Although *in vivo*, such EV might be targeted to several different types of cells, we here focused on their effects on DC and T cells. Effects were studied early during suboptimal DC-T cell interactions to maximize the window in which modulatory signals can be observed. We analyzed EV recruitment onto DC and T cells, and the effect of these EV on cytokine production and expression of activation markers by both cell types (**Figure 1**). This chapter provides first indications for a physiological role of EV released into the extracellular milieu during cognate DC-T cell interactions.

Materials and Methods

The cartoon in **Figure 1** provides a summary of the experimental setup.

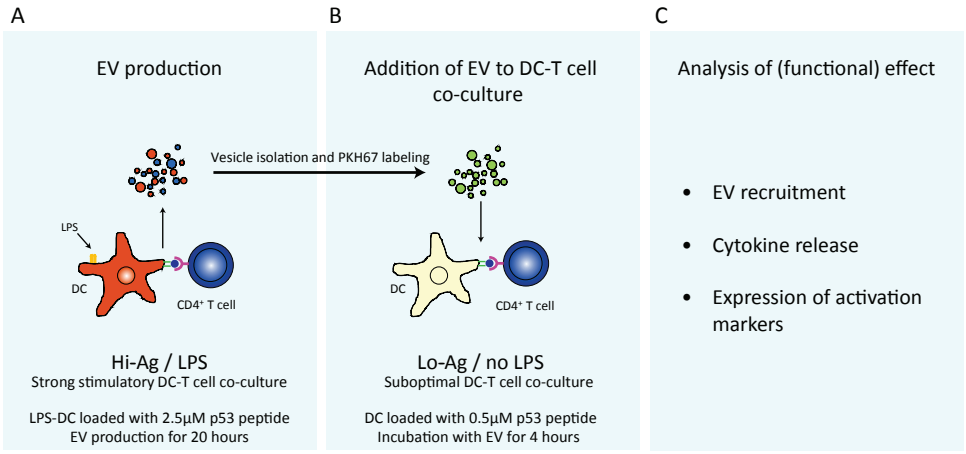

Figure 1 – Experimental setup to test functional effects of extracellular vesicles released during strong stimulatory cognate DC-T cell interaction (**A**) For extracellular vesicle (EV) production, p53 peptide-loaded (Hi-Ag) LPS-activated D1-DC were cultured together with the p53-specific $CD4^+$ T cell clone (KO4C1) for 20 hours. After overnight culture, EV were isolated from the co-culture supernatant by differential centrifugation and stained with PKH67. (**B**) D1-DC and KO4C1 T cells engaged in suboptimal interactions (Lo-Ag) were incubated with the PKH67-stained EV or medium control (not shown) for 4 hours. (**C**) The amount of recruited PKH67 label on DC or T cells was analyzed by flow cytometry. The released cytokine concentrations were measured by a multiplexed cytokine assay. Expression of activation markers on DC or T cells was analyzed by flow cytometry after immuno-labeling.

Cell culture

The p53-specific $CD4^+$ T cell clone (KO4C1), generated in a C57BL/6 p53 knockout mouse, recognizes the peptide corresponding to amino acids 77-96 of murine p53 (23). As previously described (5), T cells were restimulated with peptide-pulsed irradiated splenocytes for 3 days and isolated through centrifugation onto Ficoll-Hypaque, after which they were expanded with recombinant human IL-2 (Roche). The mouse immature DC cell line D1 is derived from a C57BL/6 mouse (24). Both DC and T cells were maintained in IMDM (Gibco) with 10% fetal bovine serum (PAA), 100 UI/ml penicillin, 100 µM streptomycin (both Gibco), 2 mM Ultraglutamine (Biowhittaker) and 30 µM βmercapto-ethanol (T cell medium) at 37°C, 5% CO2. DC culture medium (D1 medium) was further supplemented with 30% conditioned medium from GM-CSF producing NIH 3T3 cells (R1). To deplete R1-conditioned medium or fetal bovine serum (FBS) from exosomes and other EV, R1-conditioned medium or 30% FBS in IMDM was ultracentrifuged for at least 15

hours at 100,000g (SW28 rotor of Beckman Coulter Optima L-90K). Experiments were approved by the institutional ethical animal committee at Utrecht University (Utrecht, The Netherlands).

DC-T cell co-cultures for EV production

Approximately 7 x 10^6 DC per 10 cm culture dish were pulsed overnight with 2.5 µM p53 peptide in the presence of 10 µg/ml LPS (E. coli, from Fluka), after which medium was replaced with 12,5 ml fresh EV-depleted D1 medium. T cells were directly added to DC in a 1:1 ratio and co-cultured for 20 hours (**Figure 1**). As a negative control plain EV-depleted D1 medium supplemented with p53 peptide and LPS (medium control) was incubated under cell culture conditions for 20 hours.

EV isolation and labeling

EV were isolated from co-culture supernatants by differential steps of (ultra)centrifugation as described previously (25). In short, culture supernatants were cleared from cells by centrifugation at 200g and 500g. Both steps were performed twice for 10 min. Larger debris was removed from supernatant by centrifugation at 10,000g for 30 min using a SLA-600TC rotor in a Sorvall RC5Bplus centrifuge. Subsequently, EV were pelleted for 65 min at 100,000g using a SW28 rotor in a Beckman Coulter Optima L-90K ultracentrifuge. EV pellets were stained with the intercalating fluorescent membrane dye PKH67 (7.5 µM, Sigma Aldrich) according to manufacturer's protocol and as previously described (15). The staining procedure was stopped and EV were washed by adding 12ml EV-depleted T cell medium. The EV were pelleted once more at 100,000g for 65 min, resuspended in D1 medium and added to DC-T cell co-cultures. Differential centrifugation and PKH67 staining were also performed on the medium control. All centrifugation steps were performed at 4°C.

EV recruitment by DC-T cell co-cultures

For EV recruitment, 10^6 DC were loaded with 0.5 µM p53 peptide or no peptide for 2 hours. After peptide incubation, medium was replaced with 1ml fresh D1 medium (6-well plate). PKH67 labeled EV were added directly to DC and within 15 minutes 10^6 T cells were added and co-cultured for 4 hours (**Figure 1**). EV recruited by 10^6 DC and 10^6 T cells were derived from cognate co-cultures of approximately 5.5 x 10^6 DC and 5.5 x 10^6 T cells.

Flow cytometric analysis of cells

DC-T cell co-cultures were harvested and immuno-labeled for 30 min on ice in phosphate-buffered saline (PBS)/1% bovine serum albumin (BSA) and fixed with 4% paraformaldehyde for 5 minutes. Anti–CD69-PE (H1.2F3), anti-TCR-Vβ11-PE (CTVB11), anti-MHC class II-PE (M5/114.15.2), anti-CD25-PE (PC61.5), anti-CD86-PE (GL1), anti-CD4-APC (GK1.5), anti-

CD11c-PerCP (N418) and isotype control antibodies were from eBiosciences. Cells were analyzed by flow cytometry using a FACSCanto and FACSDiva software (BD Biosciences) or FCS Express software (De Novo Software). CD4/CD11c-staining was used to gate DC or T cell populations.

Multiplexed cytokine assay

Cytokine concentrations in supernatant of DC-T cell co-cultures were determined using a multiplexed cytokine assay (26). Briefly, fluorescent micro-sized beads (MicroPlex Microspheres, Luminex) were coated with different antibodies against IL-2 (JES6-1A12), IL-4 (BVD4.1D11), IL-5, (TRFK5), IL-6 (MP5-20F3), IL-10 (JES5-2A5), IL-12p70 (9A5), IL-17a (TC11-18H10), IFN-γ (AN18) and TNF-α (G281.2626). A series of two-fold dilutions of recombinant cytokines was used to create a calibration curve. The beads were added to the culture supernatant or diluted recombinant cytokines and allowed to capture cytokines overnight. Cytokines were detected by biotinylated antibodies against IL-2 (JES6-5H4), IL-4 (BVD6-24G2), IL-5 (TRFK4), IL-6 (MP5-32C11), IL-10 (SXC-1), IL-12p70 (C17.8), IL-17a (TC11-8H4.1) IFN-γ (XMG1.2) and TNF-α (MP6-XT3) followed by PE-labeled streptavidin (all BD Biosciences Pharmingen). Fluorescence per bead was measured using a Luminex model 100 XYP (Luminex). Per cytokine, at least 100 beads were measured. Trimmed means of fluorescence were used for analysis.

Statistics

Results are expressed as mean ± standard deviation. Significance of differences in EV recruitment, surface marker expression and cytokine production by DC and T cells, after incubation with co-culture EV or medium control, was tested using the paired student's T-test. In all cases, a two-sided p-value ≤ 0.05 was considered statistically significant. Asterisks indicate p-values: $p \leq 0.05$ (*) or $p \leq 0.01$ (**).

Results

We set out to investigate whether EV released during strong stimulatory DC-T cell interactions (high-dose antigen and LPS (Hi-Ag/LPS)) could influence DC and T cells engaged in suboptimal low-dose antigen (Lo-Ag) interactions.

The DC used in our model system is a DC cell line (D1) which upregulates CD80 and CD86 in the presence of LPS (27), but which is in its non-activated state well capable of activating antigen-experienced T cells. The KO4C1 T cell used in our model system is a p53-specific $CD4^+$ T cell clone and can be regarded as an antigen-experienced T cell. In previous experiments, we determined the antigen dose response curve of the KO4C1 T cells, by culturing them with DC loaded with different concentrations of cognate p53 peptide (unpublished data). The respective 0.5 µM and 2.5 µM p53 peptide used in the present study can be regarded as suboptimal (Lo-Ag) and optimal (Hi-Ag) peptide concentrations for KO4C1 T cell stimulation.

We first investigated whether EV released by DC and T cells during Hi-Ag/LPS interactions were recruited to DC and T cells engaged in suboptimal interactions with the same antigen specificity (Lo-Ag). EV released during Hi-Ag/LPS DC-T cell interactions were labeled with the intercalating membrane dye PKH67. The labeled EV were added to DC-T cell cultures in the presence of Lo-Ag and EV recruitment was monitored after four hours. As a negative control also plain culture medium was centrifuged (100,000g) and labeled with PKH67. We found that both DC and T cells acquired PKH67 during cognate interaction, but DC acquired relatively more PKH67 than T cells (**Figure 2A and B**). DC incubated with the medium control also acquired PKH67 signal. This may be due to uptake of PKH67 aggregates and/or uptake of residual PKH67-stained serum-derived EV (even after thorough EV depletion of the medium). Nevertheless, the PKH67 acquisition from this medium control was significantly lower than the acquisition seen after incubation with PKH67-positive EV from Hi-Ag/LPS DC-T cell interactions (**Figure 2A and B**). Thus, EV from Hi-Ag/LPS DC-T cell interactions are recruited by both DC and T cells engaged in suboptimal Lo-Ag interactions.

We next investigated whether EV released during Hi-Ag/LPS DC-T cell interactions could functionally influence Lo-Ag DC-T cell interactions. Hereto we first analyzed cytokine levels produced during non-cognate and Lo-Ag DC-T cell interactions in the presence or absence of EV from Hi-Ag/LPS DC-T cell interactions. In previous experiments, we found that the KO4C1 T cell clone produced IFN-γ, IL-2, IL-6 and TNF-α after 4 hours of activation with anti-CD3 and anti-CD28, whereas LPS-activated D1-DC produced only IL-6 and very little amounts of IL-2 (data not shown). We here observed that addition of EV from Hi-Ag/LPS interactions to the Lo-Ag DC-T cell co-cultures did not influence the early antigen-dependent production of IFN-γ, IL-2, IL-6 or TNF-α (**Figure 3**).

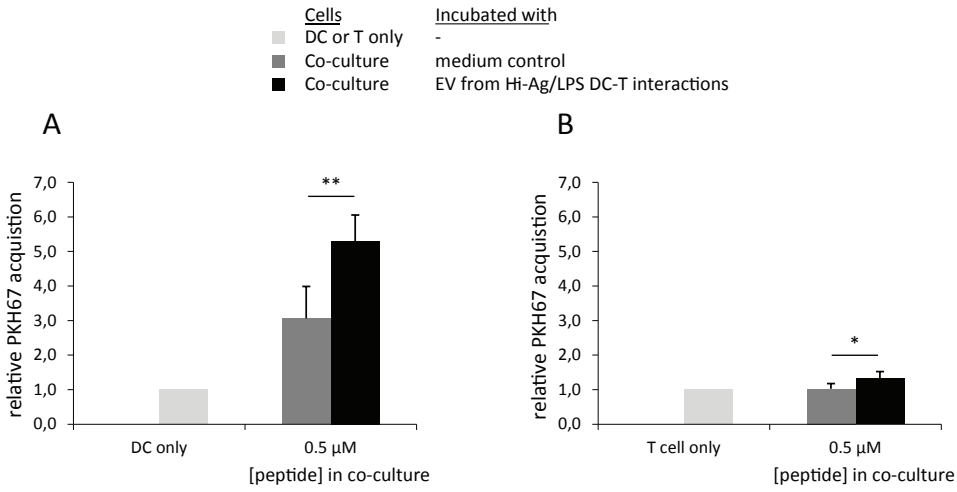

Figure 2 (left) - Recruitment of PKH67-labeled EV from Hi-Ag/LPS DC-T cell interactions by DC and T cells EV production, isolation and staining was performed as described in Figure 1. Plain DC-culture medium was used as a control. DC and T cells engaged in Lo-Ag interactions (0.5 µM peptide) were incubated with the PKH67-stained EV or medium control for 4 hours. The amount of acquired PKH67 label on DC (**A**) or T cells (**B**) was analyzed by flow cytometry. Indicated is the relative amount of acquired PKH67, normalized to DC (**A**) or T cells (**B**) without addition of PKH67-stained EV or medium control (set to 1, light grey bars). The bar graphs show the amount of PKH67 acquired either by DC (**A**) or T cells (**B**) from medium control (dark grey bars) or from Hi-Ag/LPS DC-T cell interactions (black bars). Data are expressed as mean ± standard deviation of 3 independent experiments. Asterisks denote significant differences (* = $p \leq 0.05$, ** = $p \leq 0.01$).

IL-4, IL-5, IL-10, IL-12p70 and IL-17 could not be detected in the supernatant of these co-cultures collected after 4 hours (data not shown).

Besides effects on cytokine release we analyzed whether recruitment of EV from Hi-Ag/LPS DC-T cell interactions influenced the expression of immune activation markers on DC and T cells engaged in Lo-Ag cognate interaction. After 4 hours of EV incubation, DC and T cells were harvested and stained with fluorochrome-conjugated antibodies and analyzed using flow cytometry. DC or T cell populations were gated based on CD4 and CD11c staining. Lo-Ag cognate DC-T cell interactions led to slight upregulation of MHCII and CD80 and to clear upregulation of CD86 and CD69 on DC already after 4 hours (**Figure 4A-C**). However, the expression levels of MHCII, CD80 and CD86 were not significantly altered due to addition of EV from Hi-Ag/LPS DC-T cell interactions (**Figure 4A-C**). Interestingly, the expression of the early activation marker CD69 on DC in these co-cultures was slightly but significantly increased after addition of these EV (**Figure 4D**). T cells were analyzed for expression of TCR, CD69 and CD25 (**Figure 5**). Although CD25 and CD69 expression already increased upon 4 hours of cognate interaction, their expression levels were not significantly altered by the presence of EV from Hi-Ag/LPS DC-T interactions (**Figure 5A,B**).

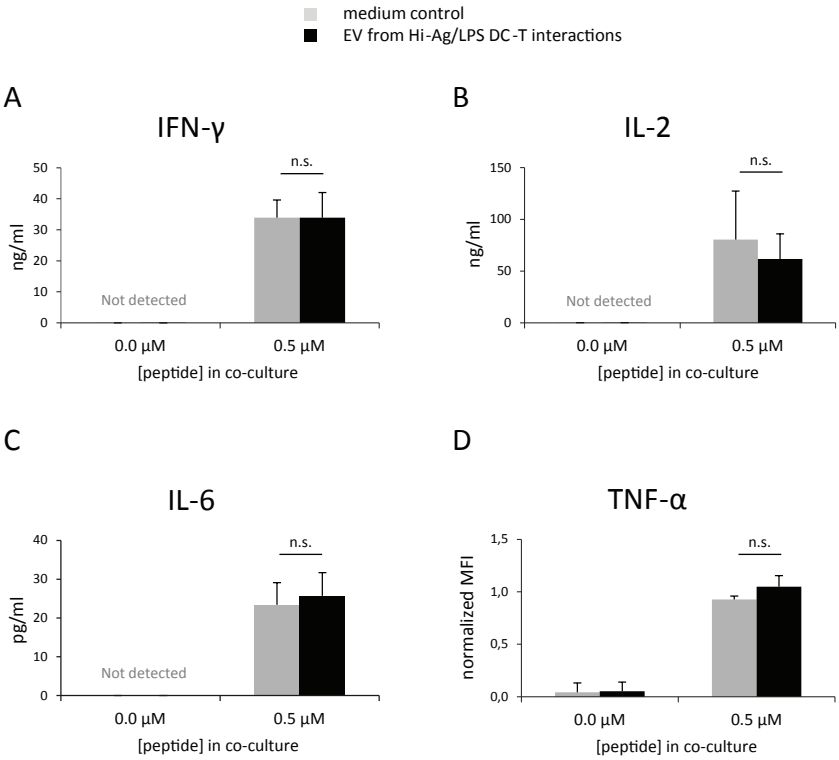

Figure 3 - Cytokine production during Lo-Ag DC-T cell co-cultures upon incubation with EV from Hi-Ag/LPS DC-T cell interactions EV production, isolation and staining was performed as described in Figure 1. Suboptimal Lo-Ag (0.5 µM peptide) or non-cognate (0 µM peptide) DC-T cell co-cultures were incubated with EV from Hi-Ag/LPS DC-T cell interactions or medium control for 4 hours. Culture supernatant was harvested and secretion of IL-2, IL-4, IL-5, IL-6, IL-10, IL-12p70, IL-17, IFN-γ and TNF-α was tested using a multiplexed cytokine assay. Indicated are the concentrations of IFN-γ (**A**), IL-2 (**B**) and IL-6 (**C**) and the normalized mean fluorescence intensity (MFI) of TNF-α (**D**) (all mean ± sd) after incubation with medium control (grey bars) or EV from Hi-Ag/LPS DC-T cell interactions (black bars) of 3 independent experiment. Since recombinant TNF-α was not stable enough to create a calibration curve, absolute concentrations could not be determined. Instead MFI values of TNF-α (**D**), normalized to cognate co-cultures incubated with medium control, are indicated. IL-4, IL-5, IL-10, IL-12p70 and IL-17 could not be detected in Lo-Ag DC-T cell co-culture supernatants.

In contrast, TCR levels were altered upon incubation with Hi-Ag/LPS DC-T cell-derived EV. The TCR is generally downregulated upon engagement with its cognate MHCII-peptide complex, as can be seen in the medium control condition (**Figure 5C**). Interestingly, in the presence of EV from Hi-Ag/LPS DC-T cell interactions no downregulation in TCR expression levels could be observed (**Figure 5C**). The observed effects on DC and T cells were not due to residual LPS or p53 peptide since both components were also added to the medium control (at concentrations equal to the co-culture supernatant). To further exclude effects of possible residual soluble factors (e.g. cytokines) supernatant of the last EV isolation

step was added to the DC-T cell co-cultures. However we found no effect on CD69 or TCR staining levels (data not shown). Thus, addition of EV from Hi-Ag/LPS DC-T cell interactions led to a rapid higher expression of the activation marker CD69 on DC and sustained TCR levels on T cells during Lo-Ag cognate interactions.

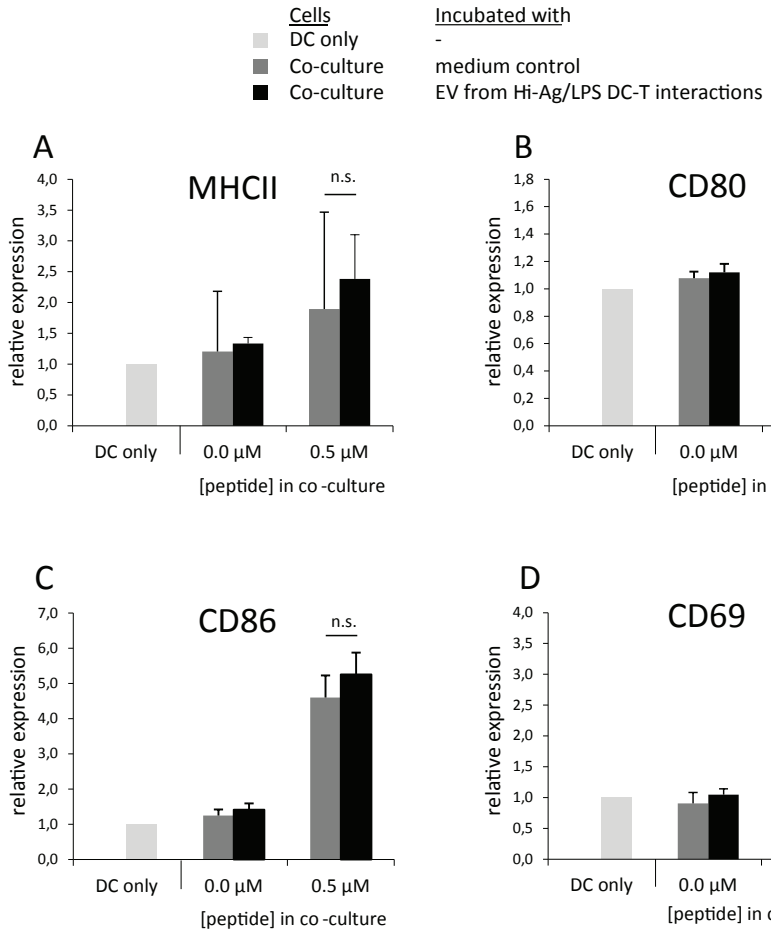

Figure 4 – Analysis of activation marker expression by DC upon incubation with EV from Hi-Ag/LPS DC-T cell interactions EV production, isolation and staining was performed as described in Figure 1. Suboptimal Lo-Ag (0.5 µM peptide) or non-cognate (0 µM peptide) DC-T cell co-cultures were incubated with EV from Hi-Ag/LPS DC-T cell interactions or medium control for 4 hours. Expression of MHCII (**A**), CD80 (**B**), CD86 (**C**) and CD69 (**D**) on DC was analyzed using flow cytometry. T cells and DC-T cell clusters were excluded from analysis based on gating for $CD4^{-}CD11c^{+}$ DC (not shown). Bar graphs show the expression of indicated markers normalized to the expression levels on DC alone (set to 1, light grey bars) of 3 independent experiments. Averages and standard deviations of indicated markers are displayed for co-cultured DC incubated with medium control (dark grey bars) or EV from Hi-Ag/LPS DC-T cell interactions (black bars). Asterisk denotes significant difference (* = $p \leq 0.05$).

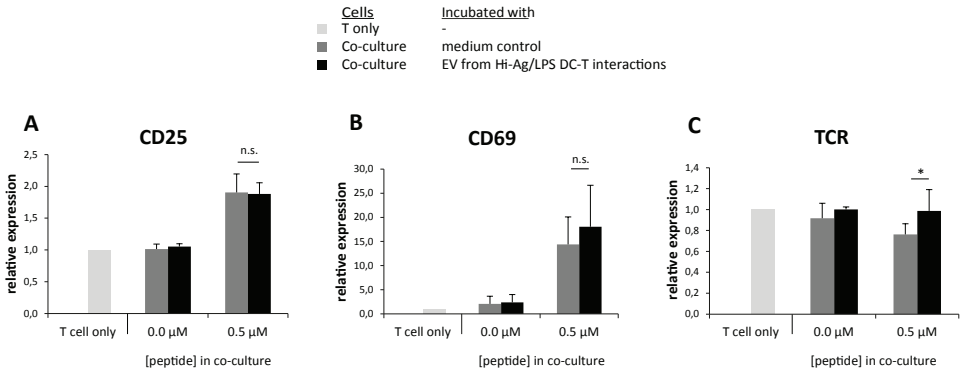

Figure 5 – Analysis of activation marker expression by T cells upon incubation with EV from Hi-Ag/LPS DC-T cell interactions EV production, isolation and staining was performed as described in Figure 1. Suboptimal Lo-Ag (0.5 µM peptide) or non-cognate (0 µM peptide) DC-T cell co-cultures were incubated with EV from Hi-Ag/LPS DC-T cell interactions or medium control for 4 hours. Expression of CD25 (**A**), CD69 (**B**) and TCR (**C**) was analyzed using flow cytometry. DC and DC-T cell clusters were excluded from analysis based on gating for $CD4^{+}CD11c^{-}$ T cells (not shown). Bar graphs show the expression of indicated markers normalized to T cells alone (set to 1, light grey bars) of 3 independent experiments. Averages and standard deviations of indicated markers are displayed for co-cultured T cells incubated with medium control (dark grey bars) or EV from Hi-Ag/LPS DC-T cell interactions (black bars). Asterisk denotes significant difference (* = $p \leq 0.05$).

Discussion

We here investigated in an *in vitro* model system whether EV released into the extracellular milieu during strong stimulatory DC-T cell interactions (Hi-Ag/LPS) could influence neighboring DC and T cells engaged in suboptimal cognate interactions (Lo-Ag). In other *in vitro* studies often very high ratios of vesicle-producing versus vesicle-recruiting cells are used (e.g. (16, 28)). In our *in vitro* model system, we added EV derived from approximately six times more producing cells compared to recruiting cells to mimic a more physiological situation.

In our model system we observed that DC recruited more EV than T cells during suboptimal cognate interactions. An explanation for this might be that DC have a much larger plasma membrane surface than T cells and can therefore bind more EV. Additionally, DC continuously sample their environment and while doing so they might take up more EV than T cells. T cells on the other hand, only recruit DC-derived EV after activation via high-affinity LFA-1 (21). The low vesicle binding observed on the T cells here might be due to the relative short co-culture time, which might have been insufficient for LFA-1 to obtain its fully active conformation. In the current experimental setup we cannot distinguish between the recruitment of DC versus T cell-derived EV since both are labeled with PKH67. In future experiments, the labeling of EV with an additional cell type-specific

fluorescent label would allow the discrimination between these EV subsets and their recruitment by specific target cells.

Expression of CD69 significantly increased on cognate interacting DC in the presence of Hi-Ag/LPS DC-T cell-derived EV. CD69 has neither been reported on DC or T cell EV (8, 14, 29) nor has it been identified as an EV-associated protein in large proteomic studies (30). This suggests that incubation with EV induced higher endogenous CD69 expression on DC. Endogenous CD69 expression on DC has been described to increase in response to pathogen-associated molecular patterns (PAMPs), such as CpG or LPS, as well as in response to IFN-γ (31, 32). Unlike activation of DC with PAMPs, addition of EV did not result in significantly altered expression levels of MHCII, CD80 or CD86. However, we cannot rule out that increased levels of these molecules can be detected at later time points. Enhanced CD69 expression might alter DC function in different ways. First, CD69 expression on DC leads to decreased migration and has been implicated in retention of activated DC in peripheral tissues (31). It is, however, unclear whether CD69 expression on DC, like on T cells (33), also results in the retention of these cells in secondary lymphoid organs. Second, crosslinking of CD69 on plasmacytoid DC has been shown to induce expression of IL-2 by these DC, which enhances T cell proliferation (34). However, after 4 hours of co-culture we observed no effects on IL-2 levels produced during DC-T cell interactions in the presence of EV. A third possibility, not described in literature, is that signaling via CD69 upon binding to a currently unknown ligand on T cells modifies DC or T cell function.

Another remarkable effect of the addition of EV from Hi-Ag/LPS DC-T cell interactions to suboptimal DC-T cell co-cultures was observed on the TCR levels of T cells. Upon addition of these EV we observed no decrease in TCR levels, which is normally seen upon cognate interaction. The T cells in these cognate interaction exhibited TCR levels comparable to TCR levels of non-cognate T cells or resting T cells in single cell type cultures. The observed effect could result from an indirect effect of the EV on DC. Added TCR-carrying EV could, for example, have blocked the MHCIIp complexes on the DC. This blocking would hamper TCR ligation on the interacting T cells leading to less TCR downregulation and decreased T cell activation. However, we observed no inhibitory effects of the EV on the expression levels of T cell activation markers CD25 and CD69 or on IFN-γ and IL-2 production (**Figure 5A,B** and **Figure 3A,B**). Besides modulation of the DC, EV might also directly affect T cells and their TCR levels. First, T cells might recruit TCR-carrying EV. Recruitment of TCR-carrying EV by T cells without fusion with the plasma membrane might result in decoy TCR complexes, whereas binding and fusion might lead to functional transfer of these TCR complexes. The ultimate effects of these recruited TCR complexes thus depend on the further processing of the TCR-carrying EV. Second, EV might transfer ceramide to the T cells, which is a signaling lipid that induces TCR upregulation (35). Ceramide is present in EV (36, 37) and is involved

in the budding of luminal vesicles (exosomes) into multivesicular bodies (35). Incubation of T cells with free ceramide has been shown to quickly induce TCR upregulation from the intracellular recycling pool, thereby increasing T cell responsiveness (38). Transfer of EV-derived ceramide to the T cell might be an additional mechanism to further increase T cell responsiveness.

Based on the analysis of rapidly produced cytokines, we found no indications that EV from Hi-Ag/LPS DC-T cell interactions influenced the type or the strength of the immune response. However, it is well possible that cytokine levels are affected by these EV at later time points. Previously, it has been shown that the D1-DC cell line, after maturation with TNF-α, can produce IL-12 during subsequent overnight cognate co-culture with T cells (24). One of our own pilot experiments showed that IL-5 can be detected in the supernatant of overnight suboptimal DC-T cell co-cultures (data not shown). In future experiments longer co-culture periods will be included to investigate whether EV from Hi-Ag/LPS DC-T cell interactions affect cytokine production at later time points.

Thus far, it is not clear whether the observed relatively small effects of EV on only a selective set of activation markers suggest that the physiological role of EV is marginal. There are several possible explanations why, after incubation with EV in our model system, we observed relatively small effects. First, signaling via these EV may mainly affect cell functions other than we have tested, or cause effects that can only be detected later during DC-T cell interactions. Second, the suboptimal cognate interaction between our DC line and antigen-experienced T cell clone may still be strong enough to overrule signals derived from the recruited EV. The functional effects of the EV should therefore be tested at even lower antigen doses or during cognate interaction between DC and naive p53-specific $CD4^+$ T cells. Naive $CD4^+$ T cells have a higher threshold for activation in comparison to antigen-experienced $CD4^+$ T cells (39) and might therefore be more susceptible for additional EV-derived signaling. Third, these EV may *in vivo* be released in secondary lymphoid organs in which soluble factors are present that are absent in *in vitro* culture systems. *In vivo*, soluble factors like MFG-E8 (36) or cytokines such as TNF-α (37) and IL-15 (38) can bind specifically to DC-derived EV. These soluble factors can contribute to binding, uptake or signaling of EV (reviewed in (40)).

Our experimental set-up in which we studied the effects of EV from Hi-Ag/LPS DC-T cell interactions on Lo-Ag DC-T cell interactions was designed as a model to analyze functional effects of EV from strong stimulatory DC-T cell interactions on suboptimal DC-T cell interactions within the same secondary lymphoid organ (**Figure 6**). We found that EV derived from strong stimulatory DC-T cell interactions induced a small but selective increase in CD69 levels on DC and sustained TCR levels on T cells upon cognate antigen stimulation. At this moment, it is not clear whether the observed effects on CD69 and TCR levels are involved in amplification or dampening of immune responses (**Figure**

6). Based on cytokine expression, we found no indication that the early response was skewed towards a different type of response after incubation with EV from Hi-Ag/LPS DC-T interactions (**Figure 6**). In summary, this chapter provides first clues on a possible functional role of EV released during strong stimulatory DC-T cell interactions. Further research is needed to reveal how the effects of EV on neighboring DC and T cells, found in this study, ultimately affects the type and strength of the immune response.

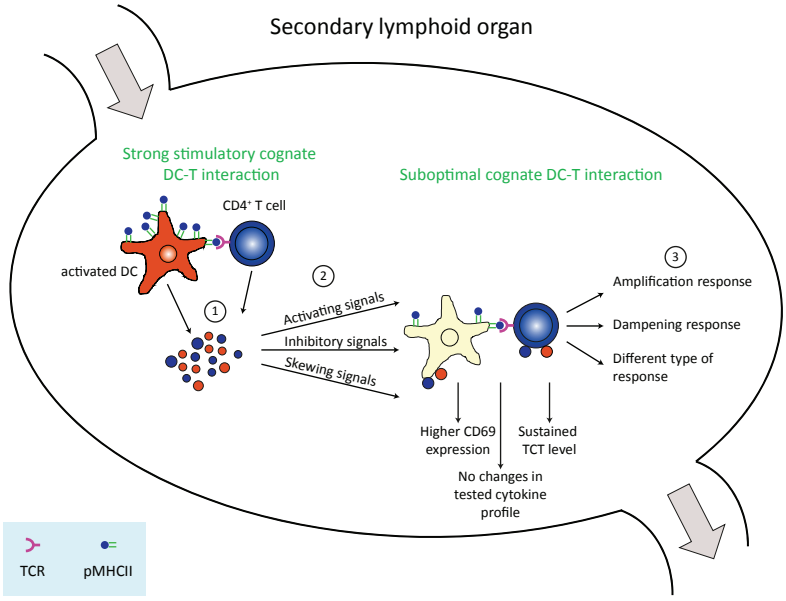

Figure 6 – Model for possible functional effects of EV from strong stimulatory DC-T cell interactions on suboptimal DC-T cell interaction within the same secondary lymphoid organ (**1**) EV produced during Hi-Ag/LPS DC-T cell interactions can be targeted to neighboring DC and T cells, engaged in suboptimal Lo-Ag interactions, within the same secondary lymphoid organ. (**2**) These EV can transfer activating, inhibitory, skewing or a mixture of these signals to neighboring DC and T cells. We found that recruitment of these EV by neighboring DC and T cells led to increased CD69 levels on DC and a lack of decreased TCR levels on T cells and did not affect cytokine levels. (**3**) It is not clear whether these altered CD69 and TCR levels will have a activating of dampening effect on the immune response. Based on cytokine expression, we found no indications in our model system that EV play a role in skewing the early response towards a different type of response. For simplicity, only one interacting T cell per DC is shown.

Acknowledgements

We thank Mieke de Boer-Brouwer, Wilco de Jager, Bram Margry and Peter van Kooten for their excellent technical assistance. We thank Chris van der Lest for his excellent help with statistical analyses. We thank Willem Stoorvogel for useful discussions and critical reading of the manuscript.

References

1. Cocucci E, Racchetti G, Meldolesi J. Shedding microvesicles: Artefacts no more. Trends in cell biology. 2009 Feb;19(2):43-51.
2. Thery C, Ostrowski M, Segura E. Membrane vesicles as conveyors of immune responses. Nature reviews. 2009 Aug;9(8):581-93.
3. Nolte-'t Hoen EN, van der Vlist EJ, de Boer-Brouwer M, Arkesteijn GJ, Stoorvogel W, Wauben MH. Dynamics of dendritic cell-derived vesicles: High-resolution flow cytometric analysis of extracellular vesicle quantity and quality. J Leukoc Biol. 2012 Dec 17;[Epub ahead of print].
4. Soo CY, Song Y, Zheng Y, Campbell EC, Riches AC, Gunn-Moore F, et al. Nanoparticle tracking analysis monitors microvesicle and exosome secretion from immune cells. Immunology. 2012 Jun;136(2):192-7.
5. Buschow SI, Nolte-'t Hoen EN, van Niel G, Pols MS, ten Broeke T, Lauwen M, et al. MHC II in dendritic cells is targeted to lysosomes or T cell-induced exosomes via distinct multivesicular body pathways. Traffic. 2009 Oct;10(10):1528-42.
6. Thery C, Duban L, Segura E, Veron P, Lantz O, Amigorena S. Indirect activation of naive CD4+ T cells by dendritic cell-derived exosomes. Nat Immunol. 2002 Dec;3(12):1156-62.
7. Qazi KR, Gehrmann U, Domange Jordo E, Karlsson MC, Gabrielsson S. Antigen-loaded exosomes alone induce Th1-type memory through a B-cell-dependent mechanism. Blood. 2009 Mar 19;113(12):2673-83.
8. Segura E, Nicco C, Lombard B, Veron P, Raposo G, Batteux F, et al. ICAM-1 on exosomes from mature dendritic cells is critical for efficient naive T-cell priming. Blood. 2005 Jul 1;106(1):216-23.
9. Utsugi-Kobukai S, Fujimaki H, Hotta C, Nakazawa M, Minami M. MHC class I-mediated exogenous antigen presentation by exosomes secreted from immature and mature bone marrow derived dendritic cells. Immunol Lett. 2003 Oct 31;89(2-3):125-31.
10. Andre F, Chaput N, Schartz NE, Flament C, Aubert N, Bernard J, et al. Exosomes as potent cell-free peptide-based vaccine. I. dendritic cell-derived exosomes transfer functional MHC class I/peptide complexes to dendritic cells. J Immunol. 2004 Feb 15;172(4):2126-36.
11. Chaput N, Thery C. Exosomes: Immune properties and potential clinical implementations. Semin Immunopathol. 2011 Sep;33(5):419-40.
12. Yang X, Meng S, Jiang H, Zhu C, Wu W. Exosomes derived from immature bone marrow dendritic cells induce tolerogenicity of intestinal transplantation in rats. J Surg Res. 2011 Dec;171(2):826-32.
13. Peche H, Renaudin K, Beriou G, Merieau E, Amigorena S, Cuturi MC. Induction of tolerance by exosomes and short-term immunosuppression in a fully MHC-mismatched rat cardiac allograft model. Am J Transplant. 2006 Jul;6(7):1541-50.
14. Blanchard N, Lankar D, Faure F, Regnault A, Dumont C, Raposo G, et al. TCR activation of human T cells induces the production of exosomes bearing the TCR/CD3/zeta complex. J Immunol. 2002 Apr 1;168(7):3235-41.
15. van der Vlist EJ, Arkesteijn GJA, van de Lest CHA, Stoorvogel W, Nolte - 't Hoen,Esther N.M., Wauben MHM. CD4+ T cell activation promotes the differential release of distinct populations of nanosized vesicles. Journal of Extracellular Vesicles. 2012;1(1):18364.
16. Zhang H, Xie Y, Li W, Chibbar R, Xiong S, Xiang J. CD4(+) T cell-released exosomes inhibit CD8(+) cytotoxic T-lymphocyte responses and antitumor immunity. Cell Mol Immunol. 2011 Jan;8(1):23-30.
17. Busch A, Quast T, Keller S, Kolanus W, Knolle P, Altevogt P, et al. Transfer of T cell surface molecules to dendritic cells upon CD4+ T cell priming involves two distinct mechanisms. J Immunol. 2008 Sep 15;181(6):3965-73.
18. Martinez-Lorenzo MJ, Anel A, Gamen S, Monle nI, Lasierra P, Larrad L, et al. Activated human T cells release bioactive fas ligand and APO2 ligand in microvesicles. J Immunol. 1999 Aug 1;163(3):1274-81.

19. Monleon I, Martinez-Lorenzo MJ, Monteagudo L, Lasierra P, Taules M, Iturralde M, et al. Differential secretion of fas ligand- or APO2 ligand/TNF-related apoptosis-inducing ligand-carrying microvesicles during activation-induced death of human T cells. J Immunol. 2001 Dec 15;167(12):6736-44.
20. Mittelbrunn M, Gutierrez-Vazquez C, Villarroya-Beltri C, Gonzalez S, Sanchez-Cabo F, Gonzalez MA, et al. Unidirectional transfer of microRNA-loaded exosomes from T cells to antigen-presenting cells. Nat Commun. 2011;2:282.
21. Nolte-'t Hoen EN, Buschow SI, Anderton SM, Stoorvogel W, Wauben MH. Activated T cells recruit exosomes secreted by dendritic cells via LFA-1. Blood. 2009 Feb 26;113(9):1977-81.
22. Helft J, Jacquet A, Joncker NT, Grandjean I, Dorothee G, Kissenpfennig A, et al. Antigen-specific T-T interactions regulate CD4 T-cell expansion. Blood. 2008 Aug 15;112(4):1249-58.
23. Lauwen MM, Zwaveling S, de Quartel L, Ferreira Mota SC, Grashorn JA, Melief CJ, et al. Self-tolerance does not restrict the CD4+ T-helper response against the p53 tumor antigen. Cancer Res. 2008 Feb 1;68(3):893-900.
24. Winzler C, Rovere P, Rescigno M, Granucci F, Penna G, Adorini L, et al. Maturation stages of mouse dendritic cells in growth factor-dependent long-term cultures. J Exp Med. 1997 Jan 20;185(2):317-28.
25. Raposo G, Nijman HW, Stoorvogel W, Liejendekker R, Harding CV, Melief CJ, et al. B lymphocytes secrete antigen-presenting vesicles. J Exp Med. 1996 Mar 1;183(3):1161-72.
26. de Jager W, te Velthuis H, Prakken BJ, Kuis W, Rijkers GT. Simultaneous detection of 15 human cytokines in a single sample of stimulated peripheral blood mononuclear cells. Clin Diagn Lab Immunol. 2003 Jan;10(1):133-9.
27. ten Broeke T, van Niel G, Wauben MH, Wubbolts R, Stoorvogel W. Endosomally stored MHC class II does not contribute to antigen presentation by dendritic cells at inflammatory conditions. Traffic. 2011 Aug;12(8):1025-36.
28. Wahlgren J, Karlson Tde L, Glader P, Telemo E, Valadi H. Activated human T cells secrete exosomes that participate in IL-2 mediated immune response signaling. PLoS One. 2012;7(11):e49723.
29. Thery C, Regnault A, Garin J, Wolfers J, Zitvogel L, Ricciardi-Castagnoli P, et al. Molecular characterization of dendritic cell-derived exosomes. selective accumulation of the heat shock protein hsc73. J Cell Biol. 1999 Nov 1;147(3):599-610.
30. Mathivanan S, Simpson RJ. ExoCarta: A compendium of exosomal proteins and RNA. Proteomics. 2009 Nov;9(21):4997-5000.
31. Lamana A, Martin P, de la Fuente H, Martinez-Munoz L, Cruz-Adalia A, Ramirez-Huesca M, et al. CD69 modulates sphingosine-1-phosphate-induced migration of skin dendritic cells. J Invest Dermatol. 2011 Jul;131(7):1503-12.
32. Bieber T, Rieger A, Stingl G, Sander E, Wanek P, Strobel I. CD69, an early activation antigen on lymphocytes, is constitutively expressed by human epidermal langerhans cells. J Invest Dermatol. 1992 May;98(5):771-6.
33. Cyster JG, Schwab SR. Sphingosine-1-phosphate and lymphocyte egress from lymphoid organs. Annu Rev Immunol. 2012;30:69-94.
34. Alari-Pahissa E, Vega-Ramos J, Zhang JG, Castano AR, Turley SJ, Villadangos JA, et al. Differential effect of CD69 targeting on bystander and antigen-specific T cell proliferation. J Leukoc Biol. 2012 Jul;92(1):145-58.
35. Trajkovic K, Hsu C, Chiantia S, Rajendran L, Wenzel D, Wieland F, et al. Ceramide triggers budding of exosome vesicles into multivesicular endosomes. Science. 2008 Feb 29;319(5867):1244-7.
36. Wang G, Dinkins M, He Q, Zhu G, Poirier C, Campbell A, et al. Astrocytes secrete exosomes enriched with proapoptotic ceramide and prostate apoptosis response 4 (PAR-4): Potential mechanism of apoptosis induction in alzheimer disease (AD). J Biol Chem. 2012 Jun 15;287(25):21384-95.
37. Brouwers JF, Aalberts M, Jansen JWA, van Niel G, Stout TAE, Helms JB, et al. Distinct lipid compositions of two types of human prostasomes. Proteomics:[Accepted for publication].

38. Menne C, Lauritsen JP, Dietrich J, Kastrup J, Wegener AM, Odum N, et al. Ceramide-induced TCR up-regulation. J Immunol. 2000 Sep 15;165(6):3065-72.
39. London CA, Lodge MP, Abbas AK. Functional responses and costimulator dependence of memory CD4+ T cells. J Immunol. 2000 Jan 1;164(1):265-72.
40. Nolte-'t Hoen EN, Wauben MH. Immune cell-derived vesicles: Modulators and mediators of inflammation. Curr Pharm Des. 2012;18(16):2357-68.

Above all, don't fear the difficult moments. The best comes from them
- Rita Levi – Montalcini

Chapter 7

General Discussion

Els J. van der Vlist

Many cell types release nano-sized vesicles, which carry a selective set of proteins, lipids and RNA. These extracellular vesicles (EV) can be found in body fluids as well as in cell culture-conditioned medium. They have been identified as vehicles for intercellular communication and are thought to be involved in many (patho)physiological processes. EV have also gained interest due to their potential clinical application as biomarkers and therapeutic agents. However, the exact mechanisms through which EV exert their functions are largely unknown. Knowledge on how the molecular composition and number of released EV is regulated upon different environmental triggers is needed to gain more insight in the physiological role of EV in intercellular communication. In the first part of this chapter, the importance to analyze the composition of EV populations at the level of individual vesicles will be discussed with a focus on the data presented in **Chapters 4 - 6** of this thesis. In the second part of this chapter, the high-resolution flow cytometric method (described in **Chapter 2 and 3**) will be compared to nanoparticle tracking analysis (NTA), a technique that is now widely used for the analysis of individual vesicles.

The importance of individual vesicle analysis

Up to now, bulk isolates of EV have mostly been used to analyze the composition of EV populations, e.g. by using proteomics and western blotting. There are two important reasons why analysis of individual EV is preferable over bulk-based analysis: it has been demonstrated that i) total vesicle isolates often consist of a mixture of different EV subsets and ii) the composition (quality) and number (quantity) of EV released by cells is dynamic.

Cells can release different EV subsets which are either derived from late endosomal compartments (referred to as exosomes) or shed directly from the plasma membrane (1, 2). Moreover, cells might simultaneously release EV subsets with a different molecular composition from the same subcellular compartment. One of the first indications that cells can release different vesicle subsets came from Van Niel *et al*. who showed that the population of EV isolated from the apical site of epithelial cells had a different protein content compared to the EV isolated from the basolateral site (3). Another recent report demonstrated that at least two distinct EV subsets could be obtained from a mouse tumor cell line. After silencing of Rab27a, a small GTPase involved in exosome secretion, the release of EV-associated proteins CD63, Hsp70, Tsg101 and Alix was decreased, whereas the release of other EV-associated proteins MFG-E8 and CD9 remained unaffected (4). These two studies indicate that cells can release a mixture of different EV subsets.

The molecular composition of EV and dynamics of their release are not only determined by their subcellular origin, but also by the activation status of the donor cell. In previous studies, this was concluded based on protein analysis of bulk isolates of EV. For instance, the amount of MHCII within total populations of EV derived from intestinal epithelial cells (IEC) was increased in response to IFN-γ. These EV populations are functionally different

from control vesicles, since only EV from IFN-γ-treated IEC were able to induce a specific humoral response (5). Other studies indicated that vesicle populations derived from immature and LPS-matured DC also differed in their protein content and function. The total pool of vesicles derived from LPS-matured DC contained higher amounts of MHCII, CD86 and ICAM-1 and were more potent in inducing antigen-specific T cell responses both *in vitro* and *in vivo* (6, 7). These two examples show that the composition of total EV populations is dynamic and that this can be reflected in the effects these EV populations impose on other cells. However, the use of bulk-based analysis of EV does not allow discrimination between changes in the number of vesicles versus changes in the number of molecules per EV, due to the lack of invariable vesicle-associated 'household' markers. Furthermore, these techniques cannot discriminate between different EV subsets, and crucial changes in small numbers of EV might be missed. These limitations hamper further research on EV functions.

To determine quantitative and qualitative changes within a heterogeneous EV population, analysis of large numbers of individual vesicles with multiple parameters (e.g. surface markers, size) is required. Since the majority of EV is smaller than 300 nm (8-10), visualization and characterization of individual EV requires high resolution techniques. In this thesis we describe the development of a flow cytometric method employing the BD Influx™, a commercially available high-resolution flow cytometer, with an optimized configuration. This high-resolution flow cytometric (FC)-based method further involves the bright fluorescent labeling of EV and their floatation into density sucrose gradients, which allows separation of EV subsets based on their buoyant density (**Chapters 2 and 3**). We have used this method to analyze the quantitative and qualitative differences in DC and T cell-derived EV subsets that are released upon different activation triggers (**Chapters 4 and 5**). We provided direct proof that DC increased the release of EV in response to activation with LPS and that such an activation signal also increased the MHCII content of individual EV. Furthermore, we found that vesicle subsets with different buoyant densities differed in their MHCII content and in the extent to which their MHCII content changed upon LPS treatment. We concluded that DC release a heterogeneous EV population of which both the molecular composition and dynamics of release are influenced by the activation status of the DC (**Chapter 4**). Also for $CD4^+$ T cells we found that the number of vesicles released by these cells increased with TCR-triggering and that additional co-stimulatory signals had potentiating effects on EV release in a dose dependent manner. Furthermore, EV released by $CD4^+$ T cells were composed of different vesicle subsets and the release of these subsets was differentially regulated, depending on the activation level of the T cell (**Chapter 5**).

Although we provided evidence that vesicle populations released by DC and T cells are heterogeneous, it is not known whether the EV subsets that we defined based on buoyant density, light scattering and molecular content also represent functionally different EV subsets. Two observations described in this thesis might indicate that the observed vesicle subsets may differ in their function. First, the differential release of distinct vesicle subsets by T cells appeared to be tightly regulated (**Chapter 5**). Second, we observed that activated T cells preferentially recruited DC-derived EV with a high MHCII content (**Chapter 4**). EV with an intermediate or low MHCII content might therefore be targeted to cells other than the cognate interacting T cells. Indeed, EV released in the extracellular medium during cognate DC-T cell interactions can be recruited by bystander DC and T cells where they induce small changes in the expression of a selective set of activation markers (**Chapter 6**). Whether the recruitment of different EV subsets by different target cells indeed reflects a difference in the function of these EV will need to be further addressed. Developing a suitable model system to study the function of these EV subsets requires more knowledge on factors that regulate their release and molecular composition and on the criteria for target cell binding. Part of these factors may be elucidated by the accurate analysis of the changes in composition and release of these EV subsets upon different environmental triggers. Isolation of different EV subsets by flow cytometric sorting would be a big step forward in the analysis of EV subsets, but is not yet feasible. Until then, other isolation strategies such as enrichment or depletion using immune-capture or isolation based on size or differences in density equilibration speed (11) could be applied.

Analysis of individual EV: pros and cons of NTA and high resolution flow cytometry

Over the last few years the field of EV research has quickly expanded and the need for nanotechnology to study EV at the individual vesicle level has strongly increased. New techniques have recently been developed and existing techniques further improved and tested for their ability to analyze individual vesicles. The pros and cons of different techniques for the analysis of individual EV are currently a highly debated topic within the field of EV research. Here our high-resolution FC method is compared with another recently developed method for analysis of individual EV, nanoparticle tracking analysis (NTA). We discuss NTA because it is currently widely used for the quantification and sizing of EV, especially in clinical settings. Moreover, we have used NTA in parallel to our FC method to characterize liposomes, virus particles and DC and T cell-derived EV (**Chapters 2 and 5**). Recently, also other commercial high-resolution flow cytometers became available. However, the discussion here focuses on the high-resolution FC method described in this thesis, since this method has been extensively validated for its suitability to analyze

individual nano-sized EV (**Chapters 2 and 3**). For both methods, the time and expertise required for sample preparations and analysis will be compared. Furthermore, their detection parameters and limits, their accuracy in size and concentration measurements and their suitability to analyze heterogeneous EV populations will be compared (and are summarized in **Table I**). Finally, the pitfalls and possible future improvements of both techniques will be discussed.

Required time and expertise for sample preparation and analysis

Independent of the analysis method, differential steps of (ultra)centrifugation are required to clear EV samples from cells and large cell fragments. For NTA measurements, EV are most often pelleted at 100,000g in a final centrifugation step and resuspended for analysis. Both our high resolution FC method and fluorescence-based NTA measurements require additional fluorescent labeling of the EV and removal of the unbound dye. The latter can only be achieved efficiently when labeled vesicles are floated into density gradients or sedimented into block gradients, which severely increases sample preparation time. Concurrently, however, separation of EV based on buoyant density allows the discrimination between EV and large protein aggregates, which are co-pelleted at 100,000g, and between EV subsets with different density characteristics.

Besides calibration, NTA does not require additional instrumental set-up. Operating the NTA instrument requires some experience, but no high level of expertise. On the NTA roughly 100 to 1000 EV can be measured within one minute. Highly concentrated particle suspensions that are homogeneous in size can thus be analyzed within a short period of time. EV populations, however, are often heterogeneous in size and their analysis requires different instrument settings (as will de be discussed in the subsequent paragraphs). Additionally, per instrument setting multiple movies need to be recorded to analyze sufficient numbers of EV. As a result, the analysis of one heterogeneous EV sample will take about 30 minutes. Instrument set-up and calibration for our FC method requires an experienced flow cytometer operator. After calibration, the FC method can be used for high-throughput analysis since roughly 10.000 to 100.000 EV can be measured within one minute. Analysis of one EV sample will take about 1.5 minutes independently of EV size heterogeneity.

Detection parameters and lower detection limits

During NTA measurements, a laser beam illuminates particles in suspension. The light scattered by these particles is focused via a conventional light microscope onto the image sensor of a video camera. This scattered light is used by the NTA software for the detection of individual particles (12, 13). The lower detection threshold for NTA is therefore dependent on the intensity of scattered light and the camera sensitivity. The intensity of scattered light depends on the particle size and refractive index, and the wavelength

of the laser used to illuminate the particle. NTA instruments equipped with the most sensitive available camera (CMOS) and the available shortest laser wavelength (currently 405 nm) allows detection of silica beads down to 60 nm (14). The lower detection limit of NTA for EV is difficult to determine since EV are heterogeneous in their molecular composition and thus also in their refractive index. Heterogeneity in refractive indices is a general problem that hampers the assessment of absolute EV sizes based on light scattering, independent of the analysis method used. As a consequence, the predictive value of calibration particles (e.g. silica beads) for light scatter-based size measurements of EV is limited. The lower detection limit of NTA can be reduced by detecting EV based on fluorescence instead of light scattering, since fluorescence-based detection is more sensitive than scatter-based detection (10). Fluorescent particles can be detected and tracked on NTA instruments that are equipped with fluorescence filters. However, in case of EV this requires additional labeling of the vesicles with a fluorescent dye (as discussed in the previous section).

Our high resolution FC method uses fluorescence signals for the detection of individual EV. Detection of the majority of nano-sized EV based on light scattering using this technology is hampered by the fact that light scattering signals of EV and noise (e.g. electronic noise, sheath contamination or nano-sized bubbles induced in pressurized fluidics) partially overlap. Therefore, we applied fluorescence threshold triggering to discriminate between fluorescently labeled EV and non-fluorescent noise. As a consequence, this method relies on the homogeneous fluorescent labeling of vesicles. The lower detection limit is determined by the fluorescent signal that can be obtained from a single EV. The amount of fluorescence per EV is in turn determined by the size of the vesicle, labeling efficiency, and brightness of the fluorescent dye. Detection of the acquired fluorescence further depends on efficient depletion of contaminating unbound dye, the power of the exciting laser and the sensitivity of the fluorescence detector. In our FC method we combined high power lasers and high-performance PMTs with bright labeling of vesicles with the intercalating fluorescent dye PKH67. Labeling with this dye allowed us to detect the vast majority of DC-derived EV, which appeared well above the fluorescence threshold. With PKH67 labeling we could detect EV smaller than 70 nm in size, based on the analysis of a prostasome subset (EV from prostate cells) with a size range of 43-69 nm, as determined by electron microscopy (11).

Accuracy and resolution in EV size measurements

By NTA, Brownian movements of multiple individual EV can be tracked. The mean square displacement of EV, together with information on the temperature and viscosity of the liquid containing the EV are used to calculate EV size, using the Stokes-Einstein equation (12). Since these size calculations are based on a stochastic process (Brownian motion)

measured over a limited amount of time, size distributions may appear broader than they actually are (13). For example, mixed populations of 100 and 200 nm polystyrene beads cannot be resolved as fully separated peaks (12). Based on the lowest detection limit for NTA (discussed in the previous section), EV that are smaller than 60 nm and larger EV with low light scattering properties may not be detected. When an EV population contains many small vesicles, this will result in an overestimation of the EV population's mean size and an underestimation of the EV concentration.

Using our FC method, fluorescence-based detection is followed by the detection of scattered light between 15° and 25° (reduced wide-angle forward scatter, rw-FSC). The resolving power for detection of differently sized beads based on light scattering between these angles was high, as indicated by the clear separation of 100 and 200 nm polystyrene bead populations (**Chapters 2 and 3**). Reduced wide-angle FSC can be used for approximate and relative sizing of EV. Calculation of absolute EV sizes based on the amount of scattered light is hampered by the fact that the refractive indices of EV are difficult to assess. Furthermore, FSC signals of nano-sized particles are relatively strongly influenced by their shape, surface roughness, and possibly light absorption (15, 16). The influence of these factors are not well understood yet and further complicate absolute sizing based on FSC signals.

Recommendations for improved detection of EV

The use of laser light with shorter wavelengths (e.g. 405 nm instead of the 488 nm laser currently used in the BD Influx™) will increase the intensity of light scattered by EV. This might allow the detection of smaller and/or low(er) scattering EV above detection thresholds on NTA instruments and flow cytometers. Furthermore, the use of shorter wavelength will increase the resolution in rw-FSC.

Our high resolution flow cytometer has a superior FSC detection compared to conventional flow cytometers, due to the adaptation of the FSC detection angle (15-25°). Increasing the minimum FSC detection angle from 2° to 15° largely improved the signal-to-noise ratio. Furthermore, collection of scattered light over larger detection angles (15-25°, compared to 2°-7°/10° on conventional flow cytometers) is beneficial since nano-sized particles scatter relatively more light to larger angles in comparison to cells (16-18). However, it is worthwhile to investigate if light scattering at even larger angles (19) or at a broader range of angles (17) would further improve the signal-to-noise ratio and resolving power for analysis of EV. Other next generation flow cytometers, such as the BC Gallios™ can also measure FSC over wider detection angles. However, unlike other next generation flow cytometers, the BD Influx™ has an open architecture and flexible modular detection systems, which uniquely allows manual adjustment of various parameters for optimization of EV analysis.

Table I – Comparison of high-resolution flow cytometry-based analysis and Nanoparticle Tracking Analysis to study individual EV

Tracking Analysis to study individual EV	High-resolution flow cytometry	Nanoparticle Tracking Analysis
Sample preparation and analysis		
Preparation requirements	Differential (ultra) centrifugation, fluorescent labeling and removal of unbound dye	Differential (ultra) centrifugation When using f-NTA: additional fluorescent labeling and removal of unbound dye
Estimated sample preparation time	24 hours	3 – 24 hours
Analysis of large EV numbers in short time	++ In the range of 10,000 – 100,000 EV / minute	+/- In the range of 100 – 1000 / minute
Analysis time for heterogeneous EV sample	1.5 minute	30 minutes
Size and concentration measurements		
Lower detection limit	Dependent on labeling intensity, for EV at least ~70 nm	Dependent on light scattering, for silica beads ~60 nm
Resolution	Excellent separation between 100 and 200 nm polystyrene beads	Individual, but somewhat overlapping peaks for 100 and 200 nm polystyrene beads
Size measurements	Relative, based on scatter intensities or intensity general fluorescent membrane dye	Absolute, calculated based on Brownian motion measurements
Concentration measurements	Absolute	Absolute
Heterogeneity in size (polydispersity)	Does not hamper analysis, since EV are analyzed one-by-one	Severely hampers analysis, since multiple EV are simultaneously tracked with the same instrument settings

Table I (*continued*)

Analysis of heterogeneous composition		
Multi-parameter analysis	Large amount of parameters can be analyzed	Limited amount of parameters can be analyzed
Integration of multiple parameters	Integration of multiple fluorescence signals and scattering per individual EV	Uncoupled detection of either fluorescence or light scattering signals to track EV
Main references	(10, 15, 22, 23)	(10, 12-14)

EV, extracellular vesicle(s); f-NTA, fluorescence-based nanoparticle tracking analysis

Quantification of EV

With NTA, EV concentrations are estimated by extrapolating the number of EV seen at any given instant within the known scattering volume (field of view x depth laser beam) to an EV concentration per unit volume (13). Besides the underestimation of EV concentrations due to EV scattering below the detection threshold, also size heterogeneity within EV populations hamper accurate concentration measurements. This is due to the fact that simultaneously tracked events are measured with the same instrument settings, whereas the optimal settings for the detection of small EV (e.g. < 100 nm) significantly differ from the optimal settings for detection of larger EV (e.g. 200 nm, (14) and our own unpublished data). Quantification of heterogeneously sized EV populations is therefore less precise than for homogeneous populations. Since cells often release EV with a size range between 50 and 1000 nm, multiple analyses at different instrument settings may be necessary (13, 14). It should therefore be noted that reported values for EV concentrations represent the concentration of only a limited range of EV of which the scatter could be detected with the applied instrument settings. Furthermore, NTA cannot discriminate between EV and protein aggregates (such as immune complexes derived from plasma (8)) which are co-pelleted with EV at 100,000g. As a result, EV concentrations within plasma or other fluids containing protein aggregates might be overestimated.

Quantitative measurements performed with our FC method can be used to accurately determine concentration differences between EV samples. Additionally, absolute particle concentrations can be calculated upon careful determination of the flow rate (the amount of volume that passes by the laser per time unit). Unlike NTA, quantitative measurements using our FC method are not hampered by size heterogeneity since EV analysis is performed in a one-by-one fashion. Recently, van der Pol and colleagues showed that flow cytometric measurements of EV can be influenced by a phenomenon named 'swarm detection' (20). They demonstrated that multiple 89 nm silica beads ('a swarm of small

particles') can be identified as a single event when the concentration of particles within the core stream is high enough for multiple particles to be detected simultaneously. In this situation, the detected scatter and fluorescence signals represent the sum of signals generated by multiple individual particles. This leads to underestimation of the particle concentration and overestimation of their size. We observed the same phenomenon while analysing different liposome samples (our own unpublished data) and adjusted our protocol accordingly. Thus, care should be taken when quantifying EV populations: the use of multiple flow rates and careful titration of EV samples are important to ensure single vesicle detection.

Determining the molecular composition of individual EV

Within a pool of EV, both the size and the molecular composition of vesicles may be heterogeneous. Differences in expression of surface markers on EV can, for example, be studied by labelling them with fluorochrome-conjugated antibodies. Both NTA and our FC method are limited by the low overall labeling intensities of EV due to their very small surface area and low number of epitopes. The efficiency with which surface proteins can be detected on EV depends not only on their abundance, but also on the affinity of antibodies, the number of fluorochromes conjugated to antibodies, and the brightness of fluorochromes.

NTA instruments can detect immuno-labeled EV when they are equipped with an appropriate laser and fluorescence filters. By using these filters only fluorescent labeled vesicles will be detected and tracked. A separate measurement based on scatter is needed to determine how fluorescently labeled EV relate to the total EV population. This comparison falls short when small vesicles are detected by fluorescence but not by light scattering-based measurements. Hence, the uncoupled fluorescence and scatter measurements and the differences in detection sensitivity of these two parameters hampers the phenotyping of EV by NTA. Furthermore, photobleaching of fluorochromes due to the long tracking time of particles is a significant problem for fluorescence NTA measurements (14). This can be circumvented by labelling EV with quantum dot-conjugated antibodies (Qdot-Ab) (13). However, labelling of EV with Qdot-Ab can influence size and concentration measurements, since quantum dots are relatively large structures (12-20 nm) and can bind multiple EV due to their multivalency. Although supporting data are lacking, it was claimed that Qdot-Ab labelling has no significant effect on EV size (14).

With our FC method, general fluorescent labelling of EV (e.g. with PKH67) can be combined with epitope specific labelling with antibodies using multiple different fluorochromes, and multiple lasers and detectors. In contrast to NTA, detection of a surface protein can be directly related to the expression of other surface proteins on the same vesicle and to the total EV population. Our flow cytometric method is therefore ideal

to study heterogeneity between and within EV populations, provided that the fluorescent signals are high enough for detection.

Recommendations for improving specific protein detection on individual EV

Further development of brighter fluorescent dyes and more sensitive detectors may allow detection of low abundance proteins and the use of low(er) affinity antibodies. Alternatively, it is worthwhile to develop methods for the amplification of fluorescence signals. Enhancing labeling intensity with secondary fluorochrome-conjugated antibodies labeling steps or fluorochrome-conjugated streptavidin is not advisable since these multivalent molecules might induce EV clustering (our own unpublished data). Other amplification methods such as enzyme-catalyzed deposition of a fluorescent reporter substrate (CARD) have been used to increase the intensity of intracellular stainings (21). This involves, for example, the labeling of surface proteins with HRP-conjugated antibodies. In the subsequent step an HRP substrate coupled to a fluorescent dye is oxidized in the presence of hydrogen peroxide and deposited on the EV surface. It is worthwhile to test if such signal amplification protocols are suitable for characterization of EV. Initial experiments should include careful assessment of non-specific staining and testing the possibility to reduce washing steps in which selective EV subsets could be lost.

Final conclusions

In this chapter, the importance of individual vesicle analysis was discussed and two techniques for the analysis of individual vesicles, NTA and our high-resolution FC method, were compared. The latter method is superior in the analysis of heterogeneous EV populations since integrated information can be obtained on multiple parameters for large numbers of vesicles in a short amount of time. Another advantage of the flow cytometric approach is that it might allow sorting of EV subsets in the future. The heterogeneity in the composition of EV precludes absolute sizing based on light scattering as detected by flow cytometers. NTA size measurements of EV based on Brownian motion may complement FC-based measurements, for example when information is required on the size of EV subsets sorted on flow cytometers .

High-resolution techniques for the analysis of individual vesicles uniquely allow accurate quantification of EV. Combined with their suitability to analyze various parameters for characterization of EV, these techniques are excellent tools to study basic aspects of EV in fundamental research. Furthermore, in clinical settings these techniques can be used for detailed analysis of EV-based biomarkers and quality control of (artificial) vesicles used as therapeutic agents. Hence, the utilization and further improvement of techniques for the analysis of individual vesicles are essential to gain insight in the functions and potential applications of extracellular vesicles.

References

1. Thery C, Ostrowski M, Segura E. Membrane vesicles as conveyors of immune responses. Nature reviews. 2009 Aug;9(8):581-93.
2. Cocucci E, Racchetti G, Meldolesi J. Shedding microvesicles: Artefacts no more. Trends in cell biology. 2009 Feb;19(2):43-51.
3. van Niel G, Raposo G, Candalh C, Boussac M, Hershberg R, Cerf-Bensussan N, et al. Intestinal epithelial cells secrete exosome-like vesicles. Gastroenterology. 2001 Aug;121(2):337-49.
4. Bobrie A, Colombo M, Krumeich S, Raposo G, Théry C. Diverse subpopulations of vesicles secreted by different intracellular mechanisms are present in exosome preparations obtained by differential ultracentrifugation. Journal of Extracellular Vesicles. 2012;1(1):18397.
5. Van Niel G, Mallegol J, Bevilacqua C, Candalh C, Brugiere S, Tomaskovic-Crook E, et al. Intestinal epithelial exosomes carry MHC class II/peptides able to inform the immune system in mice. Gut. 2003 Dec;52(12):1690-7.
6. Segura E, Nicco C, Lombard B, Veron P, Raposo G, Batteux F, et al. ICAM-1 on exosomes from mature dendritic cells is critical for efficient naive T-cell priming. Blood. 2005 Jul 1;106(1):216-23.
7. Segura E, Guerin C, Hogg N, Amigorena S, Thery C. CD8+ dendritic cells use LFA-1 to capture MHC-peptide complexes from exosomes in vivo. J Immunol. 2007 Aug 1;179(3):1489-96.
8. Gyorgy B, Modos K, Pallinger E, Paloczi K, Pasztoi M, Misjak P, et al. Detection and isolation of cell-derived microparticles are compromised by protein complexes resulting from shared biophysical parameters. Blood. 2011 Jan 27;117(4):e39-48.
9. Yuana Y, Oosterkamp TH, Bahatyrova S, Ashcroft B, Garcia Rodriguez P, Bertina RM, et al. Atomic force microscopy: A novel approach to the detection of nanosized blood microparticles. J Thromb Haemost. 2010 Feb;8(2):315-23.
10. van der Pol E, Hoekstra AG, Sturk A, Otto C, van Leeuwen TG, Nieuwland R. Optical and non-optical methods for detection and characterization of microparticles and exosomes. J Thromb Haemost. 2010 Dec;8(12):2596-607.
11. Aalberts M, van Dissel-Emiliani FM, van Adrichem NP, van Wijnen M, Wauben MH, Stout TA, et al. Identification of distinct populations of prostasomes that differentially express prostate stem cell antigen, annexin A1, and GLIPR2 in humans. Biol Reprod. 2012 Mar 22;86(3):82.
12. Filipe V, Hawe A, Jiskoot W. Critical evaluation of nanoparticle tracking analysis (NTA) by NanoSight for the measurement of nanoparticles and protein aggregates. Pharm Res. 2010 May;27(5):796-810.
13. Dragovic RA, Gardiner C, Brooks AS, Tannetta DS, Ferguson DJ, Hole P, et al. Sizing and phenotyping of cellular vesicles using nanoparticle tracking analysis. Nanomedicine. 2011 May 4;7(6):780-8.
14. Gardiner C, Ferreira YJ, Dragovic RA, Redman CWG, Sargent IL. Extracellular vesicle sizing and enumeration by nanoparticle tracking analysis. J Extracellular Vesicles. 2013;2:19671.
15. Lacroix R, Robert S, Poncelet P, Dignat-George F. Overcoming limitations of microparticle measurement by flow cytometry. Semin Thromb Hemost. 2010 Nov;36(8):807-18.
16. Shapiro HM. Practical flow cytometry. 4th edition ed. New York: Wiley-Liss; 2003.
17. Steen HB. Flow cytometer for measurement of the light scattering of viral and other submicroscopic particles. Cytometry A. 2004 Feb;57(2):94-9.
18. Kerker M, Chew H, McNulty PJ, Kratohvil JP, Cooke DD, Sculley M, et al. Light scattering and fluorescence by small particles having internal structure. J Histochem Cytochem. 1979 Jan;27(1):250-63.
19. Mullier F, Bailly N, Chatelain C, Dogne JM, Chatelain B. More on: Calibration for the measurement of microparticles: Needs, interests, and limitations of calibrated polystyrene beads for flow cytometry-based quantification of biological microparticles. J Thromb Haemost. 2011 Aug;9(8):1679,81; author reply 1681-2.
20. van der Pol E, van Gemert MJ, Sturk A, Nieuwland R, van Leeuwen TG. Single vs. swarm detection of microparticles and exosomes by flow cytometry. J Thromb Haemost. 2012 May;10(5):919-30.

21. Clutter MR, Heffner GC, Krutzik PO, Sachen KL, Nolan GP. Tyramide signal amplification for analysis of kinase activity by intracellular flow cytometry. Cytometry A. 2010 Nov;77(11):1020-31.
22. Nolte-'t Hoen EN, van der Vlist EJ, Aalberts M, Mertens HC, Jan Bosch B, Bartelink W, et al. Quantitative and qualitative flow cytometric analysis of nano-sized cell-derived membrane vesicles. Nanomedicine. 2011 Jul Oct 21;8(5):712-20.
23. van der Vlist EJ, Nolte - 't Hoen,Esther N.M., Stoorvogel W, Arkesteijn GJA, Wauben MHM. Fluorescent labeling of nano-sized vesicles released by cells and subsequent quantitative and qualitative analysis by high resolution flow cytometry. Nature Protocols. 2012 Jun;7(7):1311-26.

The most exciting phrase to hear in science, the one that heralds new discoveries, is not 'Eureka!' but 'That's funny...' - Isaac Asimov

Appendices

Nederlandse samenvatting

Nederlandse samenvatting voor niet-ingewijden

Veel organismen zoals wij die kennen (dieren, planten) zijn opgebouwd uit een groot aantal cellen. Elke cel is een op zichzelf functionerende eenheid die bestaat uit een kern, cytoplasma en een celmembraan (**Figuur 1**). In de kern bevindt zich de genetische informatie van het organisme in de vorm van DNA. Om de kern heen bevindt zich het cytoplasma, een waterige oplossing (het cytosol) met daarin allerlei eiwitten en organellen. Organellen ('organen van de cel') zijn aparte compartimentjes in de cel die elk hun eigen functie vervullen. Zowel de organellen als de gehele cel worden omgeven door een membraan. Membranen bestaan uit een dubbele laag vetten (lipiden) met daarin membraaneiwitten. Organellen die deel uitmaken van het endosomale systeem, zoals endosomen en lysosomen, kunnen met elkaar en met het celmembraan communiceren door middel van membraanblaasjes ('vesicles' in het Engels) die van het ene organel afsnoeren en met het andere kunnen versmelten (**Figuur 1**). Op die manier kan er binnenin de cel transport

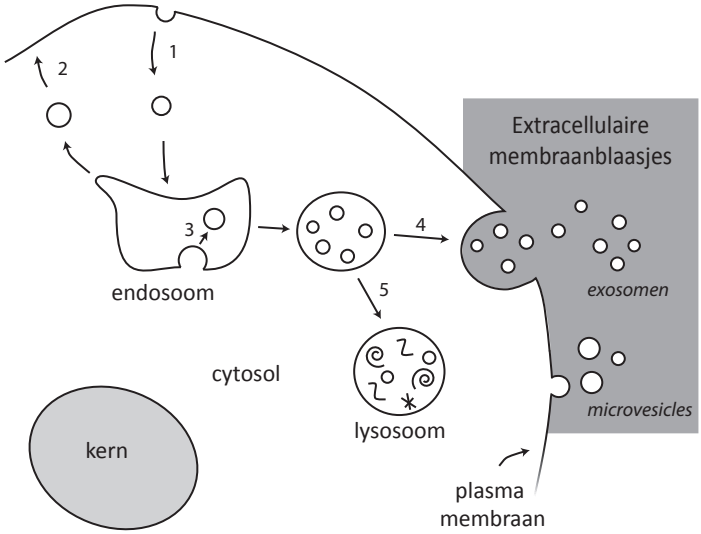

Figuur 1 - Schematisch overzicht van de cel en het endosomale systeem. Een cel kan stofjes uit de omgeving opnemen door het afsnoeren van een membraanblaasje naar binnen toe, dit wordt endocytose genoemd (1). Via het omgekeerde proces (exocytose) kunnen stofjes worden afgegeven aan de omgeving van de cel (2). Tevens kunnen op die manier membraaneiwitten op het plasmamembraan van de cel worden gezet. Stofjes die via endocytose worden opgenomen komen in een endosoom terecht. Eiwitten uit het cytosol en membraaneiwitten kunnen ook binnenin het endosoom terechtkomen door membraanblaasjes die in het endosoom worden gevormd (3). De membraanblaasjes in een endosoom kunnen worden uitgescheiden als exosomen. Dit gebeurt wanneer het membraan van het endosoom versmelt met het plasmamembraan (4). Wanneer het endsoom versmelt met een lysosoom worden de membraanblaasjes afgebroken (5). Naast het uitscheiden van exosomen kunnen cellen ook membraanblaasjes direct van hun plasmamembraan afsnoeren (microvesicles). (Aangepaste figuur uit het proefschrift van Sonja Buschow.)

plaatsvinden van lipiden en eiwitten. Wanneer een membraanblaasje versmelt met het celmembraan wordt de inhoud van het membraanblaasje uitgescheiden buiten de cel. Via het omgekeerde proces kunnen stoffen door de cel worden opgenomen. Cellen kunnen ook membraanblaasjes afgeven aan hun omgeving. Deze membraanblaasjes kunnen direct afgesnoerd worden van het plasmamembraan (microvesicles) of worden afgegeven door fusie van een endosoom, gevuld met membraanblaasjes, met het plasmamembraan (exosomen) (**Figuur 1**).

Ondanks dat cellen als individuele eenheid kunnen functioneren, is het voor een meercellig organisme erg belangrijk dat cellen met elkaar kunnen communiceren. Een voorbeeld hiervan is de communicatie tussen cellen van het afweersysteem (immuunsysteem). Een goed functionerend immuunsysteem zorgt voor het onschadelijk maken en afvoeren van ziekteverwekkers zoals virussen en bacteriën of ontspoorde lichaamscellen (zoals kankercellen). Dendritische cellen en T cellen zijn twee soorten witte bloedcellen die beiden onderdeel uitmaken van het adaptieve immuunsysteem. De cellen van het adaptieve immuunsysteem zijn samen in staat om heel specifieke afweerreacties tegen ziekteverwekkers en ontspoorde lichaamscellen te ondernemen. De dendritische cellen patrouilleren door weefsels en nemen daarbij continu materiaal uit hun directe omgeving op. Wanneer een dendritische cel een ziekteverwekker tegenkomt herkent hij deze als gevaarlijk en wordt de cel geactiveerd. De dendritische cel stabiliseert dan de expressie van MHCII membraaneiwitten (MHCII, major histocompatibility complex klasse II) op zijn celoppervlak. Aan deze MHCII eiwitten zijn eiwitfragmenten van de ziekteverwekker (antigenen) gebonden. Gedurende het activatieproces verplaatst de dendritische cel zich van het weefsel naar een lymfeknoop. In de lymfeknoop presenteert de dendritische cel het antigeen van de ziekteverwekker via MHCII aan de T cellen. Tussen alle T cellen in het lichaam zitten maar enkele T cellen die het antigeen specifiek kunnen herkennen. Wanneer een T cel het gepresenteerde antigeen herkent raakt deze geactiveerd. Naast de antigeen-presentatie worden er nog extra activatiesignalen door de dendritische cel aan de T cel gegeven (dit wordt co-stimulatie genoemd), hierdoor zal de T cel een verdedigingsaanval starten. In een gezonde situatie presenteren dendritische cellen fragmenten van lichaamseigen eiwitten gebonden aan MHCII eiwitten op hun oppervlak, maar dan zonder co-stimulatie signalen. In afwezigheid van co-stimulatie zullen T cellen niet tot aanval overgaan, maar het gepresenteerde eiwitfragment juist tolereren.

Om te voorkomen dat T cellen lichaamseigen cellen ten onrechte aanvallen is een goede communicatie tussen dendritische cellen en T cellen noodzakelijk. Wanneer deze twee type immuuncellen bij elkaar in de buurt zijn kunnen ze overleggen via direct celcontact (**Figuur 2A**). Deze communicatie vindt plaats doordat verschillende eiwitten op het celmembraan van de immuuncellen aan elkaar kunnen binden en signalen doorgeven naar de binnenkant van de cel. Wanneer de immuuncellen zich op afstand van elkaar

bevinden kunnen ze met elkaar communiceren via de afgifte van eiwitten (bijvoorbeeld cytokinen, dit zijn 'hormonen' van het immuunsysteem (**Figuur 2B**)). Deze cytokinen kunnen bijvoorbeeld via het bloed vervoerd worden van de cytokine-producerende cel naar de cel waarvoor het signaal bedoeld is. Het voordeel van deze vorm van communicatie is dat de cytokinen over grote(re) afstanden vervoerd kunnen worden. Een nadeel is echter dat alle cellen in het lichaam die gevoelig zijn voor dit cytokine beïnvloed kunnen worden. Met andere woorden, het signaal kan niet heel specifiek aan een bepaalde cel afgeleverd worden. Een andere manier waarop cellen kunnen communiceren is via het afsnoeren of uitscheiden van membraanblaasjes (**Figuur 2C**). Communiceren via membraanblaasjes heeft verschillende voordelen. Net als cytokinen kunnen membraanblaasjes over grote afstand vervoerd worden. Daarnaast kan belangrijke informatie (in de vorm van genetische signaalstoffen of eiwitten) verpakt worden in het membraanblaasje. Deze verpakte stoffen zijn dan niet bereikbaar voor andere cellen en worden beschermd tegen afbraak. In het membraan van het membraanblaasje kunnen specifieke membraaneiwitten ingebouwd

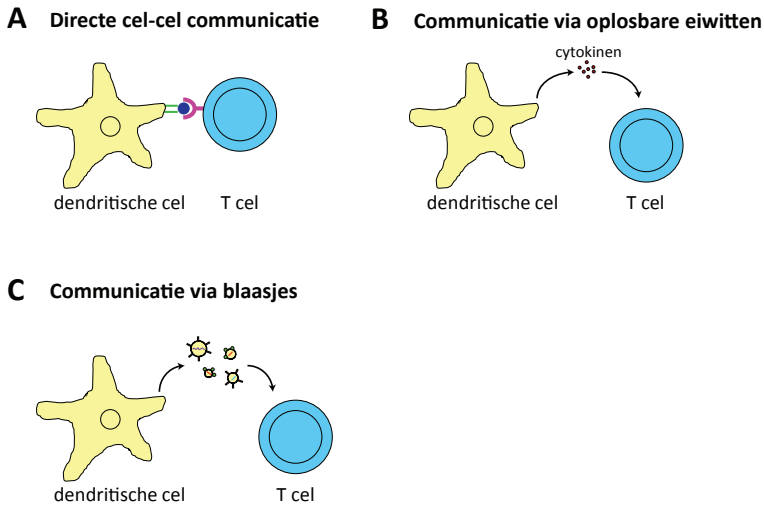

Figuur 2 – Verschillende manieren van communicatie tussen immuuncellen
(**A**) Wanneer een dendritische cel en een T cel vlak bij elkaar in de buurt zijn, kunnen ze direct communiceren via membraaneiwitten die wederzijds kunnen binden. (**B**) Door het afgeven van wateroplosbare eiwitten zoals cytokinen kunnen dendritische cellen en T cellen over grote afstand met elkaar communiceren. (**C**) Door afgifte van membraanblaasjes kunnen dendritische cellen en T cellen over grote afstand met elkaar communiceren. Deze membraanblaasjes kunnen verschillende membraaneiwitten bevatten en ook hun inhoud (genetisch materiaal of eiwitten uit het cytosol) kan variëren. Omwille van de duidelijkheid is in subfiguren B en C alleen de cytokine- en membraanblaasjes-afgifte door de dendritische cel weergegeven. In werkelijkheid kunnen beide celtypen cytokinen en membraanblaasjes afgeven.

worden. Op deze manier kan een 'postcode' toegevoegd worden aan het membraanblaasje, waardoor dit membraanblaasje heel specifiek naar een doelcel gestuurd kan worden.

Alle zoogdiercellen die tot nu toe zijn onderzocht vormen membraanblaasjes die ze afgeven aan hun omgeving. Deze membraanblaasjes zijn gevonden in vrijwel alle lichaamsvloeistoffen zoals bloed, lymfevocht, urine en speeksel. In de wetenschappelijke literatuur bestaan er veel verschillende namen voor deze membraanblaasjes waaronder exosomen en microvesicles. Voor de duidelijkheid en correctheid zullen de membraanblaasjes onderzocht in dit proefschrift extracellulaire membraanblaasjes genoemd worden (**Figuur 1**, grijze kader).

Een heel belangrijk en interessant kenmerk van extracellulaire membraanblaasjes is dat de inhoud (eiwitten, lipiden, genetische informatie) en de hoeveelheid uitgescheiden membraanblaasjes afhangen van de status van de cel. Dat wil zeggen dat wanneer een cel gestrest of geactiveerd raakt, de hoeveelheid en de inhoud van afgegeven membraanblaasjes kan veranderen. Membraanblaasjes van een geactiveerde cel geven dus andere informatie af aan een doelcel dan membraanblaasjes die door een niet-geactiveerde cel worden geproduceerd. Door per celtype te bestuderen hoe de inhoud en het aantal afgegeven membraanblaasjes varieert onder verschillende omstandigheden kunnen we inzicht krijgen in de communicatie tussen dit celtype en andere cellen van het organisme. Dit is allereerst belangrijk voor het verkrijgen van fundamenteel inzicht in cel-cel-communicatie, maar daarnaast is deze informatie belangrijk voor het gebruik van deze membraanblaasjes in de diagnostiek of als therapie. Aangezien membraanblaasjes uit lichaamsvloeistof geïsoleerd kunnen worden, kunnen deze gebruikt worden om normale fysiologische processen of juist ziekteprocessen in het organisme te monitoren. Een andere samenstelling van de membraanblaasjes in bloed kan bijvoorbeeld wijzen op de aanwezigheid van een tumor of een infectie in het lichaam. Daarnaast wordt er onderzoek gedaan naar de mogelijkheid om deze membraanblaasjes in te zetten als therapie, bijvoorbeeld als anti-tumortherapie bij kanker. Ingespoten membraanblaasjes moeten dan immuuncellen instrueren om kankercellen aan te vallen.

Twee aspecten die het bestuderen van de inhoud van membraanblaasjes en de hoeveelheid membraanblaasjes erg moeilijk maakt zijn de grootte en de heterogeniteit van membraanblaasjes. Membraanblaasjes die worden uitgescheiden door cellen hebben een diameter tussen 30 en 1000 nanometer (1 nanometer = 0,000001 millimeter) en zijn daarmee grofweg 100x kleiner dan cellen. Kleine membraanblaasjes kunnen niet met gewone lichtmicroscopie gedetecteerd worden, daarvoor moeten andere technieken met een hogere resolutie, zoals elektronenmicroscopie, gebruikt worden. Het tweede aspect dat het bestuderen van membraanblaasjes moeilijk maakt is hun heterogeniteit in grootte en samenstelling. Om een goed beeld te krijgen van alle verschillende type membraanblaasjes is het dus belangrijk om een techniek te gebruiken die in staat is om grote hoeveelheden individuele membraanblaasjes te bestuderen.

Dit proefschrift

In dit proefschrift wordt een nieuwe methode beschreven waarmee grote hoeveelheden individuele membraanblaasjes kunnen worden gedetecteerd en geanalyseerd. Vervolgens is deze methode gebruikt om de membraanblaasjes die worden uitgescheiden door twee verschillende immuuncellen, dendritische cellen en T cellen, te bestuderen. Ten slotte is in een *in vitro* modelsysteem onderzocht wat de mogelijke functie(s) van de membraanblaasjes uitgescheiden tijdens de interactie tussen dendritische cellen en T cellen kan (kunnen) zijn.

In **hoofdstuk 1** wordt allereerst een overzicht gegeven van de bestaande kennis over de afgifte, samenstelling en functie van membraanblaasjes afkomstig van T cellen en dendritische cellen. Vervolgens is in **hoofdstukken 2 en 3** een flow cytometrische methode beschreven die kan worden gebruikt voor de kwantitatieve en kwalitatieve analyse van extracellulaire membraanblaasjes. Een flow cytometer is een apparaat dat gebruikt wordt voor het detecteren, tellen en analyseren van grote hoeveelheden deeltjes, meestal zijn dit cellen. In een flow cytometer worden één of meerdere lasers gericht op een vloeistofstraal (**Figuur 3**). Door gebruik te maken van sterk verdunde monsters en van drukverschillen in de 'sheath' vloeistof en de vloeistof waarin zich de deeltjes bevinden ('sample' vloeistof), worden de deeltjes gedwongen om één voor één de laser(s) te passeren. Wanneer een deeltje een laserstraal passeert, verstrooit deze het laserlicht. De mate van lichtverstrooiing is afhankelijk van de grootte en andere eigenschappen van het deeltje. Deze lichtverstrooiing kan onder verschillende hoeken gemeten worden. Veelal meet men de voorwaartse lichtverstrooiing (in het Engels: forward scatter (FSC)) en de zijwaartse lichtverstrooiing (in het Engels: side scatter (SSC)). Wanneer het deeltje in de vloeistofstroom vooraf gemarkeerd is met een fluorescente marker kan naast de lichtverstrooiing ook de hoeveelheid fluorescent licht afkomstig van het deeltje worden bepaald. Een fluorescente marker kan bijvoorbeeld heel specifiek worden gebonden aan een eiwit op de buitenkant van het deeltje (cel of membraanblaasje). Met behulp van zo'n marker kan vervolgens voor de gehele populatie deeltjes in kaart worden gebracht welke deeltjes het eiwit wél bevatten en welke niet. Per deeltje kunnen dus zowel twee typen lichtverstrooiing als fluorescente signalen worden gedetecteerd. Met andere woorden: er kunnen meerdere parameters op hetzelfde deeltje worden uitgelezen.

Conventionele flow cytometers kunnen over het algemeen alleen deeltjes van 300nm of groter detecteren. Het overgrote deel van de membraanblaasjes afgeven door cellen is echter kleiner dan 300nm. Om deze membraanblaasjes toch te kunnen detecteren is de methode zoals beschreven in **hoofdstukken 2 en 3** ontwikkeld. Deze methode bestaat uit (1) aanpassingen van een flow cytometer met een hoge resolutie en (2) het labelen van de membraanblaasjes met een sterk fluorescente stofjes. Door de membraanblaasjes

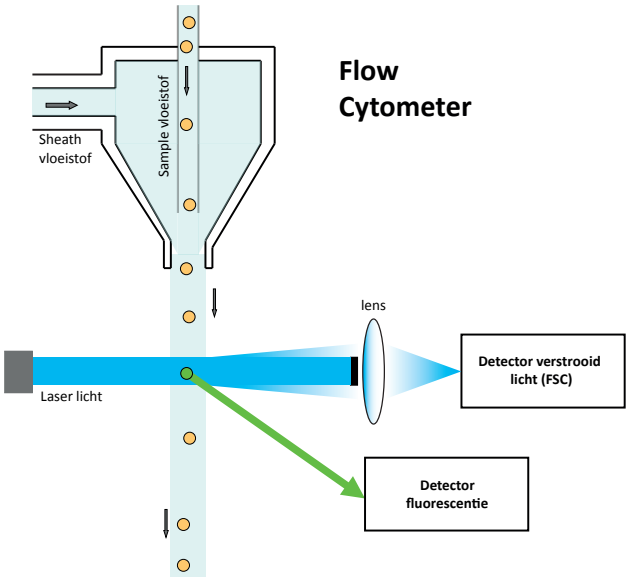

Figuur 3 – Schematisch overzicht van de werking van een flow cytometer. Met behulp van een drukverschil tussen de sheath vloeistof en de sample vloeistof (waar zich de cellen of membraanblaasjes in bevinden) worden deeltjes gecentreerd in de vloeistofstroom en één voor één langs de laser gestuurd. Wanneer het deeltje een laser passeert zal allereerst het laserlicht verstrooid worden door interactie met het deeltje. Dit verstrooide licht wordt via een lens op een detector gefocusseerd. Wanneer een deeltje gelabeld is met een fluorescente stof (en de juiste laser wordt gebruikt om deze stof in zijn lichtgevende toestand te brengen), zal het deeltje fluorescent licht uitstralen. Dit fluorescente licht kan worden gedetecteerd door een tweede detector. In werkelijkheid bevatten de meeste flow cytometers meerdere lasers met verschillende kleuren (golflengtes) en meerdere detectoren voor fluorescentie. Daarnaast is in dit figuur de tweede detector voor zijwaartse lichtverstooiing (side scatter, SSC) niet weergegeven. (Aangepaste versie figuur uit de masterscriptie van Hendrik Mertens.)

te labelen met een fluorescente stof kunnen ze worden onderscheiden van andere niet-fluorescente deeltjes die ongewenste achtergrond signalen geven (zoals stofdeeltjes of kleine luchtbelletjes in de vloeistofstraal van de flow cytometer). Een cruciaal aspect voor de detectie van fluorescente membraanblaasjes is het scheiden van deze membraanblaasjes en de overgebleven ongebonden fluorescente stof na de labelingsprocedure. Naast het analyseren van extracellulaire membraanblaasjes is deze flow cytometrische methode ontwikkeld en uitgebreid getest met behulp van verschillende modeldeeltjes zoals fluorescente bolletjes ('beads' in het Engels) van 100nm en 200nm en fluorescent gelabelde virusdeeltjes met een grootte van 100nm. De resultaten beschreven in **hoofdstukken 2 en 3** laten zien dat met behulp van deze flow cytometrische methode kwantitatieve (hoeveelheid membraanblaasjes) en kwalitatieve ('inhoud' van de membraanblaasjes) informatie verkregen kan worden voor grote aantallen membraanblaasjes. Deze methode vormde de basis voor het onderzoek beschreven in **hoofdstukken 4 en 5**.

In **hoofdstuk 4** is de kwantiteit en de kwaliteit van membraanblaasjes uitgescheiden door dendritische cellen onder verschillende activatiecondities beschreven. Dit hoofdstuk laat zien dat dendritische cellen meer membraanblaasjes uitgescheiden wanneer ze geactiveerd raken door LPS (een 'gevaar-stofje' afkomstig van een bacterie). Daarnaast bevatten de membraanblaasjes van deze geactiveerde dendritische cellen meer MHCII-eiwitten per membraanblaasje dan membraanblaasjes van niet-geactiveerde cellen. Ook binnen de populatie van membraanblaasjes afkomstig van dezelfde geactiveerde dendritische cellen, is te zien dat de hoeveelheid MHCII per membraanblaasje varieert. Alhoewel de dendritische cellen allemaal in dezelfde activatietoestand zijn, scheidden ze dus verschillende membraanblaasjes uit.

Uit eerder onderzoek binnen onze groep bleek dat T cellen MHCII-bevattende membraanblaasjes afkomstig van dendritische cellen op hun oppervlak kunnen binden. Wanneer de dendritische cellen samen met T cellen in één schaaltje gekweekt worden, verdwijnt opmerkelijk genoeg selectief de populatie membraanblaasjes met veel MHCII eiwitten. Het lijkt er dus op dat T cellen specifiek membraanblaasjes met een hoge hoeveelheid MHCII kunnen binden. Dit zou erop kunnen wijzen dat membraanblaasjes met veel MHCII op hun oppervlak bedoeld zijn voor communicatie met T cellen, terwijl membraanblaasjes met lagere hoeveelheden MHCII naar andere type (immuun)cellen kunnen gaan.

In **hoofdstuk 5** zijn de membraanblaasjes afkomstig van T cellen bestudeerd. Hiertoe werden de T cellen geactiveerd met behulp van bepaalde antistoffen. Deze antistoffen binden aan oppervlakte-eiwitten van T cellen en bootsen zo antigeen-presentatie via MHCII en de co-stimulatie (het extra activatiesignaal) na, dat normaal gesproken wordt afgegeven door een geactiveerde dendritische cel. Dit hoofdstuk laat zien dat zowel antigeen-presentatie via MHCII als de mate van co-stimulatie bepalen hoeveel membraanblaasjes er uitgescheiden worden door de T cel. T cellen scheiden een heterogene populatie aan membraanblaasjes uit, die op de flow cytometer op basis van lichtverstrooiing en hoeveelheid fluorescent label ingedeeld kunnen worden in drie verschillende subpopulaties. Hoeveel membraanblaasjes er van elke subpopulatie afgegeven worden is afhankelijk van de activatie signalen die de T cel heeft gekregen. Communicatie door de T cel via membraanblaasjes verandert dus als de activatiestatus van de T cel verandert.

In **hoofdstuk 6** hebben we in een *in vitro* ('*in vitro*' betekent in dit geval dat het proces in een kweekschaaltje bestudeerd wordt) modelsysteem gekeken wat de mogelijke rol kan zijn van membraanblaasjes die worden uitgescheiden tijdens interactie (directe cel-cel communicatie) tussen dendritische cellen en T cellen. De membraanblaasjes-producerende dendritische cellen en T cellen waren beiden in een sterk geactiveerde staat. Vervolgens werd gekeken wat het effect was van deze afgegeven

membraanblaasjes op dendritische cellen en T cellen in een zwak geactiveerde staat. De afgegeven membraanblaasjes werden gebonden door zowel dendritische cellen en in mindere mate door T cellen. Incubatie van dendritische cellen en T cellen met deze membraanblaasjes leek geen effect te hebben op de vroege afgifte van cytokinen door deze zwak geactiveerde dendritische cellen en T cellen. De membraanblaasjes hadden wel een effect op de expressie van oppervlakte-eiwitten door beide celtypen. Van deze oppervlakte-eiwitten is bekend dat ze een regulerende werking op afweerreacties kunnen hebben. De membraanblaasjes afkomstig van sterk geactiveerde dendritische cellen en T cellen zouden dus betrokken kunnen zijn bij het beïnvloeden van andere dendritische cellen en T cellen. Hier moet echter nog verder onderzoek aan gedaan worden.

Met het onderzoek beschreven in dit proefschrift is meer inzicht verkregen in de dynamiek van membraanblaasjes afgifte door dendritische cellen en T cellen. De ontwikkelde flow cytometrische methode voor de analyse van individuele membraanblaasjes was hierbij onmisbaar. Met deze methode kan heel precies de hoeveelheid uitgescheiden membraanblaasjes worden bepaald en kan de inhoud van de membraanblaasjes verder worden bestudeerd. Deze techniek is daarom zeer geschikt om de fundamentele aspecten van intercellulaire communicatie via membraanblaasjes te bestuderen. Daarnaast kan deze techniek gebruikt worden om membraanblaasjes uit lichaamsvloeistoffen te bestuderen. Zo'n karakterisering kan bijdragen aan het toekomstig gebruik van deze membraanblaasjes als (bio)marker voor normale fysiologische processen of ziekteprocessen. Tenslotte leent deze techniek zich ook om kwaliteitscontroles uit te voeren op membraanblaasjes die zijn geproduceerd voor therapieën, bijvoorbeeld tegen tumoren. Het gebruik van deze methode en andere technieken voor de analyse van individuele membraanblaasjes is cruciaal voor het verkrijgen van meer inzicht in de functie en mogelijke toepassingen van extracellulaire membraanblaasjes.

Dankwoord

Hendrik Mertens en Sonja Buschow wil ik bedanken voor het beschikbaar stellen van de originele figuren. Joost van der Lit, bedankt voor het aanpassen van deze figuren. Tot slot wil ik Marleen Hessel en Annelies van der Vlist bedanken voor het kritisch doorlezen van deze samenvatting.

Life is what happens, while you're busy making other plans
– John Lennon ('Beautiful Boy')

Appendices

Curriculum Vitae

Curriculum Vitae

Els (Elizabeth Johanan) van der Vlist werd op 30 mei 1985 geboren in Zaltbommel. Ze behaalde haar VWO diploma, met als richting Natuur & Gezondheid in de zomer van 2003 aan scholengroep het Cambium in Zaltbommel. In september van datzelfde jaar startte zij met haar studie Biologie aan de Universiteit Utrecht. Gedurende haar studie was ze actief lid van de algemene Utrechtse studenten roeivereniging Orca. Na het behalen van haar bachelor diploma vervolgde zij in september 2006 haar studie met de prestige master Biomolecular Sciences. Haar eerste onderzoekstage over de transcytose van hpIgR-bindende VHHs (lama antilichaam fragementen) werd uitgevoerd onder begeleiding van Dr. Edward Dolk en Dr. Paul van Bergen en Henegouwen binnen het departement Cellular Architecture and Dynamics van de faculteit Biologie, Universiteit Utrecht. Haar tweede onderzoeksstage voerde zij uit binnen de afdeling Onderzoek & Ontwikkeling van het Nederlands Vaccin Instituut onder begeleiding van Dr. Cecile van Els. Gedurende deze stage werkte zij aan een *in vitro* assay om de immuunmodulerende eigenschappen van kinkhoest (*Bordetella pertussis*) antigenen te bestuderen op het niveau van dendritische cellen. Zij sluitte haar master af met het schrijven van haar thesis genaamd 'Exosomes - Vehicles in intercellular communication between immune cells' onder begeleiding van Dr. Marca Wauben aan het departement Biochemie en Celbiologie van de faculteit Diergeneeskunde, Universiteit Utrecht. Na het behalen van haar masterdiploma startte zij in september 2008 aan haar promotieonderzoek getiteld 'Unravelling the physiological role of vesicles released during cognate interaction between DC and T cells' onder begeleiding van prof. dr. Marca Wauben, Dr. Esther Nolte-'t Hoen en prof. dr. Willem Stoorvogel binnen het eerder genoemde departement Celbiologie en Biochemie. De resultaten van haar promotieonderzoek staan beschreven in dit proefschrift. Aanvullend heeft zij het Infection & Immunity PhD programma gevolgd en heeft zij binnen dit programma tweemaal de 'PhD Spring Meeting' georganiseerd. Daarnaast heeft zij zich gedurende haar promotietraject ingezet om de belangen van AiO's te behartigen binnen verschillende commissies waaronder als voorzitter van de AiO commissie van de Graduate School of Life Sciences (GSLS), als secretaris van de AiO commissie van Diergeneeskunde en als AiO-vertegenwoordiger binnen het dagelijks bestuur van de GSLS.

Sinds november 2012 is Els werkzaam als docent bij de afdeling Farmacologie van het departement Farmaceutische wetenschappen aan de Bèta faculteit van de Universiteit Utrecht. Per april 2013 is Els daarnaast werkzaam als beleidsmedewerker bij onderwijszaken van Biomedische Wetenschappen in het Universitair Medisch Centrum Utrecht.

The distance between insanity and genius is measured only by success
- Bruce Feirstein

List of publications

List of publications

Els J. van der Vlist, Esther N.M. Nolte-'t Hoen and Marca H.M. Wauben **Extracellular vesicles in Immunology.** *In:* Micro/nanovesicles and exosomes in health and disease, Pan Stanford Publishing (*in press*)

Esther N.M. Nolte-'t Hoen, Els J. van der Vlist, Mieke de Boer-Brouwer, Ger J.A. Arkesteijn, Willem Stoorvogel and Marca H.M. Wauben **Dynamics of dendritic cell-derived vesicles: High-resolution flow cytometric analysis of extracellular vesicle quantity and quality.** Journal Leukocyte Biology. 2013 Mar;93(3):395-402

Els J. van der Vlist, Esther N.M. Nolte-'t Hoen, Willem Stoorvogel, Ger J.A. Arkesteijn and Marca H.M. Wauben **Fluorescent labeling of nano-sized vesicles released by cells and subsequent quantitative and qualitative analysis by high-resolution flow cytometry** Nature Protocols. 2012 Jun 14;7(7):1311-26

Els J. van der Vlist, Ger J.A. Arkesteijn, Chris H.A. van de Lest, Willem Stoorvogel, Esther N.M. Nolte-'t Hoen and Marca H.M. Wauben **$CD4^+$ T cell activation promotes the differential release of distinct populations of nanosized vesicles** Journal of Extracellular Vesicles. 2012;1:18364

Esther N.M. Nolte-'t Hoen, Els J. van der Vlist, Marian Aalberts, Hendrik C.H. Mertens, Berend Jan Bosch, Willem Bartelink, Enrico Mastrobattista, Ethlinn V.B. van Gaal, Willem Stoorvogel, Ger J.A. Arkesteijn and Marca Wauben **Quantitative and qualitative flow cytometric analysis of nanosized cell-derived membrane vesicles** Nanomedicine. 2012 Jul;8(5):712-20

Chris D. Emmerson, Els J. van der Vlist, Myrthe R. Braam, Peter Vanlandschoot, Pascal Merchiers, Hans J. de Haard, C. Theo Verrips, Paul M.P. van Bergen en Henegouwen and Edward Dolk **Enhancement of polymeric immunoglobulin receptor transcytosis by biparatopic VHH** PLoS One. 2011;6(10):e26299

A little nonsense now and then is relished by the wisest men - Roald Dahl

Dankwoord

Dankwoord

Het feit dat jij dit proefschrift nu in handen hebt, betekent dat je -in welke vorm dan ook- hebt bijgedragen aan de totstandkoming ervan. Bedankt daarvoor!

Hoera, mijn boekje is af! Ik kijk op mijn promotietraject terug als een enorm leerzame periode waarin ik me niet alleen als wetenschapper, maar ook als persoon verder heb kunnen ontwikkelen. Net als bij veel promovendi ging dit ook bij mij met de nodige pieken en dalen. Gelukkig waren er dan altijd mensen op het lab of juist daarbuiten die me oppepten wanneer het tegen zat, zorgden voor de nodige afleiding of juist mee feestvierden wanneer er een piekmoment was bereikt.

Marca, ik ken geen enkel ander persoon die naast een geweldig wetenschapper ook zo'n (mensen-)managementtalent is. Je beschikt over een buitengewone hoeveelheid mensenkennis en je vertaalt dit in een tailor-made ;-) begeleiding van je AiO's. Doordat jij soms beter dan ikzelf in de gaten had hoe ik met zaken om zou gaan, heb ik weleens gedacht dat je stiekem een wekelijks telefonisch overleg met mijn ouders hield. Vaak waarschuwde je me van tevoren al voor mijn valkuilen, liet je me gaan wanneer ik vervolgens alsnog in die valkuil liep en evalueerden we (veelal zonder veroordeling van jouw kant) achteraf hoe het was gelopen. Wat ik daarnaast erg bewonder en wat kenmerkend is voor jou, zijn de kwaliteitseisen die je stelde aan mijn werk en vaardigheden en het feit dat je daar absoluut geen concessies in deed. Hierdoor eiste je vaak het uiterst haalbare, maar kreeg je ook enorm veel voor elkaar. Zoals je ook al hebt kunnen lezen op het cadeau dat je kreeg tijdens je oratie: jij hebt mij als geen ander de ruimte en stimulans gegeven om te groeien, als wetenschapper en als persoon.
Esther, ik ben heel blij en vereerd dat jij mijn co-promotor bent. Alhoewel we eerst aan elkaar moesten wennen, is jouw bijdrage aan dit proefschrift onmisbaar geweest. Jouw praktische insteek ('dit is wel haalbaar, dit niet meer') waren een welkome tegenhanger van het overheersende optimisme in onze driekoppige werkbesprekingen en heeft erg geholpen bij de invulling van mijn hoofdstukken in het laatste jaar. In dit laatste jaar ben jij ook degene geweest die mij de kneepjes (of kan ik beter zeggen 'de basis'?) van het wetenschappelijk schrijven hebt geleerd. Dit heeft je ongetwijfeld enorm veel tijd gekost en ik ben je hier erg dankbaar voor. Tot slot was je er ook voor me op (stress-)momenten wanneer ik met zaken bleef worstelen. Jij wees me dan op hetgene waar ik tegenaan liep en gaf me de juiste inzichten en motiverende woorden ('Nu moet je gaan staan!') om de situatie om te buigen in mijn eigen voordeel.
Willem, je begon oorspronkelijk als mijn enige promotor, maar inmiddels heb je als 2e

promotor mijn promotietraject met wat meer afstand meegemaakt. Hoewel we het af en toe niet met elkaar eens waren, heb ik je kritische vragen en input altijd erg gewaardeerd. Daarnaast heb ik veel gehad aan jouw tekstuele input. De zinnen die ik na lange tijd ploeteren in elkaar had gedraaid wist jij vaak nog iets mooier en nog iets duidelijker te maken. Tot slot wil ik je bedanken voor de vrijheid die je me gegeven hebt om samen met Marca en Esther aan dit project te werken.

Ger, zonder jouw technische kennis en inzet waren de eerste vier experimentele hoofdstukken uit dit boekje er nooit geweest. Ik werd altijd erg blij als je weer eens zei: 'Ik bedacht me vannacht ineens, als we nu eens dit en dit testen…'. Het is geweldig dat onze flow cytometrische methode ook door anderen op waarde wordt geschat en dat er nu een tweede Influx op de afdeling staat! Hopelijk kunnen de kennis en de toepassingen nu nog verder worden uitgebreid. Er was voor de ontwikkeling van deze methode wel veel uithoudingsvermogen nodig: allereerst voor het ontwikkelen en daarna voor het vele testen en gebruiken (eindeloos gradiënten doormeten). Deze vele metingen werden natuurlijk opgeleukt door 'FIETS!', het uitwisselen van restaurant-tips, kabouter Wesley en talloze andere hilarische Youtube-filmpjes.

Marian (Mjan!) en **Marijke**, wat fijn dat jullie me tijdens mijn promotie bij willen staan als paranimf. **Marian**, je bent ruim 3 jaar mijn roomie geweest. Ondanks dat we tegenpolen zijn (zowel in de lengte als) wat betreft onze karakters, waren we een goede mix van rust en stuiter, van direct reageren en nuance. Samen pret hebben om LOLcats, uitspraken en appelstickertjes verzamelen op de deur, maar ook heerlijk klagen over tegenvallende resultaten of andere AiO sores. Tot slot vind ik het super leuk dat we elkaars wederzijdse paranimf zijn! **Marijke**, toen de AiO-populatie bij B&C behoorlijk begon uit te dunnen, kwam jouw vrolijke persoonlijkheid gelukkig het Celbiologie-team versterken. Het was heel fijn dat ik mijn laatste-jaars-stress altijd bij jou kwijt kon. Daarnaast vond ik het heel gezellig dat we nog een weekendje Göteborg aan het ISEV-congres vast hebben geplakt. Misschien moeten we nog eens proberen om daar met Deense kronen te betalen! ;-) Heel veel succes met je promotieonderzoek verder! **Toine**man, wat een eer dat ik je paranimf mocht zijn. Jij was voor mij altijd een rustpunt in het lab, waar ik terecht kon met mijn (al dan niet lab-gerelateerde) verhalen. Daarnaast was je altijd bereid om met jouw enorme technische kennis mij wat technische kneepjes bij te brengen. Ook jouw kennis van InDesign kwam goed van pas toen ik aan de lay-out van mijn boekje moest beginnen. Buiten het lab heb ik veel plezier beleefd aan de pannenkoeken-etentjes met Despina en de kids en ik hoop dat we dat in de toekomst zeker blijven doen. **Mieke**, bedankt voor de enorme bergen (kweek)werk die jij hebt verzet. Hierdoor had ik meer tijd en ruimte om mijn proeven goed uit de verf te laten komen. Daarnaast heb ik het ook altijd heel erg gewaardeerd om trouw elke morgen begroet te worden met een vrolijk 'Goedemorgen!' of 'Ha meissie!'. **Richard** en **Esther V.**, hoewel ik helaas niet veel

microscopiewerk heb gedaan, was het altijd erg prettig om gebruik te maken van jullie kennis en ideëen die veelal in de vrijdagochtend-werkbespreking geopperd werden. Daarnaast **Richard**, waarde collega, waren onze mailwisseling ook altijd erg grappig! **Theo**, **Carla** en **Caspaar**, ik heb altijd heel prettig met jullie samengewerkt binnen het onderwijs dat aan de diergeneeskunde of biomedische studenten werd gegeven. **Theo**, wat fijn dat ik mijn optimisme kon afzetten tegen jouw cynisme. Daarnaast wil ik je bedanken voor het actief meedenken met het voortzetten van mijn carrière binnen het hoger onderwijs. **Petra**, jouw eindeloze multi-inzetbaarheid was geweldig. Van het bestellen van mappen, even stoom kunnen afblazen, tot attente briefjes (of zelfs kleine kadootjes) in mijn postvak en zelfs een vlucht in jullie zweefvliegtuig. Bedankt! **Chris**, jouw deur stond altijd open voor de statistische problemen waar ik (voor de zoveelste keer) op stuk liep. Weliswaar in ruil voor een zak dropjes had jij altijd het geduld om mij weer op het juiste statistische spoor te brengen.
Alle andere collega's en ex-collega's en studenten van **Biochemie en Celbiologie**, bedankt voor de fijne samenwerking en alle gezelligheid binnen en buiten het lab. Zonder paaslunches, kerstdiners, 80/90ties feestjes, het sinterklaas-dobbelspel, maar ook de gezellige en/of pittige gesprekken aan de koffietafel was het de afgelopen vier jaar een stuk minder leuk geweest. In het bijzonder wil ik **Jaël**, **Julia**, **Ruud** (psst!), **Martijn**, **Maria**, **Francesca**, **Jeroen**, **Jan**, **Jason**, **Mokrish**, **Wangsa**, **Mijke**, **Nicole**, **Arjan**, **Koen**, **Janny**, **Ignace**, **Nick**, **Maidina**, **Janneke**, **Renske**, **Hanneke** en **Ruben** bedanken. **Hendrik**, bedankt voor je pionierswerk op de Influx en de gezellige samenwerking en muzikale sessies achter de FACS. **Jim**, wat heb jij tijdens je masterstage een berg werk verzet! Je werkte niet alleen hard, maar was ook een hele gezellige kamergenoot ('Krèg nou de blafhik!'). **Suus**, het half jaar dat wij kamergenootjes waren heeft zijn weerslag gehad op onze werkefficiëntie (en die van Theo!), maar ik had het voor geen goud willen missen. Ik hoop nog vaak buiten het lab verder te blijven kletsen en giechelen. **Diana**, **Maaike**, **Liset**, **Kirsten** en **Casper**, bedankt voor de gezellige sfeer en het luisterend oor op kamer 245.

Naast mijn collega's van Biochemie en Celbiologie hebben ook veel mensen buiten de afdeling een steentje bijgedragen aan dit proefschrift. Tijdens de stages binnen mijn masteropleiding ben ik begeleid door **Edward Dolk** en **Cécile van Els**. Bedankt voor jullie goede begeleiding en het doorgeven van jullie enthousiasme voor Celbiologie dan wel Immunologie. Mijn stage bij Celbiologie was nooit zo leuk / nuttig geweest zonder zzz**Jarno**, **Erik** (Enrique), **Renée** (Ronnie), **Paul** en mede-mastergenootjes **Annette**, **Chris** (Chrizz!) en **Matthia**. Tijdens mijn stage bij het NVI was ik blij om onder andere deel uit te maken van het 'drietal' samen met **Mieke** (Kwek) en **Harry** (Kwak).
Gedurende mijn AiO project heb ik ook vele uren doorgebracht op de **afdeling Immunologie** van Diergeneeskunde om metingen op de flow cytometer en later op de Luminex te doen.

Alle mensen die me hebben geholpen met het oplossen van technische problemen of zorgden voor een gezellig praatje tijdens het meten ofwel de pauzes: bedankt! In het bijzonder wil ik **Marij**, **Natascha** (met onze wekelijkse 'Janeway'club), **Martijn**, **Bram**, **Chantal**, **Rachel**, **Peter**, **Aad**, **Femke**, **Eveline** en **Jeroen S.** noemen. **Alice**, bedankt voor het kritische doorlezen van één van mijn manuscripten. **Mies**, bedankt dat je met op weg hebt geholpen op de NTA bij Biofarmacie. **Wilco**, bedankt voor je last-minute hulp met jullie supergave Luminex. **Ethlinn** en **Enrico**, bedankt voor de fluorescente liposomen. **Willem** en **Berend-Jan** bedankt voor jullie hulp bij het produceren van de fluorescente virusdeeltjes. Tijdens de PhD retreats en al het PhD gerelateerde commissiewerk was het fijn om samen te werken met **Jos**, **Erna** en **Saskia** en de gezellige groep AiO's van I&I waaronder **Matthijn**, **Evelien**, **Ewoud**, **Thijs**, **Arjan** (Arie!) en **Daphne**. **Krijn**, **Mariëtte** en **Niek**, super leuk dat jullie ook onderzoek doen naar extracellulaire vesicles. Het was leuk om (zijdelings) met jullie samen te werken.

Alle **mede-docenten bij Farmacie**, bedankt voor de fijne samenwerking en het meeleven met mijn promotietraject. **Marleen** en **Marije**, fijn om als drie beginnende docenten onze ervaringen en frustraties met elkaar uit te kunnen wisselen. Ik heb het naar mijn zin! En voor mijn (terwijl ik dit schrijf) nét nieuwe **collega's bij onderwijszaken van Biomedische Wetenschappen**: ik heb er zin in!

Ik ben een rijk mens met zo veel lieve vrienden en (schoon)familie, die altijd klaar stonden om naar mijn enthousiaste of soms moedeloze (maar in ieder geval vaak: onbegrijpelijke) verhalen te luisteren. Dank jullie wel voor alle afleiding en ruimte die jullie mij hebben gegeven, jullie zijn onmisbaar! **Hilde**, bedankt dat je altijd voor me klaar stond met een luisterend oor en een bakkie thee, met goede adviezen of juist voor een (klets)rondje op de spinning- of racefiets. Er is veel te weinig ruimte om hier te beschrijven hoeveel je voor me betekent! **Matti**, dank voor onze fijne diepgaande gesprekken. **Matthia**, bedankt voor onze fijne vriendschap (UBV rules!). En samen met **Victor** verheug ik me al op ons volgende zeskoppige 'UBV vs. Proton'-weekendje weg ofwel op een volgende borrel in de Primus.
Lil, **Ilse**, **Willy**, **Mel** en **Troedy** ('Schatjes') onze vriendschap stamt al uit de onderbouw van de middelbare school. Van boterhammen eten tussen de kluisjes, via 't Stadscafé, Duitse herders, telefoontjes met 'Jan', verschillende feestvakanties en zelfgemaakte carnavalskostuums, zijn we inmiddels beland bij de huizen kopen, kinderen en belangrijke banen! Zullen we afspreken om nooit helemaal volwassen te worden? ;-) **Ilse**, wij kennen elkaar zelfs sinds groep 2 van de basisschool. Bedankt voor het ontwerpen van de kaft van dit proefschrift! **Lilianske**, je bent mijn vriendinnetje door dik en dun. Onze levens lopen niet altijd helemaal synchroon, maar in geval van een (relatie)crisis had jij altijd aan een

half woord genoeg om vervolgens met stapels chocolade voor mijn deur te verschijnen.
Renée, **Desiree**, **Eva** en wederom **Ilse** en **Lil** ('Seven Sins') we waren een enorm gezellig en ondernemend, maar niet zo hard roeiend roeiteam onder de bezielende coaching van **Matthijs** (Matti). Inmiddels is de meerderheid van ons definitief uit de boot gestapt. Gelukkig is onze vriendschap gebleven.
Gisela, **Sanne**, **Sanne** en **Selma**, ik ben blij dat wij nog steeds, met enige regelmaat, onze klaverjasavondjes houden. Fijn om zo, na het afronden van onze studie, van elkaars reilen en zeilen op de hoogte te blijven. **Gisela**, naast klaverjassen was jij samen met Selma ook supergezellig en culinair huisgenootje en ben je een fijne vriendin. **Edwin**, bedankt voor de vele rondjes op de racefiets ('Welk fietsknooppunt was dat nou?). Nog maar een keertje Utrecht-Bommel-Utrecht doen? Daarnaast heb ik gedurende mijn AiO tijd met veel plezier gevolleybald bij team **Hebbes** (Van Slag) en speel ik inmiddels bij **Dames11** van VVU (Kaboem!) Bedankt meiden (en kerels)!

Kees en **Marjo**, **Daan** en **Kirsten**, **Thijs** en **Jennifer** en **Thomas**: Wat fijn om jullie als schoonfamilie te hebben! Dank voor jullie steun en interesse. **Kees** en **Marjo**, wat heerlijk dat er (aangekondigd of niet) altijd een bordje eten klaar stond. Daarnaast ben ik jullie ook dankbaar voor de grote hoeveelheid kluswerk die jullie hebben verzet op de Faustdreef.
Lieve **broer** en **Nancy**, ondanks dat wij heel verschillende levens hebben kon ik de verhalen over mijn onderzoek ook bij jullie kwijt. Ik vond het enorm leuk om jullie een rondleiding te geven op het lab. **Broer**, de wetenschap dat jij er altijd voor me bent, op de moeilijkste en mooiste momenten, is van onschatbare waarde.
Lieve **ouders**, jullie liefde, steun en vertrouwen hebben ervoor gezorgd dat ik mijn hele schoolcarrière zorgeloos heb kunnen doorlopen. Ook toen ik Biologie ging studeren, op kamers ging en begon aan mijn promotieonderzoek hebben jullie mij onvoorwaardelijk gesteund en soms ook jullie zorgen geuit ('Werk je niet te hard?'). Jullie zijn altijd trots geweest op wat ik deed, onafhankelijk van het eindresultaat. Dankzij jullie sta ik hier!
Lieve **Joost**, ondanks dat jij in dit proefschrift verder niet beschreven staat, ben *jij* de allermooiste ontdekking die ik heb gedaan tijdens mijn promotietraject. Wat begon halverwege mijn eerste jaar met honingdropjes en een AFM voor biologische samples is inmiddels uitgegroeid tot een fijn huisje (met twee katten) waarin we alweer een jaar samenwonen. Lief, dank je wel voor jouw rust, flexibiliteit, incasseringsvermogen wanneer ik weer eens 'de diva' uithing en al dat andere wat niet in een paar regels te vatten is. Zonder jou had ik het echt niet gered. Ik hoop jou evenveel steun te kunnen bieden de komende drie jaar, wat zeg ik… de rest van onze toekomst!

The only constant thing in life is change – Heralitus